Extracellular Polysaccharides in *Pseudomonas aeruginosa* Biofilms

Kelly Marie Colvin

A dissertation
submitted in partial fulfillment of the
requirements for the degree of

Doctor of Philosophy

University of Washington
2012

Matthew Parsek, Chair
Caroline Harwood
Wendy Thomas

Program Authorized to Offer Degree:
Microbiology

University of Washington

ABSTRACT

Extracellular Polysaccharides in *Pseudomonas aeruginosa* Biofilms

Kelly Marie Colvin

Chair of the Supervisory Committee:
Professor Matthew Parsek
Microbiology

Biofilms are a prominent mode of bacterial growth in the environment and in disease. Biofilm development involves specific stages including surface adherence, proliferation, cell-cell cohesion and dispersion. Each of these stages is dependent on either the reinforcement or modulation of the extracellular matrix. A key component of the biofilm matrix is extracellular polysaccharides. Many organisms that are adept biofilm producers including *Escherichia coli*, *Vibrio* spp, *Salmonella* spp, *Burkholderia* spp. and *Pseudomonas aeruginosa* maintain the genetic material necessary to synthesize multiple types of polysaccharides. In many cases, the different polysaccharides are niche-specific and allow the organism to thrive in a variety of environments. *P. aeruginosa* is a model organism for biofilm studies and produces three extracellular polysaccharides that have been implicated in biofilm development, alginate, Psl and Pel. Significant work has been conducted on the roles of alginate and Psl in biofilm development, however we know little regarding Pel. In this study, I demonstrated that Pel can serve two functions in biofilms. The first is that Pel provides cell-cell adhesion during biofilm growth and can act as the primary structural scaffold. The second is that Pel enhances tolerance to aminoglycoside antibiotics in biofilm populations, a property unique to Pel. Additionally, this work has laid the foundation for Pel purification and carbohydrate

structural analysis and contributed to the biochemical analysis of two proteins involved in Pel synthesis, PelD and PelF. Furthermore, I demonstrated that Pel and Psl polysaccharides provide structural redundancy in the biofilm matrix and the structural contribution of each polysaccharide was highly variable between clinical and environmental isolates. This led us to propose four classes of strains based upon their Pel and Psl functional and expression profiles. From this work, we have gained important insight on the unique and redundant roles of two distinct polysaccharides that are important factors in the adaptation of *P. aeruginosa* for successful chronic infections in cystic fibrosis patients and biofilm growth.

TABLE OF CONTENTS

ACKNOWLEDGEMENTS

During my first rotation in grad school, a senior graduate student Val Morris once told me that a thesis is a marathon and not a sprint. While, there were many periods of sprinting, maintaining a consistent and fruitful effort could only be accomplished through the training, support and encouragement of many people. I am indebted to them and am honored to have them in my corner.

First and foremost, I would like to thank my advisor, Matthew Parsek, who is an unbelievable mentor. His consistently positive attitude about research has been a *key* factor in this marathon. Without it, many successful projects may not have begun or finished without his expertise or advice. Matt has always allowed me to work independently and encouraged me in my own research endeavors. He also has an incredible ability to collaborate and find experts in a field we don't know much about. This has been invaluable in finding scientific support for multiple projects. I am surely a better scientist having been trained by him.

I would also want to thank my wonderful thesis committee, Caroline Harwood, Wendy Thomas, Pradeep Singh and Joseph Mougous for giving generously of their time and mental energy. They have been an incredible source of wisdom and support. Carrie for her limitless enthusiasm for science, critical eye in experimental design and expertise in *Pseudomonas* signaling. Pradeep for reminding me to keep in mind the environmental context where biofilms form when studying biofilm physiology. Joseph for his insights on bacterial interactions and making sure my experiments answers the question I ask. And Wendy for encouraging me to consider the physical properties of biofilms. I feel I was truly mentored by a family of wonderful scientists.

I want to thank my undergraduate advisors Victor Nizet and John Buchanan for fostering my scientific endeavors. Without them I would not be here. I could not be

more thankful for their encouragement to continue my science education. Their passion for science was contagious.

Teaching two undergraduate laboratory courses grossly enriched my graduate school experience. Despite my initial fear of public speaking, I fell in love with teaching. I couldn't be more thankful to Mark Chandler and Kendall Gray for serving as my teaching advisors. They were an endless source of creative teaching strategies, problem solving skills and inspiration.

In the lab I never would have succeeded without the advice and camaraderie of many lab members. The members of the Parsek lab including Brook Peterson, Brad Borlee, Yasuhiko Irie, Joe Harrison, Boo Shan Tseng, Laura Hmelo, Tam Quach and Laura Jennings have made graduate school so much more enjoyable. Our lab is intertwined with the Singh lab and for many years I shared a bay with Richard Siehnel and he was an incredible source of old-school techniques and endless puns. Other members of the Singh lab including Dao Nguyen, Joy Fraga Muller, Angus Angermeyer, Amruta Joshi, Elizabeth Bauerle, Rakesh Chaudhary and Ben Staudinger have been an incredible source of information and endless fun. I have also had the wonderful opportunity to mentor two undergraduates, Vivian Lee and Catherine Tart and two rotation students, Rudy Urbano and Becky Scholz. In many ways, I have learned so much from them. In particular Catherine has been an invaluable contributor to the environmental and clinical isolate project. This lab of people is a random assortment of personalities, scientific knowledge and wacky humor. I can't imagine a better group of people.

The graduate students in the Microbiology department have become part of my extended family. There are so many moments in this process that required drinking, complaining and just plain comforting. I couldn't be more grateful to them. Ruth Hall, Kristin Adams, Julie Silverman, Kim Gutierrez and Laura Icenogle have become lifelong friends that I dearly cherish. While we may be geographically parting, I am so exciting to see what these incredibly talented ladies discover in the future.

To my friends and family who have been my personal cheerleaders. In particular, my parents, Linda and Ed, and Jim and Debbie, my sisters, Julie and Kristel, my brother, Justin, my new family, Fred, Debbie and Ashlee and my lifelong friends from Junior High, Lauren Reid, Brittany Liu Girgis, Robin Hatch, Kelley Hutchinson, Sara Harvey, Michael Maxwell, Eric Fontes, Kevin Elliot and Kevin Lamar for believing in me. Even though they may not understand what I was trying to accomplish and at points believed I may cure cancer, they have been a wonderful source of support and encouragement.

And finally I would like to thank my husband, my love, Adam. He has been unflinching in his love and support throughout the ups and downs of research. During times when I struggled, he would make me dinner, tell me jokes or rejuvenate me with a quick trip to Vancouver or Portland. He is such an important part of my success and happiness. I am very thankful for him.

INTRODUCTION:

Extracellular Polysaccharides in Bacterial Biofilms

Bacterial biofilms are ubiquitous.

Microbiologists have studied bacterial cells for centuries. Traditionally bacteria are cultured in a planktonic form, or more simply stated single species of cells grown in pure culture in liquid medium. While there have been enormous advances in bacterial genetics, physiology and metabolism from studying planktonic cells, microorganisms do not live in pure cultures of dispersed single cells. Rather they accumulate at interfaces to form polymicrobial aggregates such as flocs, films or mats (62). Collectively, these aggregates are referred to as biofilms. Biofilms are multicellular communities encased in a hydrated extracellular matrix (42, 168, 180, 226). Biofilms exist on almost every imaginable environment supporting microbial growth including human teeth and medical implants to thermal hot springs and glaciers in the Antarctic (77). The ubiquitous nature of biofilms and the discovery that planktonic cells and biofilm cells exhibit distinct phenotypes makes biofilm research industrially and clinically relevant.

Biofilm formation is not a passive assembly of cells but rather is a dynamic and active process. Biofilm development can be separated into five stages. The first and second stages involve the transient association with a surface, followed by tight adherence known as irreversible attachment (226). This initial surface colonization is often mediated by surface-associated polysaccharides or appendages such as pili, flagella or fimbriae (169). After the cells are firmly attached, they form microcolonies and mature into large structures accompanied by the secretion of copious amounts of matrix material resulting in distinct structures (226). The final stage of biofilm development is achieved as some bacteria begin transitioning back into planktonic cells, presumably to begin the biofilm cycle at a separate location (226).

Biofilms are important in disease pathogenesis.

It is estimated that bacteria living in biofilms are responsible for between sixty-five and eighty percent of all bacterial infections requiring treatment by physicians (42). Biofilm infections tend to be chronic and difficult to treat due to their ability to resist robust immune responses and antibiotic treatment (180). Biofilm infections develop preferentially on a substratum and are generally confined to a particular location (180).

Known biofilm infections include endocarditis, infectious kidney stones, and in-dwelling medical device infections (180). Arguably the most well studied complex biofilm infections occur within the airways of cystic fibrosis (CF) patients (42, 180).

Cystic fibrosis (CF) is a recessive genetic disorder that affects the lungs and digestive system of humans, causing progressive decline in lung function and eventual death (134). CF was first recognized in the 1930s. According the World Health Organization, CF is most commonly found in Caucasian populations of European ancestry with a carrier frequency of 1 in 25 and prevalence rates as high as 1 out of every 3500 births in the United States. CF is caused by a mutation in the cystic fibrosis transmembrane conductance regulator (CFTR) (134). CFTR is an ABC transporter that transports chloride ions across epithelial cell membranes. Mutations in this gene result in altered chloride transport and multi-organ complications (180). One important symptom is the excess mucus secretions clogging the lungs and providing an altered environment that facilitates heavy bacterial colonization (249). Microscopic analysis of mucus secretions has revealed that within the lung, bacteria form biofilms as evidenced by multicellular clusters surrounded by matrix material (211). Despite a robust immune response and aggressive antimicrobial therapy, a number of bacterial species can chronically colonize the lungs of CF patients. *P. aeruginosa* is regarded as the major cause of morbidity and mortality in patients with CF (249). Interestingly, *P. aeruginosa* bloodstream infections can result in death within a few hours, while CF patients are often colonized with 10^8 to 10^{10} organisms of *P. aeruginosa* in their lungs for years, despite aggressive treatment (180, 249).

Biofilms exhibit multidrug tolerance.

There are many advantages to existing as a biofilm. One advantage is that a biofilm community is often more tolerant to antimicrobials and host factors (55, 138, 164). Biofilms often survive in the presence of antibiotics at concentrations that are hundreds to thousands of times higher than the minimum inhibitory concentration measured for planktonic cells (164). This is an extremely important biofilm trait because *in vivo* treatment with antibiotics may suppress infection symptoms by killing any planktonic

cells, but fail to eradicate the bacterial cells still embedded in the biofilm. When antibiotic treatment stops, the biofilm can act as a source for recurrent infections. Because of this feature, biofilms are difficult to eradicate and usually persist until the biofilm is physically removed (223). In addition to antibiotics, biofilms have increased resistance to a range of antimicrobial agents including heavy metals, host immune factors and desiccation (42, 102, 231).

Biofilm's enhanced antimicrobial tolerance is thought to be multi-factorial. One hypothesis is that biofilms are composed of distinct subpopulations, some of which are particularly tolerant to antimicrobial treatment (19, 224). The interior of a biofilm has reduced oxygen and nutrient levels, resulting in bacterial subpopulations that have low metabolic activity and slow growth rate (253). Thus, antibiotics that target actively growing cells will be less effective against this subpopulation, including tobramycin (inhibits mRNA translation), tetracycline (inhibits protein synthesis) and ciprofloxacin (inhibits DNA replication) (253). On the contrary, cells within the biofilm interior are more susceptible to antimicrobial peptides such as colistin (176). Phenotypic resistance to colistin occurs in metabolically active cells that can modify their LPS structure and induce expression of antibiotic efflux pumps (176). In addition to colistin, the transition metal gallium also preferentially kills the biofilm interior subpopulation due to this subpopulation being iron limited (107). Iron metabolism is essential for many biological processes including DNA replication, electron transport and oxidative stress defense (24). Since gallium and iron are chemically very similar, gallium can compete with iron and disrupt essential iron-dependent processes resulting in cell death (107). These examples provide evidence that biofilm subpopulations display differential antibiotic tolerance.

A second contributing factor towards antibiotic tolerance is poor penetration of the antibiotic through the biofilm matrix (223). Altered penetration patterns appear to be antibiotic specific. For example, fluoroquinolones such as ciprofloxacin rapidly penetrate through biofilms of *P. aeruginosa*, while penetration of aminoglycoside antibiotics, such as tobramycin and gentamicin, are retarded (253). The delayed

penetration of aminoglycosides is likely due to greater binding of the cationic molecule to biofilm components. *P. aeruginosa* biofilm cells also produce negatively charged polymers in the biofilm matrix, such as alginate and cyclic glucans. These polymers have been shown to bind and sequester aminoglycosides providing increased antibiotic tolerance to the biofilm (139, 163, 201, 253). Adsorption of antibiotics to the biofilm matrix may result in increase tolerance by preventing the antibiotic from reaching its site of action and/or slow antibiotic penetration to allow the bacteria to implement a protective stress response.

A third hypothesis of antibiotic tolerance involves the presence of specialized persister cells (81, 130). Persister cells represent a small subpopulation of cells that spontaneously enter a metabolically quiescent state. Transcriptomic analyses of persisters showed biosynthetic genes were down-regulated and several toxin/antitoxin systems and multidrug efflux pumps were up-regulated (131). In this temporary metabolic dormancy, cells neither grow nor die in the presence of bactericidal agents and thus exhibit multidrug and multimetal tolerance (81, 131, 132). The presence of persister cells occur in biofilms at a frequency that is 100 to 10,000 times higher than seen in planktonic cultures (220).

More recently a fourth hypothesis was proposed, involving an active starvation response (162). In 2007, it was demonstrated that bactericidal antibiotics, irrespective of target, induce cell death through a common mechanism by stimulating a lethal dose of hydroxyl radicals (115, 116). These radicals are extremely toxic and can cause cell death by damaging proteins, lipids, and DNA (116). Bacteria have developed mechanisms to combat hydroxyl radicals produced as a result of antibiotic treatment. One antioxidant mechanism is the induction of the stringent response (162). The stringent response is induced when nutrients are sparse and reduces the production of prooxidants and increases antioxidant defenses by elevating catalase and superoxide dismutase activity, thus providing tolerance to bactericidal antibiotics (162). Biofilms are inherently nutrient limited and were demonstrated to depend on the activation of the stringent response for broad-spectrum antibiotic tolerance (162, 224). This

provides evidence for an antibiotic tolerant state that does not directly depend on antibiotic target activity, drug uptake, efflux or inactivation.

Composition and function of the extracellular matrix.

In most biofilms, the cells account for less than 10% of the biofilm biomass, whereas the extracellular matrix accounts for more than 90% (62). The matrix is the extracellular material, typically self-produced, in which the cells reside. It is composed of a mixture of polysaccharides, lipids, proteins and nucleic acids (41). The extracellular matrix composition can vary greatly between biofilms, depending on the organism, fluid dynamics, temperature and nutrient availability (62).

The extracellular matrix has many functions in bacterial biofilms. First and foremost, the biofilm structure and architecture is dependent on the extracellular matrix. Many of the matrix components such as polysaccharides, proteins and DNA are involved in adhesion, which is the initial step of colonization to abiotic or biotic surfaces, followed by bacterial aggregation and microcolony development, and biofilm cohesion, which mediates mechanical stability and architecture of the biofilm (62). Biofilm morphology can be smooth, flat, rough or fluffy with various amounts of channels between biofilm structures (62). In all cases, the biofilm matrix transiently immobilizes cells to the surface.

The extracellular matrix also provides protection to embedded cells. The matrix retains water at high concentrations and protects cells from desiccation (62). In addition cells are protected by the matrix from nonspecific and specific host defenses, such as phagocytosis during infection and also have enhanced tolerance to many antimicrobial agents (62). The matrix also functions by absorbing or sequestering organic compounds and inorganic ions, thus participating in nutrient accumulation and environmental detoxification. The matrix also serves as a nutrient source by storing carbon, nitrogen and phosphorus in the forms of extracellular DNA, polysaccharides and proteins that could be utilized by the biofilm community.

Common functions of extracellular polysaccharides.

Bacteria are known to produce extracellular polysaccharides during biofilm growth and polysaccharides represent a major fraction of the matrix (62). Extracellular polysaccharides can be relatively complex. They are polymers composed of monosaccharides joined together by glycosidic bonds, composed of many repeating units leading to large, often branched, macromolecules (243). Some are homopolymers such as cellulose, which consists of linear chains made up of β(1-4)-D-glucose repeating units (229). Cellulose is found in many bacterial and plant species including *Gluconacetobacter xylinus*, *Agrobacterium tumefaciens*, *Acetobacter xylinum*, *Rhizobium* spp., and some Enterobacteriaeceae and Pseudomonadaceae strains. Many polysaccharides are heteropolysaccharides consisting of neutral and/or charged subunits, such as colonic acid. Colanic acid is composed of fucose, glucose, galactose and glucuronic acid and is found in many Enterobacteriaceae (228). While many examples of polyanionic polysaccharides exist typically due to the presence of uronic acids, very few examples of polycationic extracellular polysaccharides have been described (62). Polysaccharides can also be modified by the presence or absence of acyl substituents, such as O-acetyl or O-succinyl groups (62). The sugar composition and modifications can greatly affect the physical and chemical properties of the polysaccharide, such as hydrophobicity and viscosity. In addition, the nature of the sugar linkage such as 1,4-β or 1,2-β alters the rigidity of the polymer (62). Straight chains are more rigid, while buckled chains tend to be more flexible. These properties are important features that contribute to the functions polysaccharides provide in the biofilm matrix (62).

Extracellular polysaccharides carry out a wide range of functions, including adherence to surfaces and other cells, structurally supporting biofilms and protection against physical stress, such as shear. Extracellular polysaccharides are also important in resisting desiccation, oxidative killing, phagocytosis, and antimicrobial stress (102, 174, 198). Protection may result from the polysaccharide sequestering or creating a physical barrier in the biofilm that inhibits the penetration of antimicrobials to the residing bacterial cells (55).

Introduction to *Pseudomonas aeruginosa*.

The opportunistic pathogen, *P. aeruginosa*, is a model organism for biofilm research. *P. aeruginosa* forms robust biofilms under a variety of laboratory conditions and grows as a biofilm during human and plant infections (211, 252). Most notably, *P. aeruginosa* chronically infects the lungs of CF patients, persisting as biofilms during infection. In addition, it is a genetically tractable organism, easy to handle, and has been extensively studied for genetic determinants that contribute to biofilm development (discussed below). Each of these characteristics make *P. aeruginosa* ideal for studying biofilm development.

P. aeruginosa is a Gram-negative rod-shaped bacterium belonging to the γ-proteobacteria class (28) . Other members of the γ- proteobacteria class are important human pathogens, including Enterobacteriaceae (*Escherichia. coli*), Vibrionaceae (*Vibrio. cholerae*), and Francisellaceae (*Francisella. tularensis*) (28). *P. aeruginosa* is a versatile Gram-negative bacterium that grows in soil, marshes, marine habitats, as well as on plant and animal tissues (28).

The basis of this environmental ubiquity is *P. aeruginosa's* minimal growth requirements and nutritional flexibility (28). These features may be reflected by its large genome size, 6.3 Mbp, about one-third larger than *E. coli* (227). The large genome size allows for greater genetic and functional diversity. In addition to an increased number of paralog genes, this larger genome is predicted to encode 521 genes involved in regulation, corresponding to 9.4 percent of the genome (227). The high number of regulatory genes correlates to bacteria that can survive in diverse environments (227). For example, *E. coli* dedicates 5.8 percent of its genome to regulation, while *Helicobacter pylori,* a highly specialized bacterium with a small genome, has much less regulatory potential - only 1.1 percent of the genes are predicted to have regulatory function (227). *P. aeruginosa* is particularly well suited to adapt to changing environments with its large genomic repertoir and diverse metabolic capacity.

***P. aeruginosa*, an opportunistic pathogen.**

P. aeruginosa is an opportunistic pathogen that causes disease in patients with physical, phagocytic or immunologic defects. The advent of antibiotic treatment prolonging the lives of immune-compromised patients has been thought to increase the prevalence of *P. aeruginosa* infections. According to the Center for Disease Control and Prevention (CDC), the overall incidence of *P. aeruginosa* infections in US hospitals averages about 0.4 percent. However, this opportunistic pathogen thrives in the hospital environment and accounts for 10 percent of all hospital-acquired infections. In particular, *P. aeruginosa* is a leading common cause of hospital-acquired and ventilator-associated pneumonia (28). Pneumonia is an acute inflammation of the lungs caused by infection and is typically acquired by inhaling endogenous oral flora or through the aspiration of cells from contaminated ventilator tubing or other healthcare devices (28). An estimated three million people in the US develop pneumonia each year, about 50,000 of them die (61). The susceptibility of colonization is inversely correlated to the basic health of the individuals. While *P. aeruginosa* can cause community-acquired pneumonia, it is extremely rare (196).

Pneumonia is only one of many infections that *P. aeruginosa* can cause. Other examples include urinary tract infections, dermatitis, bacteremia, endocarditis, soft tissue infections, bone and joint infections, gastrointestinal infections and a variety of systemic infections, particularly in burn patients or cancer and AIDS patients who are immunosuppressed (28). Any *P. aeruginosa* infection represents serious problems for patients hospitalized with cancer, CF and burns as the case fatality rate reaches 50 percent (28). By the broad range of infections *P. aeruginosa* can cause, it seems that there is no tissue it cannot infect. The pathogenicity of this organism is believed to be multi-faceted. The combination of many virulence and biofilm factors are believed to enable this opportunistic pathogen to cause a wide variety of diseases.

In addition to the broad range of infections *P. aeruginosa* can cause, it is well known for its chronic colonization of the airways of CF patients. CF patients have a mutation in the CFTR gene that is important in proper regulation of chloride transport through

epithelial cells (28). The disease manifests itself in multiple organs, including increased mucus secretions from the lungs. This altered environment is almost immediately colonized by bacteria and fungi after birth (28). Until the advent of antibiotics, most CF patients died in infancy from staphylococcal infection (74). In 2010, the average lifespan of a CF patient had increased to 38 years (143). This rise in survival is due to many improvements in treatment. However, despite aggressive antibiotic therapy, ultimately 80 to 95 percent of CF patients succumb to respiratory failure brought on by chronic bacterial infection (134). Often CF patients are colonized with multiple bacterial species, but the primary pathogen responsible for morbidity and mortality is *P. aeruginosa*. The microbiology of CF lungs is complex and changes over time (143). Typically, lungs of CF patients are initially colonized by *Staphylococcus aureus* and *Haemophilus influenza* in infancy and early childhood (143). These species decline over time and are taken over by the emergence of methicillin-resistant *S. aureus* (MRSA), *Stenotrophomonas maltophilia*, *Achromobacter xylosoxidans*, *P. aeruginosa* and *Burkholderia cepacia* complex (143). By late adolescence, 80 percent of CF patients are colonized by *P. aeruginosa* (143). Chronic colonization of *P. aeruginosa* is recognized as a poor prognosis indicator (74).

Genetic variants are selected for in the lung of CF patients.

During the course of chronic CF lung infections, *P. aeruginosa* undergo both phenotypic and genetic changes to enhance persistence. One manifestation of this is the appearance of colony morphology variants during the course of infection. These phenotypic changes can be due to genetic mutations. For example, *P. aeruginosa* will persist for years in the CF lung as a clonal strain, undergoing mutational changes that can lead to loss of motility, overproduction of alginate, altered LPS, quorum sensing deficiency and reduced virulence factor expression (100, 140, 215, 250). These changes are hypothesized to aid in the persistence of *P. aeruginosa* in the CF airways as evidenced by parallel evolution (99). In addition to these phenotypic and genetic alterations, isolates from CF sputum have been demonstrated to include morphologically distinct colonies referred to as, mucoid and rugose small colony variant (RSCV) (134).

Mucoid conversion is considered a poor prognosis indicator for CF disease (134). Interestingly, *P. aeruginosa* in up to 90 percent of CF patients have converted to a mucoid phenotype. The CF lung is an extremely inflammatory environment with a high concentration of polymorphonuclear leukocytes (PMNs), reactive oxygen species and tissue damage (198). Studies have demonstrated that PMNs and their toxic oxygen by-products select for mucoid conversion of *P. aeruginosa* (144). It should be noted that the CF lung environment is a unique site of perpetual inflammation and mucoid strains are rarely observed elsewhere in nature or disease. *In vitro* growth of mucoid strains often leads to spontaneous conversion to the non-mucoid form (134). A mucoid strain overproduces the extracellular polysaccharide alginate, which is composed of mannuronic and guluronic monomeric sugars (63).

RSCVs form colonies on solid medium that are phenotypically different from the smooth colonies of wild-type cells. They autoaggregate in liquid culture, hyperadhere to abiotic surfaces and have increased resistance to antibiotics (221). Unlike mucoid strains, RSCVs are routinely isolated from the environment, after exposure to certain antibiotics and from *in vitro* biofilm reactors (17, 25, 56, 65). In addition to *P. aeruginosa*, RSCV colonies have been observed for different bacterial species including *Burkholderia cepacia, Staphylococcus aureus, Salmonella enterica* and *Vibrio cholerae* (93, 186). In all cases, a predicted extracellular polysaccharide(s) is up-regulated and is required for the rough colony morphology and autoaggregative phenotype (186). In *P. aeruginosa* RSCVs, two predicted polysaccharide operons, *pel* and *psl,* are up-regulated (136). Both *pel* and *psl* are required for the wrinkly colony morphology and autoaggregative phenotype (221). Mutations in both of the biosynthetic loci result in a smooth colony and loss of aggregation in liquid culture, similar to wild-type (221). Furthermore, RSCVs have elevated levels of the intracellular signaling molecule, c-di-GMP (221).

During a 2-year study, RSCVs were isolated from 33 of 86 *P. aeruginosa* positive CF patients (100). The appearance of RSCVs was associated with patients who received a daily inhalation of tobramycin and colistin and correlated with declining lung function (100). In addition, comparison of clonal longitudinal isolates by genetic sequences

reveal that mutations conferring the RSCV phenotype are selected for in the lung (215). Characterizing the determinants responsible for the RSCV phenotype may provide information regarding the persistence of bacterial biofilms in natural systems and chronic infections. In addition to being isolated from CF sputum, RSCVs can also be isolated in the laboratory from the long-term cultivation of biofilm reactors (111). These laboratory conditions may simulate the pressures involved in the CF lung and may provide insights as to the survival advantage conferred by RSCVs.

Factors involved in biofilm development and structure.

Biofilm development is a complex, coordinated developmental process that begins with free-floating planktonic cells attaching to a surface, multiplying, maturing and finally dispersing back into the milieu as planktonic cells. Many factors are required for this process to be successful including surface motility, extracellular polysaccharides, proteins, nucleic acids and lipids. This process is tightly regulated and affected by hydrodynamics, nutrients and environmental conditions. Furthermore, there is an increasing appreciation that the extracellular matrix is not simply a random assembly of extracellular components encasing bacterial cells, but rather a highly ordered structure consisting of intricate and specifically designed webs of polymers, proteins and nucleic acids.

Extracellular polysaccharides

Extracellular polysaccharides are the most well studied component of bacterial biofilms. It is estimated that the dry weight of a biofilm is primarily composed of polysaccharides and these polysaccharides are a necessary component for biofilm development. *P. aeruginosa* has the genetic capacity to synthesize at least three extracellular polysaccharides, Alginate, Psl and Pel (198).

Alginate

Alginate biosynthesis requires proteins encoded by 13 genes. Most lie in a single operon, but one is located at a separate site on the chromosome within a gene cluster required for LPS synthesis. Alginate is a high molecular weight linear polysaccharide

composed of β 1-4 linked D-mannuronic acid and L-guluronic acid residues with O-acetyl side groups found on the C-2 and C-3 of the mannuronic acid residues (213). Besides *Pseudomonas* species, the bacterial genera *Azotobacter* and farmed brown seaweeds, *Laminaria hyperborean* and *Marcrocystis pyrifera*, are also capable of producing alginate (63). Interestingly alginate's structure is somewhat random and varies depending on the organism or strain producing the polymer. This is because alginate is modified twice during the transport across the periplasm (63). Alginate is first synthesized as a linear homopolymer of D-mannuronic acid and transported into the periplasm. Once there, the C-2 and/or C-3 position of the mannuronic acid residue can be acetylated by the concerted actions of AlgI, AlgJ and AlgF (63). The non-acetylated D-mannuronic acids can then be epimerized to L-guluronic acid by the enzyme AlgG (63). Alginates produced from *P. aeruginosa* typically contain primarily D-mannuronic acid residues randomly interspersed with L-guluronic acid residues (54).

Overexpression of alginate leads to the production of colonies that resemble mucus, also known as the "mucoid" phenotype. Alginate production inhibits phagocytosis by monocytes and neutrophils both *in vitro* and *in vivo* and protects cells from reactive oxygen species by savaging free radicals released by activated macrophages (9, 74). Alginate can also bind to aminoglycoside antibiotics like tobramycin and inhibit their penetration (82). This feature is predicted to be the mechanism responsible for elevated tolerance to aminoglycoside antibiotics during biofilm growth (87). In support of this notion, co-administration of gentamicin and an enzyme that can degrade alginate, alginate lyase, resulted in sensitivity to the antibiotic (3).

Overexpression of alginate results in significant architectural changes to biofilm development *in vitro*. Under conditions tested, a wild-type strain produced a flat homogeneous biofilm, while a strain overexpressing alginate formed large heterogeneous biofilms despite being initially impaired for attachment (87). Moreover, expressing the alginate lyase *algL* from an inducible promoter led to alginate degradation and greater cell detachment from established biofilms compared to the un-induced control (21). Recent studies demonstrated that biofilms formed by mucoid

strains rely on the Pel and Psl polysaccharides for biofilm development (266). Mutation of *pel* and *psl* genetic loci resulted in significantly reduced biofilm biomass and failure to form macrocolonies (266). Interestingly, alginate does not appear to be a significant component in the non-mucoid laboratory strains, PAO1 and PA14 (265). Genetic mutations in necessary genes for alginate synthesis resulted in no detectable change in biofilm development (265). However, overproduction of alginate clearly affects both structural and protective properties of the biofilm.

Additional studies evaluated the effects of alginate composition and acetylation on biofilm development. Mucoid strains isolated from CF patients have reportedly different amounts of acetylation and different proportions of D-mannuronic acid and L-guluronic acid (149). Altering these properties can dramatically change the polysaccharide structure and physicochemical properties (167, 190). For example, increased acetylation impairs the cooperative binding of calcium ions. Reduction in the cooperative binding of calcium ions will reduce both the strength and number of crosslinks in the polymer and thus contribute positively to polymer swelling and viscosity (212). Thus, alginates with increased acetylation are more hydrophobic and flexible compared to non-acetylated alginates (212). A non-acetylated mucoid strain was severely impaired for attachment and biofilm development despite proficient biofilm development in both the acetylated parental mucoid strain and the non-mucoid isogenic strain (167). Further studies demonstrated that alginate acetylation was necessary for the aggregation of bacteria into microcolonies (235). Thus, it appears that acetyl groups help mediate interactions between neighbor cells and surface colonization.

Apart from acetylation, altering the proportions of D-mannuronic acid and L-guluronic acid can also affect the chemical and physical properties of the polymer, including viscosity and calcium ion interactions (67). For example, strings of D-mannuronic acid will form an extended ribbon structure, analogous to cellulose, whereas those rich in L-guluronic acid will form a buckled chain, more similar to an egg crate (67). Both uronic acids bind calcium ions, but the strings of poly L-guluronic acid have an additional metal

chelation feature which results in a much stronger polymer interaction (67). Thus, alginates rich in L-guluronic acid form strong but brittle gels whereas those rich in D-mannuronic acid are weaker but more flexible (67). How the proportion of D-mannuronic acid to L-guluronic (or if it) affects biofilm structure has not been evaluated but it can be speculated that the proportion of D-mannuronic acid and L-guluronic acid will effect strength and viscoelasticity properties and may have profound effects.

Psl

Psl is synthesized by proteins encoded by 12 genes (*pslA-L*), located in a single operon (198). The genes contain homology to known carbohydrate biosynthesis genes (63). Psl is a branched polysaccharide consisting of a repeating pentasaccharide composed of D-mannose, D-glucose and L-rhamnose subunits (27). Interestingly, the size of Psl is highly variable with a high molecular weight cell-associated form > 100 kDa and a low molecular weight form approximately 2 to 6 kDa (or one to five repeating units) that can be isolated from the cell-free culture supernatant (27). Only the high molecular weight form reacts to Psl-specific antisera (27). It still remains to be determined which form is synthesized and/or is important during initial adherence and biofilm development.

Psl is extremely important for initial adherence of planktonic cells to biotic and abiotic surfaces, including glass, polyvinyl chloride (PVC), mucin and epithelial cells (26, 136). Overexpression of Psl resulted in liquid culture aggregation and increased surface colonization and biofilm formation (136). Using a Psl-conditional expression strain, Psl was also found to be important in cell-cell adhesion and biofilm development post-attachment (136). In addition, continuous Psl synthesis is necessary to maintain normal biofilm structure (136).

A fluorescent HHA lectin and Psl-specific antisera have been used to visually monitor Psl on single cells and during biofilm growth (135, 137). The HHA lectin is from *Hippeastrum hybrid* and specifically binds α-D-mannosyl residues (106). The Psl localization patterns changes throughout biofilm development. During early

developmental stages, Psl is either cell-associated or surface-associated. Cell-associated Psl was found to localize to the bacterial cell surface in a helical pattern, similar to the bacterial cytoskeleton protein MreB (135). The authors suggested that this helical pattern might promote cell-cell interactions with neighboring cells thus encouraging biofilm development (135). The surface-associated Psl may act as an adhesive or signal for other cells to also begin biofilm development. As the biofilm matures, Psl localization shifts from cell-associated to predominantly located on the periphery of the microcolony (135). As the biofilm continues to mature and prepare for bacterial dispersion, a hollow cavity full of swimming cells forms within the mushroom-shaped microcolony. Psl remains localized to the exterior of the microcolony that is immobilized and surrounding the hollow cavity (135). Through imaging Psl localization patterns, we may achieve a better understanding of the dynamics of matrix formation and degradation that occur through biofilm development.

Psl production also provides *P. aeruginosa* with protection against the immune system by limiting complement-mediated opsonization (160). Psl protects against macrophage and neutrophil phagocytosis by inhibiting the complement components C3, C5 and C7 from being deposited on the cell surface (160). Furthermore, neutrophils exposed to serum-opsonized with wild-type *P. aeruginosa* had a reduced neutrophil oxidative burst response compared to the neutrophils exposed to serum-opsonized with the *psl* mutant (160). Finally, Psl provides protection from intracellular neutrophil-mediated killing and promotes the survival of *P. aeruginosa* in the host (160).

Pel

The *pel* operon is composed of seven-genes and was originally identified in a transposon mutagenesis screen for strains defective for biofilm formation at the air-liquid interface of a standing test-tube culture in *P. aeruginosa* strain PA14 (64). This particular strain does not synthesize Psl. These biofilms are referred to as pellicles and is the basis of naming the "*pel"* operon. The pellicles formed by PA14 are extremely rigid and resistant to extensive vortexing, boiling and enzymatic treatments including DNase I, RNase A and Proteinase K. Pellicles could form when grown in minimal media

or in rich media like LB over a range of temperatures (15-37°), although the pellicle thickness and strength changes (64). In each condition, a *pel* mutant is unable to form a pellicle.

The Pel proteins are predicted to have polysaccharide synthesis, transport and processing functions (63). Thus, it was speculated that the genes encoded on the *pel* operon might be required for the synthesis of a novel polysaccharide in the biofilm matrix (64). Evidence that *pel* mutants are defective in the production of an extracellular polysaccharide stems from initial carbohydrate analysis comparing PA14 pellicles to Δ*pel* standing cultures. PA14 pellicles were enriched for glucose subunits (64). Cellulase treatment did not break down the pellicle into single cells but did break the pellicle into smaller fractions, suggesting that either 1-4 or 1-6- linked glucose polymers are present, but cellulose is not the primary component of the pellicle (64). Further evidence supporting the *pel* genes being involved in the synthesis of an extracellular polysaccharide comes from the ability of PA14 to bind Congo red, whereas the *pel* mutant does not (64). Congo red is a dye that binds neutral polysaccharides or polysaccharides containing β-1,3- or β-1,4-glucopyranosyl linkages (214, 270). A third piece of evidence is that PA14 produced rugose colonies, while *pel* mutations in rugose backgrounds produced smooth colonies (64). Scanning electron microscopy (SEM) analysis of bacterial colonies revealed that wild-type cells were encased within an extracellular matrix that was not apparent in the *pel* mutant (64). Rugose colonies in other organisms such as *V. cholerae, Salmonella* and *P. fluorescens* also result from the overexpression of an extracellular polysaccharide (219, 268, 270).

In addition to pellicle formation and colony morphology, Pel is important in static biofilms (64). A static biofilm assay can measure initial bacterial attachment at short incubations, such as one hour, while longer incubations assess biofilm formation. Bacteria are grown in 96-well plates, washed and the adherent cells remaining on the surface of the polystyrene microtiter wells are quantified by crystal violet staining. Δ*pel* strains produced biofilms that had significantly less stained material than wild-type

cultures (64, 245). These data suggest that Pel is required for mature microtiter dish biofilms (64).

Extracellular proteins and appendages

Flagellar-mediated motility is required for biofilm formation in many organisms including *P. aeruginosa* (185). *P. aeruginosa* synthesizes one polar flagellum which allows the cell to swim in aqueous environments and in low-agar (<0.4 percent) medium (121). Mutants defective in swimming motility were identified in a transposon screen for isolates unable to adhere to microtiter dishes in the initial stages of biofilm development (169). These mutants are considered to be surface attachment defective (sad) and are unable to form biofilms (169). However, this finding is dependent on the carbon source used to grow the biofilm (113). A mutant deficient in flagella-mediated motility was unhindered in biofilm development when citrate was the carbon source, but severely reduced when glucose or casamino acids were used (113). The mechanism behind flagella-dependent adhesion has been postulated to be multi-factorial. These include: (1) flagella-mediated chemotaxis to move towards favorable environments and away from non-favorable ones; (2) flagella-mediated motility could enable bacteria to reach a surface, over-coming repulsive surface-bacterial forces; and (3) the flagella could function as an adhesin capable of physically anchoring cells to a surface (185).

In addition to flagella motility mutants, twitching motility mutants were also found to be surface attachment defective (169). Twitching motility occurs by the extension, tethering and then retraction of polar pili, thus propelling the cell across the surface in a "slingshot" manner (104). The "slingshot" mechanism allows the cell to efficiently move through viscous fluids between surface interfaces (104). In *P. aeruginosa*, type IV pili mediate twitching motility. Similar to flagella-mutants, type IV pili mutants are defective for initial adhesion, but this is dependent on the growth medium and strain background (112). Biofilm growth in glucose and casamino acids is severely attenuated in the absence of type IV pili, but this defect is not seen when biofilms are cultured with citrate as the carbon source (113). Besides being important in abiotic adherence, type IV pili have been shown to be important for bacterial adhesion to eukaryotic cell

surfaces and pathogenesis, suggesting an overlap in factors required for biofilm initiation and bacterial attachment *in vivo* (13). Type IV pili serve a second function in biofilm development. After non-motile microcolonies develop, twitching motility is important for bacterial expansion across the substratum (112). Bacterial expansion occurred in two types of type IV pili-dependent motility, "walking" and "crawling" (70). Cells that "crawled" were oriented parallel to the surface and moved with high directionality, while cells that "walked" were oriented perpendicular to the surface and moved in an irregular and unpredictable fashion (70). Both types of motility appear to be important in surface exploration and cell migration, thus affecting biofilm structure (70). Type IV pili are also important in the formation of the mushroom-shaped cap in structured biofilms (113). Interestingly, the cap formation does not require twitching motility but does require the type IV pili, providing evidence that type IV pili may function as specific matrix adhesins (8). A subsequent study demonstrated that type IV pili directly and specifically bind DNA (242). Since eDNA is also an important component of the biofilm extracellular matrix, the direct binding by type IV pili may help form a more stable biofilm. These data indicated that type IV pili are involved in multiple stages of biofilm development.

Bacterial attachment and biofilm formation is also dependent on the c*up* fimbriae (241). Three gene clusters in *P. aeruginosa* encode the necessary elements for the synthesis of fimbriae via the "*chaperone-usher pathway*" after which they were named (241). They are the *cupA*, *cupB* and *cupC* clusters (241). *Cup* fimbriae are proteinaceous appendages that are thinner and shorter than flagellum and are often important in attachment to eukaryotic cells. The *cupA* gene cluster consists of five genes, annotated *cupA1-A5*, and is important in biofilm development. A *cupA* mutant shows an adhesion-deficient phenotype, with only 10% of the bacteria adhering relative to the non-piliated or piliated parental strain (241). Upon extended biofilm cultivation, the *cupA* mutant fails to form structured biofilms (241). When *cupB* and *cupC* mutants were analyzed for their contribution to adhesion and biofilm development, no differences were seen compared to the non-piliated or piliated parental strain (241). However, overexpression of *cupA*, *cupB* and *cupC* each resulted in increased biofilm formation

suggesting that perhaps the laboratory conditions do not produce the environmental signals necessary for *cupB* and *cupC* expression (120). Interestingly, all three *cup* gene clusters are negatively regulated by MvaT (240). MvaT is a transcriptional regulator involved in the growth phase-dependent control of some QS genes (263). *mvaT* mutants exhibit enhanced biofilm formation and this phenotype is suggested to be due to the overexpression of the *cup* operons (240). A fourth cluster named *cupD* was identified within the PAPI-I pathogenicity island found in PA14 but not in PAO1 or PAK (156). Upon *cupD* overexpression, CupD fimbriae were detected on the cell surface and resulted in increased bacterial attachment (156). Collectively, the Cup adhesins appear to be important in surface colonization.

Another key feature of the biofilm matrix is the large protein adhesin, CdrA (20). CdrA shares structural similarities to other extracellular adhesins that belong to a two-partner secretion system (20). *cdrA* is found in a two-gene operon that also encodes a protein transporter, CdrB (20). Expression of *cdrAB* results in the synthesis and export of CdrA to the bacterial cell surface (20). In addition, expression of *cdrAB* leads to bacterial aggregation and increased biofilm formation compared to the vector control (20). Expression of *cdrAB* increases during biofilm growth and under conditions of high c-di-GMP (20, 221). Interestingly, aggregation mediated by CdrA is dependent on the Psl polysaccharide (20). CdrA specifically binds to the Psl polysaccharide and this tethering action is important for the formation of stable biofilm structures (20). This study combined with other work that demonstrated Psl is localized in the biofilm periphery suggests that the extracellular matrix is organized and not simply a random distribution of polysaccharides and proteins (135). *P. aeruginosa* has five additional predicted gene clusters to be involved in the synthesis of large protein adhesins and future studies may reveal them as important adhesins in the biofilm matrix (20).

Recent studies have demonstrated that extracellular enzymes can be important for biofilm development (234). Overexpression of the extracellular proteolytic elastase LasB, lipase lipC and esterase *estA* dramatically reduced the ability of mucoid strains to form biofilms (234). Expression of *estA* and *lasB* affected the extracellular concentration

of rhamnolipids, alginate levels and swarming motility, whereas, *lipC* expression affected twitching motility (234). Consequently, extracellular enzymes appear to be an important part of the extracellular matrix since they can modulate factors important for biofilm development and structure.

Lipids and nucleic acids

Another important component of the matrix is extracellular DNA (eDNA). eDNA serves as an adhesion factor particularly in young biofilms (258). Biofilm cells exposed to DNase I prevented the initial establishment of biofilms (258). However, DNase I did not disrupt pre-grown biofilms (258). Additional studies demonstrated that eDNA is spatially organized. In young biofilms, eDNA is primarily localized to the periphery of microcolonies and on the substratum (4). As the biofilms age and become mushroom-like, eDNA localized to the periphery of the stalk forming a border or glue between the cap and stalk portions (4). The eDNA generated in biofilms is due to the lysis of a small population of cells from at least two distinct pathways (4). The first is responsible for a basal level of eDNA in the biofilm and is QS-independent. The second pathway is linked to QS and results in the release of larger amounts of DNA. Biofilms formed by a *lasIrhlI* and *pqsA* mutants exhibited reduced eDNA in the biofilm matrix and were thin and flat (4).

Typical biofilm architecture produced by *P. aeruginosa* can be described as three-dimensional mushroom-shaped microcolonies that are surrounded by open channels. While the formation of heterogeneous biofilm structures depends on extracellular polysaccharides, eDNA and surface motility, the maintenance of the open channels depends on the production of rhamnolipids (47). The channels throughout the biofilm serve a beneficial purpose by providing a means to deliver oxygen and nutrients to bacteria deep within the biofilm. Rhamnolipids are a surfactant that modulate both cell-to-cell and cell-to-surface interactions (47). One benefit of surfactant production is that it blocks initial adhesion of other bacteria to the biofilm community (47). This is one mechanism that *P. aeruginosa*, *Lactobacillus spp*., and *B. subtilis* employ to non-specifically prevent other microbes from colonizing the channels within the biofilm (47,

159, 246). A second function attributed to rhamnolipids is biofilm detachment (16). Strains overexpressing rhamnolipids accelerate detachment. Moreover, exogenous addition of rhamnolipids induces the hollowing out within established biofilms observed during normal detachment events (16). Thus, rhamnolipids are important in the maintenance of open channels and detachment of cells from the biofilm. Interestingly, rhamnolipid production is subject to QS control. The transcriptional regulator, AlgR, binds to the promoters and represses expression of *rhlI* and *rhlA* (the first gene in the rhamnolipid operon) (161). Since an *algR* mutant was impaired in biofilm development, it was proposed that AlgR repression of rhamnolipid synthesis and *rhl* QS is critical for normal biofilm maturation (161).

Lipopolysaccharide (LPS) is an integral component of the cell envelope in Gram-negative organisms. LPS is primarily known for being an important virulence factor in *P. aeruginosa* (110). However, LPS modifications can alter surface properties of the bacterium and thus affect adhesion and biofilm development (141, 189). LPS is composed of three structural domains, lipid A, core oligosaccharide and the distal O antigen (124). *P. aeruginosa* produces two distinct forms of O-antigen, one is a homopolymers of D-rhamnose referred to as common polysaccharide antigen (CPA, formerly called A-band), and the other is a heteropolymer consisting of three to five sugar repeats referred to as O-specific antigen (OSA, formerly B-band) (124). In PAO1, the OSA structure consists of three repeating sugar subunits consisting of two uronic acid derivatives and one N-acetylfucosamine residue (124). Strains expressing both forms of O-antigen have a relatively hydrophilic surface (141). In the absence of OSA, PAO1's cell surface becomes more hydrophobic, even more so than a mutant devoid of either O antigen (141). This analysis suggests that OSA has hydrophilic properties and CPA has hydrophobic properties. These surface properties greatly influence surface adhesion depending on the physicochemical characteristics of the substratum. When strains were analyzed for binding to glass, a hydrophilic surface, greatest adhesion was seen for strains possessing OSA (141). However, the opposite was true in binding to a hydrophobic surface, such as polystyrene (141). While the contribution of LPS to biofilm development is still being studied, LPS undergoes modifications during biofilm

growth such that its chemical structure is distinct from cells grown planktonically (38). Biofilm growth results in LPS transition to a CPA+ and OSA- phenotype from a CPA+ and OSA+ phenotype typical of planktonic cells. This phenotypic change was reversible when cells were regrown planktonically (12). In addition, chronic colonization of *P. aeruginosa* in the CF lung selects for isolates that either lack OSA completely or express reduced quantities, while the level of CPA is maintained (78, 215). Two explanations exist as to why these modifications occur in the CF lung. First, OSA is very immunogenic; loss of OSA may be beneficial to evading the immune system. Second, loss of OSA confers resistance to aminoglycoside antibiotics (193).

Another unique feature of Gram-negative cells is that they are continuously releasing membrane vesicles (MV) from the cell surface (11). These MVs carry OMPs, LPS, phospholipids, toxins and periplasmic constituents (11). An important feature of MVs is that the natural outer membrane arrangement is generally maintained. However, this is not the case for LPS. Only OSA LPS is found in MVs (11). Recently, MVs were identified to be a component of the *P. aeruginosa* biofilm matrix (205). One place MVs localized was at the substratum-biofilm interface (205). Other studies have demonstrated that MVs aid in both surface adherence and cell aggregation (148). Therefore, planktonic *P. aeruginosa* cells may have deposited MVs prior to biofilm development to aid bacterial adherence. Substratum-associated MVs only account for a fraction of MVs observed in biofilms. The other population is thought to be important in mediating complex interactions with matrix polymers and eDNA or serving a second function by absorbing or neutralizing extraneous agents, thereby protecting the cells (206).

Environmental Factors that impact biofilm development

Biofilm structure can change in the face of different carbon sources (208). *P. aeruginosa* grown on glucose produces a heterogeneous biofilm with mushroom-shaped microcolonies, while growth on amino acids or citrate forms flat, uniform biofilms (112). Mathematical modeling and experimental evidence demonstrate that these structural differences are dependent on swarming motility, which depends on both type IV pili- and flagella-mediated motility (208). Under conditions that promote swarming

motility (growth on citrate), cells are continuously moving on a surface and produce a flat, uniform biofilm. Conditions with limited swarming motility produce cell aggregates (stalks) and have the potential to expand into mushroom-capped biofilms (208). Immobile stalks can be climbed by a motile subpopulation, which ultimately form the mushroom cap (112). Consequently biofilms are composed of both motile and non-motile subpopulations. Interestingly, swarming motility can be controlled by QS. However, this was dependent on the carbon source (208). For instance, swarming motility was QS regulated when grown on succinate but not glucose or citrate (208). These results combined suggest that nutrient conditions dictate the contribution of quorum sensing and swarming motility in biofilm development.

An additional nutrient signal for biofilm formation is iron. In the presence of subinhibitory concentrations of lactoferrin, an antimicrobial that sequesters iron, *P. aeruginosa* biofilm growth is stunted and fails to form microcolonies or differentiate into biofilm structures (209). Similarly, growth in iron-limited minimal media or strains deficient in the ability to sequester iron has markedly reduced biofilm yields (7, 182). This is a result of low iron conditions, which stimulates type IV pili-mediated surface motility that results in flat, undifferentiated biofilms (209). Thus, a critical concentration of iron needs to be present in order to promote biofilm formation (7). It is well established that QS gene expression is enhanced under iron-limiting conditions (18). This is one way that bacteria can sense and respond to their environment. Since iron is necessary for bacterial survival but often a limited commodity, stimulated motility under low iron conditions prevents biofilm development in locations where this critical nutrient is in short supply.

Signaling determinants that regulate biofilm formation

Biofilm cells differ from their planktonic counterparts in the genes and proteins that they express. As such, the process of planktonic cells transitioning to the biofilm life cycle is governed by the activities of intricate regulatory networks that coordinate motility, adhesion and extracellular polysaccharide expression. The coordination of

gene expression is dependent on inter- and intracellular signaling molecules and environmental stimuli.

Quorum sensing

Bacteria are highly social organisms, with many being capable of cooperative behaviors mediated through chemical communication or quorum sensing (QS) (263). QS is defined as a pattern of gene regulation in response to certain extracellular signals (autoinducers), usually self-produced, in a density-dependent manner (263). One common QS system involves N-acyl homoserine lactone signals. The basic system is comprised of an autoinducer signal synthase and a cognate signal response receptor. The response receptor contains two functional domains, a receptor to bind the signal and a helix-turn-helix motif to bind target promoters (34). QS-controlled genes often encode virulence factors required for host-pathogen interactions, antimicrobials important in competition with other bacterial species and gene products required for biofilm development (158). One of the best-described QS systems is that of *P. aeruginosa*.

P. aeruginosa utilizes multiple QS systems. In the *las* system, the *lasI* gene product synthesizes N-(3-oxododecanoyl)-HSL ($3OC_{12}$-HSL), which interacts with the response receptor LasR and activates target promoters (66, 158). In the *rhl* system, the *rhlI* gene product synthesizes N-butyryl-HSL (C_4-HSL), which interacts with the response receptor RhlR and activates target promoters (66, 207). Interestingly, a third response receptor, QscR, was identified without a cognate signal synthase, but was found to modulate gene expression of a particular regulon in response to $3OC_{12}$-HSL (37). While the *las, rhl* and *qsc* systems control distinct sets of target promoters, these systems are intimately connected and are organized in a hierarchy in which LasR bound to $3OC_{12}$-HSL drives the expression of *lasI* (leading to a positive feedback loop) and *rhlI* and *rhlR* (263). In addition to $3OC_{12}$-HSL and C_4-HSL, *P. aeruginosa* synthesizes a third signaling molecule, 2-heptyl-3-hydroxyl-4-quinolone, called *Pseudomonas Quinolone Signal* (PQS) (183). PQS binds to and activates the transcriptional regulator PqsR (60). The *pqs* system appears to be linked with the *rhl* QS system but the exact nature is still unclear

(150). QS is an extremely complicated in *P. aeruginosa* with intricate layers of regulation and feedback that we are just beginning to tease apart. This complexity of regulation is important since these systems can directly or indirectly regulate 10% of the genome in *P. aeruginosa* (207).

QS in *P. aeruginosa* regulates multiple virulence factors including extracellular enzymes (LasA protease, elastase, alkaline protease, lipase), secondary metabolites (hydrogen cyanide, pyocyanin), and toxins (exotoxin A) (207). These virulence factors are believed to contribute to both acute and chronic *P. aeruginosa* infections. In several animal models, QS mutants are severely attenuated for virulence compared to wild-type (217). In addition to virulence factors, QS also regulates the complex developmental process required for mature biofilm development. Under certain conditions, a *lasI* QS mutant, despite equal adherence and proliferation in flow cells, forms an undifferentiated, thin biofilm that achieves only 20% of the wild-type thickness (49). Studies following this initial discover began to unravel and identify specific biofilm factors that are QS regulated, including the *pel* operon (202). Moreover, QS signaling molecules could be extracted from sputum of CF patients colonized with *P. aeruginosa* confirming their presence *in vivo* (211).

C-di-GMP

Bis-(3',5')-cyclic-di-guanidine monophosphate (c-di-GMP) is a ubiquitous second messenger in many bacterial species (103). In particular, c-di-GMP signaling plays an important role in many species in the transition to and from biofilm growth. This includes *P. aeruginosa*. In general, increased intracellular c-di-GMP stimulates the production of extracellular biofilm matrix components and inhibits motility, whereas low intracellular levels promotes motility and inhibits synthesis of extracellular matrix components (2, 90, 237). The level of intracellular c-di-GMP is controlled by the opposing activities of two enzymes, diguanylate cyclases (DGCs) and phosphodiesterases (PDEs). DGCs synthesize c-di-GMP from two molecules of GTP and PDEs break down c-di-GMP into pGpG (86). DGC activity requires the conserved GG[D/E]EF motif (103). PDE activity requires the EAL or HY-GYP domain (68). Often a

GGDEF and/or EAL/HY-GYP domains are located at the C-terminus of a protein that contain a sensory or signal transduction domain in the N-terminus. These domains are capable of sensing and responding to environmental cues (200). *P. aeruginosa* contains 17 GG[D/E]EF-containing proteins, 5 EAL-containing proteins, 3-HD-GYP-containing proteins and 16 proteins that contain both GG[D/E]EF and EAL domains (119). Currently, it is unknown if all of these proteins are catalytically active but there lies the potential to extensively fine tune c-di-GMP concentrations depending on the environmental conditions.

Increased levels of c-di-GMP are thought to promote biofilm development. Strains mutated for PDE activity or that have hyperactive DGC activity have increased c-di-GMP levels, reduced motility and increased extracellular matrix production (86). In *P. aeruginosa* a mutation in *wspF*, a negative regulator of the DGC WspR, results in elevated biofilm formation and the RSCV phenotype (89). Transcriptomic analysis demonstrated that the *pel* and *psl* polysaccharide operons, *cdrAB* operon, and *PA2440-PA2441* are up-regulated in a high c-di-GMP background (90). PA2440 is a predicted polysaccharide deacetylase and perhaps is involved in modifying the physical properties of Pel and/or Psl. Genes that were down regulated in a high c-di-GMP background included genes involved in flagellar motility (90, 221). There is increasing evidence that the effects of c-di-GMP may, in part, be localized subcellularly. For example, mutations in different DGCs can make distinct contributions towards biofilm development (154). Strains mutated for two DGCs, SadC and RoeA, had similar reduction in total concentration of c-di-GMP (154). However, SadC appeared to specifically affect motility and RoeA specifically affect Pel production (154). SadC and RoeA have different subcellular localization patterns and suggest that localized changes in c-di-GMP play a large role in biofilm regulation (154).

For c-di-GMP to exert its function, it has to bind to and allosterically alter the structure and output function of an effector component (86). One transcriptional regulator that binds and responds to levels of c-di-GMP is FleQ (89). FleQ is a negative regulator of the genes previously determined to be expressed in a high c-di-GMP background, including

the *pel* and *psl* operon, *cdrAB* and *PA2440-PA2441* and a positive regulator of genes involved in flagellar motility (89, 90). In the case of *pel* expression, FleQ directly binds the *pel* promoter and inhibits transcription. In the presence of c-di-GMP, FleQ binds c-di-GMP altering the complex with its antiactivator FleN and relieves repression of *pel* transcription (89).

An additional c-di-GMP binding effector is PelD (86, 129). PelD is one of the proteins necessary for Pel polysaccharide synthesis. This effector contains a motif that looks similar to an inhibition site (I site) typical in DGC proteins. C-di-GMP binds to the I site and results in product inhibition (86). PelD binds c-di-GMP and this binding event is required for Pel synthesis (129). Thus, c-di-GMP regulates Pel production both transcriptionally and allosterically.

Two-component systems

Two-component systems (TCSs) are regulatory modules that are often used by the cell to respond to environmental cues. This system consists of a histidine kinase sensor and a response regulator. The sensor consists of an input domain and the response regulator is composed of a receiver domain and output domain, typically a DNA-binding motif. Upon signal recognition, the sensor kinase autophosphoylates and the phosphate is then transferred to the response regulator for transcriptional activation (157). The PAO1 genome sequence encodes 130 TCSs, many of which are involved in biofilm development (195).

One important TCS that impacts *P. aeruginosa* biofilm formation is the GacS/GacA system. Upon activation by an unknown signal, the sensor kinase GacS phosphorylates the response regulator GacA, which activates the transcription of two small RNAs (RsmY and RsmZ) (73). These small RNAs bind to and relieve the repression exerted by the translational repressor RsmA. RsmA regulates genes involved in biofilm formation, including the *pel* and *psl* operons (73, 101, 247). In agreement with this signal transduction cascade, a *gacA* mutant is impaired for biofilm development (179). Furthermore, the activity of the GacS/GacA TCS is regulated by two orphan sensors,

RetS and LadS. RetS forms inactive heterodimers with GacS, thus inhibiting the signal cascade and inhibiting biofilm development (73). While LadS activates the GacS/GacA cascade through an unknown mechanism and promotes biofilm formation (247).

Objectives of this thesis.

Biofilm development is a fundamental process and a key survival mechanism universally employed by bacteria. Despite extensive studies on the extracellular matrix of *P. aeruginosa*, very little was known about the role of the Pel polysaccharide. This thesis work aimed to elucidate the structure, function and mechanism of biosynthesis of a polysaccharide demonstrated to be an important factor in the adaptation of *P. aeruginosa* for *in-vitro* biofilm growth and successful chronic CF infections. This research has contributed to a growing body of literature concerning the complexity of surface carbohydrates involved in biofilm formation.

CHAPTER I:

The Pel Polysaccharide can Serve a Structural and Protective Role in the Biofilm Matrix of *Pseudomonas aeruginosa*

Published as: Colvin, K.M., Gordon, V.D., Murakami, K., Borlee, B.R., Wozniak, D.J., C. L. Wong, G., and Parsek, M.R.. 2011. *PLoS Pathog*. 7(1):e1001264.

ABSTRACT

Bacterial extracellular polysaccharides are a key constituent of the extracellular matrix material of biofilms. *Pseudomonas aeruginosa* is a model organism for biofilm studies and produces three extracellular polysaccharides that have been implicated in biofilm development, alginate, Psl and Pel. Significant work has been conducted on the roles of alginate and Psl in biofilm development, however we know little regarding Pel. In this study, we demonstrate that Pel can serve two functions in biofilms. Using a novel assay involving optical tweezers, we demonstrate that Pel is crucial for maintaining cell-to-cell interactions in a PA14 biofilm, serving as a primary structural scaffold for the community. Deletion of *pelB* resulted in a severe biofilm deficiency. Interestingly, this effect is strain-specific. Loss of Pel production in the laboratory strain PAO1 resulted in no difference in attachment or biofilm development, instead Psl proved to be the primary structural polysaccharide for biofilm maturity. Furthermore, we demonstrate Pel plays a second role by enhancing resistance to aminoglycoside antibiotics. This protection occurs only in biofilm populations. We show that expression of the *pel* gene cluster and PelF protein levels are enhanced during biofilm growth compared to liquid cultures. Thus, we propose that Pel is capable of playing both a structural and protective role in *P. aeruginosa* biofilms.

INTRODUCTION

Biofilms are surface associated communities embedded within an extracellular matrix (168, 180, 225). Biofilm communities exhibit enhanced antibiotic tolerance (55, 138, 164). As a result, biofilm infections tend to be chronic and difficult to eradicate (42, 180). This enhanced tolerance is thought to be multi-factorial, owing to biofilm-associated patterns of gene expression, slow growth rate, and reduced antimicrobial diffusion within the biofilm (55). A focus of research has been to identify biofilm-associated factors that contribute to their antibiotic tolerance.

The opportunistic pathogen, *Pseudomonas aeruginosa,* is a model organism in biofilm research. *P. aeruginosa* is well known for the chronic infections it causes in individuals with the genetic disease, cystic fibrosis (CF) (42). Biofilm formation within the CF airways is believed to facilitate the infection, helping the bacteria to withstand aggressive antimicrobial treatment and host defenses (211, 249).

The extracellular matrix is a distinguishing feature of biofilms, capable of functioning as both a structural scaffold and protective barrier to antimicrobials (102, 168, 174, 180, 198). A key component of the matrix is extracellular polysaccharides. Extracellular polysaccharides carry out a wide range of functions involving surface and cell-cell interactions, as well as protecting against antimicrobials and host defenses (81, 87, 174, 223, 226). *P. aeruginosa* produces three extracellular polysaccharides, alginate, Pel and Psl, all of which have been implicated in biofilm development under different circumstances (198).

Pel's composition has yet to be fully elucidated. Initial carbohydrate analysis suggests Pel is a glucose-rich polysaccharide polymer although the exact structure remains unknown (64). Pel synthesis machinery is encoded by a seven gene operon (*pelA-F*) originally identified in a mutagenesis screen for the loss of pellicle formation in PA14 (64). Pel also appears to be important in static microtiter dish biofilm assays. A *pel* mutant strain had a defect in biofilm biomass accumulation in comparison to wild-type PA14 (64, 245). The mechanism behind this observation remains unclear. Other studies have demonstrated that in the absence of type IV pili, Pel can play a role in attachment suggesting it can compensate as an attachment factor in the absence of other adhesins (245).

In this study, we conducted an analysis of Pel function. We focused our study on two common laboratory strains, PAO1 and PA14. PAO1 is capable of making both the Pel and Psl extracellular polysaccharides, while PA14 is only capable of producing Pel since three genes of the *psl* operon are deleted in this strain. We show that Pel is critical for maintaining cell-cell interactions in developing PA14 biofilms as well as providing

protection against aminoglycoside antibiotics during biofilm growth. We also show that Pel does not appear to play any critical role in PAO1 biofilm development, where Psl appears to be the primary biofilm polysaccharide. Finally, we demonstrate that the *pel* operon is transcriptionally induced and PelF protein levels increase during biofilm growth. Thus, we propose that Pel can serve both as a structural and protective factor within a biofilm community.

RESULTS

Generation of a *pel*-inducible overexpression strain.

To initiate our study, we constructed a Pel overexpression strain. The native promoter region of *pelA* was replaced with the *araC*-P_{BAD} promoter on the chromosome in two common laboratory strains, PAO1 and PA14, allowing arabinose-dependent expression of the *pel* operon (**Figure 1A**). PA14 is a clinical strain obtained from a burn patient that has a multi-gene truncation in the N-terminal region of the *psl* operon and is incapable of synthesizing the Psl polysaccharide (128). Accordingly, PA14 serves as a useful strain to study the contribution of the Pel polysaccharide independently of Psl. In contrast, PAO1 has the necessary genes to produce both polysaccharides. The inducible strains will be referred to as PAO1P_{BAD}*pel* and PA14P_{BAD}*pel*. Quantitative RT-PCR was used to quantify *pelA* transcript level from log phase cells. The level of *pelA* transcript increased with increasing concentrations of the inducer, arabinose (**Figure 1C**). The dose-dependent increase in transcription level was similar between PA14 and PAO1. Addition of 0.2% arabinose led to 51- and 61-fold increase in expression levels in PA14P_{BAD}*pel* and PAO1P_{BAD}*pel*, respectively. *pelA* transcript is expressed 1.8 times higher in wild-type PA14 compared to wild-type PAO1 relative to the internal control transcript, *ampR* (**Figure 1C**).

Pel overexpression contributes to aggregation, Congo red binding, pellicle formation and rugose colony morphology.

We evaluated PAO1P_{BAD}*pel* and PA14P_{BAD}*pel* for the ability to conditionally produce more Pel polysaccharide with increasing *pel* transcription. Previous work has demonstrated that Pel synthesis is controlled at multiple levels, transcriptionally and

allosterically (90, 129). Congo red binding and liquid culture aggregation are two phenotypes associated with increased polysaccharide production in multiple bacterial species (90, 221, 270). Addition of 1% arabinose to both PA14P_{BAD}*pel* and PAO1P_{BAD}*pel* leads to bacterial aggregation in liquid culture relative to the uninduced strain and these bacterial aggregates hyperbind Congo red (**Figure 1B**).

Pel expression was previously demonstrated to impact pellicle formation and colony morphology (64). Wild-type PA14 forms a distinct pellicle after about two days of incubation at room temperature, which becomes more pronounced over time. When induced, PA14P_{BAD}*pel* rapidly produces a thicker pellicle compared to wild-type. A top-down view reveals that the PA14P_{BAD}*pel* stain produces a pellicle with a highly defined wrinkly architecture that is resistant to extensive vortexing (**Figure 1D, bottom panel**). Consistent with previously published data, a mutation in *pelB* leads to a dramatic reduction in pellicle formation compared to the parental strain (64, 65). Pellicles produced in wild-type PAO1 grown under the same conditions are less distinct than PA14 pellicles. No discernable difference in pellicle formation is seen between PAO1 and PAO1Δ*pelB*, but overexpressing Pel enhances pellicle formation similar to PA14 (**Figure 1D**). Overexpression of *pel* produces enhanced wrinkly colony morphology in PA14, whereas the *pelB* mutant grows as a smooth colony with little Congo red binding (**Figure 1D, top panel**). Unexpectedly, PAO1 did not produce a wrinkly colony morphology for any of the tested strains despite many attempts with varying temperature and media conditions (**Figure 1D, top panel**).

Pel contributes to biofilm development post-attachment.

We investigated the function Pel plays in biofilm development using two biofilm culturing methods, a microtiter dish assay and a flow-cell reactor. A microtiter dish assay quantifies biofilm formation on plastic during static incubation. In contrast, a flow cell bioreactor allows a microscopic analysis of live biofilms growing in dilute medium under conditions of continuous flow.

The influence of Pel on initial attachment to a plastic surface was examined. A *pelB* mutation in PA14 did not impact bacterial attachment (**Figure 2A**). However, overexpressing *pel* in either PA14 or PAO1 increased surface attachment (**Figure 2A and 2B**). Similar to PA14, no phenotype was observed in a PAO1Δ*pelB* mutant compared to wild-type PAO1 (**Figure 2B**). In contrast, but consistent with previously published work, a polar deletion in *psl* had a strong attachment defect in PAO1, indicating that Psl, and not Pel, is an important adhesin for surface attachment under these conditions (102, 136).

Crystal violet staining is an indirect measurement of bacterial attachment and thus we took a complementary, microscopic approach to evaluate Pel's role in attachment to a glass surface in a flow-cell reactor. Images were acquired by scanning confocal laser microscopy (SCLM) and analyzed by COMSTAT 1 software for surface coverage (88). No statistical differences between PA14, PA14Δ*pelB,* uninduced and induced PA14P_{BAD}*pel* for attachment are observed (**Figure 2C and 3A**). Similar to PA14, no difference is observed for any of the PAO1 strains tested under non-inducing and inducing conditions (**Figure 2D and 3A**). These results are slightly inconsistent with our microtiter dish assay, which demonstrate a modest but clear increase in attachment for the Pel overexpression strains. However, in both PAO1 and PA14, a *pel* mutation did not affect attachment in either biofilm culturing method.

Unlike surface attachment, we found that Pel has a significant impact on later stages of biofilm development and this impact was found to be strain dependent. To assess effects of Pel on later stages of biofilm development, we grew strains for 24 h in a microtiter dish assay and found that the *pelB* mutant strain of PA14 has a significant reduction in biofilm biomass compared to the parental PA14 strain, similar to previous findings (**Figure 4A**) (64, 245). The PA14Δ*pelB* biofilm defect was complemented by supplying P*pel* in trans. P*pel* contains the entire *pel* operon cloned into an arabinose-controlled expression plasmid, pMJT-1 (**Figure 4A**). Overexpressing Pel in PA14 increased biofilm biomass almost two-fold (**Figure 4A**). In contrast to PA14, no

difference is seen between PAO1 and PAO1Δ*pelB,* while overexpressing Pel results in a modest increase of biofilm biomass (**Figure 4B**). Conversely, PAO1Δ*pslBCD* has a pronounced defect, suggesting that Psl is the dominant polysaccharide in PAO1 for both attachment and biofilm maintenance, as reported by Ma, et al. (136).

Biofilm formation by these strains was monitored in a flow-cell bioreactor to allow for live imaging and structural analysis. Under these conditions, *P. aeruginosa* forms biofilms that contain mushroom-shaped multicellular structures. PA14 forms small microcolonies by day two that further develop into a structurally complex biofilm with large multicellular aggregates of bacteria by day four (**Figure 4C**). In stark contrast, PA14Δ*pelB* fails to form cellular aggregates. After four days of growth, PA14Δ*pelB* remains as a dense monolayer of cells attached to the glass surface, incapable of developing the complex three-dimensional structures typical of the wild-type strain (**Figure 4C**). The absence of cell aggregates in PA14Δ*pelB* indicates Pel may be responsible for the cell-to-cell adhesion necessary for aggregate formation. In support of this, overexpressing Pel results in larger cellular aggregates and enhanced biofilm biomass compared to wild-type PA14. Flow cell images were quantified for four properties of biofilm development using COMSTAT 1, average thickness, roughness coefficient, surface-to-volume ratio and maximum thickness (**Figure 3B**) (88). Pel overexpression in PA14 affected each property by increasing the average thickness, decreasing the roughness coefficient, decreasing the surface to volume ratio and increasing the maximum thickness.

In contrast to PA14, no major visual or quantifiable difference is seen in biofilm structure after four days of growth for PAO1, PAO1Δ*pelB* and PAO1P_{BAD}*pel* (**Figures 4D and 3B**). However, a modest, but not statistically significant, increase in average biofilm thickness is detected for PAO1P_{BAD}*pel*. We subsequently assessed whether a Pel-dependent phenotype might manifest itself in older biofilms. Yet, even after nine days no significant differences were observed for PAO1, PAO1Δ*pelB* and PAO1P_{BAD}*pel* (**Figure 5**).

Continuous expression of *pel* is required for continued biofilm growth, but not for maintenance of existing biofilm structure.

Continuous production of the Psl polysaccharide was recently shown to be required for both the addition of new biofilm biomass to a growing biofilm and for the maintenance of existing biofilm structure [26]. Conditional loss of Psl expression resulted in a halt of biofilm growth and an eventual erosion of the existing biofilm structure (136).

Using our conditional expression system we grew PA14P_{BAD}*pel* biofilms for two days in the presence of arabinose and either continued providing arabinose to the biofilm culture for an additional two days or we removed it from the growth medium (**Figure 6**). Interestingly, halting Pel expression by removing arabinose resulted in a biofilm that failed to increase in size, but retained the original shape and mass after two days as calculated by COMSTAT (**Figure 7**). The biofilm that was supplied arabinose continued to grow in size. These results suggest that continuous Pel production is important over the course of biofilm development. However, unlike Psl, continuous Pel production is not required to maintain existing biofilm structure.

5.2.5 Pel is critical for maintaining cell-to-cell interactions in PA14 biofilms.

We hypothesized that the absence of cell aggregates in the PA14Δ*pelB* mutant biofilms is due to a defect in the cell-to-cell interactions necessary to hold an aggregate together. To initially test this hypothesis, we used time-lapse microscopy to analyze the behavior of biofilm cells at an early point in biofilm development. Dividing cells on the glass surface were monitored and the fate of daughter cells were separated into two categories (210). Daughter cells that remained closely associated with the mother cell were termed “aggregate builders”. Cells that did not remain closely associated with the mother cells were designated “flyers”. We predicted if Pel were important in cell-to-cell interactions, cells incapable of Pel production would show a larger percentage of daughter cells exhibiting “flyer” behavior. Our analysis determined that Pel is a crucial determinant in daughter cell behavior in PA14 (**Figure 8**). As predicted, expression of

Pel is related to daughter cell association with the parental cell. A *pelB* mutant displayed increased "flyer" behavior (88.3%) in comparison to wild-type PA14 (40.2%) and a reduced proportion of "aggregate builders" were observed (11.7%) than in PA14 (59.8%). Overexpressing *pel* resulted in an increased proportion of aggregate builders (82%) and relatively few flyers (18%).

Conversely, in PAO1 Psl appears to be the primary polysaccharide involved in aggregate building. PAO1 and the PAO1Δ*pel* mutant display indistinguishable daughter cell behavior profiles, with 33.9% and 32.6% of "flyers", respectively. Conversely, PAO1Δ*pslBCD* exhibits a much larger proportion of "flyers" (85.3%) compared to PAO1 and PAO1Δ*pelB* (**Figure 8**). These data support our hypothesis that Pel contributes to aggregate formation in a PA14 biofilm by promoting retention of daughter cells within a growing aggregate, while Psl appears to be the critical polysaccharide for aggregate building in PAO1.

To complement the time-lapse microscopy study, we developed a novel assay involving infra-red laser (6). This assay involves maintaining an optical trap in a liquid suspension of bacteria. Once bacteria enter the trap, they remain there. Initial experiments determined that continuous trapping of PA14 cells in liquid culture promoted the formation of stable aggregates. Using this technique we are able to study the effects of the Pel polysaccharide for the ability to form and maintain bacterial clusters. Since Pel was required for maintaining cell-to-cell interactions in flow cell biofilms, we predicted that Pel would be required for maintaining stable aggregates in this assay.

Wild-type PA14 forms aggregates after 20 min of trapping in all visualized fields (**Figure 9A**). In contrast, PA14Δ*pelB* did not form aggregates, even though a significant amount of free-floating bacteria entered and remained in the trap (**Figure 9B**). Rather, the mutant strain requires a minimum of 45 min of trapping to form aggregates (**Figure 9C**). Even with the extended incubation in the trap, 16% of the fields of view are absent

of aggregates. Based on the differences in time for bacterial clustering to be observed, these data conclude Pel is an important component in the initiation of cellular clustering. Subsequently, we tested to see if Pel was important in maintaining clustering aggregates after an aggregate was formed. These experiments were set up similarly by allowing bacterial aggregation to occur for 20 min for wild-type PA14 and 45 min for the *pelB* mutant. After the designated incubation time with the laser, cluster stability was monitored by microscopy five minutes after the laser trap was disengaged. More than six aggregates in each strain were visually assessed for stability and separated into three categories as described in the figure legend (**Figure 9**). 85% of wild-type PA14 cell aggregates are stable five min after the release of the trap. In contrast, only 16% of the PA14Δ*pelB* aggregates remained after the laser trap is removed. These results further support that Pel is critical for both initiating and maintaining cell-to-cell interactions.

Pel provides biofilms protection from aminoglycoside antibiotics.

A primary function attributed to the extracellular matrix is protection (102). Several well-studied polysaccharides are known to confer resistance to a range of antibiotics. In *P. aeruginosa*, alginate and cyclic glucans have been demonstrated to protect biofilms from aminoglycosides by directly binding these cationic antibiotics (43, 87, 139). In addition, rugose small colony variants (RSCVs), which produce elevated levels of Pel and Psl, show increased tolerance to tobramycin, an aminoglycoside (111, 221). Thus, we hypothesized that Pel may provide protection from antimicrobials. Therefore we tested the sensitivity of our strains to several clinically relevant antibiotics: tobramycin, gentamicin, ciprofloxacin, kanamycin, meropenem, ceftazidime, tetracycline, and carbenicillin.

Planktonic cultures of PAO1, PAO1Δ*pelB,* PAO1Δ*psl,* PAO1P_{BAD}*pel* and WFPA801 (arabinose-inducible *psl* strain (136)) were initially tested for antibiotic susceptibility by determining the minimum inhibitory concentration (MIC) of each strain. No difference is detected between PAO1, PAO1Δ*pelB,* PAO1Δ*psl* and WFPA801 for any of

the antibiotics tested (**Figure 10**). However, overexpressing Pel in PAO1 slightly increases the MIC in comparison to wild-type PAO1 to gentamicin and tobramycin, two aminoglycoside antibiotics. No difference is seen in MICs between PA14, PA14Δ*pelB* and PA14P_{BAD}*pel* for any of the antibiotics tested (**Figure 10**).

We then assessed Pel's involvement in planktonic survival by treating log-phase cultures of our strains with both tobramycin and ciprofloxacin. Ciprofloxacin was chosen as a representative antibiotic that has the same MIC for all three strains PAO1, PAO1Δ*pelB* and PAO1P_{BAD}*pel.* Equal susceptibility is seen between the wild-type and Δ*pelB* mutants in both PAO1 and PA14 (**Figure 11**). Like the MIC experiments, overexpression of Pel in PAO1 affords a small degree of protection to killing by tobramycin and gentamycin, while Pel overexpression in PA14 does not (**Figure 11**). Similar killing curves are observed between PA14 and PAO1 strains during ciprofloxacin treatment (**Figure 11**).

We subsequently assessed Pel's role in antibiotic resistance in a biofilm model. For a valid comparison of antibiotic tolerance, the same number of cells must be challenged with the antibiotic of interest. In order to satisfy this criterion, we used a 48-h colony biofilm technique that has been demonstrated previously to capture a biofilm-specific model of antibiotic susceptibility (253). Bacterial strains were grown on polycarbonate filters for two days, allowing complete coverage of the filter and equal colony forming units (CFUs) for all strains. The filter was then transferred to solid medium containing antibiotic and incubated for 24 hours. After treatment, the viable CFUs were quantified. In PA14, a *pel* mutation rendered biofilms more susceptible to the aminoglycosides tobramycin and gentamicin, while not impacting the susceptibility to ciprofloxacin (**Figures 12** and **13**). However, a *pel* mutation in PAO1 did not influence susceptibility to any antimicrobial tested.

Overexpressing *pel* in both PAO1 and PA14 led to an elevated tolerance to tobramycin and gentamicin compared to the corresponding parental strain (**Figures 12** and **13**). To

test whether Psl overexpression might provide similar aminoglycoside protection to PAO1, we used an arabinose-inducible Psl expression strain, WFPA801. Psl overexpression strain was found not to confer protection from tobramycin (**Figure 12**).

To make a more direct comparison between planktonic and biofilm cultures, we compared 24-h-old stationary phase cells with 24-h-old biofilm cells for tobramycin sensitivity. The tobramycin sensitivity profiles of stationary phase liquid cultures are identical for PAO1 and PA14 wild-type and the corresponding *pelB* mutant strains (**Figure 14**). Interestingly, overexpression of Pel in PA14 provides protection in stationary phase cells that is not observed in log phase cells (compare **Figures 11** and **14**). Similar to log-phase treated cells, PAO1P_{BAD}*pel* provides protection to stationary phase cells. 24-h-biofilms reveal the same susceptibility profiles as the 48-h-treated biofilms shown in Figure 6, with enhanced sensitivity of PA14Δ*pelB* compared to wild-type (**Figure 14**).

To complement our analysis of colony biofilms, we determined the spatial distribution of tobramycin killing in flow cell biofilms. As expected, PA14 and its derivatives display a similar tobramycin resistance pattern as the filter biofilm. The *pelB* mutant strain produced a monolayer that is easily killed, while the PA14P_{BAD}*pel* strain biofilm is the least susceptible, probably in part due to the production of greater amounts of biofilm biomass than PA14 (**Figure 15**).

Expression of the *pel* operon is induced during biofilm growth.

Our antimicrobial tolerance data suggest that in PA14, Pel plays a more important role in biofilm communities as compared to planktonic cultures. One explanation for this observation is that *pel* expression may be enhanced during biofilm growth as compared to planktonic growth. To test this, we analyzed the expression of the *pel* operon in planktonic and biofilm cells using quantitative RT-PCR. To generate enough biofilm biomass for RT-PCR we grew the strains on the surface of silicon tubing under constant flow. We observed that *pelA* transcript in PA14 is 7.2-fold higher (+/- 2.0) when grown

as a biofilm for 48 h than in planktonic conditions (for either logarithmic or stationary phase cells), while in PAO1 it is 5.11-fold higher (+/- 3.49). The control transcripts *pslA*, *lasR* and *sadC* did not exhibit biofilm-specific induction (**Figure 16A**). The *pslA* transcript was chosen as a control because the Psl polysaccharide is an important structural component in biofilm development in PAO1. The *lasR* transcript was chosen because LasR responds to an increase in biomass and the *sadC* transcript was chosen because the product SadC is a diguanylate cyclase important in regulating biofilm advancement (153, 183). Therefore, an increase in *pelA* transcript is specific to the *pel* operon and not all genes involved in biofilm formation. Even by 24 h of biofilm growth, PAO1 shows nearly a 15-fold increase in *pelA* transcript (**Figure 17**). To corroborate our transcriptional analysis, we also demonstrate PelF protein levels are elevated during biofilm growth but went undetected in stationary phase liquid cultures (**Figure 16B**). These data suggest a biofilm-associated role for Pel.

DISCUSSION

In this study, we have identified two key biofilm-associated functions of the Pel polysaccharide. Pel is critical for initiating and maintaining cell-cell interactions. These functions have been implicated in polysaccharides in other species, such as the MDX polysaccharide of *Shewanella oneidensis* and colanic acid of *E. coli* K-12 (46, 233). This appears to be a crucial mechanism by which parent cells retain their daughter cells in the biofilm community. In the absence of Pel, biofilm formation does not progress beyond the monolayer stage in PA14.

In addition, Pel appears to provide a measure of protection from aminoglycoside antibiotics. The antibiotic susceptibility experiments suggest that Pel is capable of providing protection to planktonic cells when artificially overexpressed, although there is no phenotype for the *pel* mutant strain in liquid culture for any of the tested conditions. However, in biofilms of PA14, both *pel* overexpression and a *pel* mutation impacted aminoglycoside sensitivities. This suggests that Pel may play an important protective role in biofilms of this strain.

The mechanism responsible for protection is not clear, but if Pel behaves similarly to other polysaccharides leading to elevated aminoglycoside resistance like alginate and *ndvB*-encoded glucans, it may bind or sequester the antibiotic. Both alginate and *ndvB*-encoded glucans have a high negative charge that is consistent with their ability to bind positively charged aminoglycosides. If this model proves to be true, Pel may be an acidic polysaccharide capable of interacting with cationic antibiotics. This hypothesis helps explain why no differences were seen in killing of planktonic or biofilm cells by ciprofloxacin, an anionic antibiotic, and why no protection was afforded by overexpressing the neutral polysaccharide, Psl (**Figure 12**). Another possibility is that Pel production can influence biofilm structure, which in turn may influence antimicrobial susceptibility. However, we feel this is unlikely since the structure of colony biofilms tends to be uniform.

Using PAO1 and PA14 as representative *P. aeruginosa* laboratory strains, we see that the role Pel plays in biofilm formation can vary drastically. In PAO1, it appears that Psl is the predominate polysaccharide of the biofilm EPS matrix, while in PA14 Pel is required. However, it appears in other strains, MJK8, PAO1Δ*wspF* and ZK2870, both polysaccharides contribute to biofilm and/or autoaggregation phenotypes (64, 90, 111). Whether each polysaccharide has a distinct role in biofilm formation and/or protection, or if their functions are redundant remain to be determined. Although purely in terms of surface attachment, it appears that Psl is more important, while Pel is less so.

The enhanced expression of Pel in biofilms is noteworthy. *pelA* transcript levels were minimally expressed under the planktonic culturing conditions we used. Yet despite low *pelA* transcript in planktonic conditions, only in biofilms do we detect PelF protein expression (**Figure 16**). Therefore, the protection afforded to *P. aeruginosa* by Pel from aminoglycosides appears to be a biofilm-associated mechanism of antimicrobial tolerance. To date, only the cyclic glucans encoded by the *ndvB* locus has been shown to be a biofilm-specific mechanism of antimicrobial tolerance in this species (139).

Characterizing the structure of Pel and the specific mechanism behind aminoglycoside protection is underway.

Finally, the ability to prohibit PA14 biofilms from growing larger by arresting Pel expression is exciting. The biofilm does not dissipate indicating that continuous Pel is not necessary for biofilm maintenance. This result is contrary to PAO1 biofilms that require Psl to be continuously produced for biofilm maintenance (136). Thus, manipulating Pel and Psl expression may be a central strategy for disrupting biofilms and targeting them for antibiotic therapy.

MATERIALS AND METHODS

Bacterial strains, strain construction, and growth media. Strains used in this study are listed in **Table 1** (49, 92, 94, 107, 114, 188). Unless otherwise noted, strains were grown at 37°C in LB medium. For plasmid selection, 300 μg/ml carbenicillin or 100 μg/ml gentamicin was used with *P. aeruginosa*, and 100 μg/ml ampicillin or 10 μg/ml gentamicin was used with *Escherichia coli*.

PAO1Δ*pelB* and PA14Δ*pelB* allelic replacement strains were constructed by using an unmarked, nonpolar deletion strategy described previously (92). Flanking regions of *pelB* were amplified using primers *pelB* UP and *pelB* DN. The resultant PCR product was ligated into the suicide vector, pEX18gm, via HindIII restriction site. The plasmid pEX18gmΔ*pelB* was verified by sequencing analysis and mated into PAO1 and PA14. Single recombination mutants were selected on VBMM containing 100 μg/ml gentamicin. Double recombination mutants were selected on LB plates containing 5% sucrose and confirmed by PCR.

Construction of PAO1P_{BAD}*pel* and PA14P_{BAD}*pel* was constructed similarly to the previously described protocol (92). In order to create a *pel*-inducible strain, we removed the promoter (positions -54 to -267 upstream of *pelA* for PAO1 and positions -72 to -249 for PA14) and replaced with an arabinose-inducible promoter, araC-P_{BAD} amplified from pJN105 (170). Sewing PCR was used to construct a three-portion product including flanking regions of the native *pel* promoter and the araC-P_{BAD}

promoter. The resultant PCR product was ligated into pEX18gm. Both completed pEX18gm-P_{BAD}*pel* were verified by sequencing analysis and double recombinant mutants were generated as described above.

To complement a *pel* mutation, the entire *pel* operon was amplified using pel operon SpeI F and R primers. The resultant PCR product was ligated in the expression vector, pMJT-1, via SpeI restriction site (107). The plasmid pMJT-1 P*pel* was verified by sequence analysis and transformed into PA14 and PA14Δ*pelB*.

PelF expression vector was constructed by amplifying full-length PelF with primers that omit the PelF stop codon and subsequently ligated into pET20b(+) using NdeI and XhoI restriction sites. This design removed the pelB leader sequence and constructed a PelF C-terminal 6x-HIS fusion. The construct was transformed into BL21 cells for purification.

RNA purification and analysis. RNA was extracted using an RNeasy kit (QIAGEN) according to manufactures instructions. Contaminating DNA was removed with an on-column RNase-free DNase I treatment (QIAGEN) and remaining DNA was removed by an off-column DNase I treatment (Promega) as recommended. The RNA prep was confirmed to be free of DNA by PCR. cDNA was generated by SuperScript III First-Strand Synthesis System for RT-PCR using random hexamers (Invitrogen). cDNA synthesis was verified by PCR and quantitated by RT-PCR using the SYBR Green PCR Master Mix (Applied Biosystems) as the fluorescent dye. Fluorescence was measured using ABI Prism 7000 Sequence Detection and *pelA* transcript levels were normalized to *ampR*.

Microtiter dish biofilm. 96-well microtiter dish experiments were performed as described previously (155). For rapid attachment assays, 100 μl of log-phase cells were incubated at 37°C for one hour. Non-adherent cells were removed by thoroughly washing the microtiter dish with diH_20. Adherent biomass was stained with 150 μl of 0.1% crystal violet for 10 m. Excess crystal violet was removed by submerging the microtiter dish multiple times in diH_20. Adherent crystal violet was solubilized with

200 μl of 95% ethanol for 10 m and subsequently measured at OD_{595}. For analysis of biofilm development, log-phase cells were incubated at room temperature for 20 h.

Pellicle formation assay. Standing cultures containing 3-ml LB broth were grown at room temperature in a glass tube. Pellicles were monitored by visual inspection between four and ten d. Complete coverage at the air-liquid interface of an opaque layer of cells is considered to be indicative of pellicle formation (64).

Congo red assays. LB liquid cultures supplemented with 40 μg/ml Congo red (Sigma-Aldrich) and incubated shaking overnight 37°C. The supernatants were measured at OD_{495} to assess Congo red binding. Congo red plates contained LB without NaCl, 1% agar, 40 μg/ml Congo red and 15 μg/ml brilliant blue R (Sigma-Aldrich). Cells were diluted 1/100, 10 μl spotted and incubated at room temperature for five d.

Flow cell and tube biofilm reactor. The flow cell system and tube biofilm system was assembled as described previously (111, 204, 208). *P. aeruginosa* PA14 monocultures were tagged with GFP on the chromosome using the mini Tn7 system to allow fluorescent visualization of growing biofilms (114). PAO1 monoclutures were tagged with GFP expression vector pMRP9-1 (49). Log phase cultures grown in full-strength TSB were diluted to a final OD_{600} of 0.05 for PA14 and 0.01 for PAO1 in 1% TSB. Bacteria were inoculated into an inverted flow cell and allowed to attach for one hour. Upon initiation of media flow, fresh media of 1% TSB supplemented with 0.2% arabinose was pumped at a constant rate. Biofilms were grown at room temperature up to 9 d. Attachment images were taken one hour after flow was initiated. Cells were visualized by fluorescence by scanning confocal laser microscopy and image series were compiled using Velocity (Improvision) and analyzed using COMSTAT 1 software (88).

Tube Biofilm. Tube biofilms were conducted as previously described (111, 204). *P. aeruginosa* was grown to log phase in LB at 37°C shaking, diluted to an OD_{600} 0.05 and injected into a 6.35mm inner-diameter tube and incubated for 30 minutes. Control cells

were incubated with static conditions in a 1.5ml tube. Biofilms were grown at room temperature in LB medium containing 100mM MOPS pH 7.0 at 50ml/h flow rate for 48 hours. The tube biofilms total RNA was isolated by opening the tube and scraping the adhered biomass using a cell scraper (Costar).

Live/dead staining. Biofilms were grown in flow cells in 1% TSB as described above for 4 d and subsequently treated with 1 μg/ml of tobramycin for 24 h. The MIC for tobramycin when the cells are grown in 1% TSB is 0.03 μg/ml for PAO1 and 0.06 μg/ml for PA14. This is in contrast to the MIC of 1 μg/ml seen for PA14 and PAO1 grown in full strength LB. After treatment, flow was stopped and biofilms were stained with 500 μl of propidium iodide and SYTO 9 (Invitrogen) for 10 m according to manufactures instructions. Flow resumed and images were captured after 15 m of washing.

Biofilm daughter-cell analysis. The movement and behavior of individual daughter cells of *P. aeruginosa* monocultures were monitored in young (< 2 days old) flow cell biofilms. The flow cell setup was the same as described. Fluorescent images were taken every 45 seconds for 2 hours using the time-lapse feature of the Zeiss Axiophot microscope (Carl Zeiss). The fate of new daughter cells were visually tracked and each cell was classified as an "aggregate builder" or "flyer" (210). From one cell division to the next, "aggregate builders" remained within a 15 μm diameter circle centered at the point of cell division, while "flyers" moved further away on the surface or were dissociated from the surface by media flow. A minimum of 75 cell divisions of each strain were tracked and classified.

Laser trap experiments. An open-top chamber for microscopy was constructed by layering five Secure-Seal Imaging Spacers 13mm in diameter (Grace Bio-Labs) onto a microscope cover slip and this chamber placed on an inverted Olympus microscope above a 40x or 60x long-working-distance objective. Bacteria were grown shaking at 37°C to OD_{600} 1. Samples were incubated statically at room temperature for 1-7 hours. Static incubation of the cells prior to the experiment allowed for a slight increase (~2-

fold, data not shown) in *pel* expression, presumably for the same reasons *pel* expression is required for pellicle formation in static liquid cultures [17]. A 100 μL bacterial suspension was placed into the chamber. Laser trapping was done by focusing a 1064 nm laser through the microscope objective at the top of the sample at a transmitted power of ~50mW. For PA14 wild-type bacteria, the first trap-induced clustering was seen in samples that had been in the open-top chamber for 20 min; for Δ*pelB* bacteria the first trap-induced clustering, if any, was seen in samples that had been in the open-top chamber for 45 min. Cluster stability was evaluated by monitoring formed bacterial aggregates for cluster dispersal five min after the laser beam was blocked.

PelF purification, antisera production and immunoblot analysis. BL21 pET20b(+) PelF was grown to an OD_{600} 0.5 in LB supplemented with 100 μg/ml ampicillin at 37°C. The culture was induced with 0.5 mM IPTG overnight at 18°C. Cells were centrifuged and resuspended in 50mM Tris, pH 7.5, 500 mM NaCl and 10% glycerol. Cells were lysed by French press and protein was purified by nickel affinity chromatography and size exclusion chromatography using an FPLC. Fractions with purified PelF were combined and concentrated to 1 mg/ml. Antisera was generated in rabbits using a 70-day standard protocol (Open Biosystems). Antisera was absorbed using PAO1Δ*pelF* lysates based on standard protocols. Immunoblots were performed with whole-cell lysates as described with equal amounts of total protein in each lane (58). Protein concentration was measured using the Pierce 660 nm protein assay (Thermo Scientific). 10 μg of total protein was loaded onto a 7.5% pre-cast SDS-PAGE gel (Bio-rad). Proteins were transferred to a PVDF membrane. Membranes were blocked using 5% non-fat milk in Tris buffered saline containing 0.1% Tween (TBST) and probed with absorbed rabbit polyclonal α-PelF antibody (1:2,500). Blots were washed three times with TBST, probed with α-rabbit horseradish peroxidase-conjugated antibodies (1:25,000, Thermo Scientific) and washed three times with TBST. Membranes were incubated with the Pierce SuperSignal West Pico ECL reagent (Thermo Scientific) and detected using X-ray film (Kodak).

Antibiotic sensitivity assays. MIC growth curves were completed in a 96-well microtiter dish grown in LB broth at 37°C. Log phase bacteria were diluted to 10^5 CFU in each well. A range of concentrations was assessed for each antibiotic. Bacterial growth was measured after 24 hours of incubation using a microplate reader (OD_{590}).

For planktonic killing curves, cells were either grown to log phase in LB or grown for 24 h to assess stationary phase susceptibility. Log phase cultures were split and one culture was treated with tobramycin (Sigma), gentamicin (Sigma) or ciprofloxacin (Bayer Healthcare), while the control culture was untreated. Stationary phase cells were resuspending in fresh media containing antibiotics. The cultures were incubated shaking at 37°C. Bacterial survival was assessed over time by viable plate counts.

For biofilm killing, overnight liquid cultures were diluted 1/100 and five μl were spotted onto a UV-sterilized 25mm polycarbonate filter (GE Osmonics). Biofilms were grown for two d unless otherwise stated at 37°C and moved to fresh solid media each day. Biofilms were exposed to with 5 μg/ml tobramycin or 1 μg/ml ciprofloxacin for 24 h. Bacterial viability was obtained by resuspending the filter in 1 ml of PBS and serially diluting to obtain viability counts.

Table 1 Strains used in Chapter I

Strains	Relevant Characteristics	Reference
PAO1	wild-type	Holloway, 1955
PAO1Δ*pelB*	*pelB* nonpolar mutant of PAO1	This study
PAO1P_{BAD}*pel*	chromosomal replacement of the native promoter with *araC*-P_{BAD} promoter	This study
PAO1 pMRP9-1	harbors a *gfp* expressing plasmid	This study
PAO1ΔpelB pMRP9-1	harbors a *gfp* expressing plasmid	This study
PAO1P_{BAD}*pel* pMRP9-1	harbors a *gfp* expressing plasmid	This study
PA14	wild-type	Rehme et al., 1995
PA14Δ*pelB*	*pelB* nonpolar mutant of PAO1	This study
PA14P_{BAD}*pel*	chromosomal replacement of the native promoter with *araC*-P_{BAD} promoter	This study
PA14 miniTn7 *gfp*	Tn7 chromosomal insertion of *gfp*	This study
PA14ΔpelB miniTn7 *gfp*	Tn7 chromosomal insertion of *gfp*	This study
PA14 P_{BAD}*pel* miniTn7 *gfp*	Tn7 chromosomal insertion of *gfp*	This study
BL21	*E. coli* expression strain	Novagen
BL21 pET20b(+) PelF	C-term His-tag PelF expression strain	This study

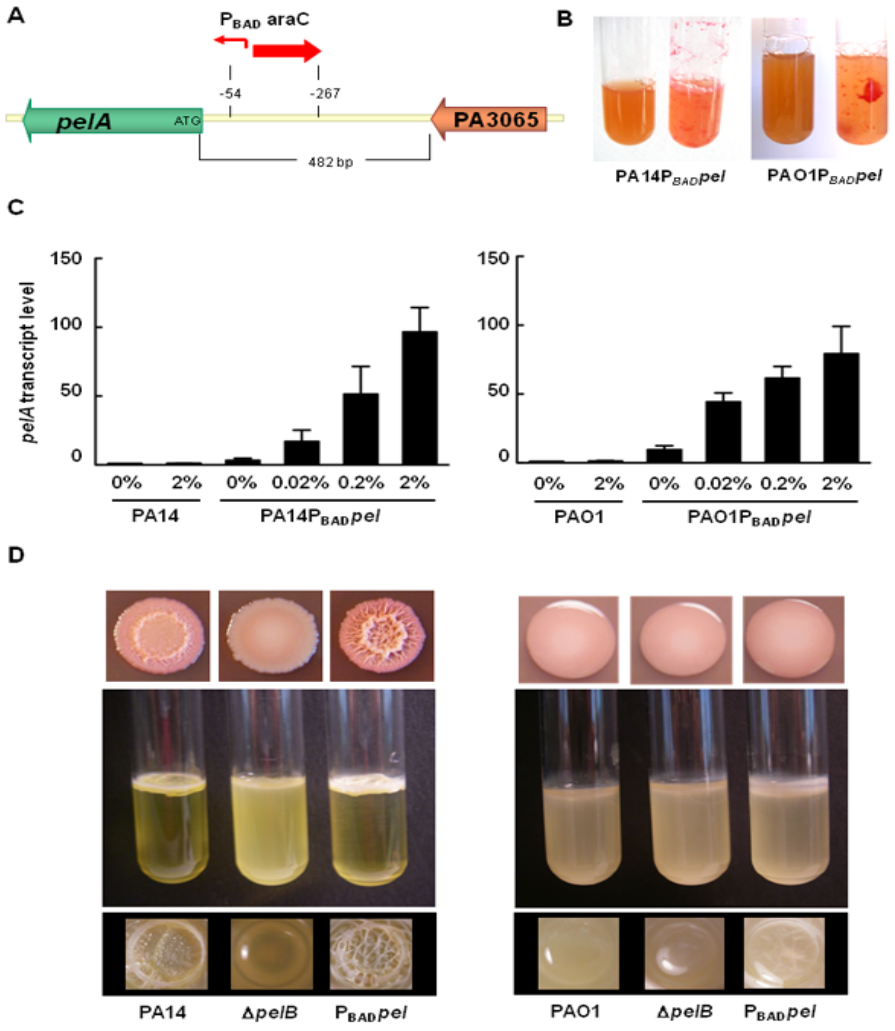

Figure 1. Generation of a *pel*-conditional strain. (A) Schematic drawing showing the replacement of the promoter region with an arabinose promoter on the chromosome to produce PAO1P$_{BAD}$*pel*. (B) Overnight growth in the presence of 1% arabinose to PA14P$_{BAD}$*pel* and PAO1P$_{BAD}$*pel* leads to visual aggregates in liquid culture (right tubes) but not seen in the un-induced culture for either PA14P$_{BAD}$*pel* and PAO1P$_{BAD}$*pel* (left tubes). Congo red was added to visually enhance the phenotype. (C) Quantitative RT-PCR analysis of *pelA* transcription in PA14 and PA14P$_{BAD}$*pel* (left) and PAO1 and PAO1P$_{BAD}$*pel* (right) in the presence of different concentrations of arabinose. *pelA* transcription is normalized to *ampR* transcription. Results shown are the mean of three independent experiments. Error bars represent the standard deviations. (D) Colony morphology (top) and pellicle formation (middle, side-view; bottom, top-down) of PA14, PA14Δ*pelB* and PA14P$_{BAD}$*pel* (left) and PAO1, PAO1Δ*pelB* and PAO1P$_{BAD}$*pel* (right) grown in LB without NaCl containing 0.5% arabinose. Photographs were taken after 5 d of growth at room temperature.

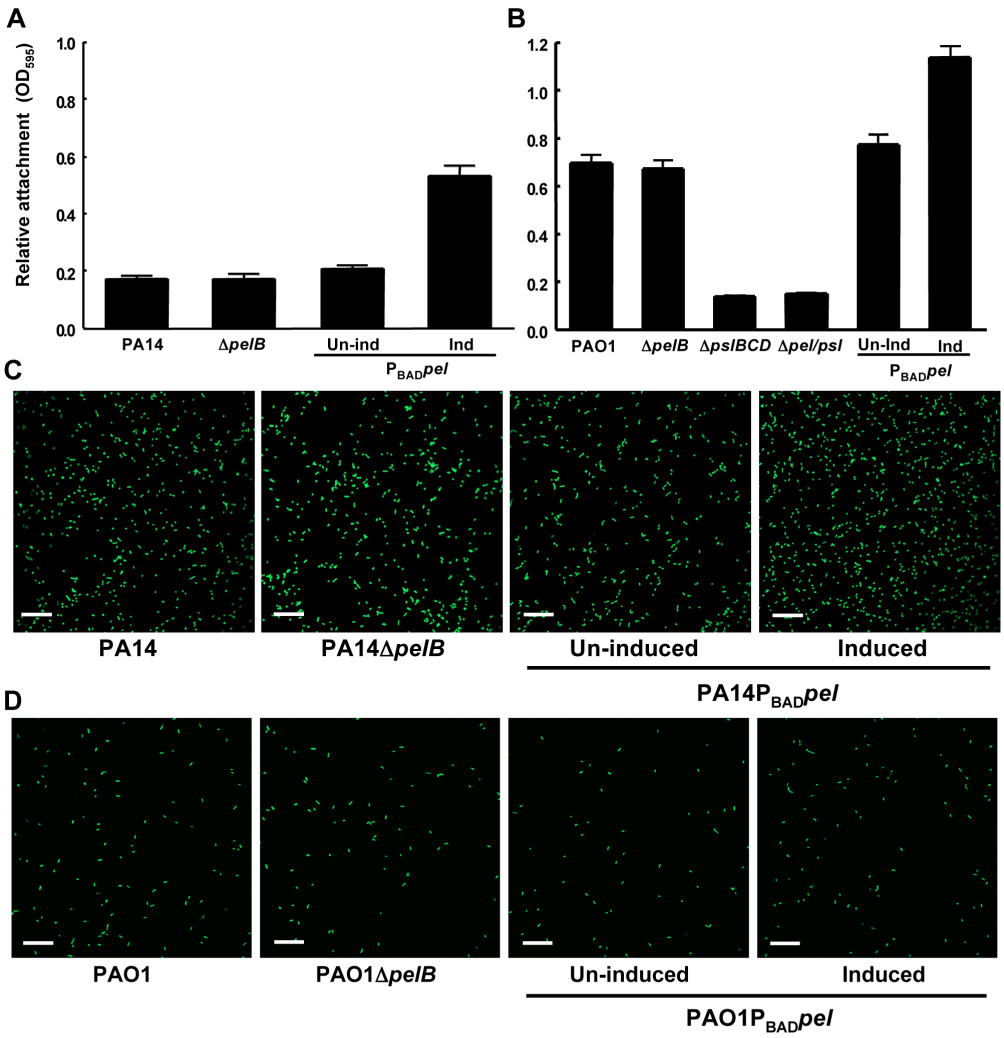

Figure 2. Pel is not required for attachment. Attachment of *P. aeruginosa* PA14 (A) and PAO1 (B) to microtiter dish wells was measured by crystal violet binding at an OD_{595}. Overexpressing *pel* by addition of arabinose increased crystal violet binding in both PA14 and PAO1, but a *pelB* mutant showed no defect. Attachment to glass slides was visualized in a flow cell after one hour of attachment and one hour of continuous flow. Medium was supplemented with 0.2% arabinose under inducing conditions. Representative SCLM images of PA14, PA14Δ*pelB* and PA14P$_{BAD}$*pel* are shown using a 40x objective (C). Representative SCLM images of PAO1, PAO1Δ*pelB* and PAO1P$_{BAD}$*pel* are shown using a 40x objective (D). Scale bars represent 25 μm. Error bars represent standard deviations.

A Substratum coverage

	Wild-type	Δ*pelB*	P_{BAD}*pel*	P_{BAD}*pel* + ara
PA14	1.085(+/- 0.43)	1.204 (+/- 0.34)	1.093 (+/- 0.46)	1.151 (+/- 0.15)
PAO1	0.478 (+/- 0.05)	0.396 (+/- 0.10)	0.322 (+/- 0.09)	0.386 (+/- 0.15)

B 4 day biofilm analysis

	Strain	Wild-type	Δ*pelB*	P_{BAD}*pel*
Average thickness (μm)	PA14	28.52 (+/- 12.8)	5.498 (+/- 2.91)	52.61 (+/- 12.1)
	PAO1	54.19 (+/- 8.34)	50.23 (+/- 9.76)	58.39 (+/- 14.3)
Roughness coefficient	PA14	0.606 (+/- 0.55)	0.786 (+/- 0.63)	0.173 (+/- 0.05)
	PAO1	0.518 (+/- 0.09)	0.516 (+/- 0.23)	0.517 (+/-0.07)
Surface to volume ratio ($\mu m^2\ \mu m^{-3}$)	PA14	0.439 (+/- 0.12)	1.749 (+/- 0.55)	0.366 (+/- 0.06)
	PAO1	0.265 (+/- 0.05)	0.262 (+/- 0.06)	0.361 (+/- 0.08)
Maximum thickness (μm)	PA14	58.30 (+/- 10.9)	37.50 (+/- 2.29)	91.65 (+/- 16.5)
	PAO1	105.2 (+/- 13.8)	106.5 (+/- 19.6)	112 (+/- 10.8)

Figure 3. Attachment and biofilm structure quantified by COMSTAT 1. (A) Using the substratum coverage variable in COMSTAT 1, the relative number of cells attached to the glass slide of a flow cell after one hour of attachment followed by one hour of continuous flow was measured. Four images per flow cell done in duplicate in three independent experiments were evaluated. (B) COMSTAT 1 assessed four variables of biofilm structure for PA14, PA14Δ*pelB*, PA14P_{BAD}*pel*, PAO1, PAO1Δ*pelB* and PAO1P_{BAD}*pel* for the SCLM image stacks of day four biofilms. Three images per flow cell done in duplicate in three independent experiments were evaluated.

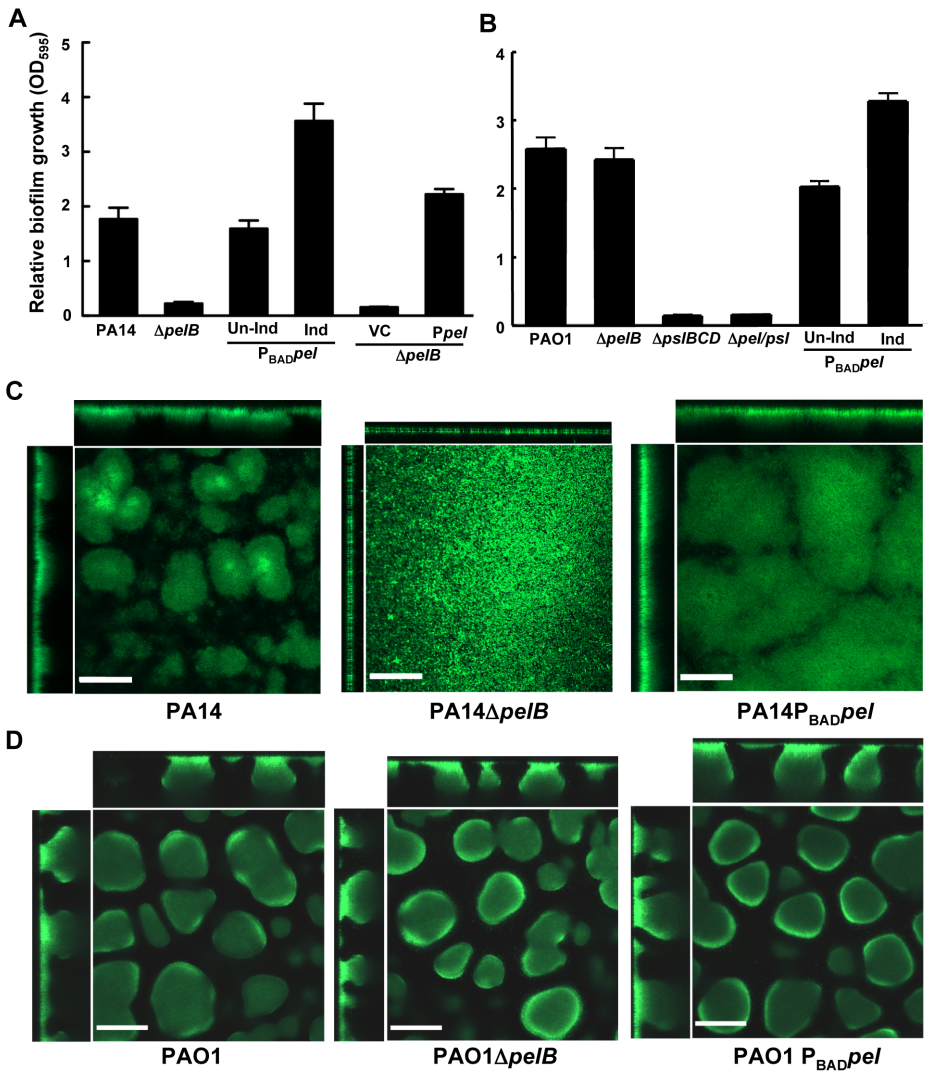

Figure 4. PA14Δ*pelB* is arrested in the monolayer stage of biofilm development. Strains PA14 (A) and PAO1 (B) were compared at 24 h for levels of biomass in microtiter dishes grown at room temperature by measuring crystal violet binding OD_{595}. Expression of the *pel* operon from an arabinose-inducible plasmid pMJT1 (P*pel*) but not in the vector control (VC) alleviated the crystal violet staining defect of PA14Δ*pelB*. Biofilm structure was visualized in a flow cell and representative top-down and side-view images are shown for PA14, PA14Δ*pelB* and PA14P_{BAD}*pel* (C) and PAO1, PAO1Δ*pelB* and PAO1P_{BAD}*pel* (D). Images were obtained using a 20x objective after four d of growth in continuous flow chambers. Scale bars represent 100 μm. Error bars represent standard deviations.

A

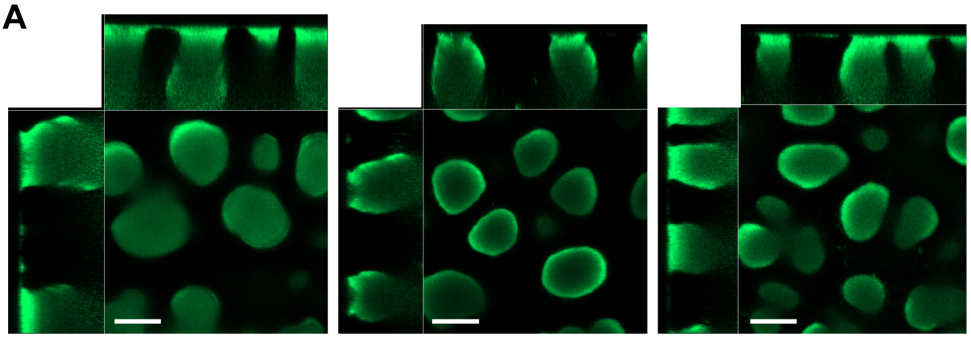

PAO1 PAO1Δ*pelB* PAO1P$_{BAD}$*pel*

B 9 day biofilm analysis

	PAO1	PAO1Δ*pelB*	PAO1P$_{BAD}$*pel*
Average thickness (μm)	63.92 (+/- 17.2)	80.45 (+/- 19.7)	71.09 (+/- 26.2)
Roughness coefficient	0.933 (+/- 0.10)	0.822 (+/- 0.07)	0.711 (+/- 0.09)
Surface to volume ratio (μm^2 μm^{-3})	0.557 (+/- 0.15)	0.734 (+/- 0.16)	0.711 (+/- 0.09)
Maximum thickness (μm)	151.6 (+/- 19.6)	156 (+/- 23.0)	142 (+/- 26.5)

Figure 5. Biofilm structure in 9 day PAO1 biofilms. (A) Biofilm structure was visualized by SCLM in a flow cell after 9 days of growth. Representative top down and side-view images are shown for PAO1, PAO1Δ*pelB* and PAO1P$_{BAD}$*pel.* Images were obtained using a 20x objective. Scale bars represent 100 μm. (B) Images were quantified for average thickness, roughness coefficient, surface to volume ratio and maximum thickness by COMSTAT 1. Four image stacks per flow cell done in duplicate in two independent experiments were evaluated.

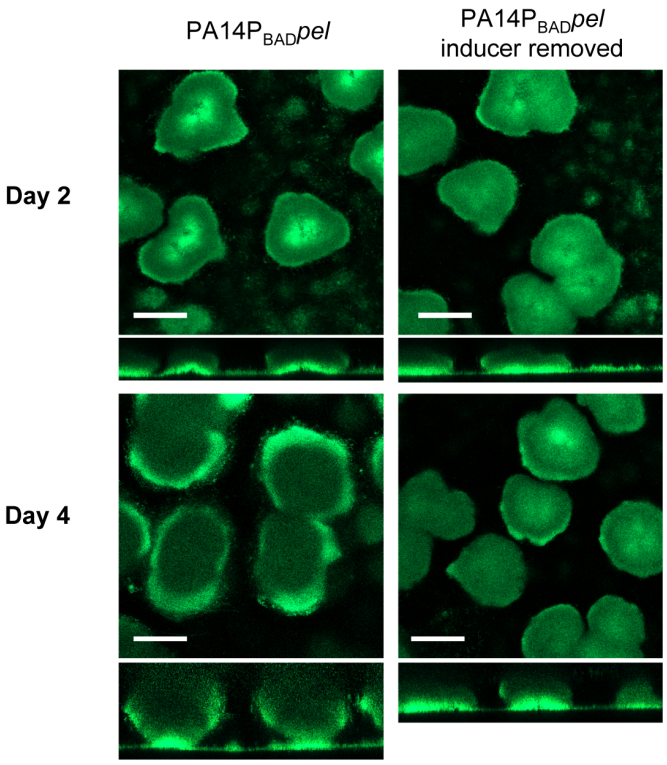

Figure 6. Continuous Pel production is required for biofilm growth, not maintenance of existing biofilm structure. PA14P$_{BAD}$*pel* was grown in 2% TSB for two days under inducing conditions (0.2% arabiniose). Biofilm growth was continued either in the presence (left) or absence (right) of the inducer arabinose. Representative top-down and side-view SCLM images from day two and day four are shown. Scale bars represent 100 μm.

	Day	PA14P$_{BAD}$*pel*	PA14P$_{BAD}$*pel* inducer removed
Average thickness (μm)	2	26.46 (+/- 2.47)	25.81 (+/- 5.52)
	4	73.36 (+/- 14.1)	33.30 (+/- 5.31)
Roughness coefficient	2	0.338 (+/- 0.06)	0.454 (+/- 0.12)
	4	0.562 (+/- 0.03)	0.505 (+/- 0.22)
Surface to volume ratio (μm^2 μm^{-3})	2	0.405 (+/- 0.08)	0.573 (+/- 0.08)
	4	1.051 (+/- 0.20)	0.574 (+/- 0.07)
Maximum thickness (μm)	2	61.00 (+/- 1.73)	61.87 (+/- 2.56)
	4	136.9 (+/- 17.0)	82.50 (+/- 6.12)

Figure 7. COMSTAT 1 analysis of arabinose removal in PA14P$_{BAD}$*pel* flow cell biofilms. PA14P$_{BAD}$*pel* biofilms were grown for two days under inducing conditions (0.2% arabinose). Biofilms were either continued to be grown in the presence or absence of the inducer, arabinose. COMSTAT 1 evaluated SCLM images for average thickness, roughness coefficient, surface to volume ratio and maximum thickness. Four image stacks per flow cell done in duplicate in two independent experiments were evaluated.

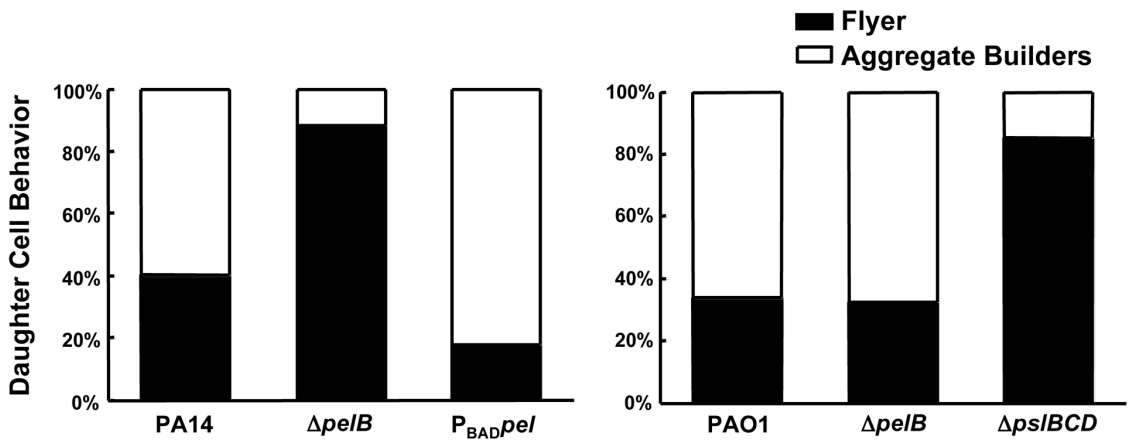

Figure 8. Pel impacts daughter cell behavior in early PA14 biofilms. Bacterial cell divisions were monitored by time-lapse microscopy in an early-stage biofilm grown in a flow cell. Daughter cells that remained within a 15 μm diameter of the mother cell are referred to as "aggregate builders", other cells were termed "flyers". A minimum of 75 cell divisions was assessed for each strain.

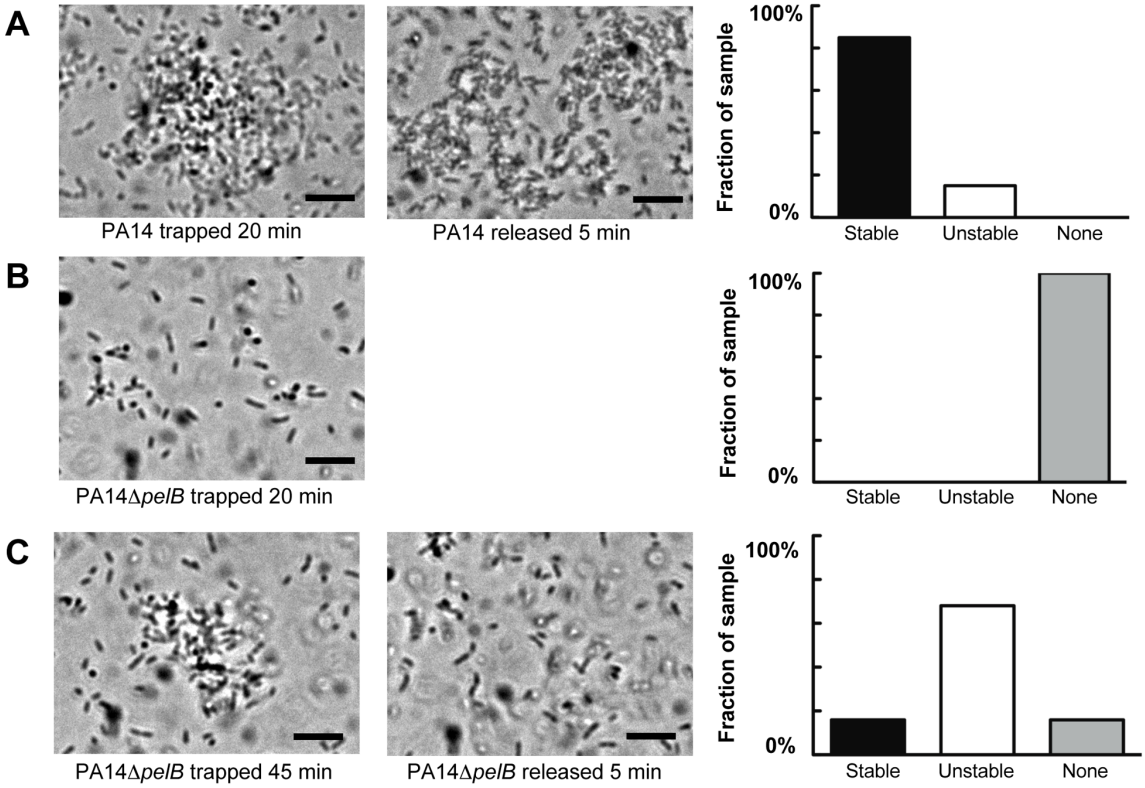

Figure 9. Pel is important for cell-to-cell interactions necessary for aggregate formation. Laser tweezers were used to trap bacteria and investigate bacterial clumping phenotypes. The captured bacteria were examined visually by light microscopy for aggregation after 20 min (A) PA14 (B) PA14Δ*pelB.* An extended trapping time of 45 min was required to initiate aggregation in PA14Δ*pelB* (C). The stability of formed aggregates was visually assessed five min after the release of the laser trap (center panel A and C). Aggregate stability was classified into three categories, "stable" if the aggregate remained intact, "unstable" if the aggregate dispersed into single cells and "none" if an aggregate did not form during the allotted time (right panels). A minimum of six replicates for each strain was assessed. Scale bars represent 10 μm. Representative phase-contrast images are shown. Experiment and analysis performed by Vernita Gordon.

	Carb	Cipro	Tob	Gent	Kan	Tet	Mero	Ceft
PAO1	64	1	1	0.25	64	8	1	1
PAO1Δ*pelB*	64	1	1	0.25	64	8	1	1
PAO1Δ*psl*	64	1	1	0.25	64	8	1	1
PAO1 P_{BAD}*pel*	64	1	4	1	128	8	1	1
WFPA801	64	1	1	0.25	64	8	1	1
PA14	128	0.06	1	2	128	8	0.5	2
PA14Δ*pelB*	128	0.06	1	2	128	8	0.5	2
PA14 P_{BAD}*pel*	128	0.06	1	2	128	8	0.5	2

Figure 10. Pel's effect on the minimum inhibitory concentration (MICs) to a wide range of antimicrobials. Strains were assessed for their MIC by broth dilution to carbenicillin (carb), ciprofloxacin (cip), tobramycin (tob), gentamicin (gent), tetracycline (tet), meropenem (mero), kanamycin (kan) and ceftazidime (ceft). Concentrations shown are μg/ml. Concentrations were empirically tested. Bacterial strains were grown in the presence of 0.5% arabinose.

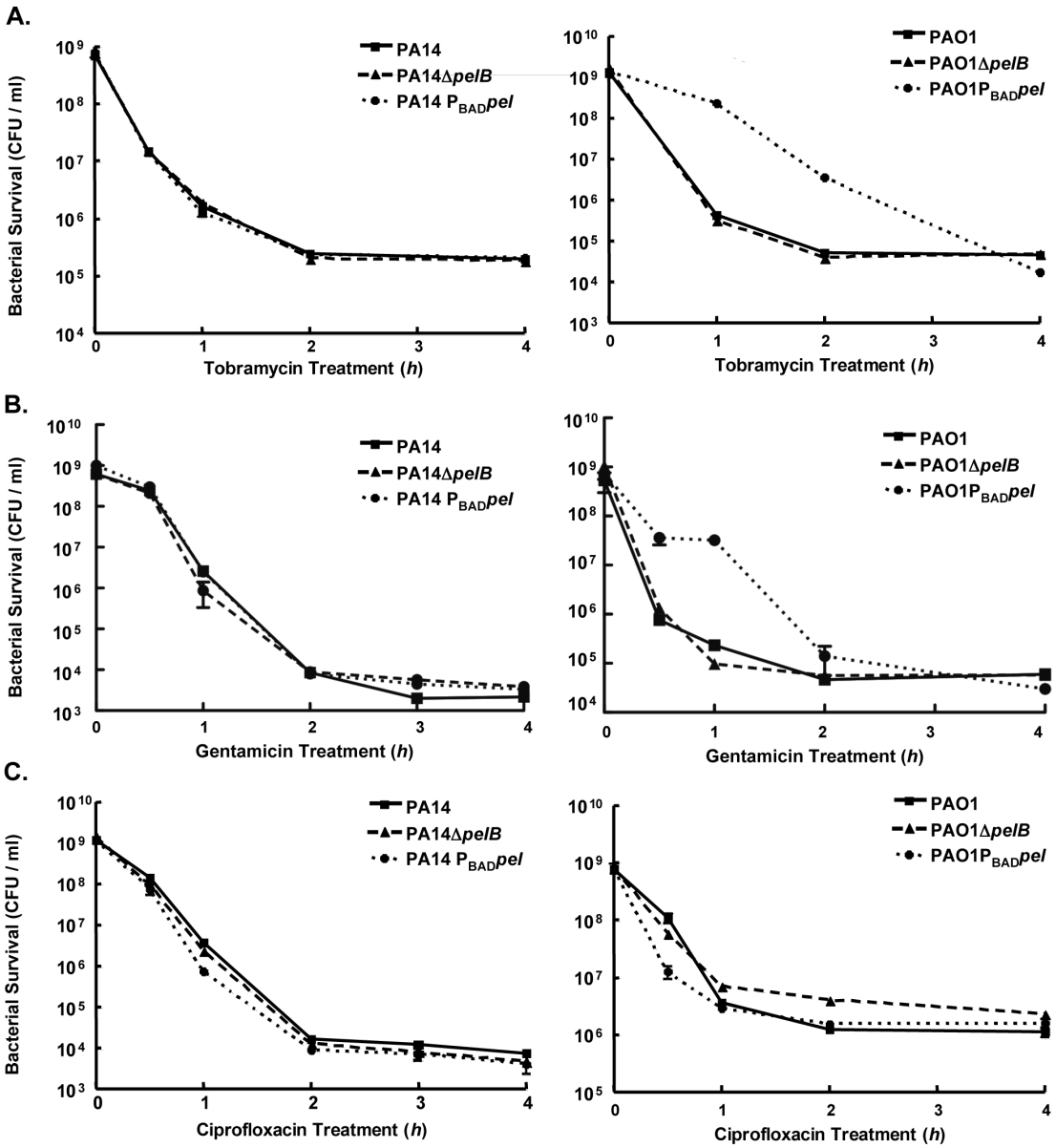

Figure 11. Analysis of Pel-mediated antibiotic tolerance in planktonic culture. Log-phase planktonic cultures were treated with either tobramycin (A), gentamicin (B) or ciprofloxacin (C). Bacterial survival was monitored over time by assessing the number of CFUs. On the left, PA14 (solid line), PA14Δ*pelB* (dashed line) and PA14P_{BAD}*pel* (dotted line) were treated with 5 μg/ml tobramycin, 2 μg/ml and gentamicin 0.1 μg/ml ciprofloxacin. On the right, PAO1 (solid line), PAO1Δ*pelB* (dashed line) and PAO1P_{BAD}*pel* (dotted line) were treated with 5 μg/ml tobramycin, 5 μg/ml gentamicin and 1 μg/ml ciprofloxacin.

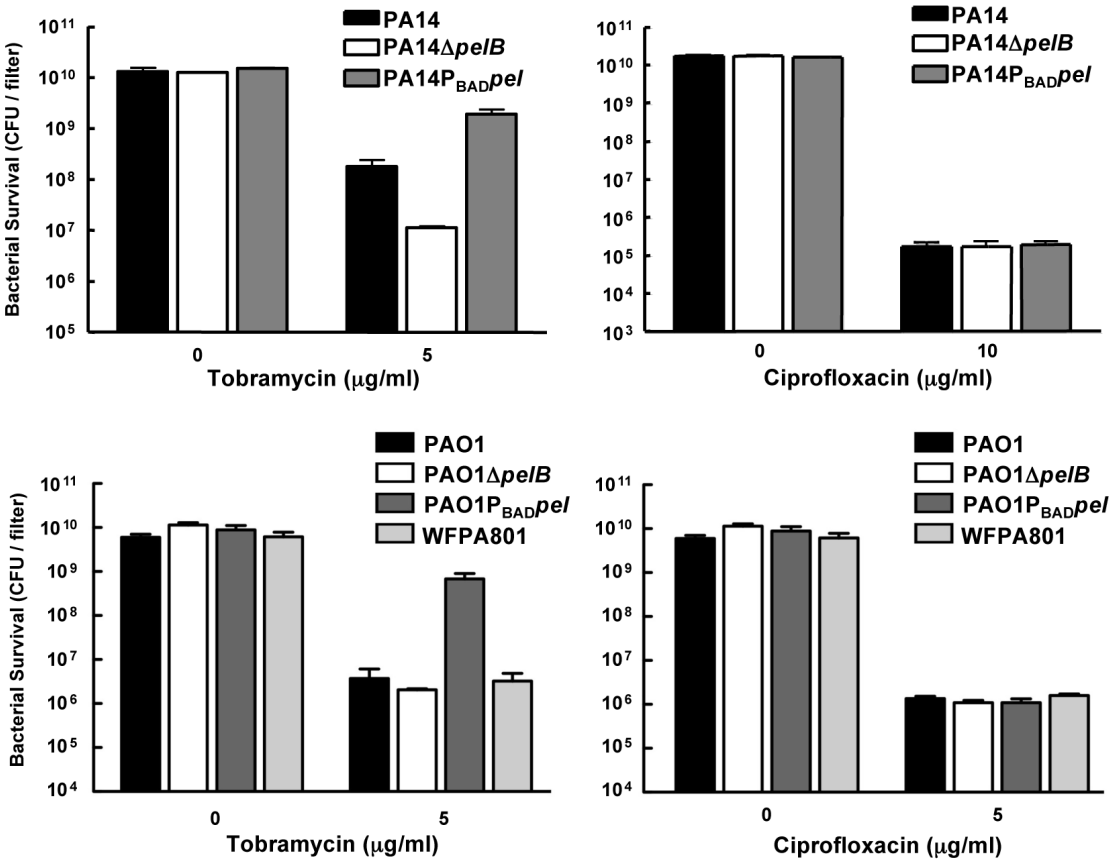

Figure 12. Analysis of Pel-mediated antibiotic tolerance in biofilms. 48-h filter biofilms were assessed for relative susceptibility. Biofilms were treated with tobramycin and ciprofloxacin for 24 h. No antibiotic controls are included for baseline comparison. WFPA801 overexpresses the Psl polysaccharide. Bacterial survival was measured by CFU counts.

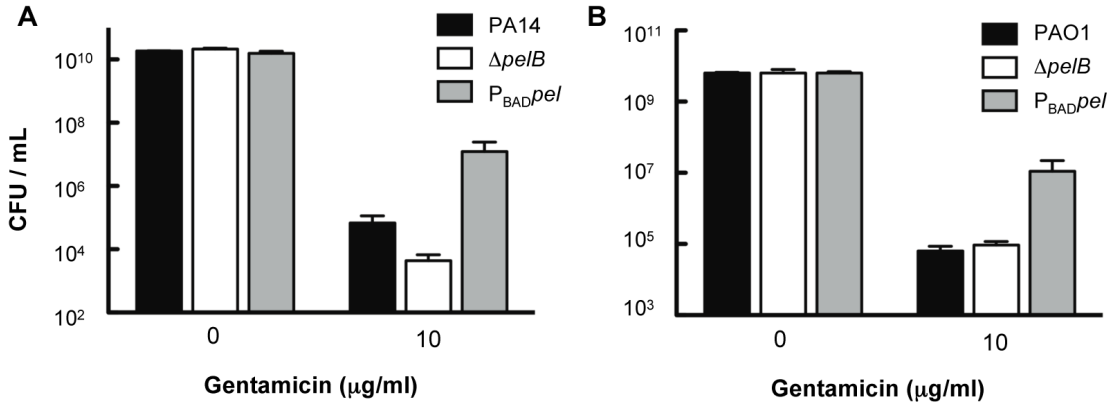

Figure 13. Pel provides tolerance to gentamicin during biofilm growth. 48 h colony biofilms were assessed for relative susceptibility. Biofilms were treated with gentamicin for 24 h. Bacterial survival was measured by CFU counts.

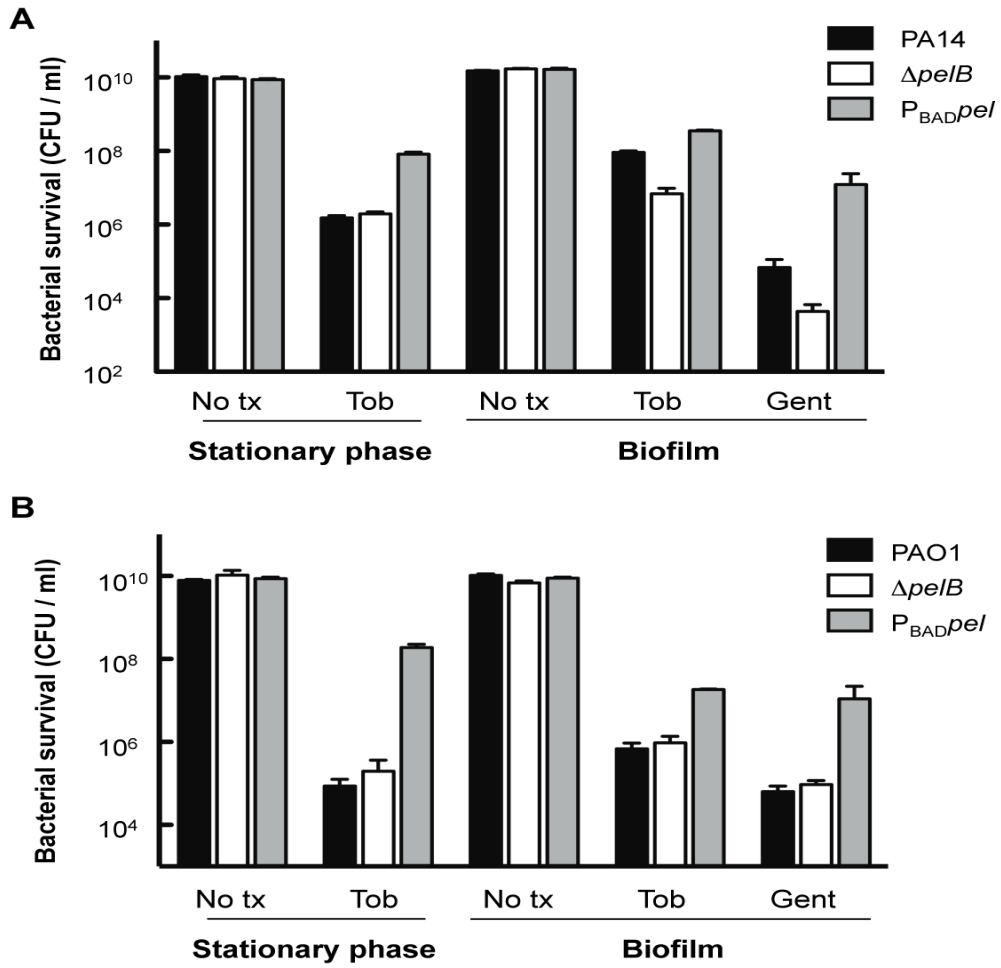

Figure 14. Analysis of Pel-mediated antibiotic resistance to stationary phase planktonic and biofilm grown cells. Bacterial survival was assessed for both PA14 (A) and PAO1 (B) 24 h stationary phase cultures and 24 h filter biofilms. Prior to antibiotic treatment, stationary phase planktonic cells were centrifuged and resuspended in fresh media containing no treatment (No tx) or indicated antibiotics. Biofilm cells were moved to a fresh media source containing no treatment (No tx) or antibiotics. Planktonic cultures were treated with 5 μg/ml tobramycin (Tob). Biofilm cells were treated with either 10 μg/ml of gentamicin (Gent) or tobramycin at 5 μg/ml for PAO1 and 150 μg/ml for PA14.

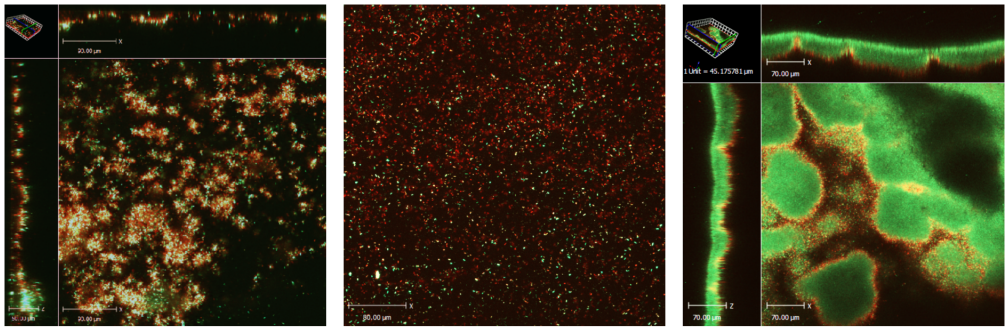

Figure 15. Live/Dead staining of tobramycin treated PA14 flow cell biofilms. 4 d old flow cell biofilms were treated with 1 μg/ml of tobramycin for 24 h. Treated biofilms were stained with syto 9 (green) and propidium iodide (red) to visually assess live and dead cells. Images were taken from a 20x objective.

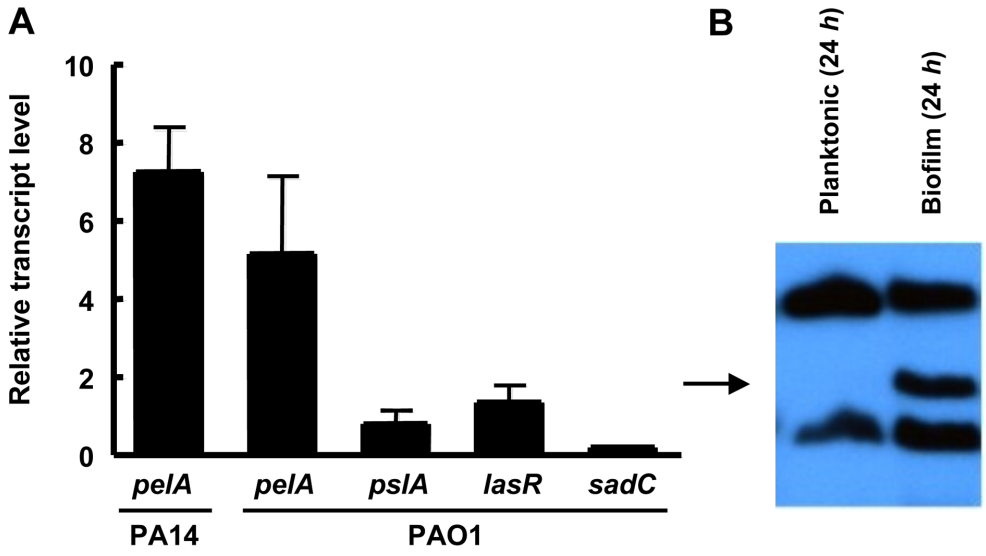

Figure 16. *pel* expression is elevated during biofilm growth. (A) Planktonic and biofilm cells are compared for transcript level by quantitative RT-PCR. In both conditions, bacteria are grown to log phase at 37°C. Planktonic cells are incubated statically in a test tube at room temperature for 30 min. Biofilm cells are grown in a tube biofilm, with an initial attachment period of 30 min followed by continuous flow for 48 h. Transcripts are normalized to *ampR* and then to the initial planktonic condition. Results shown are the mean of three independent experiments. Error bars represent the standard deviations. (B) Planktonic and biofilm cells were probed for PelF protein expression by western blot. A 24 h shaking liquid culture was compared to a 24 h grown tube biofilm at RT. Samples are normalized to total protein. The arrow indicates PelF expected protein size, 56 kDa. qRT-PCR analysis performed by Keiji Murakami.

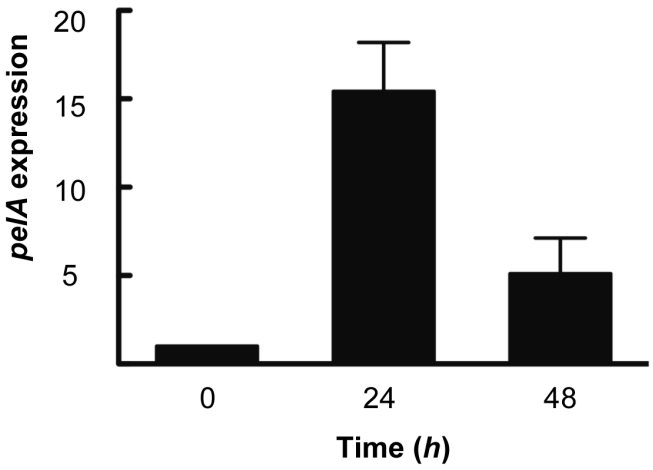

Figure 17. *pelA* expression is induced throughout biofilm growth. Biofilm cells are grown in a tube biofilm, with an initial attachment period of 30 min followed by continuous flow for 48 h. *pelA* transcripts are normalized to *ampR* and then to the planktonic condition at time 0. Results shown are the mean of three independent experiments. Error bars represent the standard deviations. Experiment performed by Keiji Murakami.

CHAPTER II:

Characterization of the Composition and Structure of Pel

INTRODUCTION

Multiple lines of evidence suggest that the *pel* operon encodes the machinery necessary for the synthesis of an extracellular polysaccharide. *P. aeruginosa* strain PA14 forms pellicles that are dependent on the production of Pel (64). These pellicles are resistant to DNase I, RNase A and Proteinase K alone or in combination did not release cells from the biofilm matrix (64). Sodium periodate treatment, which oxidizes carbohydrate rings, broke down the pellicle into small clusters releasing cells into the medium (64). Cellulase is an enzyme that hydrolyzes 1-4 and 1-6-β-D-glycosydic linkages commonly found in cellulose. Cellulase treatment led to a fragmented pellicle. In a *cupA2* background, the pellicle was broken down into single cells after cellulase treatment (64). Although the pellicle was susceptible to cellulose treatment, there are multiple lines of evidence that Pel is not cellulose. First, the concentration of cellulose used was extremely high (5 mg/ml) to treat the pellicles. The most likely explanation of pellicle susceptibility is that cellulase acted non-specifically. Second, Calcofluor, which stains cellulose, does not stain the pellicles (64, 270). Third, the *pel* operon does not contain any orthologs of the cellulose biosynthesis gene clusters.

There is no universal method to purify extracellular polysaccharides. Protocols typically use growth conditions that maximize polysaccharide yield but minimize autolysis and degradation (262). Both physical and/or chemical methods with varying stringencies are used to extract polysaccharides from the bacterial-cell surface or biofilm matrix. In some cases, such as alginate and Psl, polysaccharides can be removed by washing the cells in water, saline or buffer solutions (262). However, tightly bound polysaccharides require harsher treatments. Physical methods of disruption include sonication and boiling. Chemical methods include extraction with EDTA, formaldehyde, trifluoroacetic acid and sodium hydroxide (133). Some of these chemical treatments result in cell degradation and thus it is hard to distinguish between intra- and extracellular polysaccharides. After polysaccharides are extracted, the preparation is subsequently treated to remove contaminants such as nucleic acids, proteins and LPS. Samples can then be dialyzed and/or fractionated by size-exclusion chromatography and

subsequently analyzed for carbohydrate content by colorimetric assays, GC/MS or NMR (43, 57, 133, 216).

The first attempt at identifying Pel's carbohydrate content was done by solubilizing a PA14 pellicle in 1 M sodium hydroxide (64). The cells were removed by ultracentrifugation and filtration. Polysaccharides that remained in the supernatant were precipitated with ethanol and the carbohydrate content was identified by gas chromatography/mass spectrometry (GC/MS). One milligram of matrix contained 62.4 μg of rhamnose, 37.6 μg glucose, 28.7 μg unknown amino sugar, 19.8 μg QuiNAc, 6.5 μg GlcNAc, 6.4 μg kdo and 3.6 μg ribose (64). Most of these sugars are components of the *P. aeruginosa* PA14 LPS, which was subsequently determined (43). The second attempt compared wild-type pellicles with *pel* mutant cultures for carbohydrate content. These studies detected a 3.74-fold increase in glucose (64).

While the previous experiments suggest that Pel is a glucose-rich polysaccharide, further analysis suggest that this may not be the case. In 2010, a second group analyzed the chemical composition of the extracellular biofilm matrix of PA14 and identified the presence of cyclic-β-(1,3)-glucans (201). These cyclic glucans are composed of 12-17 glucose residues with 30-50% of the glucose residues substituted with 1-phosphoglycerol at the O-6 position (201). The presence of these cyclic glucans were attributed to the *ndvB* locus, not the *pel* operon (201). This locus was previously discovered in a transposon screen for mutants that did not develop high-level biofilm-specific tobramycin resistance (139). It was also demonstrated that these extremely anionic glucans bind tobramycin and sequester the antibiotic from reaching its target sites, thus providing the cell protection (201). In addition, *ndvB* is preferentially expressed in biofilm, suggesting that perhaps the higher concentration of glucose in the PA14 pellicle are due to the elevated production of NdvB and not Pel (139).

An additional study on the extracellular carbohydrates of PA14 was performed in 2010. In this study, the carbohydrate chemists first characterized the structure of PA14 LPS O-specific antigen (OSA). Since many treatments are relatively harsh to remove

extracellular polysaccharides from the cell surface and/or extracellular matrix, the LPS is invariably liberated from the outer membrane and is a source of carbohydrate contamination. By knowing the chemical composition of LPS, further purifications can be controlled for. PA14 OSA consists of three repeating sugar units, 2-acetamido-2-deoxy-α-L-galacturonic acid (α-L-Gal*N*AcA, unit A), 2-diacetamido-2,6-dideoxy-α-D-glucose (α-D-Qui*N*Ac, unit B) and α-L-rhamnose (α-L-Rha, unit C) (43). Subsequently, the carbohydrate composition was analyzed from pellicles of cells grown in defined media including the cell-associated extracellular matrix and the growth medium. Most carbohydrates purified from the cell-associated matrix eluted in the void volume of a Sephadex G-50 column and contained Rha, QuiNAc and Glc with small amounts of GlcNAc and Hep, indicating the presence of LPS (43). NMR showed the presence of the β-(1,3)-glucans and OSA as main components of the high molecular weight fraction (43). The growth medium also contained carbohydrate material that eluted near the void volume. The LPS was removed by ultra-centrifugation. NMR analysis revealed the presence of two components, a polysaccharide composed of the three repeating units identical to the OSA polysaccharide and β-(1,3)-glucans (43). Interestingly, the high molecular weight OSA was not detected in a PA14Δ*pelC* strain suggesting that the *pel* operon could be involved in the production of extracellular OSA (43). However, further studies are needed to confirm if Pel is a modified form of OSA LPS.

In this aim, I sought to identify the chemical composition and structure of the Pel polysaccharide. Using a Pel overexpression strain described in Chapter I to produce large quantities of polysaccharide material, polysaccharide purification methods were refined specifically for Pel. Initial GC/MS analysis suggests that Pel material is rich in glucose, rhamnose and ribose. In addition Pel-specific antiserum was generated and used to follow Pel through purification trials. Finally, I analyzed mutants deficient in OSA and CSA production for changes in PA14 colony morphology. In particular, a mutant in *orfN* (PA14_*23460*) formed a smooth colony similar to a *pel* mutant. The *orfN* gene product is a glycosyltransferase necessary for linking OSA and CSA to the outer core indicating that Pel and LPS production may be related.

RESULTS

Ethanol precipitation of PA14P$_{BAD}$*pel* cultures results in an insoluble precipitate not found in PA14Δ*pel*.

In 2009, a study demonstrated that the extracellular products of *P. aeruginosa* inhibit Staphylococcal growth and disrupt established biofilms produced by *S. epidermidis* (187). A *pel* mutant had reduced capacity to disrupt *S. epidermidis* biofilms suggesting that Pel might be secreted (187). Initial attempts at purification used culture supernatants. In order to magnify Pel production, I used the arabinose-inducible PA14P$_{BAD}$*pel* strain that aggregates in liquid culture, forms earlier and stronger pellicles and also leads to increased biofilm biomass. These phenotypes all suggest that Pel production is increased in this strain. As a negative control, I used PA14P$_{BAD}$*pel*Δ*pelF*, a strain deficient in aggregation, pellicle formation and biofilm development. PA14P$_{BAD}$*pel* and PA14P$_{BAD}$*pel*Δ*pelF* were grown in liquid culture for 24 h under a few different environmental conditions in the presence of arabinose. The supernatants were precipitated with ice-cold 70 percent ethanol overnight at -20°C, a common method for the precipitation of polysaccharides (22, 243). The ethanol precipitate from PA14P$_{BAD}$*pel* looked distinctively different from the negative control (**Figure 1A**). The precipitate was centrifuged, dried and resuspended in ddH_2O. Interestingly, PA14P$_{BAD}$*pel* ethanol precipitate was partially insoluble in ddH_2O, which was not found for PA14P$_{BAD}$*pel*Δ*pelF* (**Figure 1B**).

Further experiments evaluated the precipitate properties and determined if it was composed of carbohydrates. Multiple pieces of evidence suggested that it was. I first attempted to solubilize the precipitate in different solvents. However, it remained insoluble in ddH_20, DMSO, phenol, chloroform, ethanol, methanol and acetone. The precipitate could be hydrolyzed in acid, a method used to break down polysaccharides into oligosaccharides or individual sugars depending on the strength of the acid and length of incubation (**Figure 1C**) (85). This result was the first indication that that precipitate could be composed of a polysaccharide component. Consistent with this, the precipitate was completely resistant to enzymatic treatments by DNase I, RNase A and

Proteinase K (data not shown). The precipitate bound Congo red, a dye that binds neutral polysaccharides or polysaccharides containing β-1,3- or β-1,4-glucopyranosyl linkages (**Figure 1D**)(64, 214, 270). Since PA14 colonies producing Pel have a higher Congo red affinity than colonies not producing Pel, this was a second piece of evidence that a polysaccharide specific to the *pel* operon was found in the precipitate. Since pellicles were demonstrated to be partially sensitive to cellulase treatment, I treated the insoluble precipitate with a high concentration of cellulase. No effect was seen on the pellicle (data not shown). However, when the bacterial strains were grown in the presence of cellulase, the precipitate structure differed (**Figure 1E**). The single uniform precipitate was fragmented and more sensitive to physical disruption by vortexing than the non-treated sample.

PA14P$_{BAD}$*pel* precipitate has elevated levels of rhamnose, ribose, glucose and two un-identified amino sugars.

The insoluble precipitate was quantified for carbohydrates using the phenol-sulfuric acid assay, a common method for the detection and quantification of neutral polysaccharides (57). The insoluble precipitate was estimated to contain 5 mg of carbohydrate material (data not shown). Samples were sent to the Complex Carbohydrate Research Center (CCRC) located at the University of Georgia for the identification of monomer composition by Parastoo Azadi. The analysis checked for the presence of twelve sugars, including arabinose (Ara), rhamnose (Rha), fucose (Fuc), xylose (Xyl), glucuronic acid (GlcA), ribose (Rib), mannose (Man), galactose (Gal), glucose (Glu), N-acetyl galactosamine (GalNAc), N-acetyl glucosamine (GlcNAc) and N-acetyl mannosamine (ManNAc). Three samples were analyzed for the presence of these twelve sugars. The first sample was the soluble ethanol precipitate from PA14P$_{BAD}$*pel*Δ*pelF* (Δ*pel*). The second sample was the soluble and insoluble ethanol precipitate from PA14P$_{BAD}$*pel* (P$_{BAD}$*pel*). The third sample was the washed insoluble ethanol precipitate from PA14P$_{BAD}$*pel* (P$_{BAD}$*pel* ppt). The analysis measured both the mass and molar percent of each carbohydrate (**Figure 2A**). Δ*pelF* and P$_{BAD}$*pel* samples were nearly identical in sugar composition with mannose comprising the majority of

the sample, but P_{BAD}*pel* ppt displayed a different sugar profile that was rich in glucose, rhamnose and ribose (**Figure 2B**). In addition, the GC/MS of P_{BAD}*pel* ppt contained two large peaks that eluted after the glucose peak. The peaks have mass spectra that resembled spectra of the amino sugars run in the samples, but the retention was different from the standard (data not shown). One predicted sugar contaminant in these samples is LPS. The inner core is composed of two residues of Kdo and two residues of L -*glycero*- D -*manno*-heptose (110). The outer core is composed of D-Glc, L-Rha and D-GalN (110). PA14's O-specific antigen is a repeating trisaccharide composed of L-GalNAcA, D-QuiNAc and L-Rha (43). The common LPS antigen is composed of D-Rha (110). It is quite possible that the unknown sugars in the P_{BAD}*pel* ppt sample are GalNAcA and QuiNAc, two amino sugars that are part of the O-specific antigen but further analysis would need to be conducted. In addition the appearance of ribose may correspond with increase amounts of nucleic acids that were incompletely digested due to the protected environment of the insoluble precipitate prior to GC/MS.

Characterization of Pel antiserum.

Antiserum was raised against the insoluble precipitate from PA14P_{BAD}*pel* to generate Pel-reactive antiserum. The specificity of Pel antiserum was checked by analyzing strains previously described to have altered levels of Pel expression (39, 89, 90). The Pel antiserum was absorbed against both PA14Δ*pel* and PAO1Δ*pel* lysates to remove cross-reactive antibodies. Initially PA14, PA14Δf*leQ* (high *pel* transcription), PA14Δ*wspF* (high *pel* transcription and elevated c-di-GMP levels), PA14P_{BAD}*pel* grown in different concentrations of arabinose and PA14P_{BAD}*pel*Δ*pelF* were probed for Pel reactivity (**Figure 3A**). PA14Δ*wspF* and PA14P_{BAD}*pel* grown with 0.5 percent arabinose showed elevated reactivity to the Pel antiserum. However, there was a lot of background even when the antibody was absorbed that made differentiating between lower levels of Pel production difficult in PA14, PA14Δf*leQ* and PA14P_{BAD}*pel*Δ*pelF*. Since the antiserum was synthesized from this strain background we expected a higher level of cross-reactivity that was Pel-independent. Therefore, I analyzed Pel production in PAO1. Strains initially analyzed were PAO1, PAO1Δ*wspF*, PAO1Δ*wspF*Δ*pel*, PAO1Δ*wspF*Δ*psl*, PAO1Δ*wspF*Δ*pel*Δ*psl* and PAO1P_{BAD}*pel* (**Figure 3B**). Strains

PAO1Δ*wspF,* PAO1Δ*wspF*Δ*psl*, and arabinose induced PAO1P_{BAD}*pel* had elevated Pel reactivity compared to the negative controls (**Figure 3B**). PAO1 has reduced background and strains that overexpress Pel have a modest increase in reactivity but its difficult to discern between PAO1 and PAO1Δ*pel* (**Figure 3C**). Overall the antisera may be a useful tool for large but not small differences in Pel production.

Pel antiserum is cross-reactive to the PA14 O-antigen.

Based on the GC/MS analysis of the insoluble precipitate we sent for antisera production (**Figure 2A**), we speculated that the Pel antiserum would be cross-reactive with the O-specific antigen in PA14. PAO1 and PA14 have different O-specific antigens. PA14 O-specific antigen consists of L-GalNAcA, D-QuiNAc and L-Rha repeating units, while PAO1 O-specific antigen consists of D-ManNAcN, D-ManNAcNAc and D-FucNAc (193). To test if the Pel antiserum was cross-reactive to PA14 O-specific antigen, I purified LPS from a few PAO1 strains that differ in Pel production and PA14 strains that differ in Pel production and LPS profiles and ran them out on a polyacrylamide gel. A characteristic ladder pattern for both O-specific antigen and common antigen is typical of both PAO1 and PA14 (124, 141). We found that the Pel antiserum recognizes PA14 O-specific antigen (**Figure 4**). The antibody does not recognize any of the PAO1 strains but equally recognizes PA14, PA14Δ*pelA*, PA14Δ*pelD*, PA14P_{BAD}*pel* and PA14Δ*wspF.* PA14Δ*wspF* showed a slightly altered banding pattern that was shifted up in molecular weight. The *orfN* gene is 67% identical to *wbpL* (*PA3145*) in PAO1. WbpL is a glycosyltransferase required for the synthesis of both OSA and CSA in PAO1 (194). Therefore we predicted a PA14Δ*orfN* mutant to be defective in OSA and CSA synthesis. Consistent with this was the observation that the Pel antisera did not react with PA14Δ*orfN* (**Figure 4**). To control for CSA production, we mutated *wbpX* (PA14_*71930*), a glycosyltransferase involved in CSA synthesis (194). PA14Δ*wbpX* was still reactive to the Pel antiserum, suggesting that PA14 O-specific antigen is cross-reactive with the antiserum.

PA14Δ*orfN* is delayed for wrinkly colony morphology.

Strains mutated for the ability to synthesize OSA and CSA were evaluated for colony morphology. PA14 will wrinkle under certain growth conditions. This wrinkly colony morphology requires Pel production (39, 40). A strain incapable of synthesizing CSA, PA14Δ*wbpX*, showed no impairment in colony morphology (**Figure 5A**). Interestingly, PA14Δ*orfN* initially displays a smooth colony morphology similar to a *pelF* mutant but after prolonged incubation will begin to wrinkle on the colony edges (**Figure 5B**). A strain mutated for *pelF* retained a smooth colony morphology irrespective of the presence or absence or *orfN*. Supplying the *orfN* allele at a neutral site on the chromosome could complement the change in colony morphology.

Followed Pel through purification using the Pel antisera

In order to use the Pel antiersum as a tool to follow Pel through purification steps, I switched strain backgrounds from PA14 to PAO1. PAO1 has a different OSA polysaccharide and does not have as much cross-reactivity as PA14. In addition, I used a strain that had elevated levels of c-di-GMP, a known regulator of *pel* transcription and biosynthesis (90, 129). The Pel production strain was PAO1Δ*wspF*Δ*psl* P_{BAD}*pel* and the control strain was PAO1Δ*wspF*Δ*psl*Δ*pel*. The overexpression strain aggregated in liquid culture and formed rugose colonies that were not apparent in the control strain (**Figure 6A**). In addition, the Pel antiserum detected higher levels of Pel in the P_{BAD}*pel* strain compared to the triple mutant. Interestingly, the fraction containing Pel reactivity changed during growth. For example, cells grown in LB at 37°C under aerobic conditions showed initial Pel reactivity that was cell-associated but after 24 h was found in the supernatant (**Figure 6B**). I subsequently attempted to purify Pel from the supernatant.

While I have attempted Pel purification many times, I have been unable to find a reliable purification method. In some purification protocols a 100-kDa filter retains Pel, while in other purifications Pel is lost after dialyzing with a 2-kDa membrane. It is a possible that Pel, like Psl, and has two forms, a high molecular weight form and a low molecular weight form. In Psl the low molecular weight form is secreted into the supernatant, while the high molecular weight form is cell-associated (27). This did not

appear to be the case for Pel and seemed to be more variable (data not shown). In other cases different Pel preparations differed in the capability to bind to hydrophobic columns suggesting Pel's structure could be modified. Perhaps using the secreted form of Pel in the supernatant was not the ideal method. For one, the supernatant fraction also contains lysed cells. This may be one reason for variability between purifications. Second, using an undefined medium (LB) that is invariably different between batches may alter Pel synthesis and/or properties. Third, we don't know if the Pel antiserum is a reliable detector of Pel production. Thus, we don't want to rely solely on this method of detection.

Modified Pel purification.

I took on a new strategy to purify Pel but used the same strains as before, PAO1Δ*wspF*Δ*psl* P_{BAD}*pel* and the control strain PAO1Δ*wspF*Δ*psl*Δ*pel*. I switched to a defined medium, Jensens, that resulted in high growth yield. In this medium, the overexpression strain aggregated in liquid culture, formed rugose colonies and high amounts of biofilm formation in a crystal violet attachment assay (data not shown). These phenotypes were not apparent in the control strain. Using the defined medium to grow cells, I followed a protocol employed by Tony Romeo's lab to purify poly-β-1,6-GlcNAc (PGA) (254). Polysaccharides were extracted from bacterial cells using an EDTA/lysozyme mixture. The solubilized solution was treated with proteinase K to digest the protein contaminants. The protein contaminants were then removed by a hot phenol extraction. The aqueous layer was concentrated in a 10 kDa spin column. After a 10 min centrifugation, 20 mls of PAO1Δ*wspF*Δ*psl*Δ*pel* concentrated to 0.5 mls, while the PAO1Δ*wspF*Δ*psl* P_{BAD}*pel* solution was concentrated to 5 mls. After extended, centrifugation the PAO1Δ*wspF*Δ*psl* P_{BAD}*pel* solution was concentrated to 2 mls. These results suggest that something large is preventing the solution from concentrating, probably Pel. Samples were subsequently separated on a Sephacryl S-200 column using PBS as the running buffer. The protein absorbance spectrum (OD_{280}) is shown (**Figure 7A**). In addition I used three methods to detect the presence of Pel. The first was the phenol-sulfuric acid assay, which detects neutral hexoses at OD_{490} and neutral pentoses and uronic acids at OD_{480} (57). The second assay detects hexosamines and can equally

detect glucosamine and galactosamine (216). Lastly, I used the Pel antiserum. Each fraction from the Sephacryl S-200 column was tested with all three assays (**Figure 7B, 7C, and 7D**). The sample that extracted from P_{BAD}*pel* contained higher reactivity with the phenol-sulfuric acid assay as well as the hexosamine assay. Interestingly, the Pel antiserum reacted against the high molecular weight fractions that did not differ from each other in the other assays. Future studies would examine these fractions by GC/MS for carbohydrate material.

Lectin screen to identify Pel's composition.

A parallel approach to identify Pel's composition and linkage profile is to identify a lectin that binds to Pel. Lectins are proteins that specifically bind to carbohydrates. Commercially available fluorescent lectins were screened for the ability to bind a strain that produces Pel but not to a *pel* mutant. This type of screen successfully identified two specific lectins for the Psl polysaccharide and provided insight on the carbohydrate composition prior to the Psl structure being known (137). In addition, the fluorescent lectins have been useful in analyzing the Psl localization on single cells and during biofilm growth (135, 137). To screen for lectins that may bind Pel, we used a negative control PAO1Δ*pel*Δ*psl*Δ*alg* that was incapable of synthesizing the three known extracellular polysaccharides, Pel, Psl and alginate. Our tester strain was PAO1Δ*psl*Δ*alg*P_{BAD}*pel*. Both strains were grown in the presence of arabinose. We screened six lectins with a variety of carbohydrate affinities, Wheat Germ Agglutinin, WGA (GlcNAc-β-1,4- GlcNAc-β-1,4- GlcNAc, Neu5Ac), *Ulex europaeus* agglutinin, UEA-1 (α-L-Fuc), *Hippeastrum hybrid* lectin, HHA (α-1,3-Man or α-1,6-Man), Snowdrop lectin, GNA (α-1,3-Man or α-1,6-Man), *Dolichos biflorus* agglutinin, DBA (terminal α-d-GalNAc) and *Bauhinia purpurea* lectin, BPA (GalNAc-β-1,4- GalNAc and Gal). Unfortunately, no lectin was identified to be Pel-specific (**Figure 8**). On the contrary, the lectin analysis suggested that Pel production masked particular sugars. For examples, the UEA-1 lectin bound well to the control strain, PAO1Δ*pel*Δ*psl*Δ*alg*, but not to the tester strain, PAO1Δ*psl*Δ*alg*P_{BAD}*pel*. This was also true for the GNA lectin.

DISCUSSION

Nonmucoid strains of *P. aeruginosa* account for the vast majority of strains isolated from the environment and represent the early colonizers of the CF airways. Extracellular polysaccharides are important components of the biofilm matrix and by knowing the physical and structural properties of each polysaccharide, our understanding of *P. aeruginosa* biofilms will greatly improve. While the structure of Psl was recently identified, the structure of Pel is still unknown. A few clues have been put forth such as Pel being glucose-rich, only to be taken back when the source of glucose was found to be from NdvB and Pel independent (201). One group suggested that Pel may be involved in the secretion of non-lipid linked O-specific antigen (43). If this were the case, like O-specific antigen of the LPS, Pel's composition and structure would differ between strains.

Examples of non-lipid linked O-specific antigens exist. The first example of "O-antigen capsules" were found in *E. coli* in serotype O111, where 50% of the O-antigen is in the smooth LPS fraction and the remainder is in a LPS-unlinked capsular form (261). O-antigen capsules now comprise Group 4 capsules (261). The full distribution of O-antigen capsules is unknown, since many may have been overlooked due to earlier assumptions that the O-antigen was always lipid-A-linked. Identical structures for LPS O-antigen and O-antigen capsule have been described in a variety of Gram-negative species including *Salmonella enteritidis*, *Vibrio cholerae* O139, *Aeromonas salmonicida*, *Acetobacter methanolicus* and *Vibrio anguillarum* (75, 218, 251, 255). Importantly, some *E. coli* serotypes only express lipid-linked O-antigen suggesting that O-antigen capsule is not a simple consequence of synthesizing LPS (261). The main differences between O-antigen capsules and lipid-linked O-antigen is that O-antigen capsules tend to have a higher molecular weight and use different initiating glycosyltransferases (218, 261). In addition, the O-antigen capsule is not dependent on LPS core biosynthesis for expression at the cell surface, but rather relies on a separate biosynthetic and transport system (218). Therefore, it is still possible that the *pel* biosynthetic operon is involved in synthesis of a non-lipid linked O-specific antigen.

Consistent with the hypothesis that Pel may be a modified O-antigen capsule is the fact that our antiserum generated against Pel is cross-reactive to the PA14 O-specific antigen but not PAO1. Further studies are needed to remove LPS contamination from Pel samples and subsequently analyzed for carbohydrate content. Two common methods are used to separate out lipid-linked O-antigen and O-antigen capsule including high-speed centrifugation and polymyxin B chromatography (43, 218). Interestingly, biofilm growth and chronic colonization of CF lungs selects for strains that reduce or eliminate the ability to produce lipid-linked OSA (12, 125, 215). In contrast, Pel production is speculated to increase during both biofilm formation and chronic CF infections as demonstrated by the increase in fitness of rugose colonies during in-vitro biofilm growth and the high prevalence of *wspF* mutations isolated from CF infections (215, 221). While the molecular mechanisms responsible for the loss of lipid-linked OSA during biofilm growth and CF infections are unknown, it is possible that the polysaccharide precursors are shuttled through the Pel biosynthetic machinery instead.

Another point of interest is whether the Pel polysaccharide is modified, such as by acetylation. These physicochemical properties would affect the solubility and viscosity of the polysaccharide. Identifying these properties may allow us to purify a soluble form of Pel that can be analyzed for carbohydrate content and linkage. One piece of evidence that suggests Pel may be modified is in regulatory backgrounds that lead to *pel* up-regulation (e.g. Δ*wspF* and Δ*fleQ*), the two-gene operon *PA2440-PA2441* is also up-regulated (89, 90, 221). *PA2440* has homology to polysaccharide deacetylases and preliminary experiments demonstrate that overexpressing this operon alters the colony morphology and reduces aggregation in liquid culture in PAO1Δ*wspF*. Similarly I found that a mutant in PA2440 in the PAO1Δ*wspF* background results in increased aggregation. It remains to be determined if Pel is the target polysaccharide. If Pel is acetylated, removing acetyl groups can decrease the hydrophobic nature of the polysaccharide and perhaps increase its solubility.

During the first purification attempt, an insoluble precipitate formed in PA14P$_{BAD}$*pel* but not the *pel* mutant (Figure 1). We suspected the physical properties of Pel resulted in an insoluble precipitate. Secondary purification attempts used a different wild-type strain in a high c-di-GMP background, PAO1Δ*wpsF*Δ*psl*P$_{BAD}$*pel*. Interestingly, no insoluble precipitate formed after ethanol precipitation under identical conditions for PA14P$_{BAD}$*pel* (data not shown). While these results do not confirm that a polysaccharide deacetylase is acting on Pel, they suggest that Pel has the potential to be modified. Future purification studies will continue with PAO1Δ*wpsF*Δ*psl*P$_{BAD}$*pel* since this strain produces large quantities of Pel per cell mass and may be an important strain for reducing the hydrophobic nature of Pel (due to elevated PA2440 expression in this background).

Purification of Pel proved to be extremely challenging. The main problem is that we don't have a reliable detector of Pel. Our antiserum is cross-reactive with PA14 OSA and does not always show differential reactivity patterns in our mutants. In addition, a general method of detection for polysaccharides does not exist. If the polysaccharide composition is known, colorimetric assays and sugar detection kits are available. However, since the Pel composition is unknown the best method would be to run GC/MS profiles on each fraction from a size-exclusion column and compare them to the fraction from a *pel* mutant. Currently, we do not have the expertise or resources for this experiment and samples need to be carefully chosen for further analysis. We are optimistic that Pel's composition will be identified by the new purification techniques. In parallel, a more comprehensive lectin screen should be performed. One particular high-throughput approach would be a lectin microarray as described to determine protein modification (95, 96). Knowing the identity and being able to purify Pel will initiate many further experiments, such as identifying Pel localization within the biofilm matrix and evaluating the mechanism behind aminoglycoside tolerance.

MATERIALS AND METHODS

Bacterial strains, strain construction and growth media.

Bacterial strains in this study are listed in **Table 1.** DNA manipulations were performed using standard techniques as described in Chapter I. For routine culture, *P. aeruginosa* strains were grown at 37°C in Luria-Bertani (LB) medium (Difco). Plasmids were selected with 100 μg/ml gentamycin or 300 μg/ml carbenicillin for *P. aeruginosa* strains and 10 μg/ml gentamycin or 100 μg/ml ampicillin for *E. coli*. 25 μg/ml irgasan was used to counter select for *E. coli*. For the first Pel purification I grew cultures in Erlenmeyer flasks (50 ml per 250 ml flask) in LB medium overnight at 30°C. For the second polysaccharide purification, cells were grown in Erlenmeyer flasks (1 L per 2L flask) at 37°C for 24 h in Jensen's defined medium. 1 L of Jensen's contains 5 g NaCl, 2.51 g K_2HPO_4, 15.5 g glutamic acid, 2.8 g valine, 1.3 g phenylalanine supplemented with 25 ml 50% Glucose, 10 ml $MgCl_2$-$7H_20$ (33 g/l), 10 ml $CaCl_2$-$2H_20$ (2.1 g/l), 10 ml $FeSO_4$-$7H_20$ (0.11g/l) and 10 ml $ZnSO_4$-$7H_20$ (0.24 g/l).

Acid hydrolysis.

Samples were incubated with either 2 M trifluoroacetic acid (TFA) at 110°C for 1 h or 1 M sulfuric acid (H_2SO_4) at 100°C for 4 h for complete hydrolysis.

Cellulase Treatment.

The insoluble precipitate was treated with 20 mg/ml (final concentration) of cellulase from *Aspergillus niger* (Sigma) at 37°C overnight. Alternatively, bacterial strains were grown as described above with the addition of 1 mg/ml (final concentration) of cellulase from *Aspergillus niger* prior to ethanol precipitation (Sigma).

Congo red staining.

The ethanol precipitate was supplemented with 40 μg/ml Congo red (Sigma-Aldrich) and incubated at 37°C for 1 h.

Polysaccharide purification.

Secreted

A sample (0.5 ml) of overnight culture was added to 50 mls of LB medium supplemented with 0.5% arabinose and incubated for 20 h at 30°C. Cells were harvested by centrifugation. The supernatant was precipitated overnight at -20°C with cold ethanol to a final concentration of 70%. The precipitate was resuspended in 2 ml of buffer (50 mM Tris, pH 7.5; 1 mM $CaCl_2$ and 2 mM $MgCl_2$) and treated with 5 mg DNase I, 5 mg RNase A for 2 h at 37°C, followed by 5 mg Proteinase K treatment overnight at 37°C. This sample was lyophilized and sent to the Complex Carbohydrate Research Center at University of Georgia for analysis. This sample was also used for antisera production.

Cell-associated

A sample (1 ml) of overnight culture was added to 1 L of Jensen's medium supplemented with 0.5% arabinose and incubated for 24 h at 37°C. Cells were harvested by centrifugation and pellets were resuspended in 20 mls of 50 mM Tris, pH 8.0; 20 mM EDTA, pH 8.0; and 100 mg lysozyme. The suspension was incubated at 25 °C for 30 m followed by the addition of 7 mg of Proteinase K and overnight incubation at 37°C. The suspension was diluted with 50 ml of 50 mM Tris, pH 8.0 and polysaccharide was separated from proteins and cell debris by phenol extraction (254). Briefly, the polysaccharide mixture was stirred vigorously with an equal volume of phenol at 65-70°C for 1 h. The sample was cooled to 25°C and incubated at 4°C overnight to allow the phases to separate. The aqueous layer was extracted with an equal volume of chloroform, and concentrated by ultrafiltration (Amicon 10kDa molecular weight cutoff). Concentrated sample (1 ml) was loaded onto a Sephacryl S-200 size exclusion column equilibrated with PBS and eluted with the same buffer. 1 ml fractions were collected and assayed for hexosamine content, neutral sugar content (phenol-sulfuric acid assay) and reactivity with anti-Pel antiserum.

Phenol-sulfuric acid assay.

This assay was performed as originally described with minor modifications (57). Under the hood, 1 ml of sample was mixed with 500 µl 5% phenol in a glass test tube. This incubated for 5 m at 25°C. To each sample 2.5 ml of sulfuric acid was added quickly and

directly to the sample. Care was taken not to allow the sulfuric acid to run down the side of the glass tube but rather a direct stream to the sample. This ensured sufficient mixing and reproducibility. Samples were incubated for 5 m at 25°C and measured at OD_{490} for neutral hexoses and OD_{480} for pentoses and uronic acid.

Hexosamine assay.

This assay was performed as originally described with minor modifications (216). In a glass tube with cap, 100 µl carbohydrate sample and 100 µl 1 M HCl was added. Samples were vortexed and heated at 110°C for 2 h then cooled to 25°C. In a fume hood, 400 µl of 2.5% $NaNO_2$ was added. Samples were vortexed and allow to stand for 15 m at 25°C. 200 µl of 12.5% ammonium sulfamate was added. Samples were vortexed and incubated at 25°C for 5 m. 200 µl of 0.25% MBTH was added. Sample were vortexed and incubate at 37°C for 30 m. 200 µl $FeCl_3$ was added and samples were incubated at 37°C for an additional 5 m and subsequently cooled to 25°C. Absorbance was read at OD_{650}.

Glycosyl composition performed at the Complex Carbohydrate Research Center (CCRC).

Glycosyl composition analysis was performed by combined gas chromatography/mass spectrometry (GC/MS) of the per-*O*-trimethylsilyl (TMS) derivatives of the monosaccharide methyl glycosides produced from the sample by acidic methanolysis. An aliquot was taken from the sample and added to separate tubes with 40 µg and 60 µg of inositol as the internal standard. The samples were then combined with 400 µl of 2M TFA and set at 121°C for two h. The samples were later dried under nitrogen to remove the TFA. Methyl glycosides were then prepared from the sample following the mild acid treatment by methanolysis in 1 M HCl in methanol at 80°C (16 h), followed by re-*N*-acetylation with pyridine and acetic anhydride in methanol (for detection of amino sugars). The sample was then per-*O*-trimethylsilylated by treatment with Tri-Sil (Pierce) at 80°C (0.5 h). These procedures were carried out as previously described (152). GC/MS analysis of the TMS methyl glycosides was performed on an AT 6890N

Gas chromatograph interfaced to a 5975B mass selective detector (MSD), using a Supelco EC-1 fused silica capillary column (30m × 0.25 mm ID).

Generation of Pel antiserum and absorption.

The insoluble washed precipitate was used to generate antiserum from rabbits using a 70-day standard protocol (Open Biosystems). Antiserum was absorbed using PA14Δ*pel* and PAO1Δ*wspF*Δ*pel*Δ*psl* lysates. Lysates were generated from 100 ml of each strain grown to late-log (OD_{600} ~ 1.0). Cells were centrifuged and resuspended in 3 ml of lysis buffer (50mM Tris, pH 8.0, 10mM EDTA, pH 8.0). Cells were lysed by three cycles of freeze/thaw followed by sonication and centrifugation. The cell lysate was subsequently used for absorption by mixing 20 μl α-Pel antisera, 50 μl PA14Δ*pel* lysate and 50 μl PAO1Δ*wspF*Δ*pel*Δ*psl* lysate in 1 ml of 5% non-fat milk in Tris-buffered saline with Tween 20 (TBST)(10 mM Tris, pH 7.5, 150 mM NaCl, 0.1% Tween 20). The antiserum was absorbed for 4 h at 25°C under constant rotation.

Immunoblot Analysis.

Standard protocol

Pel immunoblots were performed as described previously for Psl with the following minor modifications (27). Cells from each growth condition described above were harvested and resuspended in 100 μl 0.5 M EDTA. Cells were boiled for 20 min with periodic vortexing and centrifuged. The supernatant fraction was treated with Proteinase K (final concentration 0.5 mg/ml) for 60 min at 60°C, followed by Proteinase K inactivation for 30 min at 80°C. Samples were stored at 4°C for immunoblotting. Polysaccharide preparations were normalized to total protein in the EDTA extraction as determined by protein assay (Bio-Rad). Sample (5 μl) was spotted onto a nitrocellulose membrane and air dried for 10 m. The blot was blocked for 1 h at 25°C in 5 percent milk TBST, followed by the absorbed α-Pel antiserum at 1:1,000 dilution in 1 percent non-fat milk TBST for 1 h. Blots were developed with goat α-rabbit HRP-conjugated secondary antibody (Thermo-Scientific) and Pierce detection kit.

Modified immunoblot protocol for LPS

LPS samples were prepared by the method of Hitchcock and Brown (91) and resolved on a pre-cast 12.5% Tris-HCl polyacrylamide gel (Bio-Rad) and transferred to a nitrocellose membrane for immunoblotting. Briefly, overnight cultures grown on LB agar medium at 37°C were harvested and diluted to an OD_{600} of 0.5 in PBS in a volume of 1 ml. Suspensions were centrifuged at 2,300 x *g* for 5 m and resuspended in 250 µl of Hitchcock and Brown lysis buffer (2% SDS, 4% β-mercaptoethanol, 10% glycerol, 1 M Tris (pH 6.8), 0.002% bromophenol blue). The samples were heated at 100°C for 30 m, cooled to room temperature and incubated with 1.5 µl of proteinase K (20 mg/ml stock) at 56°C for 2 h. 5 µl of the preparation were resolved by electrophoresis. The transferred LPS was probed for Pel similar to the above description with the following modification. The buffer was switched from TBST to PBS without Tween 20.

Lectin analysis.

Strains were grown to OD_{600} 1.0 in LB + 0.5% arabinose. A sample of each culture (1 ml) was harvested and washed twice in the appropriate buffer as described by the manufacturer (EY Laboratories). The following was mixed at incubated in the dark at 25°C, 100 µl bacteria, 80 µl buffer, 20 µl 1µM lectin. The cells were washed twice and resuspended in 50 µl. A 3 µl sample was spotted on an agarose pad. Images were acquired by fluorescence microscopy.

Table 1 Strains used in Chapter II

Strains	Relevant Characteristics	Reference
PA14	wild-type	Rehme et al., 1995
PA14P$_{BAD}$*pel*	*Pel* over-expression strain	This study
PA14P$_{BAD}$*pel*Δ*pelF*	*pelF* nonpolar deletion	This study
PA14Δ*fleQ*	*fleQ* nonpolar deletion	Varisa Huangyutitham
PA14Δ*wspF*	*wspF* nonpolar deletion	Varisa Huangyutitham
PAO1	Wild-type	Holloway, 1955
PAO1Δ*wspF*	*wspF* nonpolar mutant	Hickman et al. 2005
PAO1Δ*wspF*Δ*pel*	polar *pelA* mutation	Irie et al. 2010
PAO1Δ*wspF*Δ*psl*	polar *pslBCD* mutation	Irie et al. 2010
PAO1Δ*wspF*Δ*pel*Δ*psl*		Borlee et al. 2010
PAO1Δ*pelB*	*pelB* nonpolar mutant of PAO1	This study
PAO1P$_{BAD}$*pel*	*Pel* over-expression strain	This study
PA14Δ*pelA*	pelA nonpolar mutant	This study
PA14Δ*pelD*	*pelD* nonpolar mutant	This study
PA14Δ*orfN*	*orfN* nonpolar mutant	This study
PA14Δ*wbpX*	*wbpX* nonpolar mutant	This study
PAO1Δ*wspF*Δ*psl* P$_{BAD}$*pel*	*Pel* over-expression strain in PAO1Δ*wspF*Δ*psl*	This study
PAO1Δ*pel*Δ*psl*Δ*alg*	*algD* mutant in PAO1Δ*pel*Δ*psl*	Jocelyn Muller
PAO1Δ*psl*Δ*alg*P$_{BAD}$*pel*	*Pel* over-expression strain in PAO1Δ*psl*Δ*algD*	This study

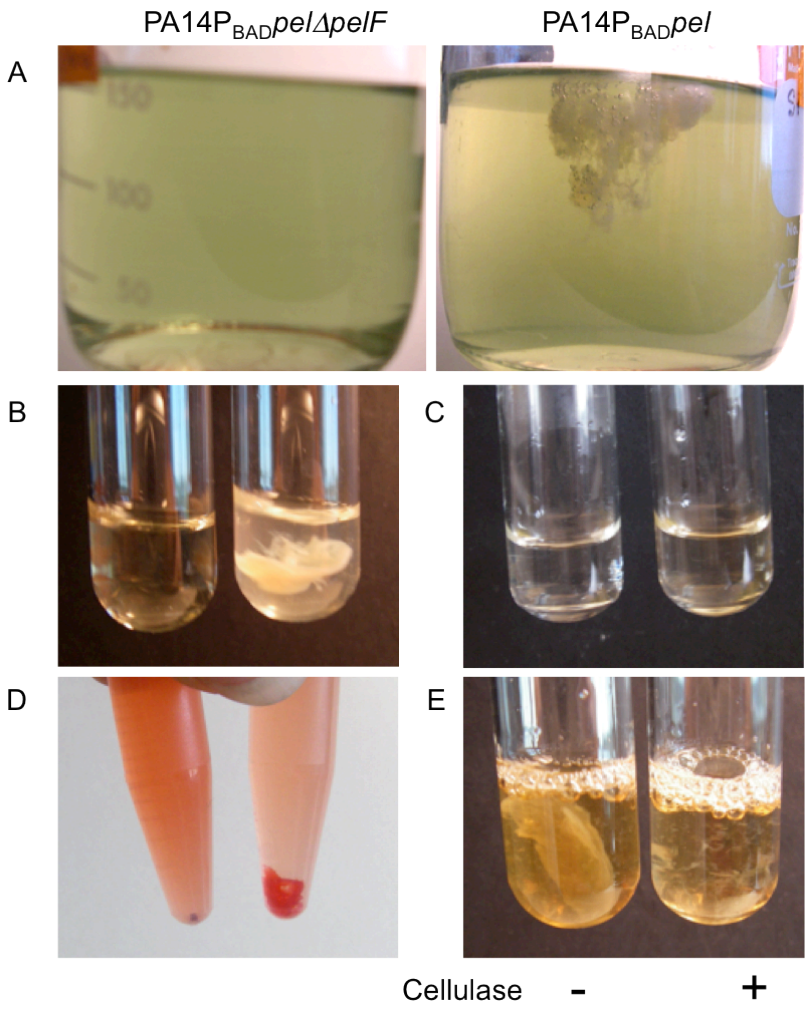

Figure 1. Insoluble Pel precipitate characteristics. Overnight ethanol precipitation of bacterial supernatants (A). Unless otherwise stated, the left tube is PA14P$_{BAD}$*pelΔpelF* and the right tube is PA14P$_{BAD}$*pel.* Image of the ethanol precipitate resuspended in water (B). The same sample in B imaged after acid hydrolysis with 2 M TFA (C). Congo red binding of the precipitate (D). PA14P$_{BAD}$*pel* was grown in the presence or absence of cellulase prior to ethanol precipitation. Pictures are the precipitate resuspended in water (E).

A

	Δ*pel*		P_{BAD}*pel*		P_{BAD}*pel* ppt	
	Mass (μg)	Mol %	Mass (μg)	Mol %	Mass (μg)	Mol %
Ara	3.4	3.5	0.7	0.8	0.7	1.9
Rha	9.6	9.0	3.4	3.7	15.5	38.8
Fuc	n.d.	-	n.d.	-	n.d.	-
Xyl	n.d.	-	n.d.	-	n.d.	-
GlcA	n.d.	-	n.d.	-	n.d.	-
Rib	5.0	3.9	1.5	1.4	8.2	17.3
Man	85.2	72.4	88.3	87.2	8.6	19.7
Gal	1.0	0.9	0.5	0.5	0.3	0.7
Glc	12.2	10.3	6.5	6.4	7.9	18.0
GalNAc	n.d.	-	n.d.	-	n.d.	-
GlcNAc	n.d.	-	n.d.	-	2.0	3.7
ManNAc	n.d.	-	n.d.	-	n.d.	-

B

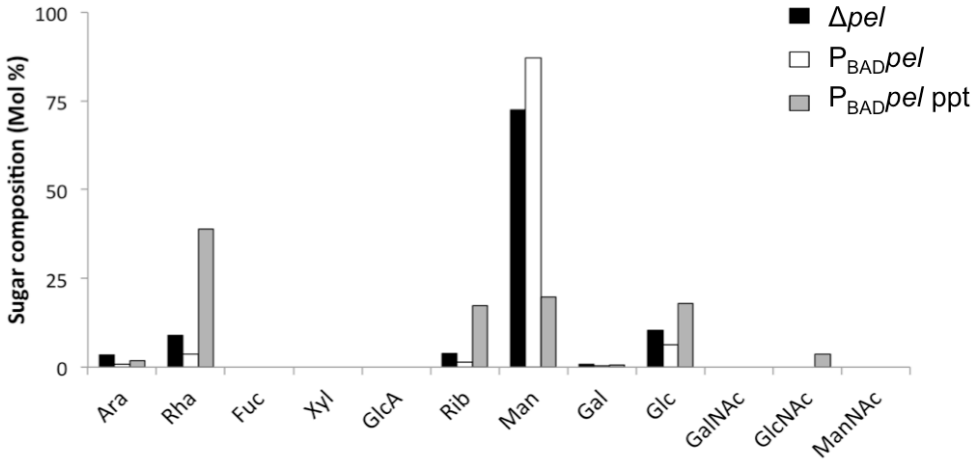

Figure 2. GC/MS analysis suggests Pel is glucose, ribose and rhamnose rich. The presence of 12 sugars were tested by GC/MS in three samples, Δ*pel* (PA14P_{BAD}*pel*Δ*pelF* soluble), P_{BAD}*pel* (PA14P_{BAD}*pel* soluble and insoluble fraction) and P_{BAD}*pel* ppt (PA14P_{BAD}*pel* insoluble precipitate washed). The raw numbers are shown in (A) and graphed in (B). Carbohydrate analysis performed by the Complex Carbohydrate Research Center at University of Georgia.

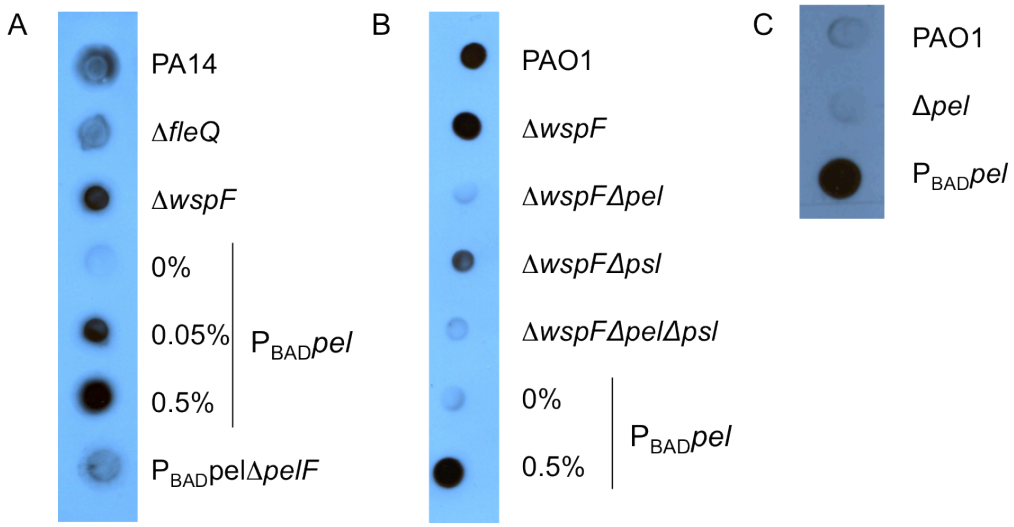

Figure 3. Pel antiserum specificity. Strains that have differential production of the Pel polysaccharide were tested with the Pel antiserum. Dot blots are shown for strain background PA14 (A) and PAO1 (B and C).

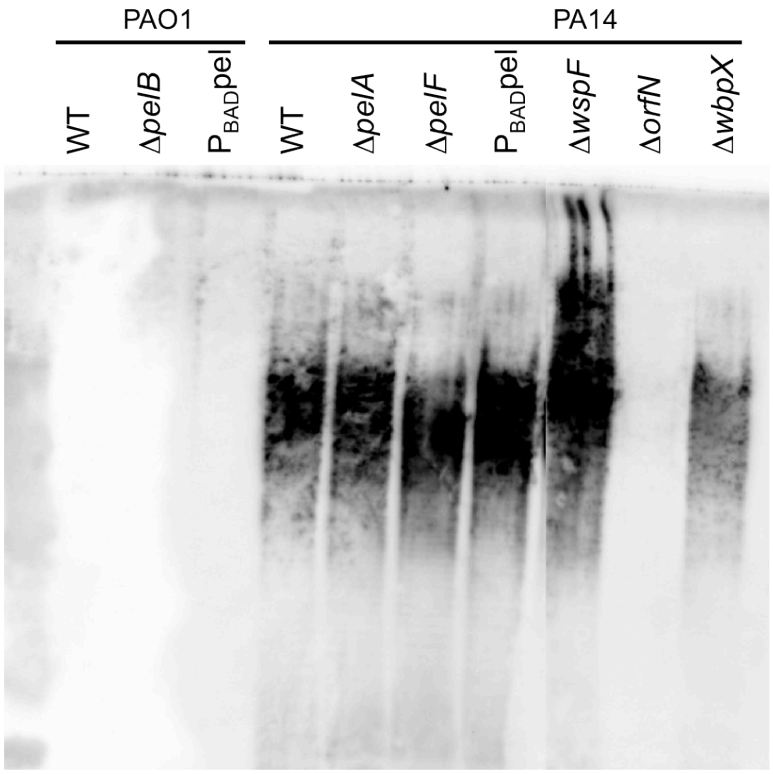

Figure 4. Pel antiserum reacts against PA14 LPS. LPS extracts from each strain were separated on a 12.5% polyacrylamide gel, transferred to a nitrocellulose membrane and probed for Pel antisera reactivity. Pel antisera is cross-reactive with PA14 LPS and not PAO1.

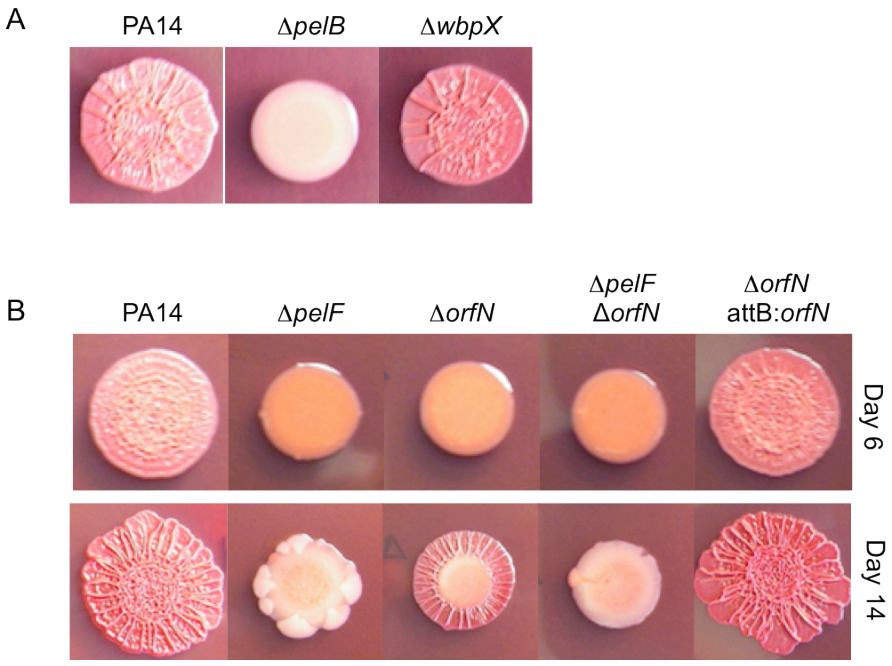

Figure 5. PA14Δ*orfN* is impaired in colony morphology. (A) Colonies were grown on T-broth + 0.5% arabinose for 6 d. (B) Colonies were grown for either 6 d (top panel) or 14 d (bottom panel).

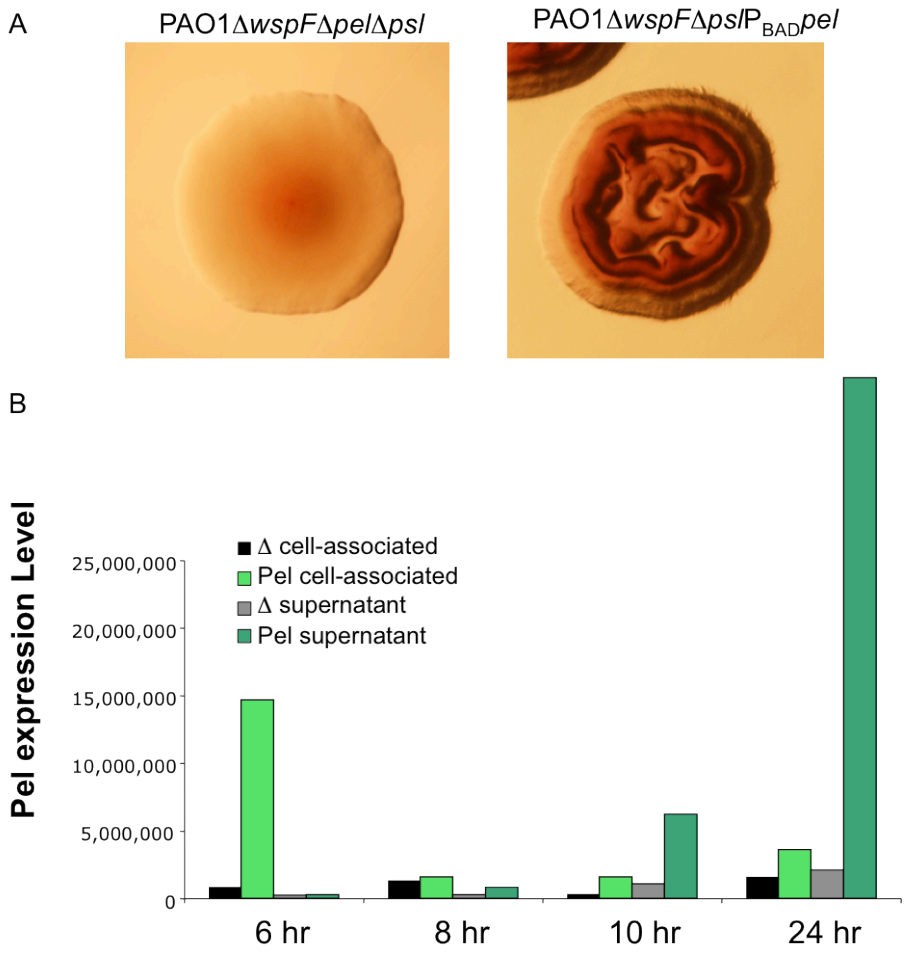

Figure 6. PAO1Δ*wspF*Δ*psl*P$_{BAD}$*pel* produces Pel in both the supernatant and cell-associated fractions. The colony morphology of PAO1Δ*wspF*Δ*psl*Δ*pel* and PAO1Δ*wspF*Δ*psl*P$_{BAD}$*pel* on agar plates supplemented with Congo red and Brilliant blue. Overexpressing *pel* results in a rugose colony morphology (A). Bacterial strains, Δ (PAO1Δ*wspF*Δ*psl*Δ*pel*) and Pel (PAO1Δ*wspF*Δ*psl*P$_{BAD}$*pel*), were analyzed for Pel reactivity throughout growth in LB. Both cell-associated and secreted fractions were analyzed for Pel reactivity with the antisera (B).

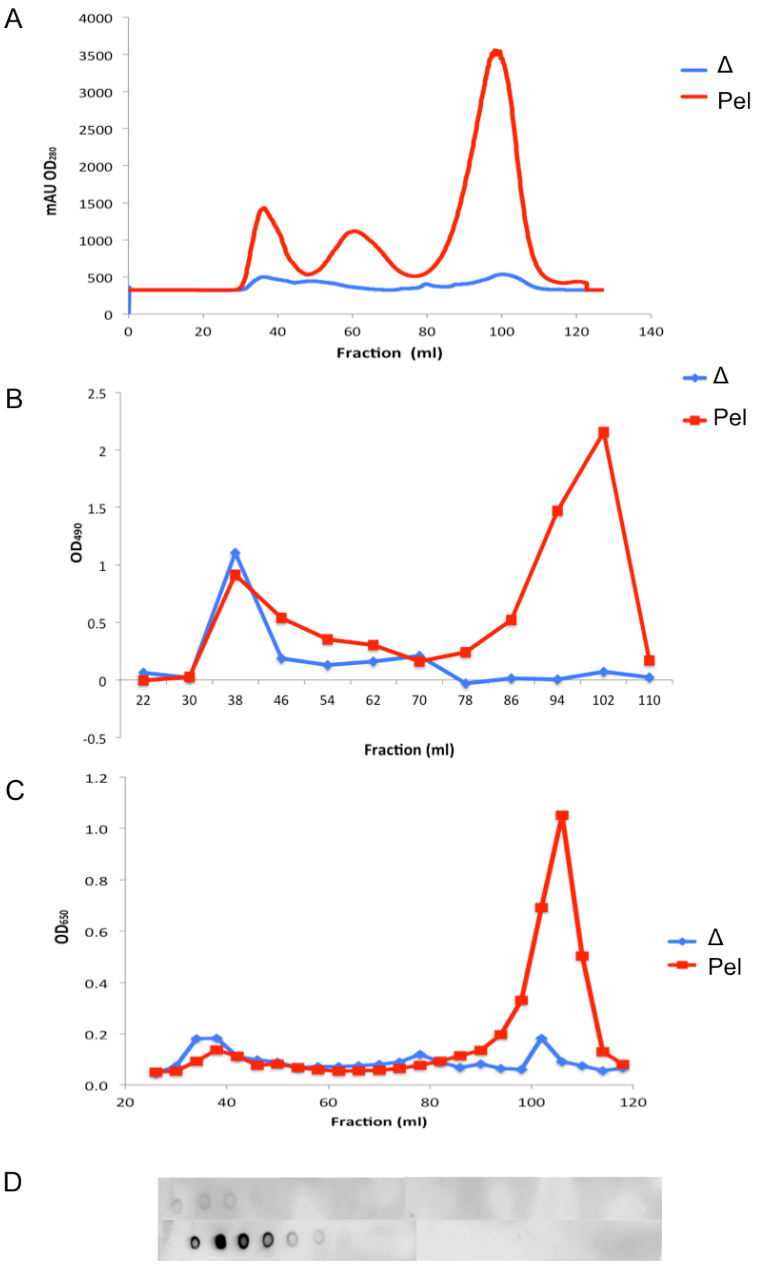

Figure 7. Elution profile of crude carbohydrate extracts. Polysaccharides were purified from Δ (PAO1Δ*wspF*Δ*psl*Δ*pel* in blue) and Pel (PAO1Δ*wspF*Δ*psl*P_{BAD}*pel* in red) and run on a Sephacryl S-200 size-exclusion column. Samples were measured for OD_{280} (A), neutral sugars (B), hexosamines (C) and reactivity towards Pel antiserum (D). The nitrocellulose blot is probing fractions from 22-120 off the size-exclusion column for PAO1Δ*wspF*Δ*psl*Δ*pel* (top) and PAO1Δ*wspF*Δ*psl*P_{BAD}*pel* (bottom).

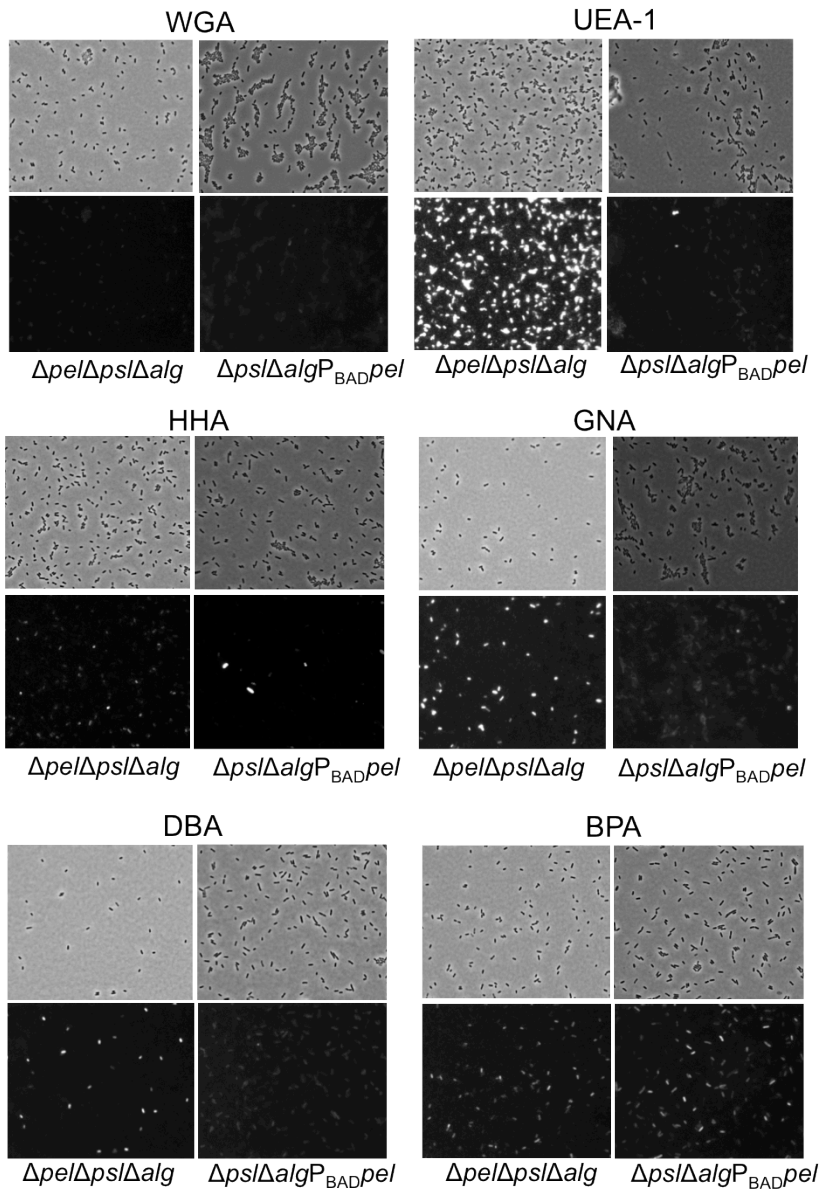

Figure 8. Lectin screen for Pel. Six fluorescent lectins (WGA, UEA-1, HHA, GNA, DBA, and BPA) were tested to see if they were Pel specific. The phase-contrast images are shown on the top panel and the fluorescent images are on the bottom. The two strains examined were PAO1Δ*pel*Δ*psl*Δ*alg* and PAO1Δ*psl*Δ*alg*P$_{BAD}$*pel*.

CHAPTER III:

Biochemical Characterization of Two Proteins Involved in Pel Synthesis

Part of this data published as: Marmont, L.S., Whitney, J.C., Robinson, H., Colvin, K.M., Parsek, M.R., and Howell, L.P. Expression, Purification, Crystalization and Preliminary X-ray analysis of *Pseudomonas aeruginosa* PelD. 2012. *Acta Crys*. F68, 181-184.

Part of this data submitted as: Whitney, J.C., Colvin, K.M., Marmont, L.S., Robinson, H., Parsek, M.R., and Howell, L.P. A Receptor for Biofilm Formation is a Degenerate Diguanylate Cyclase*. Submitted.*

Note: All crystallization experiments and ITC analysis were performed by Lynne Howell's lab from University of Toronto.

INTRODUCTION

The biosynthesis of complex carbohydrates, such as polysaccharides, involves multiple enzymatic reactions and transportation of the mature polysaccharide outside the cell membranes. Biosynthesis of extracellular polysaccharides can be divided into five different stages. Initially the precursor substrate is synthesized, which is often a nucleotide-linked sugar (243). This is followed by the polymerization of the precursor substrate onto the growing polysaccharide. The polysaccharide is transported to the periplasm where it is further modified and finally exported through the outer membrane (243).

Sugar precursors must be converted into nucleotide-linked sugars before they are recognized by specific glycosyltransferases and assembled onto a growing polymer chain. Different sugars are activated by different nucleotide triphosphate (NTP) to form nucleotide diphosphate (TDP) derivatives (79). Polysaccharide synthesis relies on a common pool of nucleotide-linked sugars, which are then further modified or directly incorporated into the growing polymer chain (193). To date, the biosynthesis pathways of more than 30 nucleotide sugars have been reported (79). *P. aeruginosa* can synthesize at least four products that rely on the common pool of nucleotide sugar precursors, including alginate, Psl, LPS and rhamnolipids (27, 193, 203, 261). Alginate synthesis begins with the common nucleotide sugar GDP-D-Man as a substrate for the enzyme AlgD, which converts GDP-D-Man to GDP-D-Mannuronate (63). Rhamnolipid synthesis requires dTDP-L-Rha. Psl synthesis requires GDP-D-Man, dTDP-L-Rha and UDP-D-Glc (27). LPS O-specific antigen is strain specific but in PAO1, O-specific antigen relies on dTDP-L-Rha and the common antigen relies on GDP-D-Man as the precursor of GDP-D-Rha. Inactivation of genes involved in the sugar nucleotide precursor of a specific polymer prevents polymer production (27).

There are two generalized mechanisms of polysaccharide synthesis (260). The first utilizes a lipid carrier, typically undecaprenyl phosphate (und-P), to transport sugar

residues in a block-wise manner across the inner membrane to the periplasm. Once in the periplasm the polymer grows by transferring the growing chain onto the nascent lipid carrier and is shuttled across the outer membrane. The second method of polysaccharide synthesis does not use a lipid carrier. Rather the polymer formation is initiated on an unknown acceptor molecule and extended by a processive glycosyltransferase in the cytoplasm. The polymer is then exported through an ABC transporter in the inner membrane and shuttled across the outer membrane by a similar mechanism as lipid-carrier synthesis.

The Pel synthesis machinery has been largely uncharacterized. However, each of the seven genes in the operon is required for Pel production (245). To date, only two proteins have been individually examined experimentally, PelC and PelD (117, 129, 244). Using these data and computational prediction software, a schematic for the localization and function of the individual Pel proteins were put forth (**Figure 1**)(63). The model more closely resembles alginate and cellulose biosynthesis than Psl or group 1 capsules from *E. coli* (63).

Similar to the cellulose biosynthesis pathway in *E. coli*, there does not appear to be gene products involved in the synthesis of the precursor substrate (197, 229). This suggests that the biosynthesis of Pel sugar-nucleotide precursors is derived from central metabolism. One example is AlgC, a phosphomannomutase required for the conversion from mannose-6-P to mannose-1-P (269). The *algC* gene (*PA5322*) is located within the LPS biosynthesis operon but is required for alginate, Psl, rhamnolipid and LPS production (27, 72, 173, 269).

Pel polymerization is suggested to begin with the only predicted glycosyltransferase PelF, which is also the only protein that localizes to the cytoplasm. Glycosyltransferases are enzymes that transfer the monosaccharide component of a high-energy nucleotide sugar donor (e.g. UDP-glucose) to a non-reducing end of an acceptor molecule (197). Acceptor molecules for glycosyltransferases are typically oligosaccharides, but proteins or lipids can also be glycosylated (197). PelF resembles enzymes of the

glycosyltransferase-4 (GT-4) family from the Carbohydrate-Active enZYmes database (CAZy) and is likely involved in polysaccharide polymerization. Structural homology indicates that PelF is a retaining glycosyltransferase with two Rossman-like domains, a common structural feature in enzymes involved in nucleotide binding (63). Retaining glycosyltransferases generate products with the same stereochemistry of the nucleotide-sugar donor (50). Since the *pel* operon only contains one predicted glycosyltransferase, the Pel polysaccharide may be a linear homopolymer or PelF could be the initiating glycosyltransferase involved in non-lipid linked OSA production.

Pel production is allosterically regulated by the secondary messenger c-di-GMP. Binding of c-di-GMP to the inner membrane protein PelD is essential for Pel production (129). C-di-GMP receptors are also found in the alginate and cellulose biosynthetic (151, 257). PelD is predicted to contain 4 transmembrane (TM) domains in the N-terminus and the C-terminus is located in the cytoplasm where it interacts with c-di-GMP and regulates polymer production (63). PelD contains a conserved inhibition site characterized by a RxxD motif and a degenerate GG[D/E]EF domain required for diguanylate cyclase catalytic activity.

The polymer is likely transferred across the inner membrane by two proteins, PelE and PelG. PelG is an inner membrane protein with 12 predicted TM domains and resembles a transport protein from the multidrug and toxic compound extrusion (MATE) family (63). MATE proteins primarily function as efflux pumps and use electrochemical gradients to drive substrate export (84). PelG's similarity to MATE proteins suggests that PelG may play a key role in exporting Pel across the inner membrane. PelE is the last inner membrane protein with two predicted TM domains. The majority of this protein, residues 90-320, is positioned in the periplasm. This C-terminal region contains multiple copies of the tetratricopeptide (TPR) motifs (63). Given that TPR motifs are involved in protein-protein interaction, PelE may function as a scaffold protein and help the assembly of a large multi-protein secretion machine (63).

The polysaccharide is then translocated through the periplasm and across the outer membrane by two proteins, PelB and PelC. PelB is the most likely candidate that Pel translocates through. The C-terminus of PelB is predicted to be rich in β-sheets in the C-terminus, a property of many outer membrane porins (63). The N-terminus is located in the periplasm and contains an extensive amount of TPR domains. One prediction is that PelB and PelE function as a structural scaffold for the assembly of the secretion complex and to protect Pel from degradation as it moves through the periplasm. The second outer membrane protein is PelC. While the exact function of this protein is unknown, PelC is essential for polymer production and predicted to be important in polysaccharide transport (117, 244).

The final protein, PelA, is located in the periplasm and has two predicted domains. The first is a glycoside hydrolase domain in the N-terminus and the second is a C-terminal carbohydrate esterase domain (63). It is speculated that PelA has a dual function. PelA could modify the polymer after polymerization by catalyzing the removal of O or N-acylation from the substituted carbohydrate. Deacetylation is a common polymer modification, including in alginate, cellulose or poly-β-1,6-N-acetylglucosamine, and in each case affects biofilm properties. In addition, PelA may also function as a Pel hydrolase and be required for determining polymer size and/or clearance of the polysaccharide from the periplasm. This function has been described before for alginate biosynthesis. If the multi-protein biosynthetic complex is not formed properly, AlgL degrades the alginate polymer into uronic acids (63).

In this study we characterize two proteins involved in Pel synthesis, PelD and PelF. The X-ray structure of PelD in its apo and c-di-GMP bound forms is presented. The structure reveals an N-terminal GAF (c**G**MP-specific phosphodiesterase, **a**denylyl cyclases and **F**hlA) domain and a C-terminal degenerate GGDEF domain that is missing several secondary structure elements normally found in enzymatically active DGCs. Residues from both the GGDEF domain and the GAF domain interact directly with c-di-GMP, however, only those in the GGDEF domain were found to be essential for ligand binding *in vitro*. Mutations to these essential c-di-GMP binding residues *in vivo* resulted in

abolishment of air-liquid pellicle formation that is characteristic of Pel polysaccharide production. Our results provide structural data that demonstrates that degenerate GGDEF domains can act as c-di-GMP receptors. Furthermore, PelD may act in an analogous manner to proteins in the alginate and cellulose secretion systems, Alg44 and BcsA, respectively, which have been proposed to control the biosynthesis and/or export of their respective polysaccharides upon c-di-GMP binding. In addition we have identified residues in the glycosyltransferase PelF that are necessary for *in vitro* binding of the UDP nucleotide. Mutations to these residues *in vivo* resulted in abolishment of wrinkly colony formation and pellicle development. Moreover, we identified a mutant in *galU*, which is unable to synthesize UDP-D-glucose, resulted in smooth colony formation, a Pel-dependent phenotype. This analysis has provided substantial insight on Pel biosynthesis.

RESULTS

PelD purification, crystallization and X-ray structure analysis.

A schematic depiction of the domain organization in PelD and the truncated cytoplasmic version used to purify PelD is shown (**Figure 2A and 2B**). The cytoplasmic region of the putative inner membrane protein from *P. aeruginosa*, $PelD_{156-455}$, has been expressed and purified to near-homogeneity using a Ni^{2+}-NTA column followed by size-exclusion chromatography (~99%). SDS-PAGE analysis revealed the protein was at its expected molecular weight of 36 kDa (**Figure 2C**). PelD eluted as a single peak (**Figure 2D**). Approximately 20 mg of purified His_6-$PelD_{156-455}$ could routinely be obtained per liter of cell culture. The purified protein was stable for two months and retained its ability to form crystals. Interestingly, the solubility of PelD was temperature dependent. When purified PelD was exposed to 4ºC or below the sample became opaque and the protein precipitates. At temperatures above 4°C the sample returns to its original state with no observable effects to the protein sample or its crystallizability.

PelD crystals were observed in medium with high concentrations of polyethylene glycol (PEG). The best crystals were obtained were from the following condition, 10% PEG 8000, 100 mM Tris, pH 7.0, 200 mM $MgCl_2$. This condition yielded crystals that grew as flat plates with sharp edges that took approximately 5 d to fully develop (**Figure 3A**). Diffraction-quality crystals were optimized by the adjustment of precipitant concentration and buffer pH. These conditions yielded crystals of identical size and morphology (**Figure 3B**). The crystals diffracted at 2.2 Å resolution. The final model was refined to an R_{work} of 19.6% and an R_{free} of 23.8%. These R-factors are a measure of agreement between the crystallographic model and the original X-ray diffraction data. An R factor greater than 50% implies that agreement between observed and calculated values is very poor, while a target R factor for a protein refined with data of 2 Å is 20%.

The overall structure of $PelD_{156-455}$ showed that the protein, as predicted, contains an N-terminal GAF domain and a C-terminal GGDEF domain (**Figure 3C**). A search of the Protein Data Bank indicates that the GAF domain had the highest structural similarity to the GAF domain of a putative two-component response regulator from the cyanobacterium *Nostoc* sp. PCC 7120. Following PelD's GAF domain is a short linker region (residues 309-317) that connects it to the GGDEF domain. Although this region is disordered in the crystal structure, the two domains still associate with one another through a 653 $Å^2$ interface, which is predominantly comprised of the interaction between the α4 helix of the GAF domain and the α1 helix of the GGDEF domain (**Figure 3D**). Notably, D305 and R330, which represent two of the most highly conserved residues among PelD homologs, form a salt bridge with one another at this interface suggesting that the interaction of the two domains may be critical for biological function and not an artifact of crystallization. Moreover, several hydrophobic residues (L165, I298, K340, K369 and K390) are solvent inaccessible as a consequence of this interface. The calculated Δ^iG for this interface is -6.3 kcal/mol suggesting that its formation is energetically favorable (118).

In functional diguanylate cyclases, the catalytic GGDEF residues required for activity are located between β2 and β3 strands. However, PelD contains the residues RNDEG at this

location, explaining the lack of diguanylate cyclase activity observed for this protein (**Figure 4A**)(129). Furthermore, when compared to the activated GGDEF domain from *Caulobacter crescentus* PleD in complex with its nucleotide ligand, GTPαS, it becomes clear that the structural elements involved in nucleotide binding are absent in PelD (**Figure 4B and C**). For example, PelD does not contain functionally equivalent residues to N335, D344, K442 and R446 of PleD, which are involved in nucleotide binding. The magnesium-coordinating residues in PleD (E370 and E371 of its GGEEF motif) are conserved in PelD (D378 and E379), however in the $PelD_{156-455}$ structure, they are found ~10 Å away from where they would be needed for substrate binding. A third magnesium-coordinating residue in PleD (D327) appears to be both conserved in sequence and location in $PelD_{156-455}$ (E348) and may represent an evolutionary relic. Despite these significant structural differences observed between the catalytically competent and degenerate active sites of PleD and $PelD_{156-455}$, the conserved RXXD motif is found between the α2 helix and β2 strand where the allosteric I-site of active diguanylate cyclases is normally located (**Figure 4B**).

Dimeric c-di-GMP binds the I-site of PelD.

To determine if the structure of PelD changed in the presence of c-di-GMP, new crystallization conditions of $PelD_{156-455}$ in the presence of c-di-GMP were screened. This new crystal form diffracted to 2.3 Å and refined to an R_{work} of 20.1% and an R_{free} of 25.2%, After structure determination by molecular replacement, electron density that resembled two mutually intercalated c-di-GMP molecules was clearly observable in the I-site of PelD and allowed for the straightforward placement of two c-di-GMP molecules into the structure (**Figure 5A**). Overall, no gross structural rearrangements were observed between the un-bound (apo) and bound (holo) forms of $PelD_{156-455}$ (Overall C_α RMSD of 1.6 Å). A C_α alignment of the apo and c-di-GMP bound GGDEF domains shows that the GAF domain undergoes a 14° rotation to facilitate ligand binding (**Figure 5B**), which slightly decreases the buried interface between the two domains from 653 $Å^2$ to 609 $Å^2$ (due to disruption of the S294/H338 interaction). This conformational change is relatively small compared to what has been observed for other c-di-GMP receptors such as *Vibrio cholerae* PlzD, which undergoes a 123° inter-domain rotation (10). Within the

I-site, two c-di-GMP molecules interact with one another through hydrogen bonds between the N1 and N2 atoms of the guanine bases and the oxygen atoms of the phosphate groups in the same manner observed previously for the ligand in the c-di-GMP bound structures of the GGDEF-containing proteins PleD from *C. crescentus* and WspR from *P. aeruginosa* (29, 51). In addition, the interaction between the conserved RXXD motif and c-di-GMP is similar to that seen in the PleD and WspR structures with hydrogen bonds existing between R367 and the guanine O6 atom and phosphate group, and between D370 and the N1 and N2 atoms of the guanine base (**Figure 5C**). Arg402, located on the α3 helix of the GGDEF domain also interacts with c-di-GMP through hydrogen bonds between its N_{ε} and $N_{\eta 1}$ atoms and the O6 and N7 atoms of guanine. R161 is the sole residue from the GAF domain that interacts with c-di-GMP through interactions with the phosphate group and the N7 atom of guanine. This inter-domain cross-linking by c-di-GMP observed between the GAF and GGDEF domains of the $PelD_{156\text{-}455}$ structure is similar to what is seen in the PleD structure where c-di-GMP interacts with both its GGDEF and Rec-like adapter domain. While domain immobilization through I-site binding serves to prevent the association of the GGDEF active half-sites in PleD, the significance of the inter-domain cross-linking observed in $PelD^{156\text{-}455}$ is not immediately obvious given the degeneracy of its GGDEF domain.

c-di-GMP binding is required for pellicle formation.

To determine the relative contribution of each of the c-di-GMP binding residues to ligand binding, isothermal titration calorimetry (ITC) was performed on wild-type $PelD_{156\text{-}455}$ as well as on R161A, D367A, R370A and R402A site-directed mutants (**Figure 6**). ITC is a method for measuring biomolecular interactions, such as protein-protein interactions and protein-small molecule interactions. When a protein binds to a small molecule heat is either generated or absorbed and ITC can directly measure the change in heat during the binding event and determine the binding parameters in a single experiment. In agreement with previous characterization, the wild-type protein bound c-di-GMP with moderate affinity (K_d of 1.9 μM)(129). In comparison, the R161A mutant showed a relatively modest but significant reduction in binding affinity (K_d of 4.9 μM). In agreement with previous surface plasmon resonance data, the R367A,

D370A and R402A mutants reduced the ligand binding affinity to below the detection limit of the calorimeter (129). These results demonstrate that most of the binding specificity for c-di-GMP resides in the GGDEF domain of PelD.

To examine the effect of c-di-GMP binding *in vivo* an unmarked, non-polar *pelD* deletion mutant was generated in *P. aeruginosa* PA14 and used for complementation studies. As expected, this mutant was deficient in both biofilm formation in a microtiter dish as well as pellicle formation in standing cultures (**Figure 7A** and **B**). When this mutant was complemented with *pelD* on a plasmid, wild-type levels of biofilm and pellicle were restored. However, when the *pelD* deletion mutant was complemented with the *pelD* gene containing the R367A, D370A or R402A point mutants, biofilm and pellicle formation were reduced to that of the non-complemented strain. Western blot analysis clearly shows that the lack of complementation is not due to lost of protein expression as comparable amounts of PelD are expressed in all cases (**Figure 7B**, bottom panel). These results correlate well with the ITC data and suggest that c-di-GMP binding is essential for Pel polysaccharide formation. Interestingly, complementation of the *pelD* deletion mutant with the *pelD* gene containing the R161A point mutant resulted in a partial recovery of biofilm formation. Additionally, pellicle formation was clearly observed in standing cultures although this phenotype was slightly delayed and some cells remained in a planktonic state. This intermediate phenotype, when taken together with the ITC data, suggests that R161 may act as a fine-tuning mechanism in that it is required for both the highest affinity binding of c-di-GMP to PelD *in vitro* as well as maximum biofilm production *in vivo.* However, when mutated it does not severely hinder binding or completely abolish biofilm and pellicle formation. The complete conservation of R161 across all PelD homologs lends further support to the functional importance of this residue. Lastly, complementation was performed with a construct containing the same boundaries as the crystallized fragment of PelD, $PelD_{156\text{-}455}$. Perhaps not unsurprisingly, this plasmid was unable to restore biofilm or pellicle formation confirming that the GAF-GGDEF containing fragment of PelD is insufficient for biological activity and the transmembrane domains of PelD are essential for function.

PelD is predicted to dimerize through coil-coil interactions.

The mechanism of PelD activation upon c-di-GMP binding is still unclear. $PelD_{156-455}$ underwent only minor structural rearrangements upon c-di-GMP binding. In addition, $PelD_{156-455}$ elutes as a monomer both in the presence (data not shown) and absence of c-di-GMP as analyzed by size-exclusion chromatography (**Figure 2**). These observations prompted us to utilize a bioinformatics approach to examine regions of the protein where overexpression and purification had proven unsuccessful. Analysis of the fourth transmembrane helix region using the coiled-coil prediction program MARCOIL (52) suggests that residues 129-153 (≥ 98% confidence level) form a coiled-coil motif implying that the oligomeric state of PelD *in vivo* may be dimeric (**Figure 8A**). The boundaries of the coiled-coil prediction lie just upstream of the α1 helix from the GAF domain, indicating that the coiled-coil may simply be an extension of this N-terminal helix (**Figure 8B**). Examining other crystal structures of GAF domains show they are often associated with α helical stalk domains (including coiled-coil motifs) (**Figure 8C**). The structure of a *P. aeruginosa* GAF domain of unknown function (PA5279) solved by the Joint Center for Structural Genomics contains an N-terminal coiled-coil that mediates dimerization of the protein. In addition, phosphodiesterase 2A from *H. sapiens* contains tandem GAF domains, both of which contain α helical stalk regions that form the homodimerization interface (177). These data suggest that PelD may regulate Pel synthesis through protein-protein interactions.

PelF purification, subcellular localization and preliminary crystallization trials.

PelF is predicted to be a cytoplasmic protein containing a glycosyltransferase domain located on the C-terminus (**Figure 9A**) (63). Full-length His_6-PelF was purified using a Ni^{2+}-NTA column followed by size-exclusion chromatography. This allele can complement a *pelF* mutation, indicating the fusion is still functional. PelF elutes as two peaks and their ratio changes between purification trials (**Figure 9B**). The size of the first peak corresponds to 142 kDa and the second to 56 kDa. SDS-PAGE analysis of the two peaks shows both peaks are purified near homogeneity (**Figure 9C**). PelF is predicted to be 56 kDa. These data suggest that PelF can oligomerize.

PelF is the only protein in the Pel complex predicted to localize to the cytoplasm (63). In order to experimentally verify that PelF localized to the cytoplasmic fraction, cells were fractionated for the cytoplasmic fraction and membrane fraction. PelF was only found in the cytoplasmic fraction for mid-log cells in PA14 (**Figure 10A**). PelC was a membrane control (244). Interestingly, overexpressing *pel* in either a PA14Δ*fleQ* (data not shown) or PA14P_{BAD}*pel* background altered PelF's subcellular localization pattern (**Figure 10B**). Overexpressing the *pel* operon resulted in a significant portion of PelF to be found in the membrane fraction. One hypothesis is that the Pel proteins form a complex during the synthesis of the Pel polymer. If this is the case, our subcellular fractionation data suggests that when Pel is being synthesized PelF moves from the cytoplasm to the membrane fraction to complete the Pel synthesis complex.

Crystal trials with full-length His_6-PelF were conducted. Purified protein was highly stable between 4-16°C and will precipitate at room temperature. Three conditions revealed small crystals. The first was 20% PEG 8000, 0.1 M citric acid, pH 5.0. The second was 50% PEG 400, 0.2 M lithium sulphate, 0.1 M sodium acetate, pH 5.1. The third was 20% PEG 3350, 0.2 M ammonium citrate, pH 5.0. Unfortunately, none of the crystals were suitable for diffraction analysis (data not shown).

Nucleotide sugar binding is required for PelF activity.

To gain insight on the potential function and residues required for activity, we took a bioinformatics approach. A Phyre analysis was conducted to identify homology to known structures. The top hit with 15% identity and 100% precision was to a CaZY type 4 glycosyltransferase, MshA from *Corynebacterium glutamicum*. MshA catalyzes the transfer of GlcNAc from UDP-GlcNAc to 1-l-myo-inositol-1-phosphate in the first step of mycothiol biosynthesis (248). PelF was modeled after MshA (**Figure 11A**). The predicted active site was modeled in the presence of a nucleotide sugar (**Figure 11B**). Three amino acids were predicted to be important in coordinating the activity of the nucleotide sugar donors, K330, E405 and E415. Sequence alignments to other

crystalized structures of GT4 glycosyltransferases demonstrate that these three amino acids are conserved (**Figure 11C**) (36, 76, 123, 181, 248).

In order to test whether these amino acids were required for PelF activity. Site-directed mutants were created on a plasmid expressing PelF. K330, E405 and E415 were each mutated to an alanine residue. Expression of wild-type PelF complements a *pelF* mutant for both colony morphology and pellicle formation (**Figure 12A**). Each site-directed mutant was incapable of complementing a *pelF* mutant, despite a similar level of protein expression (**Figure 12A** and **B**).

UDP-linked sugars are important in Pel synthesis.

In order to identify the nucleotide sugar specific to PelF and Pel synthesis two approaches were taken, one biochemical, the second genetic. The biochemical approach utilized purified PelF and performed ITC with potential nucleotide sugar donors. ITC was performed with Purified PelF and incubated with potential nucleotides including UDP, GDP, TDP, CMP and ADP. PelF showed a preferential interaction with UDP (**Figure 13**). The binding affinity constant, K_d, with UDP was 77 μM. Two UDP-linked sugars were tested for PelF binding affinity, UDP-Glc and UDP-GlcNAc. PelF had significantly reduced affinity towards UDP-GlcNAc, but did show a modest affinity towards UDP glucose albeit significantly reduced compared to UDP alone (data not shown). A second method of detecting protein-ligand interactions is differential scanning fluorimetry. Every protein has a specific melting temperature; an increase in melting temperature represents an increase in the thermal stability of a protein and serves as an indirect way to measure ligand binding. Based on the large shifts in melting temperature, PelF shows specificity for UDP and TDP (data not shown). These data sets suggest that PelF preferentially binds UDP-linked sugars and thus the PelF specific nucleotide sugar donor most likely contains UDP.

We also took a second approach using genetics. In the past few years, our knowledge of the genes predicted to be involved in the biosynthesis of nucleotide sugars has dramatically increased (79). Based on the ITC analysis and preliminary carbohydrate

data suggesting Pel to be glucose rich, we initially tested to see if UDP-D-Glucose was required for Pel production. UDP-glucose is synthesized in the common pool of nucleotide sugars. The gene required for the conversion of D-Glc-1-P to UDP-D-Glc is *galU*. The gene *galU* (PA14_*38350*) is found in a two-gene operon with another gene predicted to be UDP-Glc 6-dehydrogenase. The biosynthetic pathway for UDP-D-Glc, UDP-D-Gal, UDP-D-GlcA and UDP-D-GalA are shown (**Figure 14A**). A *galU* mutant was created and analyzed for colony morphology. PA14Δ*galU* displays smooth colony morphology similar to a *pel* mutant (**Figure 14B**). PA14P_{BAD}*pel*Δ*galU* is delayed for wrinkly colony morphology and displays an altered wrinkly phenotype. Changing the media to T-broth resulted in rugose colony development for both PA14Δ*galU* and PA14P_{BAD}*pel*Δ*galU*. However, the rugose colony morphology was delayed compared to the corresponding, wild-type strain (**Figure 14C**). A second phenotype associated with Pel production is biofilm development in a microtiter dish assay. PA14Δ*galU* is only slightly reduced in biomass whereas PA14Δ*pelA* was severely attenuated (**Figure 14D**). In addition, the PA14P_{BAD}*pel*Δ*galU* was arabinose responsive and increased the amount of biomass compared to the un-induced condition. These results demonstrate that *galU* is important in Pel-dependent colony morphology but not biofilm development.

To further evaluate gene products downstream of *galU*, mutants were created that were unable to synthesize UDP-D-glucuronic acid. The importance of UDP-D-glucuronic acid is apparent considering the downstream polymers that use the compound or its descendants, such as UDP-xylose, UDP-arabinose and UDP-galacturonic acid (98). In PAO1, two genes (*PA2022* and *PA3559*) encode functional UDP-Glc dehydrogenase proteins (98). The homologues in PA14 were mutated, PA14_*18300* and PA14_*38360*, and assessed for colony morphology. No differences in the single mutants or double mutant were observed (**Figure 15**).

Gene products involved in dTDP sugar synthesis were also examined for Pel production. The biosynthetic pathway for the production of dTDP-L-rhamnose (dTDP-L-Rha) is well characterized and begins with the conversion of D-Glc-1-P and dTTP to dTDP-D-Glc, performed by RmlA (PA14_68200) (**Figure 16A**) (79). Despite many attempts, I was

unsuccessful in constructing a *rmlA* mutant in PA14. Unpublished work from Pradeep Singh's lab had determined that in PAO1, LPS O-antigen mutants were susceptible to killing by their own self-produced R2-pyocin. This works was confirmed by the van Delden lab who demonstrated that the O-antigen provided a shield to the receptor sites found on the LPS outer core (122). We hypothesized that a PA14Δ*rmlA* would be unable to synthesize O-antigen since L-Rha is one of the three sugars found in PA14 OSA and thus be killed by its own R-pyocins (43). Using a strain background that was unable to synthesize R-pyocins, PA14:*prtR* S153A, a *rmlA* mutant was easily generated. However, no differences in colony morphology were detected between the wild-type and *rmlA* mutant (**Figure 16B**).

Lastly, I examined gene products involved in GDP sugar synthesis. Since our initial analysis of Pel composition suggested Pel could be rhamnose rich, I focused on GDP-D-Rha. The biosynthetic pathway for the production of GDP-D-Rha is outlined (**Figure 17A**)(79). GDP-D-Rha is converted from GDP-D-Man in a two step pathway requiring Gmd (PA14_71990) and Rmd (PA14_72000) functions (79). In-frame mutation of *rmd* resulted in a change in colony morphology (**Figure 17B**). In both a PA14 and PA14P_{BAD}*pel* strain background, the colonies displayed elevated wrinkles that were more defined compared to the corresponding wild-type. These results suggest that Pel production is not compromised and could possibly be overexpressed.

DISCUSSION

The Pel synthesis complex is predicted to be composed of seven proteins. In this study we characterized two, PelD and PelF. PelD is a c-di-GMP receptor that participates in the regulation of Pel synthesis. PelD was expressed, purified and crystalized in the presence and absence of c-di-GMP. Three amino acids were demonstrated to be essential for c-di-GMP binding and Pel production. A mutation in one amino acid, R161, resulted in a decreased affinity for c-di-GMP and this translated to delayed pellicle development and reduced biofilm biomass. PelF is a glycosyltransferase that most likely participates in the first step of Pel synthesis. PelF was expressed, purified and examined for the ability

to bind particular nucleotide sugars. PelF binds UDP with the highest affinity. In addition, we identified a few mutations, which altered Pel-dependent phenotypes, namely *galU* and *rmd*.

The cytoplasmic region of the putative inner membrane protein, $PelD_{156-455}$ was expressed, purified and crystalized. The structure encompasses the GGDEF domain and GAF domain and demonstrates that degenerate GGDEF domains also function as c-di-GMP receptors. Interestingly, unlike the degenerate EAL domains of FimX and LapD, which bind the monomeric dinucleotide at their degenerate active sites, PelD utilizes the allosteric I-site commonly found in active DGCs to bind dimeric self-intercalated c-di-GMP. This mode of binding has also been observed in the product-inhibited structures of the DGCs PleD and WspR. It has been proposed that c-di-GMP dimerization and I-site binding sets the upper concentration limit of c-di-GMP in the cell by preventing further biosynthesis (29, 51). The inhibition constants (K_i) for c-di-GMP binding to the I-site of both PleD and another active DGC, *C. crescentus* DgcA, are both in the range of ~1 μM (35), which is similar to the measured c-di-GMP dissociation constant for PelD (1-2 μM).

Since PelD acts as a receptor c-di-GMP, we hypothesized that the binding of c-di-GMP to the GGDEF domain would induce a conformational change. However the apo and holo forms of $PelD_{156-455}$ resulted in minor structural rearrangements. We now speculate that c-di-GMP binding may result in PelD dimerization of the predicted coil-coil domains. Dimerization may subsequently regulate the Pel polymerase activity of PelF through protein-protein interactions in an analogous manner as to the proposed alginate and cellulose secretion systems (97, 151, 171). Alginate polymerization is carried out by the inner membrane protein Alg8, which contains four transmembrane domains and a cytoplasmic family 2 glycosyltransferase domain (171, 191). The ability of Alg8 to synthesize alginate is dependent on the c-di-GMP binding activity of the PilZ domain in Alg44 and thus it has been proposed that Alg8 and Alg44 act in concert as a co-polymerase to not only synthesize alginate but also facilitate its transport across the inner membrane. In the bacterial cellulose export apparatus, BcsA is a large inner

membrane protein that contains both a family 2 glycosyl transferase domain and a c-di-GMP binding PilZ domain in the cytoplasm (199). Although PelD contains a degenerate GGDEF domain instead of a PilZ domain, it may play a functionally equivalent role in Pel polymerization and export.

Full-length PelF was expressed and purified. Two biochemical methods were attempted to identify the nucleotide sugar that binds to PelF, ITC and DSF. In both cases, PelF displayed a preference for UDP nucleotides. Follow-up experiments tested two UDP nucleotide sugars, UDP-D-Glc and UDP-D-GlcNAc for binding kinetics. Neither bound as tightly as UDP alone. One explanation is that PelF transferase activity is occurring in the presence of UDP sugars. For many glycosyltransferases water can serve as the accepting molecule and can potentially analyze the catalysis reaction of the nucleotide sugar. If this is the case, the combined binding and catalysis reactions have the potential to interfere with the ITC results.

A second approach used genetics to see if we could identify the nucleotide sugar precursor. The theory was a mutant incapable of generating the sugar precursor would be incapable of synthesizing Pel. This approach has been used to identify the nucleotide sugar precursors in both Psl and alginate (27, 63). In this study we demonstrated that a *galU* mutant is significantly delayed in colony morphology. One explanation is that Pel requires UDP-D-Glc or a downstream product for synthesis. The fact that the *galU* mutant eventually forms a wrinkly colony is perplexing. One hypothesis is that a second gene on the *P. aeruginosa* chromosome can complement the *galU* defect. It has been noted that nucleotide sugar biosynthesis proteins are difficult to predict function from sequence (79). A follow-up mass spectrometry analysis is needed to confirm the presence or absence of UDP-D-Glc from the *galU* mutant to determine if UDP-D-Glc is missing. A second hypothesis is that nutrient rich medium such as tryptone broth or LBNS provides the sugar nucleotide to cells exogenously. Perhaps examining colony morphology and biofilm development in defined media may prove to be a more clear strategy. A third explanation for the delayed colony morphology is that *galU* is important for LPS production and it is loss of LPS production, not Pel, that is

responsible for changes in colony morphology. Thus, a *galU* mutant may not affect Pel production but rather change other polymers that are important for in colony morphology. Wrinkly colony morphology requires Pel production but it may not be sufficient.

Future work will continue to identify the sugar nucleotide required for Pel synthesis. In addition, expression, purification and crystallization trials are being performed for the remaining five proteins in the Pel complex. Site-directed mutagenesis will identify key structural and functional residues involved in polymer synthesis. A complete characterization of the Pel biosynthetic complex will greatly enhance our knowledge about fundamental carbohydrate production and provide insight on a polymer important for biofilm formation by the opportunistic pathogen, *P. aeruginosa*.

MATERIALS AND METHODS

Strain Construction.

Bacterial strains in this study are listed in **Table 1.** For routine culture, *P. aeruginosa* strains were grown at 37°C in Luria-Bertani (LB) medium (Difco). Plasmids were selected with 100 μg/ml gentamycin or 300 μg/ml carbenicillin for *P. aeruginosa* strains and 10 μg/ml gentamycin or 100 μg/ml ampicillin for *E. coli*. 25 μg/ml irgasan was used to counter select for *E. coli*.

DNA manipulations were performed using standard techniques. Allelic replacement strains were constructed by using an unmarked, non-polar deletion strategy. Flanking regions of gene of interest were amplified using primers two primer sets and digested with restriction enzymes. The resultant PCR product was ligated into the suicide vector, pEX18Gm, via complementary restriction site. The plasmid was verified by sequencing analysis. Single recombination mutants were selected on LB containing 100 μg ml^{-1} gentamicin and 25 μg ml^{-1} irgasan. Double recombination mutants were selected with LB without NaCl containing 10% sucrose and confirmed by PCR.

pPelD

The *pelD* complementation plasmid was constructed by digesting the PCR product generated from the *pelD* WT primer set with HindIII and SacI. The PCR product was ligated into pUCP18. The plasmid was verified by sequencing. The same strategy was taken when generating the truncated mutant pPelD 156-455 except using the *pelD* 156 F primer instead of *pelD* WT F.

pPelF

The pelF complementation plasmid was constructed by digesting the PCR product generated from the *pelF* WT primer set with HindIII and SacI. The PCR product was ligated into pUCP18. The plasmid was verified by sequencing.

Site-directed Mutants

The R161A, R367A, D370A and R402A point mutants were generated from the pPelD plasmid by site-directed mutagenesis (Stratagene). The K330A, E405A and E413A point mutants were generated from the pPelF plasmid by site-directed mutagenesis (Strategene). Each plasmid was verified by sequencing.

Microtiter dish biofilm.

96-well microtiter dish assay was preformed as described previously with the following modifications (155, 170). 100 μl of mid-log cells (OD_{600} ~ 0.5) grown in LB was added to the wells of a 96-well polypropelene plate (Nunc) and incubated statically for 24 h at 25°C. Following incubation, non-attached cells were removed and the plate was rinsed thoroughly with water. Plates were stained with 150 μl 0.1% crystal violet for 10 min. The plate was rinsed and adhered crystal violet was solubilized in 200 μl 95% ethanol for 10 min, then 100 μl was transferred to a new 96-well plate to measure the absorbance at OD_{595}.

Pellicle assays.

Mid-log cells (OD_{600} ~ 0.5) grown in LBNS (LB without NaCl) were diluted 1/100 in 3ml LBNS broth in a glass tube and left undisturbed at 25°C. Pellicles were monitored by visual inspection between four and ten d. Complete coverage at the air-liquid interface of an opaque layer of cells is considered to be indicative of pellicle formation (64).

Colony morphology.

Overnight cultures grown in LB medium were diluted 1/100 and 5 μl spotted onto agar medium and incubated at 25 °C for 14 d. Agar medium was either LB without NaCl (LBNS) supplemented with 40 μg/ml Congo red and 15 μg/ml brilliant blue R or Tryptone plates (T-broth with 1% bacto agar) supplemented with 40 μg/ml Congo red and 15 μg/ml brilliant blue R (Sigma).

Western blot analysis

1 ml of mid-log cells (OD_{600} ~ 0.5) grown in LB were harvested and resuspended in 250 μl PBS. 50 μl sample was mixed with 50 μl 2x laemmli buffer and boiled for five m. Protein concentration was measured using the Pierce 660 nm Protein Assay and Ionic Detergent Compatibility Reagent as described by the manufacturer (Thermo Scientific). Equal total protein was loaded onto a pre-cast 12.5% Tris-HCl polyacrylamide gel and transferred to a PVDF membrane for immunoblotting (Bio-rad). The membrane was blocked in 5% non-fat milk in TBST for 1 h at 25°C. The membrane was subsequently probed with an absorbed α-PelD antibody at 1:1,000 dilution in 1% non-fat milk TBST for 1 h. Blots were developed with goat α-rabbit HRP-conjugated secondary antibody (Thermo-Scientific) and Pierce detection kit.

Antibody production and absorption

Purified PelD protein was used to generate antiserum from rabbits using a 70-day standard protocol (Open Biosystems). Antiserum was absorbed using PA14Δ*pelD* lysates. Lysates were generated from 100mls of PA14Δ*pelD* grown to late-log (OD_{600} ~ 1.0). Cells were centrifuged and resuspended in 3ml of lysis buffer (50mM Tris, pH 8.0, 10mM EDTA, pH 8.0). Cells were lysed by 3 freeze/thaw cycles followed by sonication

and centrifugation. The cell lysate was subsequently used for absorption by mixing 20 μl α-PelD antisera, 75 μl PelD lysate in 1ml of 5% non-fat milk in TBST. The antiserum was absorbed for 4 h at 25°C under constant rotation.

Protein purification

His_6-$PelD_{156-455}$.

The cell pellet from 2 one liter bacterial cultures was thawed and resuspended in 80 ml buffer A (50 mM Tris, pH 8.0, 300 mM NaCl, 10% glycerol, 1 mM tris(2-carboxyethyl)phosphine (TCEP) containing one SIGMAFAST EDTA-free protease-inhibitor cocktail tablet (Sigma). The resuspension was then lysed by French press and the soluble fraction was loaded onto a Ni^{2+}-NTA column pre-equilibriated with buffer A supplemented with 5 mM imidazole. Bound protein was washed and subsequently eluted with buffer A supplemented with 250 mM imidazole. SDS-PAGE analysis revealed the protein was ~95% pure and appeared at its expected molecular weight of 36 kDa. Fractions containing PelD were pooled and concentrated on a 30 kDa molecular weight cutoff Amicon spin column (Millipore). PelD was further purified and buffer-exchanged into buffer B (20 mM Tris, pH 8.0, 150 mM NaCl, 10% glycerol, 1 mM DTT) by size-exclusion chromatography on a HiLoad 1600 Superdex 200 gel-filtration column (GE healthcare). All PelD containing fractions were pooled and concentrated as described above.

Full-length PelD

The cell pellet from one liter bacterial culture was thawed and resuspended in 20 ml buffer C (50 mM Tris, pH 7.5, 250 mM NaCl, 10% glycerol, 400 mg lysozyme, one EDTA-free protease-inhibitor cocktail tablet (Sigma). The resuspension was then by sonication and the soluble fraction was loaded onto a Ni^{2+}-NTA column pre-equilibriated with buffer C supplemented with 10 mM imidazole. Bound protein was washed and subsequently eluted with buffer C supplemented with 250 mM imidazole.

Subcellular fractionation.

For PA14 and PA14Δ*pelF* strains were grown in 50 mls of LB to OD_{600} 0.6 at 37°C. Cells were pelleted and resuspended in 2 mls of lysis buffer (50 mM Tris, pH 7.5, 150 mM NaCl, 1 mg/ml lysozyme, 5 mM β-mercaptoethanol, Complete EDTA-free protease inhibitor (1 tablet per 10 ml lysis buffer)). Cells were lysed by three freeze/thaw cycles in a dry-ice ethanol bath followed by sonication. Cell debris and unlysed cells were removed by centrifuged at 13,000 g for 10 m. This was the whole cell fraction. The sample was further centrifuged at 55,000 g for 1 h. The supernatant was the cytoplasmic fraction and the pellet was the membrane fraction. The pellet was resuspended in lysis buffer. For PA14P_{BAD}*pel* and PA14P_{BAD}*pel*Δ*pelF* cells were grown in 50 mls of LB + 0.5% arabinose for 6 h at 37°C. Fractions were harvested the same as described above.

Crystalization Trials

Purified PelD was concentrated to 10 mg mL^{-1} and crystallized by the hanging drop vapor diffusion technique. Diffraction quality crystals belonging to the orthorhombic space group $P2_12_12$ were grown in 10% (w/v) PEG 8000, 0.1 M Tris-HCl pH 7.5 and 0.2 M $MgCl_2$. Crystals were cryoprotected with the crystallization solution supplemented with 20% (v/v) ethylene glycol prior to flash freezing. X-ray diffraction data were collection at the selenium peak on beam line X29 at the NSLS (Brookhaven National Laboratory) and processed with the HKL2000 software program (175). A total of six (out of six) selenium sites were located using HKL2MAP (178), and density modified phases were calculated using SOLVE/RESOLVE (232). The resulting solvent flattened Se-SAD map was of reasonable quality and allowed for manual model building in COOT (59). The model was then refined against the native data using PHENIX.REFINE (1) to a final R_{work}/R_{free} of 19.6% and 23.8%.

$PelD^{156-455}$ in the presence of 2.5 mM c-di-GMP (without any pre-incubation of the protein and ligand) was rescreened for crystallization conditions using commercially available sparse matrix screens. Diffraction quality crystals of $PelD^{156-455}$ in complex with c-di-GMP were obtained in 22% w/v PEG 8000, 0.1 M sodium cacodylate pH 6.1 and 0.2 M ammonium sulfate. As per the apo form of the protein, crystals of the complex

were cryoprotected in crystallization solution supplemented with 20% (v/v) ethylene glycol prior to flash freezing and data were collected at beam line X29. Data were processed using HKL2000 and the structure determined using the PHENIX AutoMR wizard. The final model was refined to an R_{work}/R_{free} of 20.1% and 25.2%.

All structural alignments were performed using the secondary-structure matching (SSM) algorithm in COOT. Structural illustrations were generated in Pymol (Schrödinger). Analysis of protein interfaces was performed using the Protein Interfaces, Surfaces and Assemblies (PDBePISA) server provided by the European Bioinformatics Institute (118). Prediction of the coiled-coil region of PelD was carried using the MARCOIL server provided by the Max Planck Institute for Developmental Biology (52). Interdomain motions were assessed using the DynDom Protein Domain Motion Analysis server (184).

Isothermal titration calorimetry.

For the ITC experiments, the PelD protein samples and c-di-GMP were prepared in 20 mM Tris-HCl, 150 mM NaCl, 10% (v/v) glycerol, 1 mM DTT. Titrations were carried out with 250 μM c-di-GMP in the syringe and 25 μM solution of the indicated PelD sample in the cuvette. For PelF samples, PelF and nucleotide ligands were prepared in 20 mM Hepes, pH 4.5, 150 mM NaCl, 10% glycerol and 10 mM DTT. Titrations were carried out with 3 mM nucleotide or 1 mM for GDP in the syringe and 60 μM solution of PelF sample in the cuvette. ITC measurements were performed with a VP-ITC microcalorimeter (MicroCal Inc., Northampton, MA). Each titration experiment consisted of twenty-five 10 μL injections with 180 second intervals between each injection. The heats of dilution for titrating ligand into buffer were subtracted from the sample data prior to analysis. The ITC data were analyzed using the Origin v5.0 software (MicroCal Inc., Northampton, MA) and fit using a single-site binding model.

Table 1 Strains used in Chapter III

Strains	Relevant Characteristics	Reference
PA14	wild-type	Rehme et al., 1995
PA14P_{BAD}*pel*	*Pel* over-expression strain	This study
PA14Δ*pelD*	*pelD* nonpolar mutant	This study
PA14Δ*pelD* pUCP18	pUCP18 multi-copy plasmid	This study
PA14Δ*pelD* pPelD	Full-length PelD expressed by pUCP18	This study
PA14Δ*pelD* pPelD R161A	Site-directed mutant of pPelD, R at aa position 161 switched to A	This study
PA14Δ*pelD* pPelD R367A	Site-directed mutant of pPelD, R at aa position 367 switched to A	This study
PA14Δ*pelD* pPelD R370A	Site-directed mutant of pPelD, D at aa position 370 switched to A	This study
PA14Δ*pelD* pPelD R402A	Site-directed mutant of pPelD, R at aa position 402 switched to A	This study
PA14Δ*pelD* pPelD$_{156\text{-}455}$	Truncated PelD mutant expressing aa 156-455	This study
PA14Δ*pelF* pUCP18	pUCP18 multi-copy plasmid	This study
PA14Δ*pelF* pPelF	Full-length PelD expressed by pUCP18	This study
PA14Δ*pelF* pPelF K330A	Site-directed mutant of pPelF, K at aa position 330 switched to A	This study
PA14Δ*pelF* pPelF E405A	Site-directed mutant of pPelF, K at aa position 405 switched to A	This study
PA14Δ*pelF* pPelF E415A	Site-directed mutant of pPelF, E at aa position 415 switched to A	This study
PA14Δ*galU*	*galU* nonpolar mutant	This study
PA14P_{BAD}*pel*Δ*galU*	*galU* nonpolar mutant	This study
PA14Δ*18300*	*18300* (PA2022 homologue) nonpolar mutant	This study
PA14Δ*38360*	*38360* (PA3559 homologue) nonpolar mutant	This study
PA14Δ*18300*Δ*38360*		This study
PA14:*prtR* S153A	Does not produce R2 pyocins	Jon Penterman
PA14:*prtR* S153A Δ*rmlA*	*rmlA* nonpolar mutant	This study
PA14Δ*rmd*	*rmd* nonpolar mutant	This study
PA14P_{BAD}*pel*Δ*rmd*	*rmd* nonpolar mutant	This study
BL21	*E. coli* expression strain	Novagen
BL21 pET20b(+) PelF	C-term His-tag PelF expression strain	This study
BL21 pET28a(+) PelD$_{156\text{-}455}$	N-term His-tage PelD truncated expression strain	This study

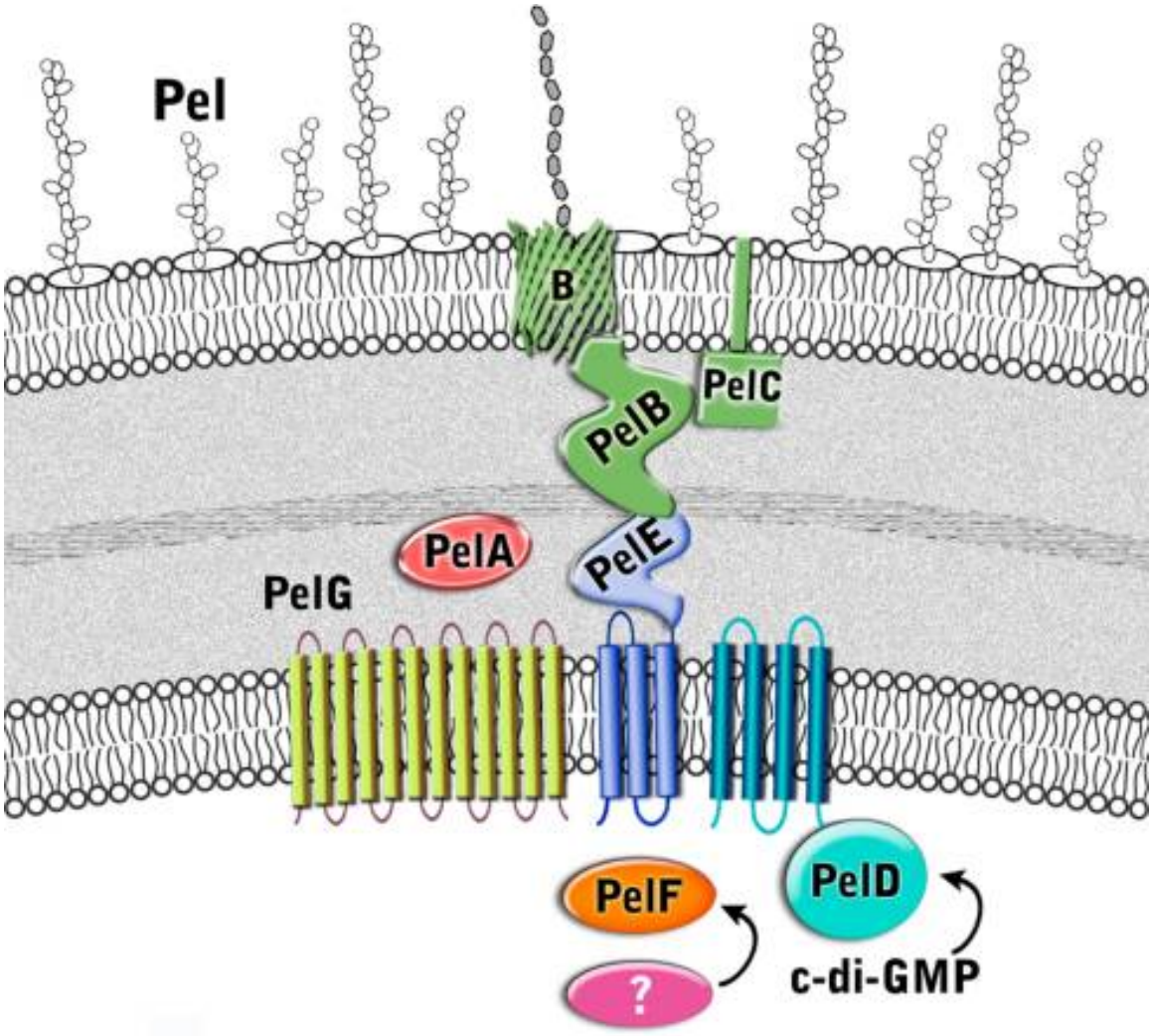

Figure 1. Proposed structure of the Pel biosynthetic complex. Figure taken from Franklin MJ, et al. 2011. *Front. Microbiol*. 2:167 (63).

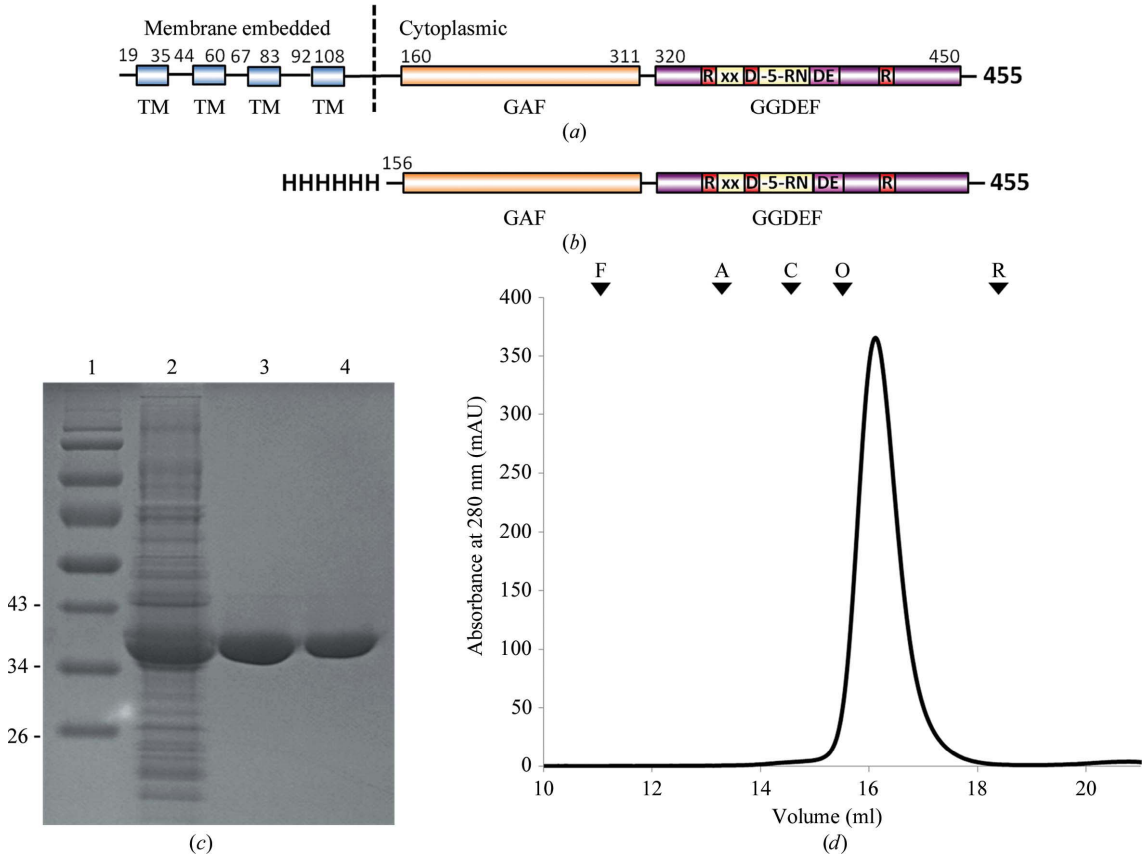

Figure 2. PelD domain organization and purification. (A) Schematic diagram of the domain organization of PelD. The boundaries of the transmembrane (TM) segments and the GAF and GGDEF domains are denoted above the schematic and were predicted using HMMTOP and Phyre2, respectively. (B) Schematic diagram of the His_6-$PelD_{156–455}$ construct using in this study. (C) SDS–PAGE analysis of His_6-$PelD_{156–455}$ during expression and purification. Lane 1, molecular-weight markers (kDa); lane 2, soluble cell lysate; lane 3, purified His_6-$PelD_{156–455}$ after nickel-affinity chromatography; lane 4, following size-exclusion chromatography. (D) Size-exclusion chromatogram of His_6-$PelD_{156–455}$. Protein standards used to calibrate the column are indicated by inverted triangles; F, ferritin; A, aldolase; C, conalbumin; O, ovalbumin; R, ribonuclease A. The molecular weights of ferritin, aldolase, conalbumin, ovalbumin and ribonuclease A are 440, 158, 75, 43 and 13.7 kDa, respectively. Figure taken from Marmont LS, et al. 2012 *Acta Crys*. F68 (142).

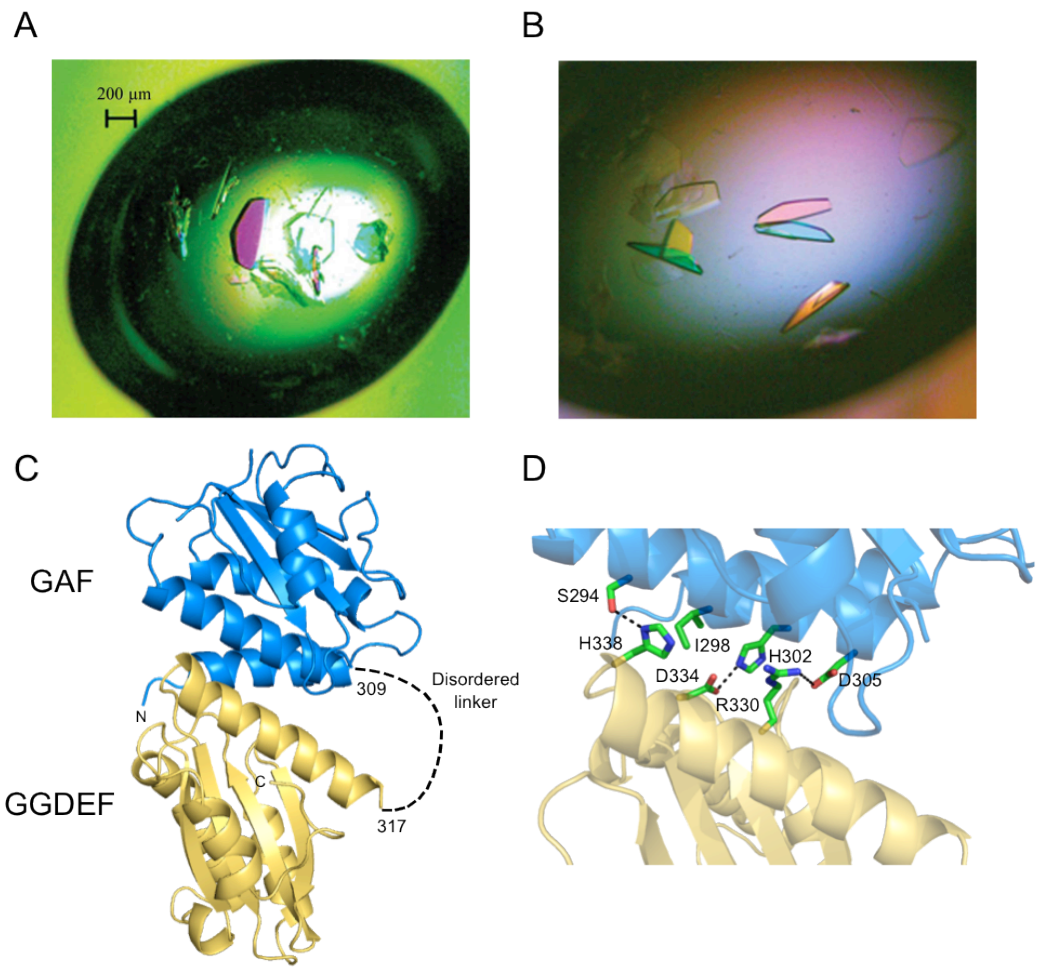

Figure 3. X-ray structure of His_6-$PelD_{156–455}$. Crystal of His_6-$PelD_{156–455}$ grown initially from Wizard 2 condition No. 43 (A) and crystal obtained after optimizations (B) The optimized crystals were grown in 11.5%(w/v) PEG 8000, 100 mM Tris–HCl pH 7.5, 200 mM $MgCl_2$. The overall structure of $PelD^{156-455}$ is displayed in cartoon representation (C). The GAF and GGDEF domains are shown in blue and yellow, respectively. The locations of the N- and C- termini are indicated with N and C, respectively. The disordered linker region (residues 309-317) is indicated by the black dashed line. (D) Stick representation of the residues involved in interactions between the GAF and GGDEF domains. Carbon, nitrogen and oxygen atoms are colored green, blue and red, respectively. Figure adapted from Figure taken from Marmont LS, et al. 2012 *Acta Crys*. F68 and Whitney JC, et al. *submitted* (142).

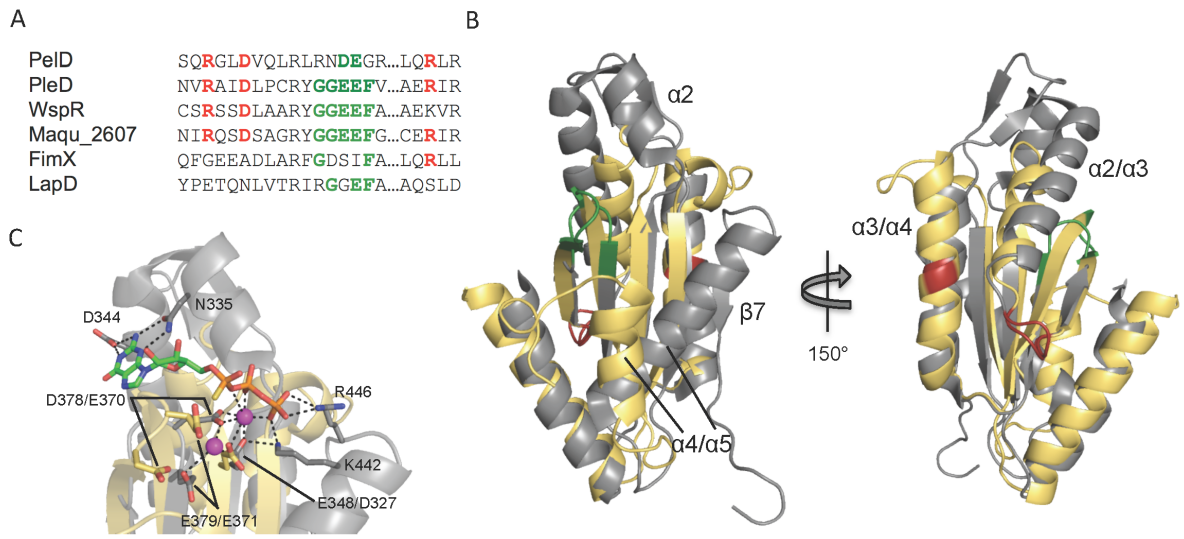

Figure 4. PelD contains a degenerate GGDEF domain with a conserved I-site. (**A**) Multiple sequence alignment of the GGDEF and I-site residues (or lack thereof) found in the GGDEF domains of *C. crescentus* PleD, *P. aeruginosa* WspR, *M. aquaeolei* Maqu_2607, *P. aeruginosa* FimX and *P. fluorescens* LapD. The alignments are based on three-dimensional superposition using the secondary-structure matching (SSM) algorithm in COOT. The catalytic and I-site residues are indicated in green and red, respectively. (**B**) Structural comparison of the GGDEF domains of PelD and the active DGC PleD as shown from two opposing views. The structures are shown as a cartoon representation with PleD displayed in grey and PelD displayed in yellow. In the left panel, secondary structure elements in PelD that are not present (α2 and β7) or are displaced significantly (α4/α5) compared to those found in canonical GGDEF domains, such as in PleD, are labeled. In the right panel, secondary structure elements that contain (α3/α4) or are adjacent to (α2/α3) the conserved I-site residues are indicated. In both structures, the catalytic and I-site residues are colored green and red, respectively. (**C**) Comparison of the active site of PleD in complex with GTPαS and PelD. Single amino acid labels indicate nucleotide or magnesium binding residues in PleD for which there are no structural equivalents in PelD. Double amino acid labels indicate conserved residues between the two proteins (with the PelD residue number indicated first). GTPαS is shown as a stick representation with the carbon, nitrogen, oxygen, phosphorous, and sulfur atoms colored green, blue, red, orange and yellow, respectively. The magnesium ions in the PleD structure are shown as magenta spheres. Image taken from Whitney JC, et al. *submitted.*

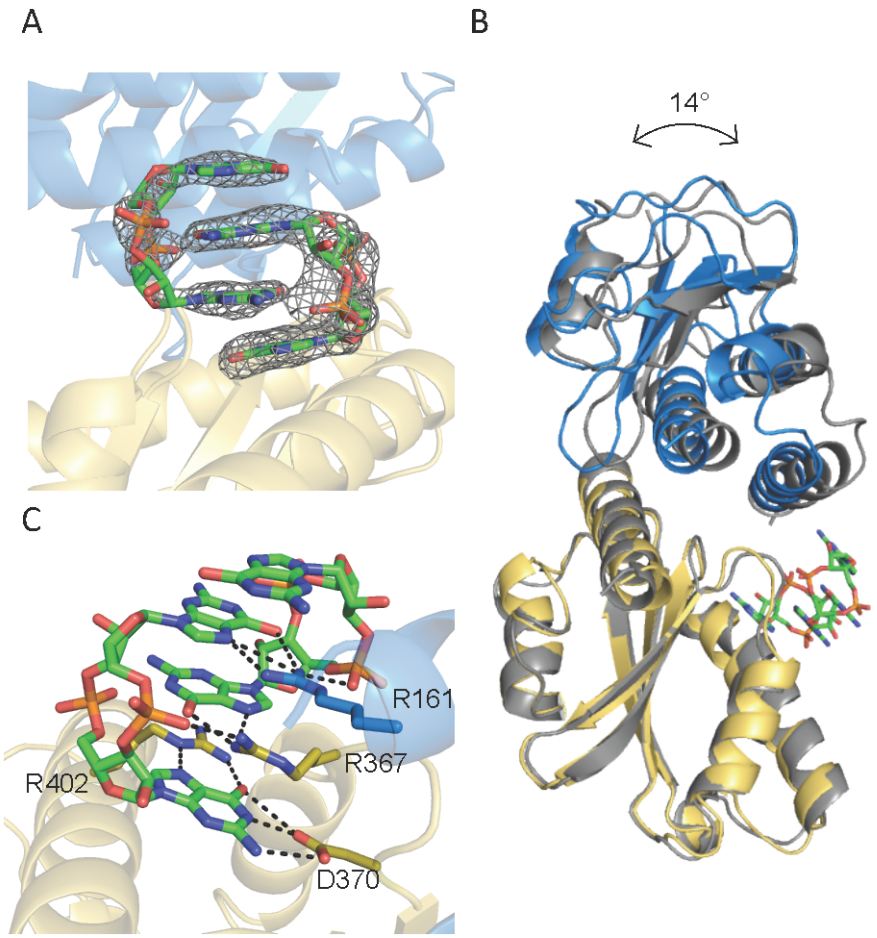

Figure 5. Comparison of the apo and holo forms of PelD$_{156-455}$. (A) Electron density map of (c-di-GMP)$_2$ after molecular replacement contoured at 3σ, shown as a grey mesh. Cyclic di-GMP is shown as a stick representation with carbon, nitrogen, oxygen and phosphorous atoms colored green, blue, red and orange, respectively. (B) C_α superposition of the GGDEF domains of the apo and c-di-GMP bound structures of PelD$_{156-455}$. The ligand free and ligand bound structures of PelD$_{156-455}$ are displayed as a cartoon representation and colored in grey and yellow/blue, respectively. (C) Close-up of I-site/c-di-GMP interactions. Cyclic di-GMP binding residues Arg161, Arg367, Asp370 and Arg402 are shown as sticks and are colored in the same manner as their associated domains. Image taken from Whitney JC, et al. *submitted.*

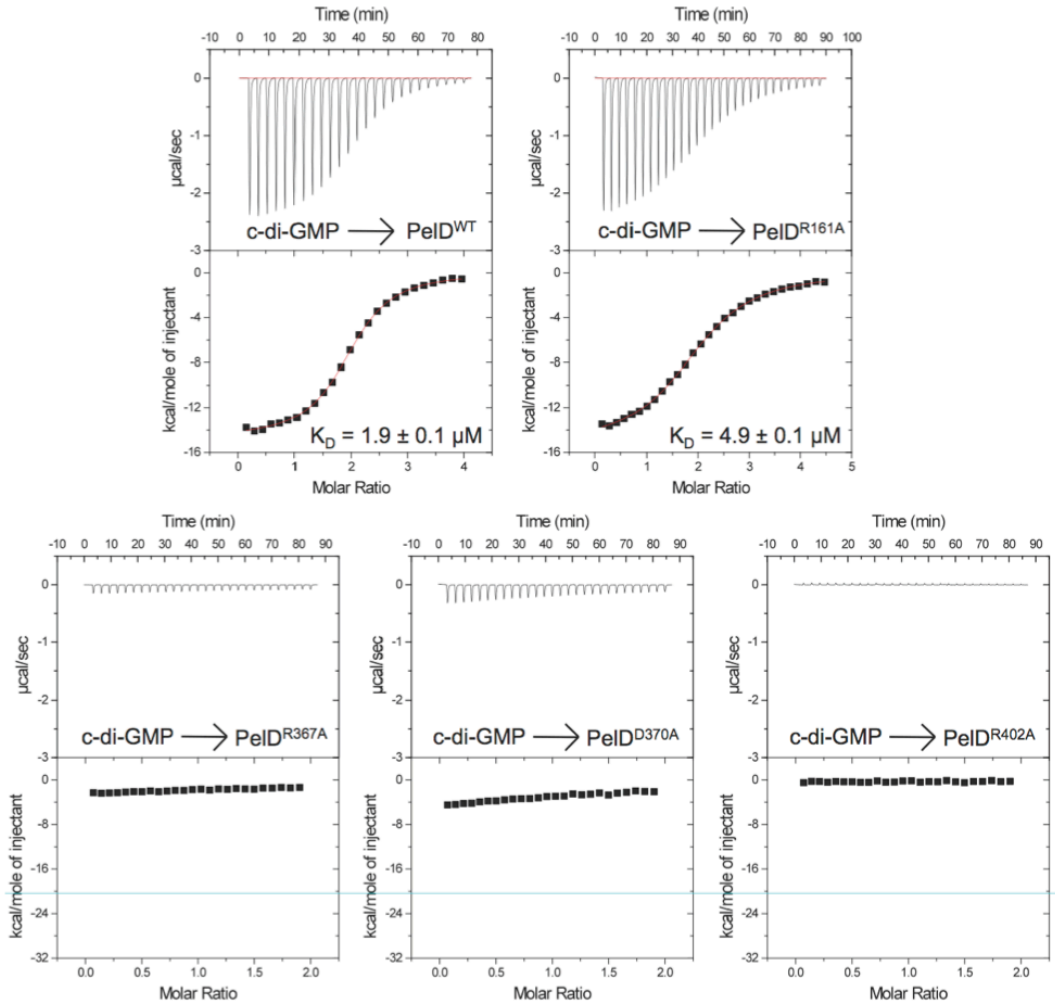

Figure 6. PelD$_{156\text{-}455}$ binds c-di-GMP with micromolar affinity. Isothermal titration calorimetry of c-di-GMP with wild-type PelD$_{156\text{-}455}$ and the indicated site-directed mutants. In each experiment, the top panel displays the heats of injection while the bottom panel shows the normalized integration data as a function of the molar syringe and cell concentrations. Where binding was observed (top panels), the red line represents the fit of the integrated data to a single-site binding model. The calculated dissociation constants (K_D) are also indicated for each experiment where binding was observed. Image taken from Whitney JC, et al. *submitted.*

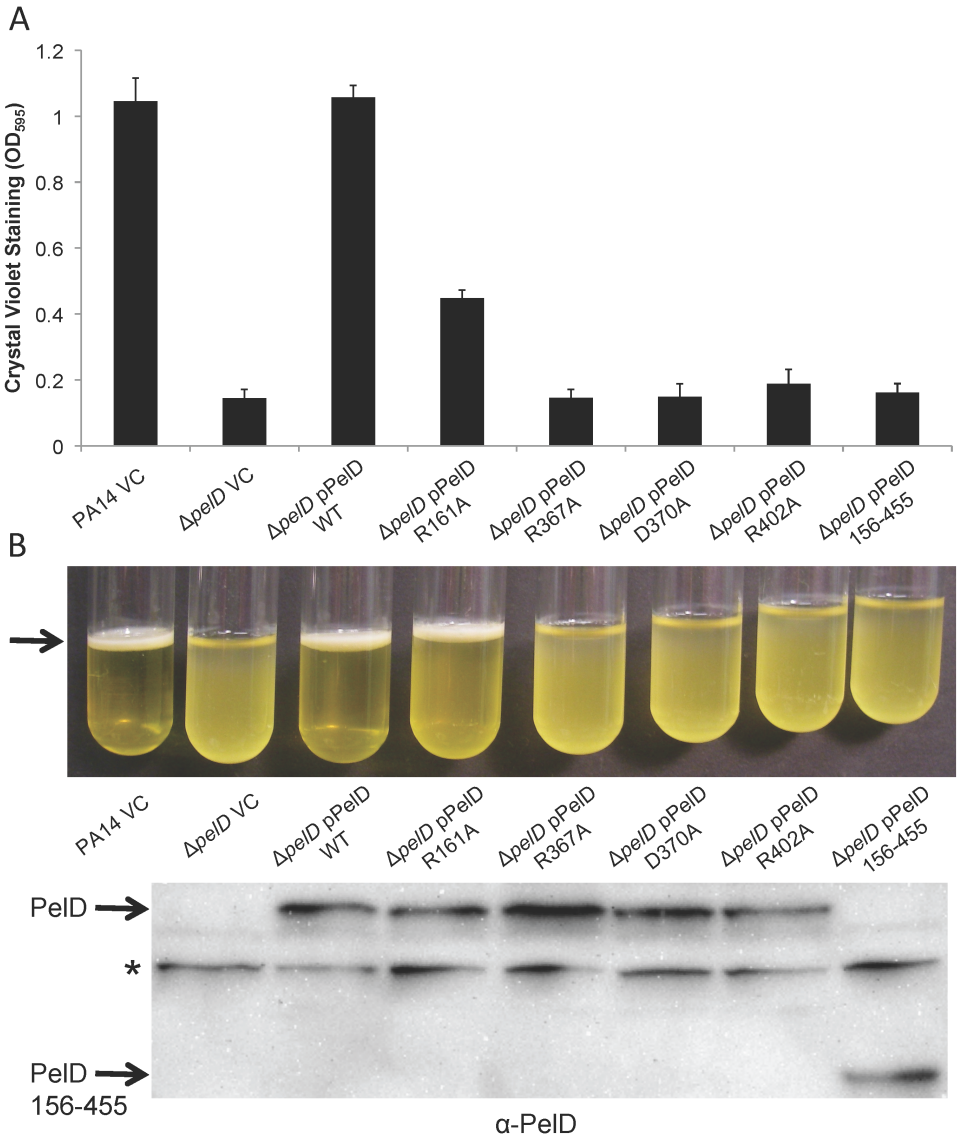

Figure 7. Effect of I-site mutations on biofilm formation. (A) Microtiter dish biofilm assay and (B) pellicle assay of *P. aeruginosa* PA14, PA14Δ*pelD*, PA14Δ*pelD* pPelD WT or the indicated point mutants and PA14Δ*pelD* pPelD$^{156\text{-}455}$ strains. The amount of crystal violet staining for each sample is the mean of three independent replicates. The error bars represent the standard errors (SEM). The pellicles form at the air-liquid interface of standing cultures as indicated by the black arrow. (C) The α-PelD western blot of each of the indicated strains shows expression of the various PelD mutants. The asterisk indicates a non-specific band that was used as a loading control. Image taken from Whitney JC, et al. *submitted.*

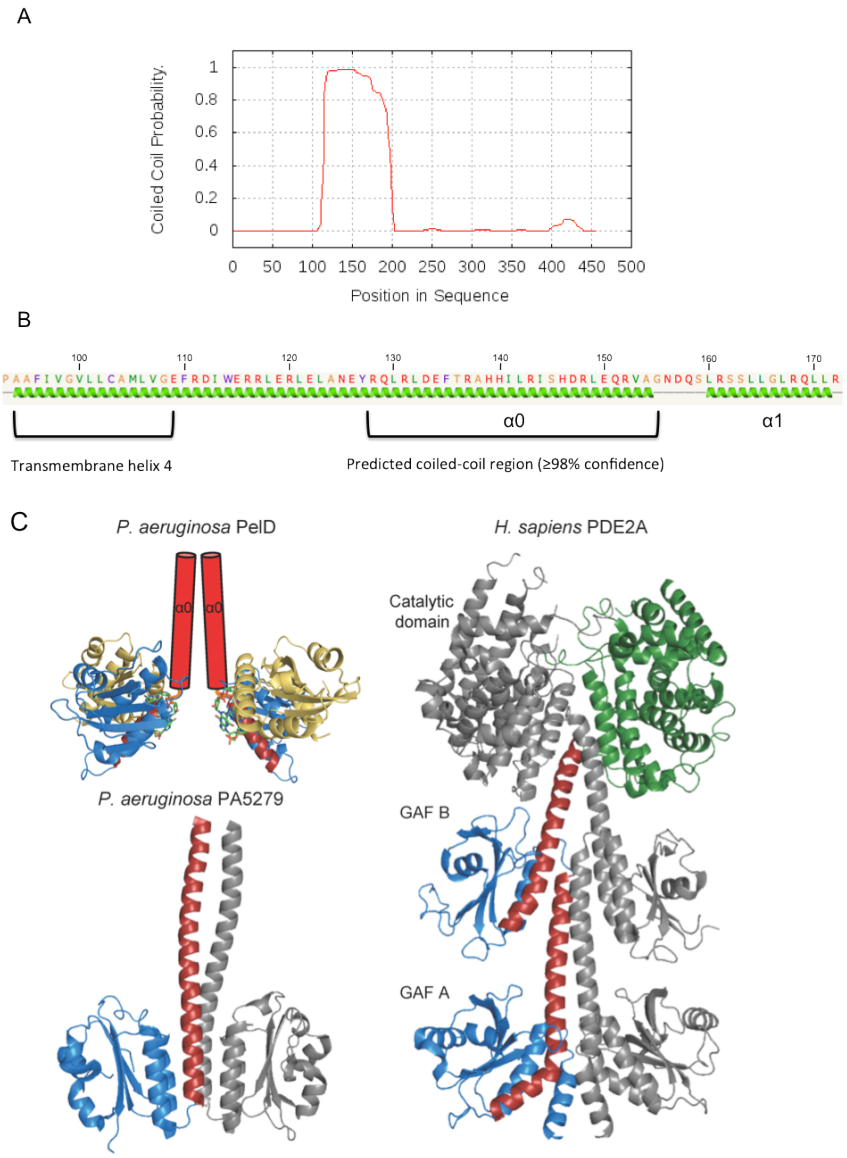

Figure 8. PelD contains a predicted coiled-coil region. (A) Graphical output from the MARCOIL coiled-coil prediction server (52). Full-length PelD from *P. aeruginosa* PA14 was used as the input sequence. (B) The location of transmembrane helix 4 (TM4) and the secondary structure prediction was obtained using HMMTOP (238) and *Phyre*^{2} (109), respectively. The helix denoted α1 is the first α helix from PelD's GAF domain. (C) Cartoon representation of *P. aeruginosa* PelD, *P. aeruginosa* PA5279 and *H. sapiens* PDE2A. For each protein, the GAF domain(s) is displayed in blue with its corresponding dimerization helix highlighted in red. As the proposed dimerization helix lies upstream of the crystallized fragment of PelD, a red cartoon cylinder was used to indicate this helix. The GGDEF domain of PelD, the catalytic phosphodiesterase domain of PDE2A and the non-crystallographic symmetry copies of PA5279 and PDE2A are colored in yellow, green and grey, respectively. Image taken from Whitney JC, et al. *submitted.*

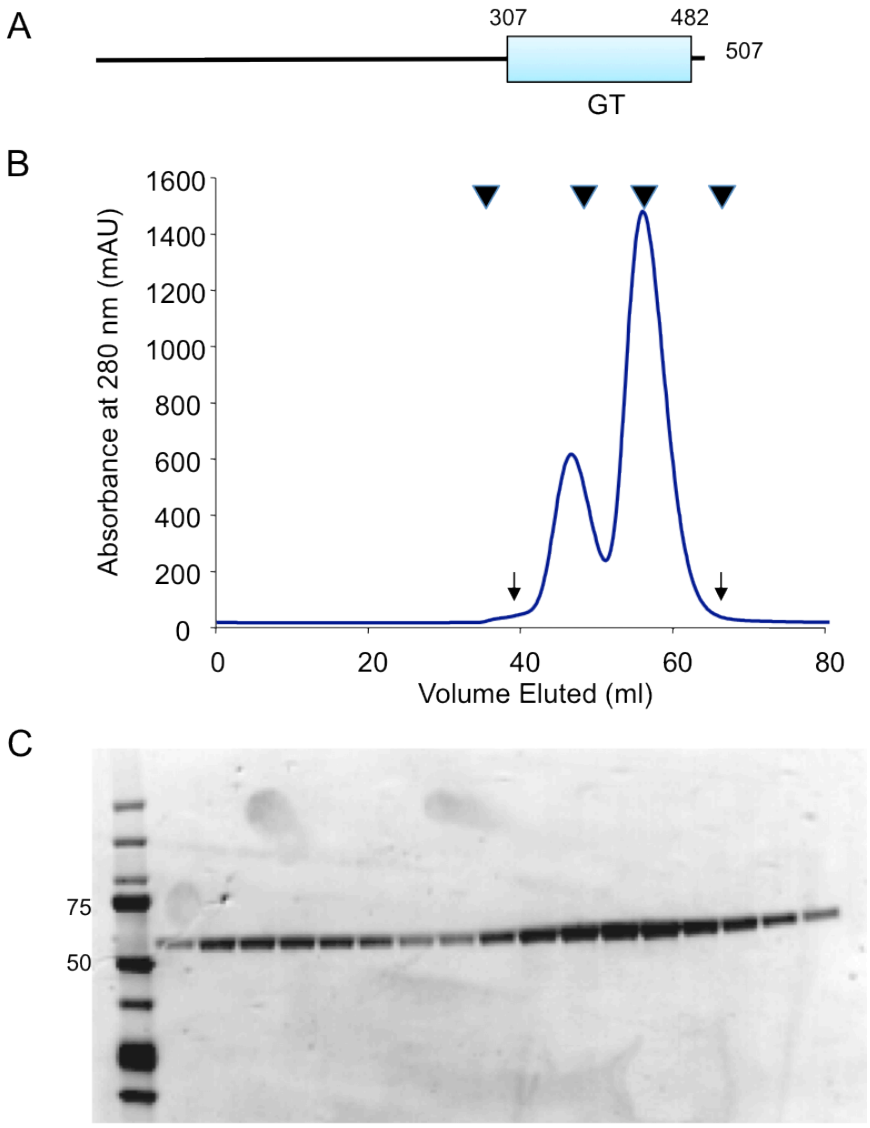

Figure 9. Purification of PelF. (A) Schematic diagram of the domain organization of PelF. The boundaries of the predicted glycosyltransferase (GT) domain are designated above. (B) Size-exclusion chromatogram of His_6-PelF. Protein standards used to calibrate the column are indicated by inverted triangles; ferritin (440 kDa); aldolase (158 kDa); conalbumin (75 kDa) and ovalbumin (43 kDa). (C) SDS–PAGE analysis of His_6-PelF after size-exclusion chromatography. Lane 1, molecular weight markers, followed by fractions from the size-exclusion chromatography as designated by arrows in (B).

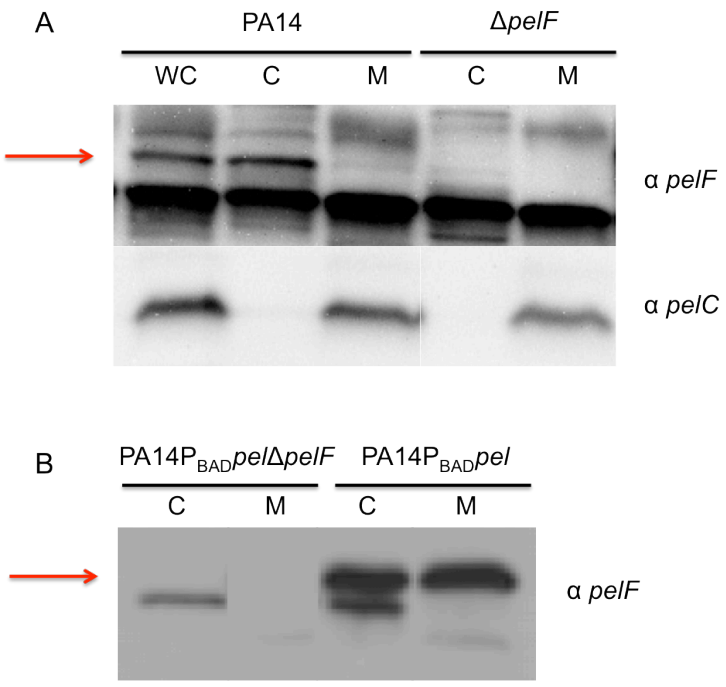

Figure 10. PelF subcellular localization shifts from the cytoplasmic to membrane fraction upon Pel production. (A) Cells were grown to log phase, lysed and fractionated by differential centrifugation. Three fractions were compared whole cell (WC), cytoplasmic fraction (C) and membrane fraction (M). Samples were probed for PelF protein (top) and PelC protein (bottom). Red arrow points to PelF. (B) Cells were grown to late-log, lysed and fractionated by differential centrifugation. Two fractions were compared, the cytoplasmic fraction (C) and membrane fraction (M).

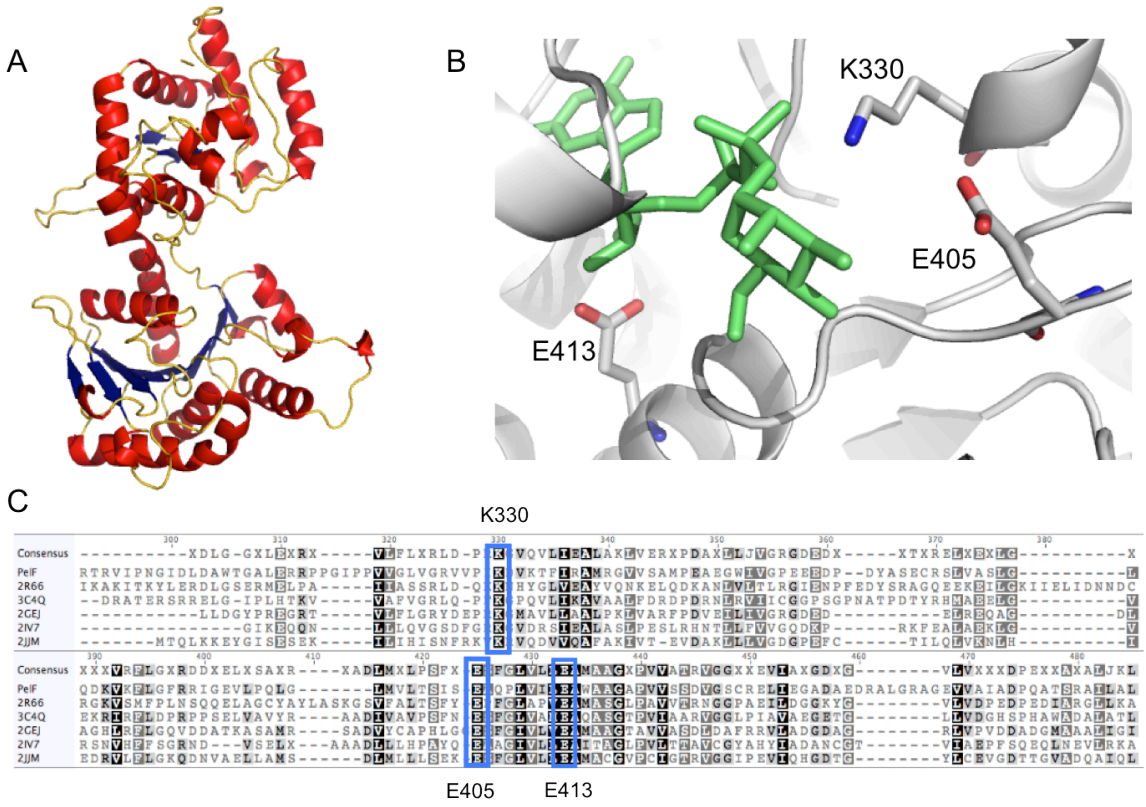

Figure 11. PelF has homology to glycosyltransferases. (A) PelF is modeled after the X-ray crystal structure of MshA from *Corynebacterium glutamicum*. (B) The nucleotide sugar, GDP-mannose, is modeled into the potential active site in PelF. (C) PelF sequence alignment with GT4 family glycosyltransferases from other organisms. K330, E405 and E415 are conserved throughout the family. 2R66 is sucrose phosphate synthase (SpsA) from *Halothermothrix orenii*. 3C4Q is MshA from *Corynebacterium glutamicum*. 2GEJ is phosphatidylinositol mannosyltransferase (PimA) from *Mycobacterium smegmatis*. 2IV7 is UDP-Glc: L-glycero-D-manno-heptose II α-1,3-glucosyltransferase (WaaG) from *E. coli*. 2JJM is UDP-GlcNAc: L-malate α-N-acetylglucosaminyltransferase (BshA) from *Bacillus anthracis*. Analysis by Serge Gueroussov.

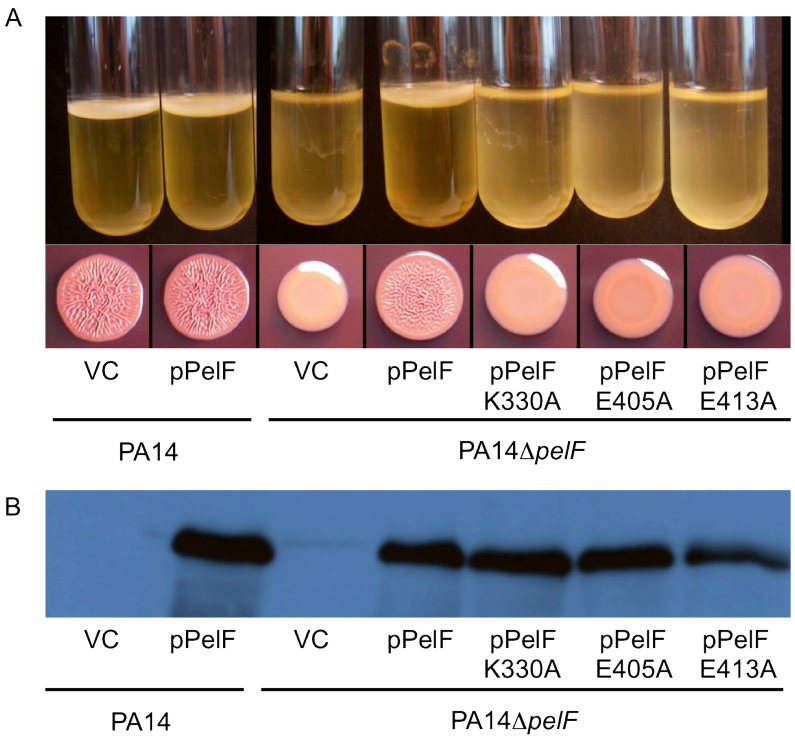

Figure 12. Effect of nucleotide sugar binding mutations on Pel function. (A) Strains containing pUCP18 (VC), pUCP18 pelF (pPelF) or mutated pPelF were monitored for pellicle formation (top) or colony morphology (bottom). Site-directed mutants were deficient in both phenotypes. (B) Western blot analysis using the PelF antibody shows equal protein expression in all strains containing pPelF.

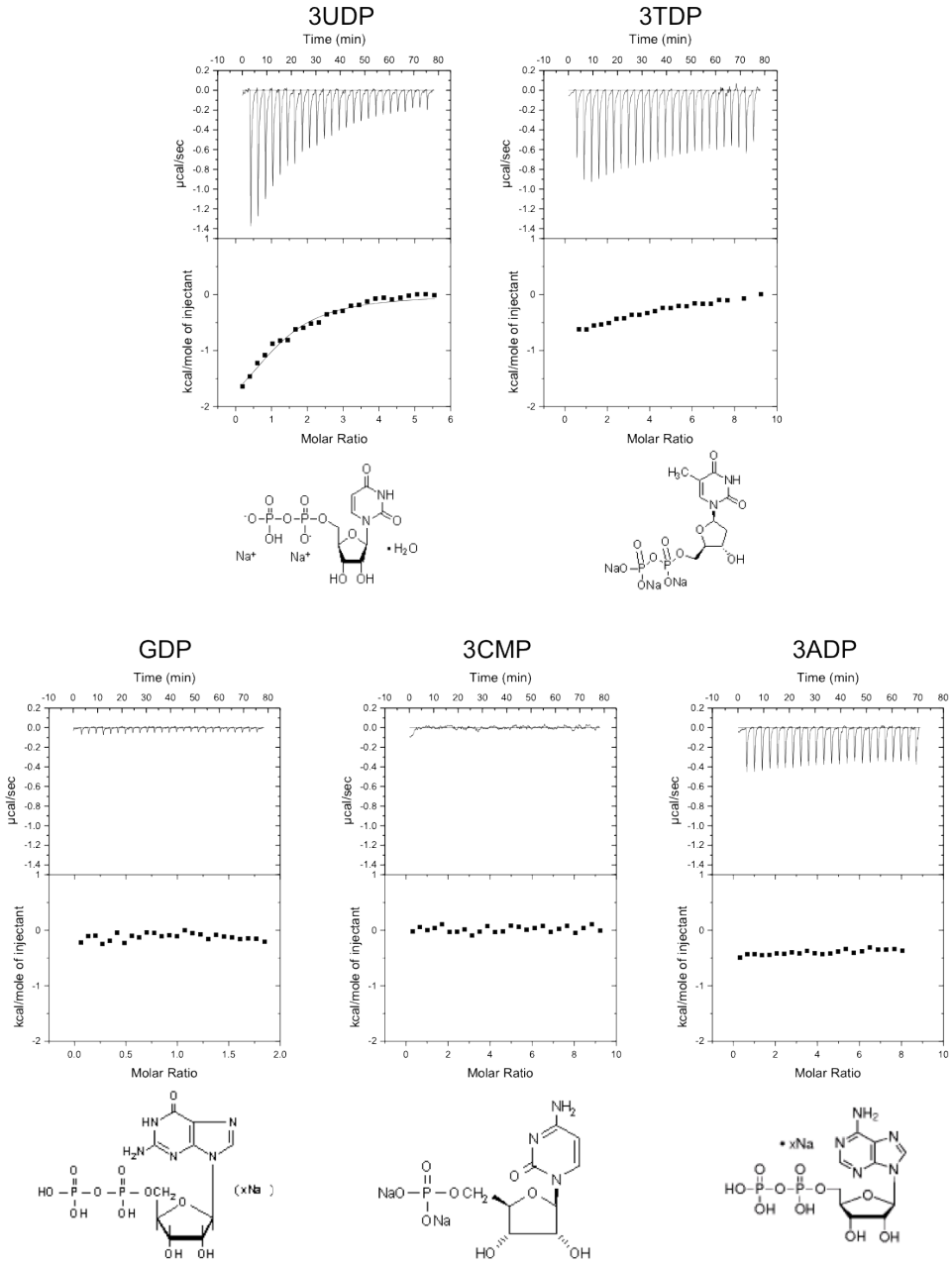

Figure 13. ITC analysis of PelF and potential nucleotide ligands. ITC of PelF and five nucleotides (UDP, TDP, GDP, CMP and ADP) without sugars attached. In each experiment, the top panel displays the heats of injection while the middle panel shows the normalized integration data as a function of the molar syringe and cell concentrations. Where binding was observed, the solid line represents the fit of the integrated data to a single-site binding model. The structure for each nucleotide is shown (bottom panel). Analysis by John Whitney and Lindsey Marmont.

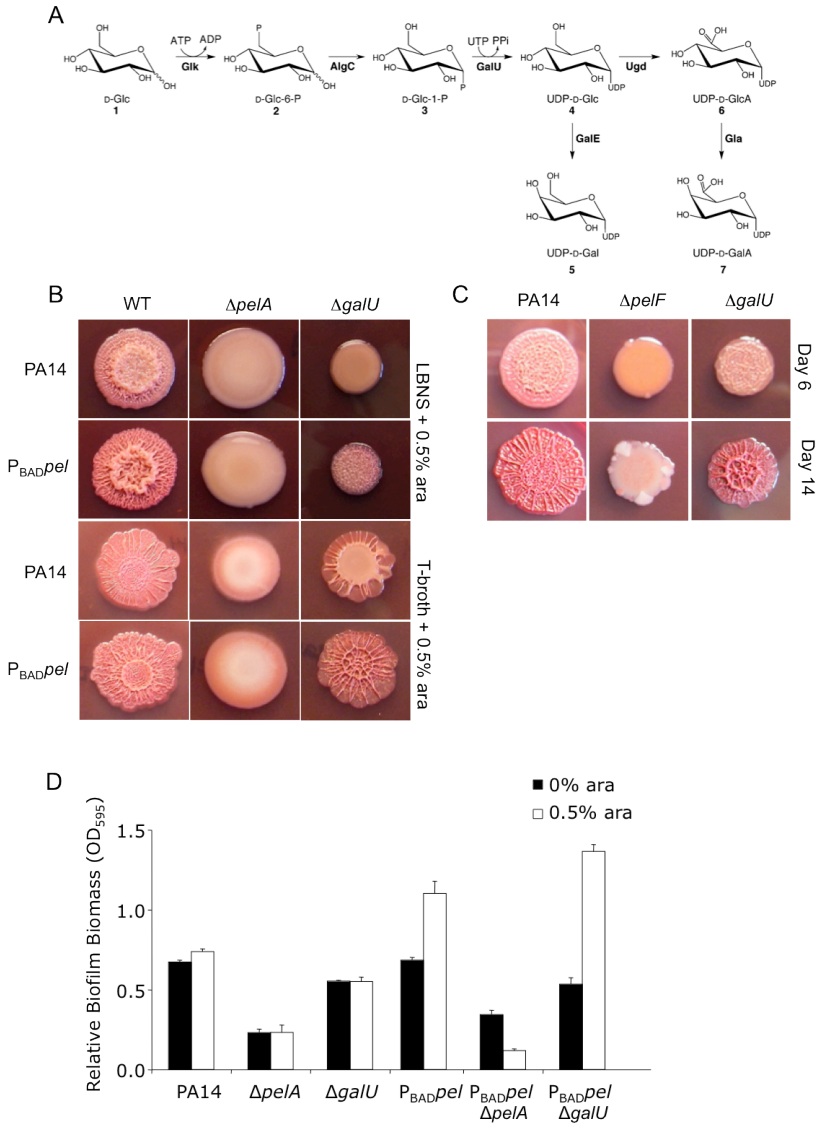

Figure 14. A *galU* mutant is delayed in wrinkly colony morphology development. (A) Biosynthesis pathways of UDP-d-glucose, UDP-d-galactose, UDP-d-glucuronic acid and UDP-d- galacturonic acid. Figure taken from Hao, Y., and Lam, J.S. 2011. *Pathways for the Biosynthesis of NDP sugars* (79). (B) Colony morphology of strains grown on two types of media for 8 days, LBNS + 0.5% arabinose (top panels) or T-broth + 0.5% arabinose (bottom panels). (C) Colony morphology of strains grown on T-broth + 0.5% arabinose for 6 days (top panel) or 14 days (bottom panel). (D) Microtiter dish biofilm assay of different mutants grown in the presence and absence of arabinose.

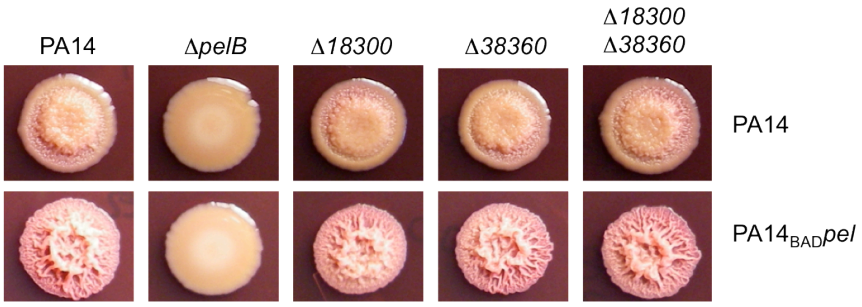

Figure 15. Colony morphology of UDP-glucose dehydrogenase mutants. Colonies were grown on LBNS + 0.5% arabinose for 6 d at 25°C. Images were captured.

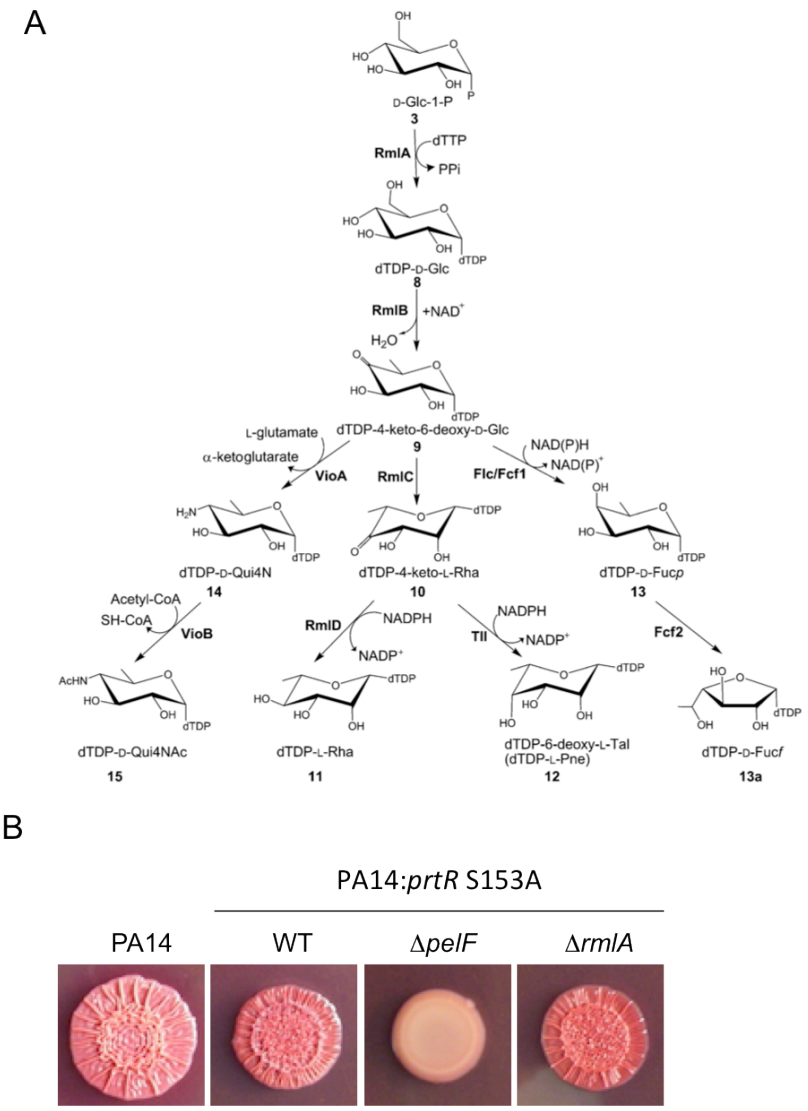

Figure 16. *rmlA* mutants do not disrupt colony morphology. (A) Biosynthesis pathways of dTDP sugars. Figure taken from Hao, Y., and Lam, J.S. 2011. *Pathways for the Biosynthesis of NDP sugars* (79). (B) Colony morphology of PA14, wild-type (WT), *pelF* and *rmlA* mutants. The WT background is PA14:*prtR* S153A and does not synthesize R2-pyocin.

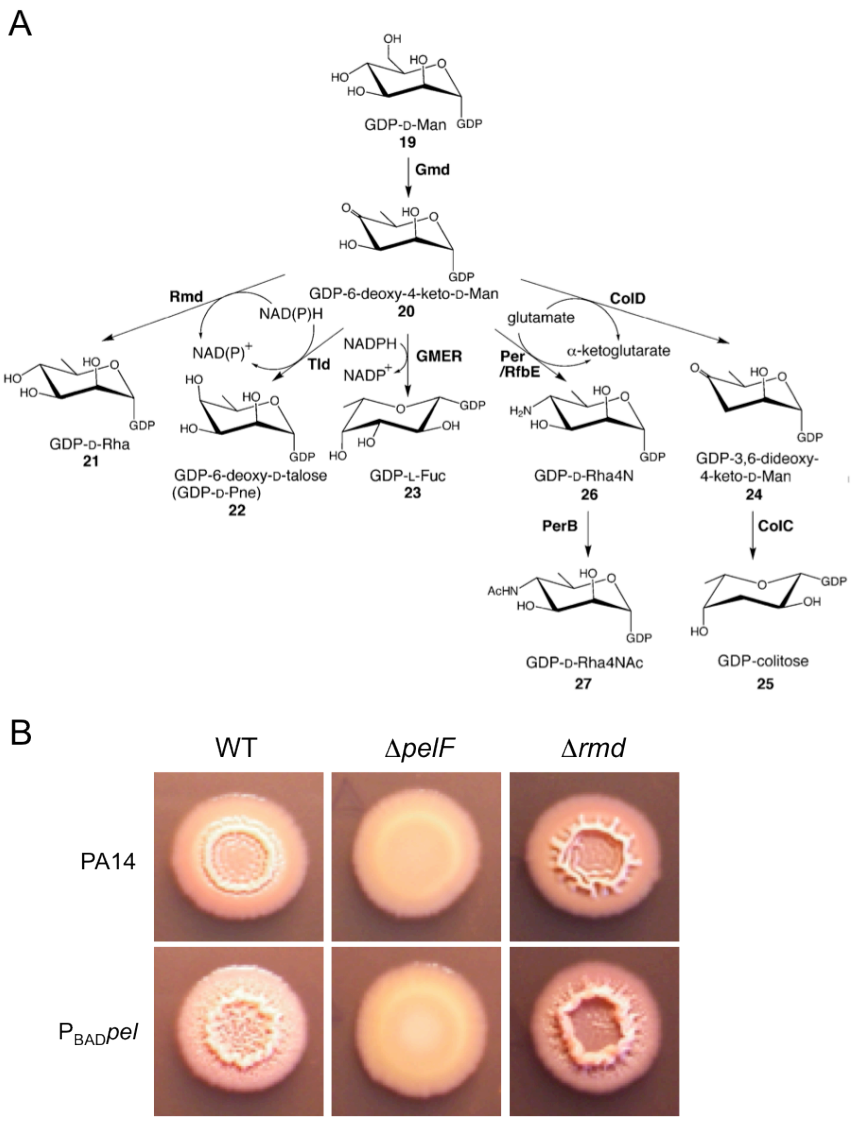

Figure 17. *rmd* mutants enhance wrinkly colony morphology. (A) Biosynthesis pathways of GDP sugars. Figure taken from Hao, Y., and Lam, J.S. 2011. *Pathways for the Biosynthesis of NDP sugars* (79). (B) Colony morphology of PA14, PA14Δ*pelF*, PA14Δ*rmd* (top row) and PA14P_{BAD}*pel*, PA14P_{BAD}*pel*Δ*pelF*, PA14P_{BAD}*pel*Δ*rmd* (bottom row). Colonies were grown on LBNS + 0.5% arabinose for 5 d.

CHAPTER IV:

Pel and Psl Polysaccharides Provide *Pseudomonas aeruginosa* Structural Redundancy within the Biofilm Matrix

Published as: Colvin, K.M., Irie, Y., Tart, C.S., Urbano, R., Whitney, J.C., Ryder, C., P. Howell, L., Wozniak, D.J., and Parsek, M.R. 2011. *Environ. Microbiol*. 10.1111/J.1462-2920.2011.02657.x.

ABSTRACT

Extracellular polysaccharides comprise a major component of the biofilm matrix. Many species that are adept at biofilm formation have the capacity to produce multiple types of polysaccharides. *Pseudomonas aeruginosa* produces at least three extracellular polysaccharides, alginate, Pel and Psl, that have been implicated in biofilm development. Non-mucoid strains can use either Pel or Psl as the primary matrix structural polysaccharide. In this study, we evaluated a range of clinical and environmental *P. aeruginosa* isolates for their dependence on Pel and Psl for biofilm development. Mutational analysis demonstrates that Psl plays an important role in surface attachment for most isolates. However, there was significant strain-to-strain variability in the contribution of Pel and Psl to mature biofilm structure. This analysis led us to propose four classes of strains based upon their Pel and Psl functional and expression profiles. Our data also suggest that Pel and Psl can serve a redundant function as a structural scaffold in mature biofilms. We propose that redundancy could help preserve the capacity to produce a biofilm when extracellular polysaccharide genes are subjected to mutation. To test this we used PAO1, a common lab strain that primarily utilizes Psl in the matrix. As expected, a *psl* mutant strain initially produced a poor biofilm. After extended cultivation, we demonstrate that this strain acquired mutations that up-regulated expression of the Pel polysaccharide, demonstrating the utility of having a redundant scaffold extracellular polysaccharide. Collectively, our studies revealed both unique and functionally redundant roles for two distinct biofilm extracellular polysaccharides.

INTRODUCTION

Pseudomonas aeruginosa thrives in diverse environments, including soil, water, insects, plants and animals (80). In humans, *P. aeruginosa* is an opportunist, capable of causing both acute and chronic infections. Examples of acute infection include, urinary track infections, respiratory infections, soft tissue infections, bone and joint infections, bacteremia and a variety of systemic infections (14). *P. aeruginosa* is also well known

for the chronic infections it causes in individuals with the genetic disease, cystic fibrosis (CF) (74). It is widely believed that biofilm growth within the lungs of CF patients is a hallmark for the facilitation of disease (180, 211). Biofilm bacteria exhibit reduced susceptibility to antimicrobials, detergents and the host immune system compared to planktonic cells (55, 81, 168). As a result biofilm infections (including CF airway infections) tend to be chronic and difficult to eradicate (42).

Biofilms are surface associated communities embedded within an extracellular matrix (168, 180, 226). The extracellular matrix consists of polysaccharides, proteins, nucleic acids and lipids and is a distinguishing feature of biofilms, capable of functioning as both a structural scaffold and protective barrier (83). Extracellular polysaccharides are a crucial component of the matrix, and carry out a range of functions including promoting attachment to surfaces and other cells, building and maintaining biofilm structure, as well as protecting the cells from antimicrobials and host defenses (223, 226).

P. aeruginosa produces at least three extracellular polysaccharides that can be important in biofilm development (198). Alginate is an important biofilm extracellular polysaccharide that is over-produced in mucoid variants, which are often isolated from lungs of chronically-colonized CF patients (74). In mucoid strains, alginate is the predominant extracellular polysaccharide of the matrix (87). Non-mucoid strains utilize primarily the Pel and Psl polysaccharides for biofilm formation (265). The *pel* locus contains seven genes encoding functions involved in the synthesis and export of an uncharacterized polysaccharide (63). The *pel* locus was identified in a transposon mutagenesis screen for loss of pellicle formation, a biofilm formed at the air-liquid interface of a static liquid culture (64). The loss of biofilm formation is specifically attributed to the capability of Pel to initiate and maintain cell-cell interactions (39). The *p*olysaccharide *s*ynthesis *l*ocus (*psl*) contains 12 genes, 11 of which are necessary for synthesis and export of the Psl polysaccharide (27). Recently, the structure of Psl was identified as repeating units of a neutral, branched pentasaccharide consisting of D-glucose, D-mannose and L-rhamnose monosaccharides (27).

Depending on the strain studied, the role of Pel and Psl in biofilm formation can vary drastically (69, 267). For example, the two most commonly studied non-mucoid laboratory strains, PAO1 and PA14, differ in the primary polysaccharide used to maintain biofilm structure (39). PAO1 relies primarily on Psl, while Pel production is required for mature biofilm development in PA14 (39, 69, 267). Collectively, these studies suggest that Pel and Psl are each capable of functioning as a structural scaffold involved in maintaining biofilm integrity.

Regulation of Pel and Psl expression is complex, with multiple levels of intricate control. Recent studies have demonstrated multiple pathways of transcriptional control for both *pel* and *psl*. FleQ represses transcription of the *pel* and *psl* operons. This repression is relieved in the presence of the intracellular signaling molecule c-di-GMP (89). RpoS acts as a positive transcriptional regulator of *psl* gene expression and quorum sensing has been suggested to positively regulate *pel* and *psl* expression as well (71, 101, 202). Another regulatory system controlling *pel* and *psl* gene expression is the Gac-Rsm signal transduction pathway (73, 247). Translation of *psl* is inhibited by the RNA binding protein, RsmA (101). Finally, c-di-GMP can act as a positive allosteric regulator of Pel synthesis through PelD binding (129).

Rugose small colony variants (RSCVs) of *P. aeruginosa* have been isolated from CF sputum and *in vitro* biofilm reactors (15, 215). RSCVs are characterized by hyperadherence and hyperaggregation that result from elevated expression of Pel and Psl (45, 101, 221). In addition, c-di-GMP signaling is linked to the RSCV phenotype (221). To date, the RSCVs described in *P. aeruginosa* all have elevated levels of c-di-GMP, and depletion of c-di-GMP suppresses the RSCV phenotype (89, 101, 221, 239). One common genetic route to the RSCV phenotype is a mutation in the *wspF* gene (215, 221). This mutation activates the diguanylate cyclase WspR and results in elevated c-di-GMP, which in turn results in the RSCV phenotype (89).

In this study, we evaluated a range of clinical and environmental *P. aeruginosa* isolates for their dependence on the Pel and Psl polysaccharides for biofilm development. Mutational analysis demonstrates that for most strains Psl plays an important role in surface attachment. However, there was significant strain-to-strain variability in the contribution of Pel and Psl to mature biofilm structure. Our study led us to propose four classes of strains based upon their dependence for and expression patterns of Pel and Psl. These data demonstrate that the relative importance of Pel and Psl is highly variable. We conclude that both Pel and Psl can each serve as the primary biofilm matrix polysaccharide, while only Psl is an important surface attachment determinant. To examine the significance of producing two extracellular polysaccharides, we performed biofilm evolution experiments and discovered in the absence of the one structural polysaccharide, the evolved biofilm population selects for the up-regulation of a secondary structural polysaccharide.

RESULTS

P. aeruginosa can use either Psl or Pel as the primary biofilm matrix polysaccharide.

Two common laboratory strains, PAO1 and PA14, differ in the primary polysaccharide used as a structural scaffold for the biofilm (39). PAO1 primarily uses Psl, while PA14, which has a three-gene deletion in the *psl* operon, uses Pel (39, 128). For the purpose of this study, we validated this observation using two distinct biofilm culturing formats. The first being a microtiter dish assay which measures biofilm biomass that forms at the air-liquid interface after static incubation. The second method utilizes confocal laser scanning microscopy (CLSM) to visually monitor live biofilms growing in dilute medium under conditions of continuous flow using a flow-cell reactor.

PAO1 and PA14 and their corresponding *pel*, *psl,* and *pelpsl* mutant strains were compared for initial attachment and biofilm formation in the microtiter dish assay (**Figure 1A** and **1B**). A *pel* mutation did not have a surface attachment phenotype in

either PAO1 or PA14 backgrounds. As expected, a PAO1Δ*psl* mutant strain was completely deficient in attachment.

Unlike surface attachment, Pel had a significant impact on later stages of biofilm development, but this result was strain dependent (**Figure 1B**). A PA14Δ*pel* mutant strain produced a substantially reduced level of biofilm biomass compared to PA14, while a PAO1Δ*pel* biofilm was indistinguishable from PAO1. In contrast, the PAO1Δ*psl* and a PAO1Δ*pel*Δ*psl* double mutant strain were impaired for biofilm formation. Similar to the microtiter dish assays, flow-cell grown PAO1 biofilms were dependent on Psl and PA14 biofilms on Pel (**Figure 1C**). PA14Δ*pel,* PAO1Δ*psl* and PAO1Δ*pel*Δ*psl* strains are arrested at the monolayer stage of biofilm development, showing an absence of microcolony growth and relatively reduced biomass compared to the parent strain. These data confirm previous observations and serve as a reference for the subsequent analysis of environmental and clinical isolates.

Pel and Psl utilization is variable among clinical and environmental isolates for biofilm development.

The data presented in **Figure 1** raise the question as to whether PAO1 or PA14 is generally representative of *P. aeruginosa* in terms of matrix polysaccharide dependence. To address this question, we examined a variety of clinical and environmental isolates for their dependency on Pel and Psl. The strain collection consisted of 20 isolates, including four environmental and sixteen isolates from diverse human infections (**Table 1**). The colony morphologies of these isolates, a phenotype that is linked to extracellular polysaccharide production (5, 30, 221, 268), was highly variable (**Figure 2**).

In-frame deletions of *pelF* and *pslD* were generated using standard allelic replacement strategies. These mutations have previously been shown to eliminate Pel and Psl production, respectively (27, 245). Due to some strains having intrinsic antibiotic resistance, mutagenesis intractability or other unknown factors, only 10 of the isolates

were successfully mutated. These strains were tested for growth on laboratory medium and found to have comparable growth rates (**Figure 3**).

We first tested the ability of these strains to attach to plastic surfaces in a microtiter dish assay. In all the strains tested, a *psl* mutation impaired attachment (**Figure 4A, B** and **C**). Additionally, *pel* mutations did not have an attachment phenotype in any tested strain. Three strains, all of which were weakly adherent, still demonstrated reduced attachment in a *psl* mutant (**Figure 4B**). Two of the strains, CF127 and 19660, showed a slight effect of Pel on attachment, but only in the absence of Psl (**Figure 4C**). Collectively, these results emphasize the importance of Psl as a surface attachment determinant.

Overall, we found that the strains were variable in their ability to produce biofilms in microtiter dishes. One strain, CF127, was a hyper-biofilm forming strain, producing 3-4 fold more biofilm biomass than the other strains (**Figure 5**). For five isolates, a *psl* mutation severely impaired biofilm formation, in a manner very similar to PAO1. In these strains, a *pel* mutation did not have a phenotype (**Figure 5A**). For three isolates, single *pel* or *psl* mutations had little effect (**Figure 5B**). Two isolates, CF127 and 19660, showed small but consistent reduced biofilm biomass for single *pel* and *psl* mutations (**Figure 5C**). All *pelpsl* double mutant strains were completely deficient for biofilm formation (**Figure 5**).

We took a complementary approach using flow-cell bioreactors to evaluate biofilm formation for a few representative strains: E2, S54485, CF127, 19660 and MSH3 (**Figure 6**). E2 formed a thick rough biofilm devoid of any cell aggregate structures. The E2 *pel* mutant strain looked identical to wild-type, while the *psl* and *pelpsl* mutants contained only a few attached cells to the glass surface. These data correlated to our microtiter dish biofilm analysis (**Figure 5A**). S54485 is similar to E2. Wild-type and the *pel* mutant formed thick, uniform biofilms. The *psl* mutant formed small aggregates of cells that were not present in the double mutant. MSH3 is capable of forming large mature cell aggregate structures, similar to PAO1 (**Figure 6**). In contrast to PAO1 *pel*,

MSH3 *pel* biofilms produced immature structures that are significantly reduced in size, suggesting that Pel production can contribute to biofilm structure for this strain under these culturing conditions. MSH3Δ*psl* and MSH3Δ*pel*Δ*psl* mutants strains both fail to form cellular aggregates and produce a monolayer of cells on the glass surface. Strain 19660 and 19660Δ*pel* produced biofilms characterized by densely packed cell aggregates. In stark contrast to the microtiter dish assay data, the 19660Δ*psl* mutant produced biofilms with more biomass and fewer cell aggregates than wild-type (**Figure 6**). We hypothesize this is partially due to an attachment defect in this strain (**Figure 7A**). The discrepancy between the 19660Δ*psl* strain microtiter dish assay and flow-cell data (**Figure 7B** verse **Figure 6**) can be explained by the fragile nature of the biofilms produced by this strain. The microtiter dish assay has a vigorous wash step, which removed what appeared to be adherent biomass. When a gentle wash is performed, the *psl* mutant has similar biomass to wild-type (**Figure 7B**). CF127 forms a thick structured biofilm with a high degree of surface roughness. Both *pel* and *psl* single mutants display similar rough, structured biofilms, slightly reduced in height (**Figure 6**). Although impaired, the CF127Δ*pel*Δ*psl* strain is not completely deficient for biofilm formation. Though, as expected, the biofilm biomass is significantly reduced from the parent and single mutant strains.

Determining the effects of *pel* and *psl* mutations on colony morphology.

Strains were grown on solid medium for 5 d at 25°C. Nearly all *pel, psl* single mutants and *pelpsl* double mutants displayed identical colony morphology to the wild-type strain (**Figure 8**). An exception to this was seen for two strains, 19660 and CF127. Both strains display a wrinkly colony morphology that is converted to a smooth colony in a *pelpsl* double mutant strain. It should be noted that the colony texture appearance between CF127 and 19660 is strikingly different (**Figure 8 and 2**). CF127 and 19660 colony morphologies are similar to the previously described rugose small colony variants (RSCVs) (45, 101, 221). We were surprised to see very little change in Congo red binding between CF127 and mutant strains. In particular, we were surprised that CF127 did not hyperbind the dye as previously reported for other RSCVs (221).

8.2.4 Strain classification based upon Pel and Psl-dependent phenotypes.

Our colony morphology and biofilm phenotypes suggest that the strains can be classified into four different classes. The first class, or Class I, is a **"Pel-dominant matrix"** (**Figure 9**). Our only current representative of this class is PA14. Class II is a **"Psl-dominant matrix"**. "Psl-dominant matrix" strains, like PAO1, relied primarily on Psl for biofilm formation. Representatives of this class includes SS4485, X13273, E2, 62, and X24509. Class III we have termed "**EPS redundant matrix users**". These are poor attaching strains, similar to PA14. Here mutations in both *pel* and *psl* are necessary to eliminate the ability of these strains to produce a biofilm in the microtiter dish assay; single *pel* and *psl* mutations do not affect biofilm formation. MSH3, MSH10, and T56593 are class III strains. Finally we propose class IV, which we term **"matrix over-producers"**. Class IV strains include CF127 and 19660. For "matrix over-producers" Pel and Psl are both important for attachment. Similarly, both single *pel* and *psl* mutants are partially impaired for mature biofilm formation. In CF127, *pel* and *psl* mutant strains are equally impaired for biofilm formation but are still capable of producing significant amounts of adhered biomass. While in strain 19660, a *psl* mutant is much more compromised than a *pel* mutant, but is not as impaired as the double mutant. This suggests both polysaccharides contribute additively to biofilm formation. Additionally, matrix overproducers are the only class where *pel* or *psl* mutations impact colony morphology (**Figure 9**). It should be noted that not all isolates fall cleanly into a single class based upon their phenotypes.

PelC protein and Psl polysaccharide expression levels correlate with biofilm phenotypes and strain class designations.

We reasoned that the observed attachment and biofilm phenotypes (**Figures 4** and **5**) are related to Pel and Psl expression levels. To explore this possibility, we measured the isolates relative PelC protein and Psl expression levels. Psl levels were measured semi-quantitatively using Psl-specific antiserum (27). Since reagents are not available for evaluating Pel directly, we used antiserum against one of the proteins necessary for its synthesis, PelC. We have generally found that elevated PelC protein levels track well with Pel-dependent phenotypes (Data not shown and (39)). To confirm the specificity

of the Psl antibody, we evaluated strains with expected reactivity results. All *psl* mutant strains showed reduced reactivity (**Figure 10**).

The first condition we tested approximated the initial planktonic attachment conditions for the microtiter dish assay data presented in **Figure 4**. In PA14, as expected, PelC is expressed but Psl polysaccharide is not detected. PAO1 expressed Psl to a high degree while PelC protein expression is reduced compared to PA14 (**Figure 11A**). Both of these strains have expression profiles that correspond to their reliance on the different polysaccharides for biofilm production. In general "Psl-dominant" (Class II) strains produce an intermediate level of Psl and low PelC protein expression. The class III "EPS redundant matrix users" expresses both PelC and Psl at low levels. "Matrix over-producers" (Class IV), 19660 and CF127, both show elevated PelC protein and Psl polysaccharide levels. These data also suggest that Psl expression correlates to initial attachment. Strains that produce little Psl: PA14, X24509, MSH3, MSH10 and T56593 show reduced initial attachment (**Figure 1 and Figure 4**).

Expression profiles were also analyzed from strains grown to closer approximate microtiter dish biofilm culturing conditions (**Figure 11B**). As expected, PA14 produced PelC at a high level, while PAO1 produced high levels of Psl. "Psl-dominant" strains (Class II) produced Psl at an intermediate to high level and PelC at an intermediate level. Class III strains had slightly elevated PelC protein expression but low levels of Psl. Class IV "Matrix over-producers" still displayed elevated expression levels of PelC and Psl. We also analyzed PelC and Psl levels for all of our original strains grown in these conditions (**Figure 12A**). Of the 10 strains for which we had no mutational data (designated "not classified" in Figure S5A), all appeared to produce Pel and Psl to some degree.

***pelA* and *pslA* transcript levels do not correlate to PelC and Psl expression levels.**
We hypothesized that variations in polysaccharide expression levels could be due to transcriptional differences. Therefore, we measured *pelA* and *pslA* mRNA levels using qRT-PCR (**Figure 11C** and **Figure 12B**). In almost all strains, the relative transcript

level was similar to PAO1. One exception was CF127, which exhibited *pelA* transcript levels 40-fold higher than PAO1 (**Figure 11C**). Differences in *pelA* and *pslA* transcript levels did not always translate to similar changes in PelC or Psl expression (**Figure 11** and **Figure 12**). For example, E2's *pslA* transcript was 3-fold higher compared to PAO1, but Psl polysaccharide levels appeared to be lower (**Figure 11**).

Despite the relatively small differences detected in *pelA* and *pslA* transcription between strains, we investigated the possibility that variations in polysaccharide expression levels could be explained by DNA sequence differences in regulatory control regions upstream of the *pel* and *psl* operons. We sequenced the upstream intergenic regions of *pel* and *psl* for each strain (data not shown). PA14 has an intergenic region of 562 bp between the ATG of *pelA* and the translational stop of the upstream ORF, *gdhB* (**Figure 13**). In contrast, PAO1 has a three-gene operon (PA3065-PA3067) inserted 484 bp upstream of the *pelA* translational start site (**Figure 13**). This operon is missing in PA14. Members from each of the other three polysaccharide classes were found to have this insertion. The first 200 bp up-stream of the *pelA* translational start site was highly conserved. Similarly, the intergenic region upstream of *pslA* (525 bp) was strongly conserved. Only one nucleotide change was seen for all 20 isolates, strain 62, within 200 bp of the translational start site, including the RsmA binding sequences.

C-di-GMP levels track with PelC expression.

C-di-GMP levels control *pel* and *psl* transcription and allosterically regulate Pel biosynthesis (73, 90, 239). We hypothesized that our protein and polysaccharide expression results (**Figure 11B**) could be explained by strain-to-strain differences in intracellular c-di-GMP concentrations. The intracellular concentration of c-di-GMP was measured from a select number of strains grown 3 d on agar media at 25°C (**Figure 14**). Intracellular c-di-GMP levels appeared to track well with PelC protein expression and less so with Psl polysaccharide expression. As expected, the RSCV, CF127, had elevated c-di-GMP levels. Interestingly, both PAO1 and 19660 displayed high Psl expression with relatively low c-di-GMP levels. Overall, c-di-GMP proved to be a poor indicator of Psl.

Pel and Psl redundancy can rescue biofilm formation in mutant strains.

We hypothesized that one advantage for strains to maintain two distinct EPS biosynthetic loci such as *pel* and *psl* would be for redundancy. This would minimize the impact of a mutation on a critical function such as biofilm formation. In the case of PAO1, Psl is the primary biofilm polysaccharide. Since PAO1 can produce Pel (39, 101, 267), we reasoned that during biofilm growth, a PAO1 *psl* mutant strain may acquire mutations that up-regulate Pel production to compensate for the loss of Psl.

To test this, we compared PAO1 and PAO1Δ*psl* for PelC expression before and after extended biofilm growth. As expected, the mutant strain was initially impaired for biofilm growth. After extended culturing, a biofilm was visible and upon harvesting the adherent biofilm biomass, we observed an increase in PelC protein levels in both PAO1 and PAO1Δ*psl* compared to the starting planktonic inoculum (**Figure 15A**). This supports previous data showing that biofilm cells exhibit elevated *pelA* transcription and PelF protein levels compared to planktonic populations (39). Interestingly, the PAO1Δ*psl* biofilm displayed PelC protein levels 3-fold higher than PAO1 (**Figure 15B**). When we plated the biofilm biomass onto solid medium, we noticed a high frequency of the RSCV phenotype in the biomass harvested from PAO1Δ*psl* biofilm (**Figure 15C**). The RSCVs are approximated half of the total population for PAO1Δ*psl* after 3 d of biofilm growth, while they account for only five percent of the total PAO1 population (**Figure 15D**).

RSCVs have elevated c-di-GMP levels and Pel and Psl expression levels (45, 90, 101). In a PAO1Δ*psl* mutant, elevated c-di-GMP still results in the RSCV phenotype. Individual smooth and RSCV colonies isolated from the biofilm were then tested for PelC expression. As expected, strains displaying the RSCV phenotype had elevated levels of PelC protein expression compared to the parental inoculum and elevated intracellular levels of c-di-GMP (**Figure 16**). Interestingly, the representative smooth isolate from PAO1Δ*psl* biofilm also displayed elevated levels of c-di-GMP compared to the parent strain (**Figure 16B**). Laboratory derived RSCVs commonly result from mutations in the

wspF gene (221). To determine if the RSCVs isolated were *wspF* mutants, we attempted complementation with pWspF (**Figure 17A**). The PAO1 RSCV was partially complemented by WspF. The colony morphology was smooth but remained small in size. In contrast, each PAO1Δ*psl* RSCV was fully complemented by WspF (**Figure 17A**). We then sequenced the *wspF* gene for each isolate (**Figure 17B**). The PAO1 RSCV has a 201 bp gene deletion including 164 bp of the C-terminus of *wspF* and 36 bp in the intergenic region between *wspF* and *wspR*. In the PAO1 *psl* RSCVs, single base pair insertions were identified producing a frameshift in the ORF.

We next tested if biofilm growth increased PelC expression in other clinical and environmental class II isolates bearing *psl* mutations. Similar to PAO1, each *psl* mutant displayed higher PelC expression compared to the corresponding wild-type strain (**Figure 18C**). To see if RSCVs are selected for in the *psl* mutant background, we plated out the biofilm biomass (**Figure 18A**). For one strain, S54485, RSCVs were detected and their presence was increased in the *psl* mutant compared to the wild-type (**Figure 18B**). RSCVs were not clearly identified in E2 or X13273 and thus not quantified. Regardless of whether RSCVs were isolated or not, PelC expression was elevated in the *psl* mutant biofilms. These data suggest that a strain relying primarily on Psl can utilize Pel to rescue biofilm growth if faced with a deleterious *psl* mutation.

DISCUSSION

Extracellular polysaccharides are a key component of the biofilm matrix. The ability to produce multiple types of polysaccharides appears to have been maintained in *P. aeruginosa*. Yet the two common laboratory strains, PAO1 and PA14, use two different polysaccharides as the major biofilm matrix polysaccharide. We sought to determine the relative prominence of Psl and Pel as the major matrix polysaccharide. In this study we propose four classes of matrix users based upon Pel and Psl dependent phenotypes. Finally, we demonstrated that elevated Pel expression can rescue biofilm formation for a Psl-utilizing strain. These data suggest that an advantage of having both Pel and Psl is

to reduce the impact of deleterious mutations on an important function such as biofilm formation.

Psl played an important role in surface attachment for all the isolates tested (Figure 4). This suggests that Psl universally plays a critical role in attachment for more *P. aeruginosa* isolates. This is also not surprising, as many polysaccharides are involved in the attachment of various bacterial species to abiotic surfaces (like plastic and glass), plant, and mammalian surfaces (32, 127, 254). However, Pel did not appear to be an important attachment determinant. Only in strains producing a large amount of Pel (class IV) was an attachment phenotype observed for a *pel* mutant strain (Figure 4C).

Unlike surface attachment, the isolates exhibited a spectrum of Pel and Psl dependencies for biofilm formation. We classified Pel polysaccharide utilizing strains class I matrix producers. PA14 was the only strain we found to use Pel as the dominant matrix polysaccharide. An extensive analysis of multiple isolates would have to be performed to determine how widespread class I strains are in the community. However, we would predict that isolates bearing *psl* mutations would probably be class I strains. Some strains, like PAO1, primarily relied on Psl for biofilm formation. Our expression data at least confirm that these strains are capable of transcribing and expressing some of the Pel biosynthetic genes/proteins. Therefore, like PAO1, their reliance on Psl is not due to the inability to express the Pel enzymes, although we cannot rule out that these strains are unable to make the Pel polysaccharide itself. We called these strains class II matrix producers.

Class III strains we called EPS redundant matrix users. These strains produced relatively low amounts of PelC and Psl. Single mutations in either *pel* or *psl* did not have a phenotype for biofilm formation in the microtiter dish assay (Figure 5B), suggesting that both Pel and Psl are individually capable of ensuring normal biofilm development in this class. The one class III strain we examined in a flow cell, MSH3, showed reduced biomass for both *pel* and *psl* single mutations relative to the wild-type. This is different from the microtiter dish biofilm assay data, where single mutations have no phenotype.

One explanation is that several factors can impact biofilm structure in the flow cell besides EPS production (e.g. relative surface motility) (208). Perhaps the longer culturing time (5 d verse 1 d) or a flowing compared to a static environment influenced biofilm resulted in the observed differences seen in the two systems. However, this data is consistent with the idea that both Pel and Psl are produced and are important in class III strain biofilms.

Finally, Class IV strains were matrix overproducers. These strains, CF127 and 19660, produced a robust biofilm, where single *pel* or *psl* mutations only slightly reduced biofilm biomass compared to the wild-type strain. This does not clearly appear to be the case for 19660, where in microtiter dish biofilms a *psl* mutation appeared to have a significant impact on biofilm formation (Figure 5C). However, analysis of the same strain in a flow cell (Figure 6) showed that it was capable of producing a significant biofilm. We speculated that our vigorous wash step removed most of the biofilm biomass in the 19660Δ*psl* mutant. By changing our microtiter wash conditions, we confirmed that the 19660Δ*psl* mutant formed significant, albeit fragile, biofilms (Figure 7). PelC and Psl expression studies showed that CF127 and 19660 strains produced both at high levels. Elevated polysaccharide expression in CF127 can be explained by high levels of intracellular c-di-GMP (Figure 14). However, this is not the case for 19660, suggesting that the underlying molecular mechanisms responsible for elevated matrix production are different in these two strains.

One might predict that the source of isolates would be a key predictor of which matrix class they belong to. However, polysaccharide dependence and the isolate source do not appear to be correlated, but a much larger number of strains would need to be tested in order to make any definite conclusions. Interestingly, phylogenetic analysis of *P. aeruginosa* strains demonstrate that strains from similar environmental or clinical sources are in general no more related than those from different sources (264). In addition, the functional significance of being placed in a given matrix class is not clear. It is reasonable to presume that each class exhibits functional differences. Pel and Psl are chemically distinct polysaccharides with unique properties that could influence

function (27, 43, 64). For example, Psl has been specifically found to be important in surface adherence and biofilm initiation on glass, polyvinyl chloride (PVC), mucin, epithelial cells and human alveolar epithelial cells (26, 65, 136, 146). Not surprisingly, PA14, a class I isolate, was the poorest at surface attachment of tested strains (Figure 6). Pel production has also been linked to aminoglycoside tolerance in biofilms (39). This suggests that biofilms produced by class II isolates might be more sensitive to this class of antibiotic.

Our evolution experiments suggest that a mutation in the primary matrix polysaccharide (Psl) will select for adaptations promoting expression of the compensatory matrix polysaccharide (Pel) during biofilm growth (Figure 15). The molecular nature of the PAO1Δ*psl* RSCV strains demonstrates elevated c-di-GMP levels similar to previously described RSCVs (90, 221). In addition, we identified the mutations responsible for the conversion to an RSCV in the PAO1Δ*psl* strains to the gene *wspF*. Mutations in the gene *wspF* activate the diguanylate cyclase WspR increasing c-di-GMP levels and result in an RSCV (44, 45, 90, 127, 221). We also demonstrated that biofilm growth of Class II *psl* mutants universally selects for increased PelC expression as demonstrated in Figure S11. For some of the isolates, RSCVs are produced and as seen in PAO1, they are produced at a greater frequency in the *psl* mutant. However, the molecular mechanism of increased PelC expression in X13273 and E2 (which did not produce RSCVs) is not clear

There are different hypotheses (not mutually exclusive) as to why a species might retain the capability of producing multiple biofilm matrix polysaccharides. One hypothesis is that depending upon the environment, different polysaccharides might be employed as the primary matrix scaffold. *P. aeruginosa* is not unique in its ability to produce multiple different extracellular polysaccharides. Other organisms such as, *Escherichia coli*, *Pseudomonas putida*, *Vibrio* spp, *Salmonella* spp. and *Burkholderia* spp. also produce multiple polysaccharides, each of which contribute to biofilm formation (108). For example, *Salmonella enterica serovar Typhimurium* produces three known extracellular polysaccharides, colanic acid, cellulose and an O-antigen capsule (44).

Interestingly, each polysaccharide has a niche-specific role in biofilm formation. For example, O-antigen capsule is critical to form a biofilm on gallstone surfaces but is not involved in glass or plastic binding (44). Colanic acid is important in biofilm formation on HEp-2 cells and chicken intestinal tissue but does not play a role in plastic surface or gallstone biofilm development (127). Finally, cellulose does not contribute to gallstone biofilm formation but does on HEp-2 cells, chicken intestinal epithelium and plastic surfaces (44, 127). Thus, *P. aeruginosa* might utilize Psl, Pel and alginate in a similar niche-specific manner.

Pseudomonas putida is another example capable of producing four unique polysaccharides, Pea, Peb, alginate and a cellulose-like polymer (Bcs) (31, 145, 165, 166). Recent studies demonstrate that Pea and Peb play important roles in *P. putida* biofilm stability, while alginate and Bcs appear to be minor contributors in laboratory grown biofilms (31, 145, 165, 166). Similar to *P. aeruginosa*, strains of *P. putida* can differentially depend on individual polysaccharides for biofilm development (31, 145, 165, 166). These polysaccharides also display unique attachment patterns. The cellulose-like polymer, but not Pea contributes to maize root colonization and neither is important in glass attachment (165). This set of work highlights that polysaccharides in the *P. putida* biofilm matrix have unique niche-colonization but display some redundant cell-cell adhesion functions.

Another hypothesis is that biofilm formation is such an important survival mechanism that maintaining the capability of producing redundant matrix polysaccharides would be an advantage. This is demonstrated in our biofilm evolution experiments. Such redundancy might be important for adverse environments, such as the CF airways, where strains arise that exhibit elevated rates of mutation (172). Redundancy of matrix polysaccharides might help reconcile high mutations rates with the maintenance of a key survival mechanism such as biofilm formation.

MATERIALS AND METHODS

Bacterial strains and growth conditions

Bacterial strains in this study are listed in **Table 1** (20, 27, 39, 49, 92, 94, 111, 126, 136, 188, 264). For routine culture, *P. aeruginosa* strains were grown at 37°C in Luria-Bertani (LB) medium (Difco). Plasmids were selected with 100 μg/ml gentamycin for *P. aeruginosa* strains and 10 μg/ml gentamycin for *E. coli*. 25 μg/ml irgasan was used to counter select for *E. coli*. For all assays comparing isolates, Tryptic Soy Broth (TSB) 30g/L and supplemented with 15g/L of bacto agar for plates (Difco).

Strain construction

ΔpelF

Allelic replacement strains were constructed by using an unmarked, nonpolar deletion strategy. Flanking regions of *pelF* were amplified using primers *pelF* UP and *pelF* DN primer sets. The resultant PCR product was ligated into the suicide vector, pEX18Gm, via *Hind*III restriction site. The plasmid pEX18GmΔ*pelF* was verified by sequencing analysis. Single recombination mutants were selected on VBMM containing 100 μg/ml gentamicin or LB containing 100 μg/ml gentamicin and 25 μg/ml irgasan. Double recombination mutants were selected on LB without NaCl plates containing 5% sucrose and confirmed by PCR.

ΔpslD

Construction of Δ*pslD* strains was performed as described before (27).

Colony morphology

Overnight cultures were diluted 1/100 in PBS. 5 μl of cells were spotted onto TSB plates supplemented with 40 μg/ml Congo red and 15 μg/ml brilliant blue R (Sigma-Aldrich) and incubated at 25°C for 5 d.

Microtiter dish biofilm

96-well microtiter dish assay was preformed as described previously with the following modifications (170). 100 μl of mid-log cells ($OD_{600} \sim 0.5$) grown in TSB was added to the wells of a 96-well polypropelene plate (Nunc) and incubated statically for 1 h (rapid

attachment) or 24 h (biofilm development) at 25°C. Following incubation, non-attached cells were removed and the plate was rinsed thoroughly with water. Plates were stained with 150 μl 0.1% crystal violet for 10 min. The plate was rinsed and adhered crystal violet was solubilized in 200 μl 95% ethanol for 10 min, then 100 μl was transferred to a new 96-well plate to measure the absorbance at OD_{595}.

Flow cell experiments

PA14 monocultures were tagged with GFP on the chromosome using the mini Tn7 system to allow fluorescent visualization of growing biofilms (33). PAO1, E2, CF127, 19660 and MSH3 monoclutures were tagged with the GFP expression vector, pMRP9-1 (49). S54485 biofilms were stained with 1 ml of 5 μM FM4-64 for 10 m. Flow resumed and images captured after 15 m of washing. Log phase cultures grown in full-strength TSB were diluted to a final OD_{600} of 0.05 for PA14 and 0.01 for PAO1, E2, S54485, CF127, 19660 and MSH3 in 1% TSB. Bacteria were inoculated into an inverted flow cell and allowed to attach for one hour. Upon initiation of media flow, fresh media of 1% TSB was pumped at a constant rate (10 ml/h). Biofilms were grown at room temperature for 5 d. Biofilms were visualized by fluorescence using a Zeiss LSM 510 scanning confocal laser microscope and image series were compiled using Velocity software (Improvision).

Tube biofilm

Tube biofilms were conducted as previously described with the following modifications (204). *P. aeruginosa* was grown to log phase in TSB at 37°C shaking, diluted to an OD_{600} 0.05 and 3 ml injected into a 30 cm long x 6.35 mm inner-diameter tube and incubated for 1 h. Biofilms were grown at 25°C in full-strength TSB medium at 10 ml/h flow rate for 72 h. The external portion of the tube was sterilized with ethanol and from each tube three 2 cm slices were extracted and placed in 2 ml PBS. Biomass was scraped from the inside of the tube, vortexed and analyzed for protein expression as described in the immunoblot analysis section. Colony morphology was assessed on LB medium with a dissecting microscope (Olympus SZX-ILLK100).

PelC purification and antibody production.

The coding sequence for the mature PelC protein (residues 20-172) was amplified from *P. aeruginosa* PAO1 genomic DNA using gene-specific primers and cloned into the pET28a expression vector (Novagen) and the sequence verified. The expression vector was then transformed into *E. coli* BL21 (DE3) cells (Agilent) and subsequently grown in 1 L Luria-Bertani (LB) broth containing 50 mg/ml kanamycin at 37°C. Once the cells reached an OD_{600} of 0.6, protein expression was induced by the addition of 1 mM isopropyl-β-D-1-thiogalactopyranoside (IPTG) followed by incubation at 25°C for 18 h. The cell cultures were then pelleted by centrifugation and flash frozen for subsequent purification. Frozen cell pellets were thawed in 40 ml of cell lysis buffer (50 mM Tris-HCl pH 8.0, 300 mM NaCl, 1 SIGMAFAST protease inhibitor EDTA-free cocktail tablet (Sigma)) and lysed by homogenization using an Emulsiflex-C3 (Avestin, Inc.) at a pressure of 10000-15000 psi (three passes total). Following centrifugation of the insoluble cell lysate, PelC was purified over Ni-NTA agarose (QIAGEN) using a linear imidazole gradient (20 mM Tris-HCl pH 8.0, 300 mM NaCl, 20-250 mM imidazole) followed by size-exclusion chromatography (20 mM Tris-HCl pH 8.0, 150 mM NaCl) using a HiLoad 16/60 Superdex 200 column (GE Healthcare). Purified PelC protein was sent to Open Biosystems for polyclonal antisera production.

RNA purification and analysis

P. aeruginosa strains were grown in TSB shaking at 37°C for 8 h or on TSB plates for 3 d at 25°C. Total RNA was stabilized for purification using RNAprotect Bacterial Reagent and extracted using the RNeasy Mini Purification kit (QIAGEN). Briefly, approximately 10^9 CFU in RNAprotect were lysed using 5 mg/ml lysozyme and tip-sonication. Genomic DNA was removed with an on-column RNase-free DNase I treatment (QIAGEN) and the RNA eluted in 30 μl RNase-free water. Remaining genomic DNA was removed by a second off-column DNase I treatment (Promega). Following purity confirmation by PCR using *rplU* primers, cDNA was synthesized using the iScript cDNA synthesis kit (Bio-Rad) and verified by PCR. 84 μl of water was added to the cDNA samples to prevent

interference of real-time PCR by reagents from the reverse transcription reaction. Quantitative real-time PCR was performed using the CFX96 Real-Time PCR Dectetion System (Bio-Rad). With iQ SYBR Green Supermix used according to manufacturer's instructions (Bio-rad). Primers are listed in Table S1. *pelA*, *pslA* and *algD* transcript levels are normalized to *rpsL* transcript levels.

Immunoblot analysis

1 ml of *P. aeruginosa* liquid culture grown in TSB for for 2.5 h to an OD_{600} ~ 0.5 followed by 1 h static incubation at 25°C were harvested and resuspended in 500 μl PBS. Alternatively, cells were collected from TSB agar surfaces grown for 3 d at 25°C and resuspended in PBS. Alternatively, biomass was collected from tube biofilms grown for 3 d at 25°C. Biomass was resuspended in PBS. 50 μl sample was mixed with 50 μl 2x laemli buffer and boiled for five m. Protein concentration was measured using the Pierce 660 nm Protein Assay and Ionic Detergent Compatibility Reagent as described by the manufacturer (Thermo Scientific). Equal total protein was loaded onto a pre-cast 12.5% Tris-HCl polyacrylamide gel and transferred to a PVDF membrane for immunoblotting (Bio-rad). The membrane was blocked in 5% non-fat milk in TBST for 1 h at room temperature. The membrane was cut in half and either probed for RNA polymerase (RNAP, Neoclone Biotechnologies) according to manufacturers instructions or with α-PelC antibodies at 1:5,000 dilution in 1% non-fat milk TBST for 1 h. Blots were developed with goat α-rabbit HRP-conjugated secondary antibody (Thermo-Scientific) and Pierce detection kit.

Psl immunoblots were performed as described previously with the following modifications(27). Cells from each growth condition described above were harvested and resuspended in 100 μl 0.5 M EDTA. Cells were boiled for 20 min with periodic vortexing and centrifuged. The supernatant fraction was treated with Proteinase K (final concentration 0.5mg/ml) for 60 min at 60°C, followed by Proteinase K inactivation for 30 min at 80°C. Samples were stored at 4°C for immunoblotting. Polysaccharide preparations were normalized to total protein in the EDTA extraction as

determined by Protein Assay (Bio-rad). 5 µl sample was spotted onto a nitrocellulose membrane and probed as described previously (27).

Nucleotide extraction and c-di-GMP measurements

P. aeruginosa strains were grown on TSB plates for 3 d at 25°C or 1 d at 37°C. Colonies were harvested using a plastic loop and quickly deposited into 1.1ml VBMM. With minimal re-suspension step, 990ml was immediately aspirated and added into 70% perchloric acid (Sigma) to a final concentration of 0.6M. 10ml of 10mM 2-chloro-AMP (internal standard compound) was added to the mixture, vortexed, and placed on ice. Each individual sample was prepared one at a time to minimise the time spent between harvesting cells and acid extraction, as bacteria rapidly alter intracellular nucleotide pools in response to changes in their growth environment (23). All subsequent extraction steps and LC/MS/MS measurements were performed as described in a forthcoming article (Irie Y *et al.*, *manuscript in preparation*).

Table 1 Strains used in Chapter IV

Strains	Relevant Characteristics	Reference
PAO1	wild-type	Holloway, 1955
PAO1Δ*pel*	*pelA;* polar mutant of the *pel* operon	Borlee *et al.,* 2010
PAO1Δ*psl*	*pslBCD;* polar mutant of *psl* operon	Kirisits *et al*., 2005
PAO1Δ*pel/psl*		Borlee *et al.,* 2010
PA14	wild-type	Rehme et al., 1995
PA14Δ*pelB*	*pelB* nonpolar mutant of the *pel* operon	Colvin *et al*., 2011
X13273	Blood isolate; Seattle, WA	Wolfgang *et al*., 2003
X13273Δ*pel*	*pelF*; non-polar mutant of the *pel* operon	This study
X13273Δ*psl*	*pslD;* non-polar mutant of the *psl* operon	This study
X13273Δ*pel/psl*		This study
S35004	Blood isolate; Seattle, WA	Wolfgang *et al*., 2003
19660	Cornea/Ocular infection; Berkeley, CA	Wolfgang *et al*., 2003
19660Δ*pel*	*pelF*; non-polar mutant of the *pel* operon	This study
19660Δ*psl*	*pslD;* non-polar mutant of the *psl* operon	This study
19660Δ*pel/psl*		This study
6077	Cornea/Ocular infection; Berkeley, CA	Wolfgang *et al*., 2003
X24509	UTI; Seattle, WA	Wolfgang *et al*., 2003
X24509Δ*pel*	*pelF*; non-polar mutant of the *pel* operon	This study
X24509Δ*psl*	*pslD;* non-polar mutant of the *psl* operon	This study
X24509Δ*pel/psl*		This study
S54485	UTI; Seattle, WA	Wolfgang *et al*., 2003
S54485Δ*pel*	*pelF*; non-polar mutant of the *pel* operon	This study
S54485Δ*psl*	*pslD;* non-polar mutant of the *psl* operon	This study
S54485Δ*pel/psl*		This study
JJ692	UTI; Minneapolis, Mn	Wolfgang *et al*., 2003
U2504	UTI; Gainesville, FL	Wolfgang *et al*., 2003
CF5	cystic fibrosis; Columbia, MO	Wolfgang *et al*., 2003
CF18	cystic fibrosis; Jackson, MS	Wolfgang *et al*., 2003
CF27	cystic fibrosis; Seattle, WA	Wolfgang *et al*., 2003
CF127	cystic fibrosis; Denver, CO	Wolfgang *et al*., 2003
CF127Δ*pel*	*pelF*; non-polar mutant of the *pel* operon	This study
CF127Δ*psl*	*pslD;* non-polar mutant of the *psl* operon	This study
CF127Δ*pel/psl*		This study
62	environmental (soil); Berkeley, CA	Wolfgang *et al*., 2003
62Δ*pel*	*pelF*; non-polar mutant of the *pel* operon	This study
62Δ*psl*	*pslD;* non-polar mutant of the *psl* operon	This study
62Δ*pel/psl*		This study
E2	environmental (tomato plant); Gainesville, FL	Wolfgang *et al*., 2003
E2Δ*pel*	*pelF*; non-polar mutant of the *pel* operon	This study
E2Δ*psl*	*pslD;* non-polar mutant of the *psl* operon	This study
E2Δ*pel/psl*		This study
MSH3	environmental (water); Spirit Lake, WA	Wolfgang *et al*., 2003
MSH3Δ*pel*	*pelF*; non-polar mutant of the *pel* operon	This study
MSH3Δ*psl*	*pslD;* non-polar mutant of the *psl* operon	This study
MSH3Δ*pel/psl*		This study
MSH10	environmental (water); Spirit Lake, WA	Wolfgang *et al*., 2003
MSH10Δ*pel*	*pelF*; non-polar mutant of the *pel* operon	This study
MSH10Δ*psl*	*pslD;* non-polar mutant of the *psl* operon	This study
MSH10Δ*pel/psl*		This study
T56593	Ear infection; Wake Forest University, NC	provided by D. Wozniak
T56593Δ*pel*	*pelF*; non-polar mutant of the *pel* operon	This study
T56593Δ*psl*	*pslD;* non-polar mutant of the *psl* operon	This study
T56593Δ*pel/psl*		This study
T53616	UTI; Wake Forest University, NC	provided by D. Wozniak
T68934	cystic fibrosis; Wake Forest University, NC	provided by D. Wozniak
X54868	Bronchial; Wake Forest University, NC	provided by D. Wozniak
WFPA801	*psl*-inducible strain, PAO1 background	Ma *et al*., 2006

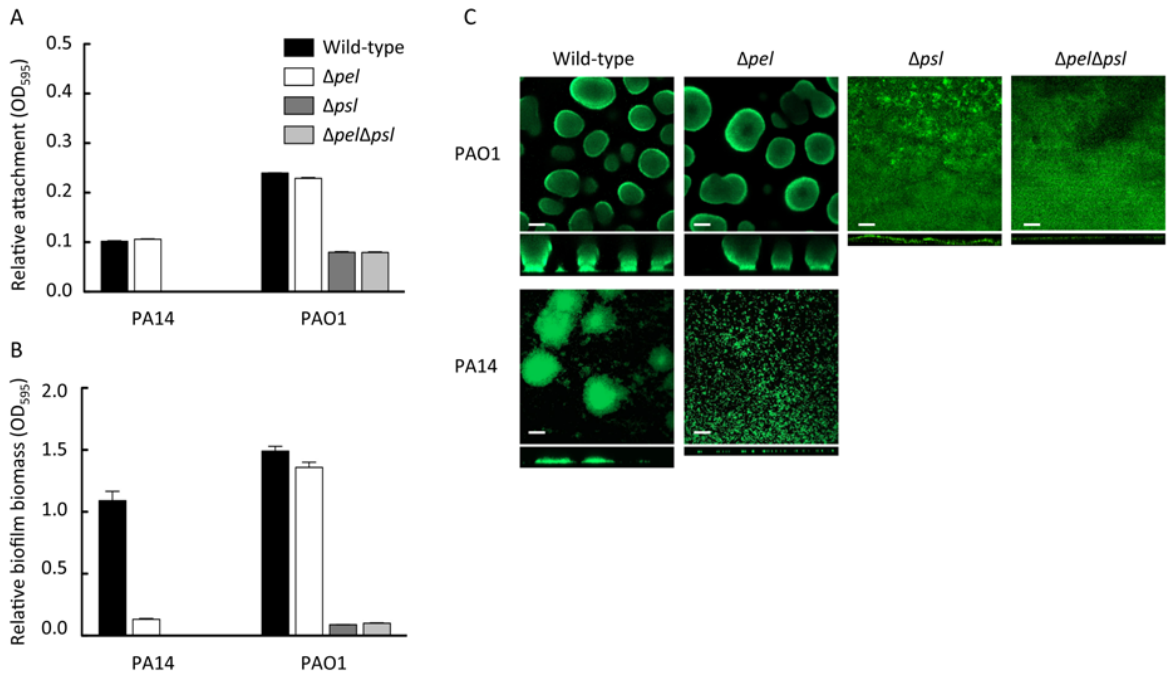

Figure 1. PAO1 and PA14 attachment and biofilm analysis. The effect of *pel* and *psl* mutations in static microtiter dish assays and flow cell experiments were analyzed. Attachment after 1 h of incubation (A) and biofilm formation after 24 h of incubation (B) were assessed by crystal violet staining for PAO1 and PA14 and the corresponding mutants. Flow cell images were acquired after 5 d of growth. Representative top down and side view CLSM images are shown using 20x objective (C). Scale bars represent 50 μm. Error bars represent standard deviation.

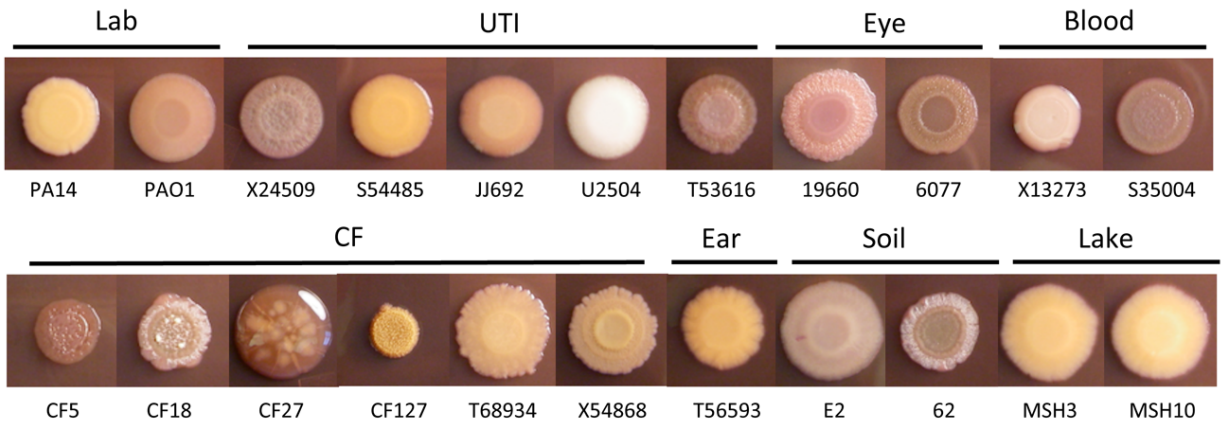

Figure 2. Colony morphology of the clinical and environmental isolates. Images of colony morphology of 5 µl spots were acquired after 5 d of growth at 25°C. Colonies are arranged according to their isolation site.

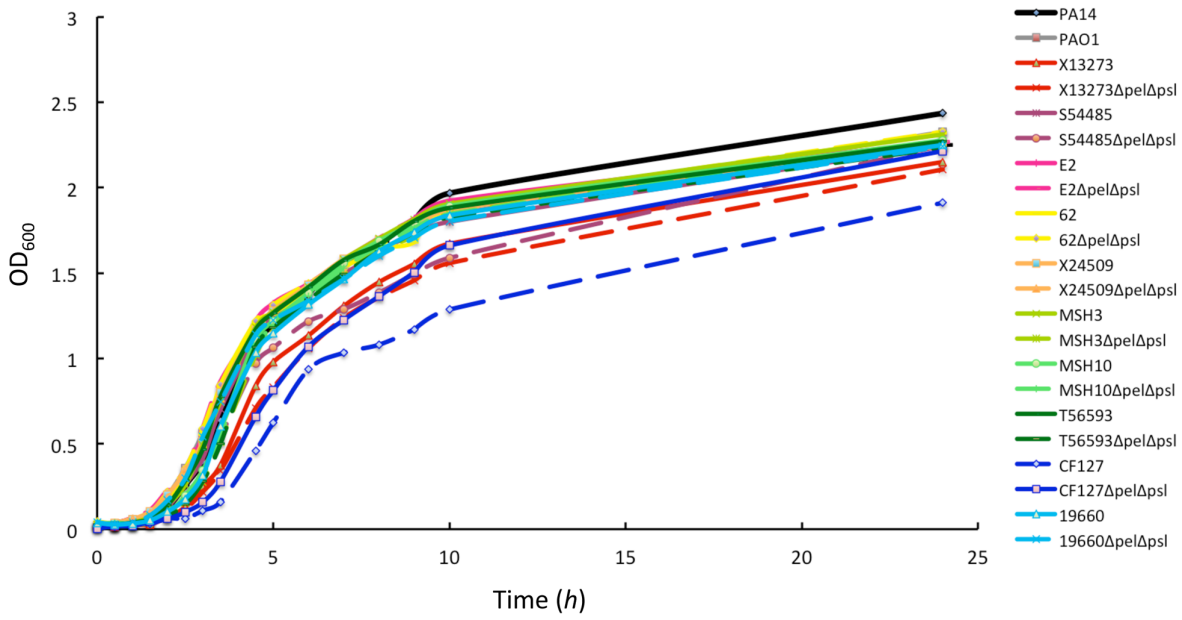

Figure 3. Growth curve of isolates and *pelpsl* mutants. Relative growth rate was monitored by OD_{600} from wild-type and *pelpsl* mutants grown at 37°C in shaking conditions.

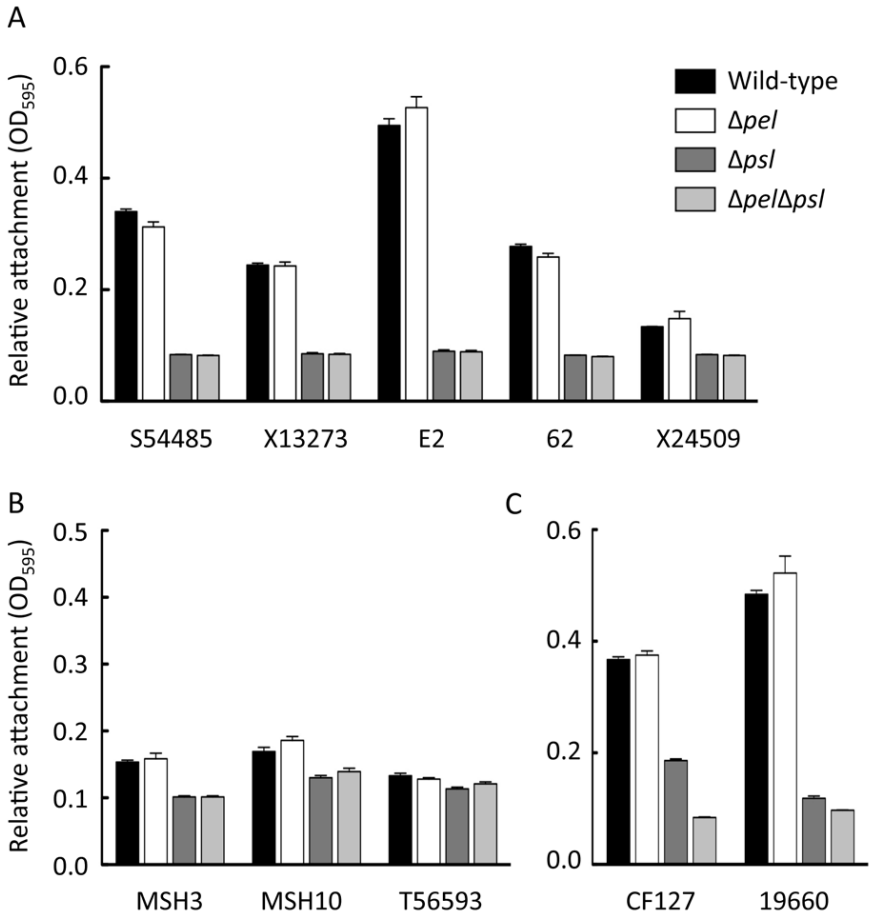

Figure 4. Relative attachment of the isolates to a microtiter plate. The effect of *pel* and *psl* mutations in static microtiter dish assays for attachment was analyzed. Strains were incubated statically for 1 h, loosely adherent material was removed through washing and the remaining biomass was stained by crystal violet. Mutants were separated based on class categorization, "Psl-dominant strains" (A), "EPS redundant matrix users" (B) and "matrix over-producers" (C). The rationale is described in the text. Error bars represent standard deviation.

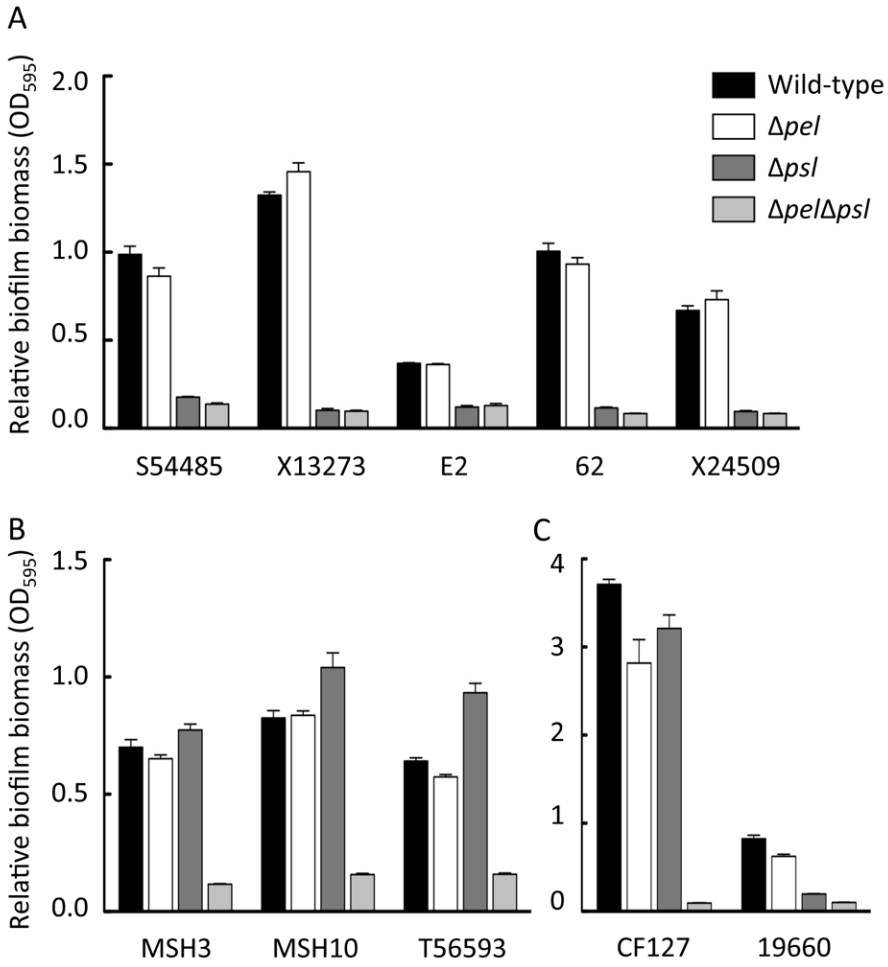

Figure 5. Relative biofilm formation of the isolates to a microtiter plate. The effect of *pel* and *psl* mutations in static microtiter dish assays for biofilm formation was analyzed. Strains were incubated statically for 24 h, loosely adherent material was removed through washing and the remaining biomass was stained by crystal violet. Mutants were separated based on class categorization, "Psl-dominant strains" (A), "EPS redundant matrix users" (B) and "matrix over-producers" (C). The rationale is described in the text. Error bars represent standard deviation.

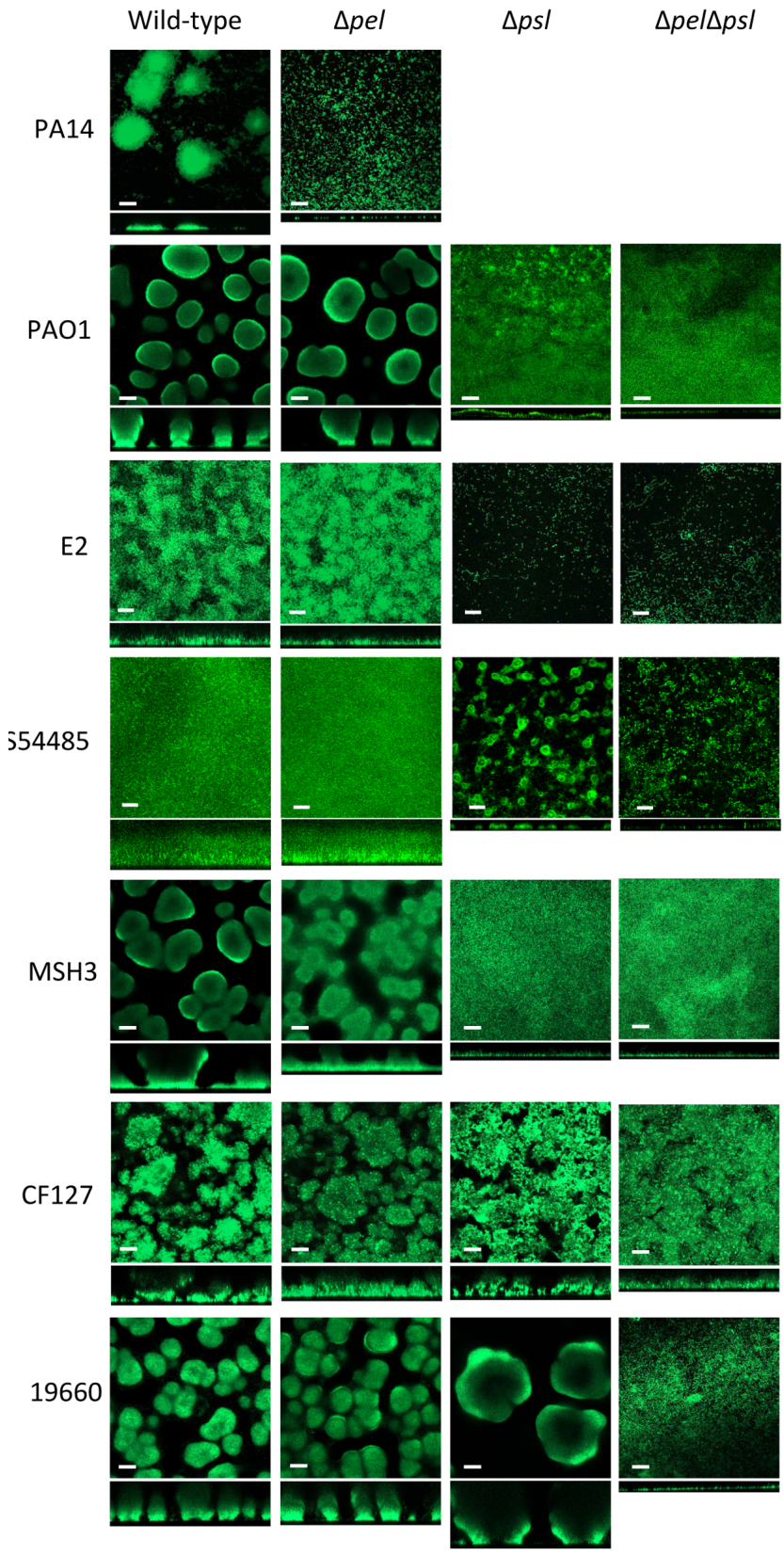

Figure 6. Flow cell analysis of select isolates.
Flow cell images of PA14, PAO1, E2, S54485, MSH3, CF127, 19660 and their corresponding mutants were acquired after 5 d of growth. Representative top down and side view CLSM images are shown using 20x objective. Scale bars represent 50 μm.

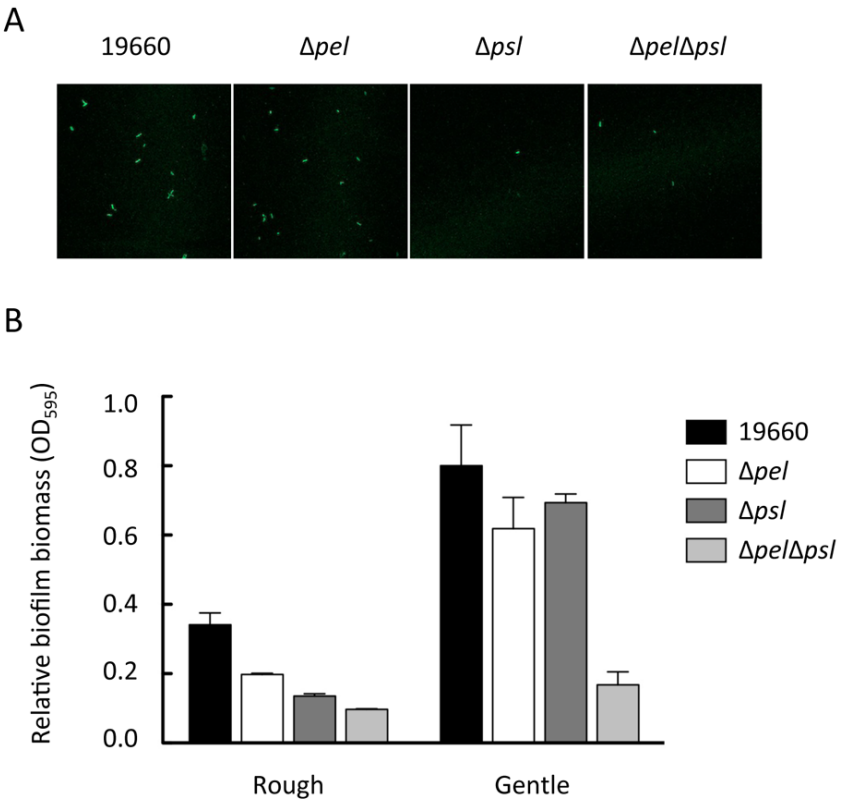

Figure 7. 19660 attachment and microtiter dish biofilm formation. Attachment to glass slides was visualized in a flow cell after one h of attachment and one h of continuous flow. Representative CSLM images are shown using a 40x objective of 19660, *pel*, *psl* and *pelpsl* (A). 19660 strains were compared for relative biomass after 24 h growth at 25°C in a microtiter dish biofilm assay using two different wash conditions (B). Rough washing is the typical method of washing by submerging the microtiter dish under water and rigorously dumping the liquid out. Gentle washing removes non-adhered biomass by gently pipetting the water washes. Error bars indicate standard deviation.

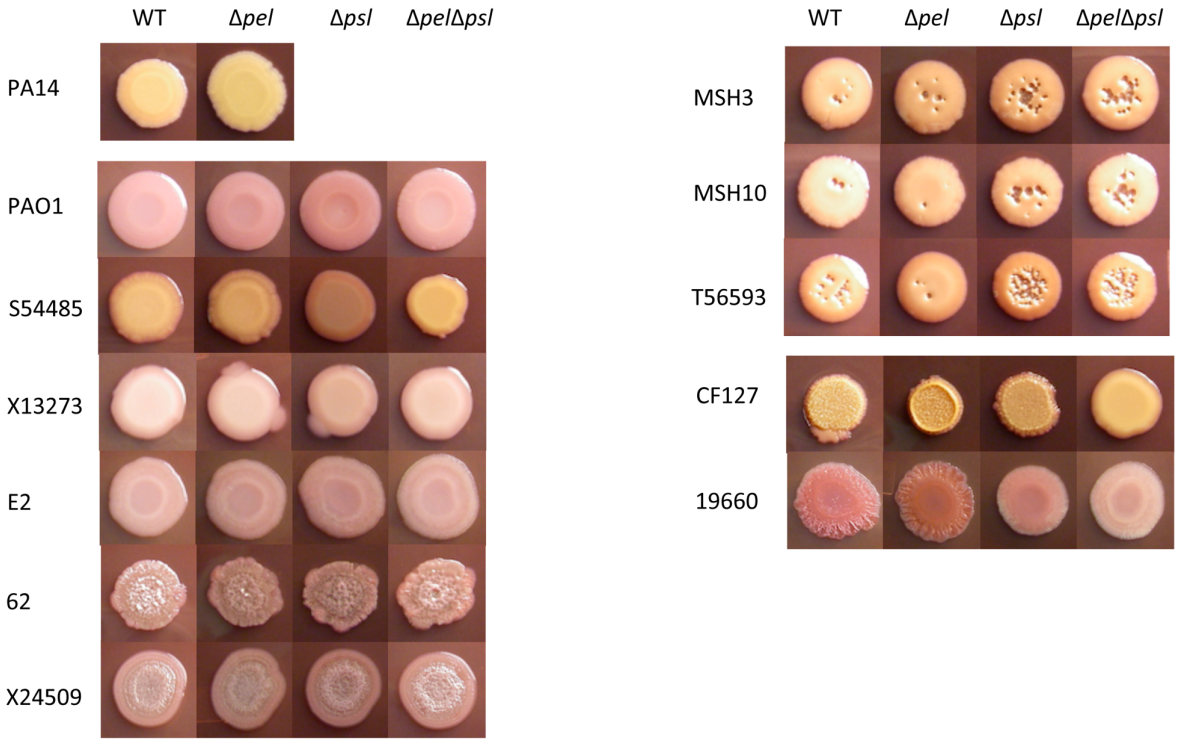

Figure 8. Colony morphology of *pel* and *psl* mutants. The colony morphology of 5 µl spots was compared for the parent strain, *pel* and *psl* single mutants and *pel/psl* double mutant. Images were acquired after 5 d of growth at 25°C.

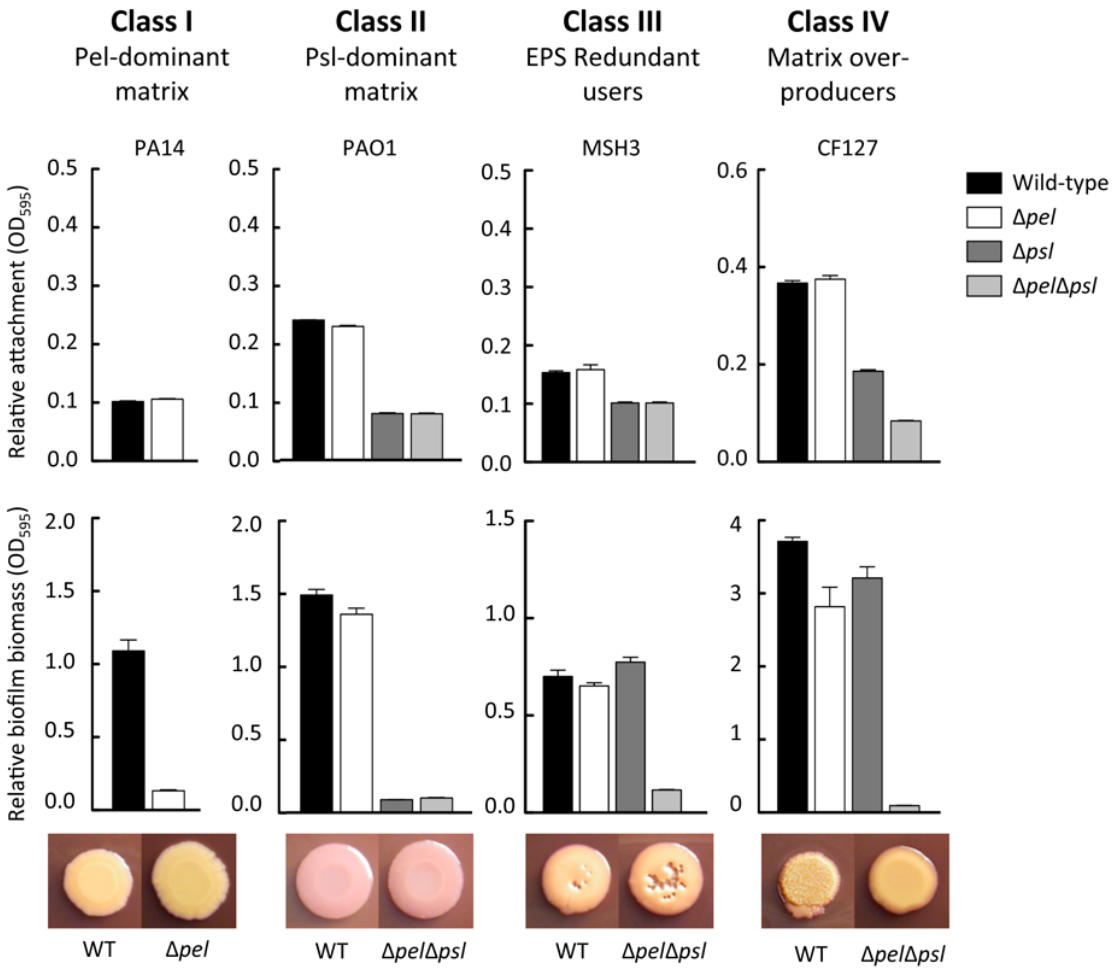

Figure 9. Representative phenotypes for class categorization. One strain from each class is chosen as a representative class isolate. The effect of *pel, psl* and *pelpsl* mutations in static microtiter dish assays and colony morphology are shown. The top panel is relative attachment, middle panel is relative biofilm formation in a microtiter assay and bottom panel shows colony morphology for wild-type and *pelpsl* mutant.

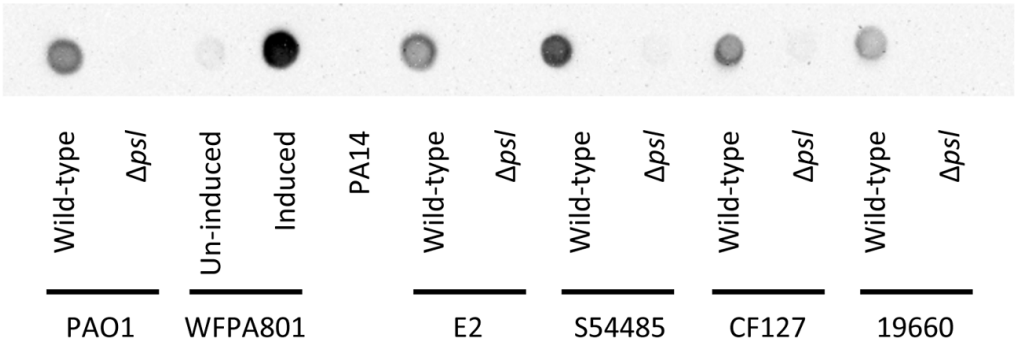

Figure 10. Verifying the Psl antisera. Psl polysaccharide dot blots were compared from strains grown overnight at 37°C. Wild-type and the corresponding *psl* mutant for PAO1, E2, S54485, CF127 and 19660 were compared for Psl expression levels. In addition PA14 and the arabinose inducible Psl strain, WFPA801 were also tested.

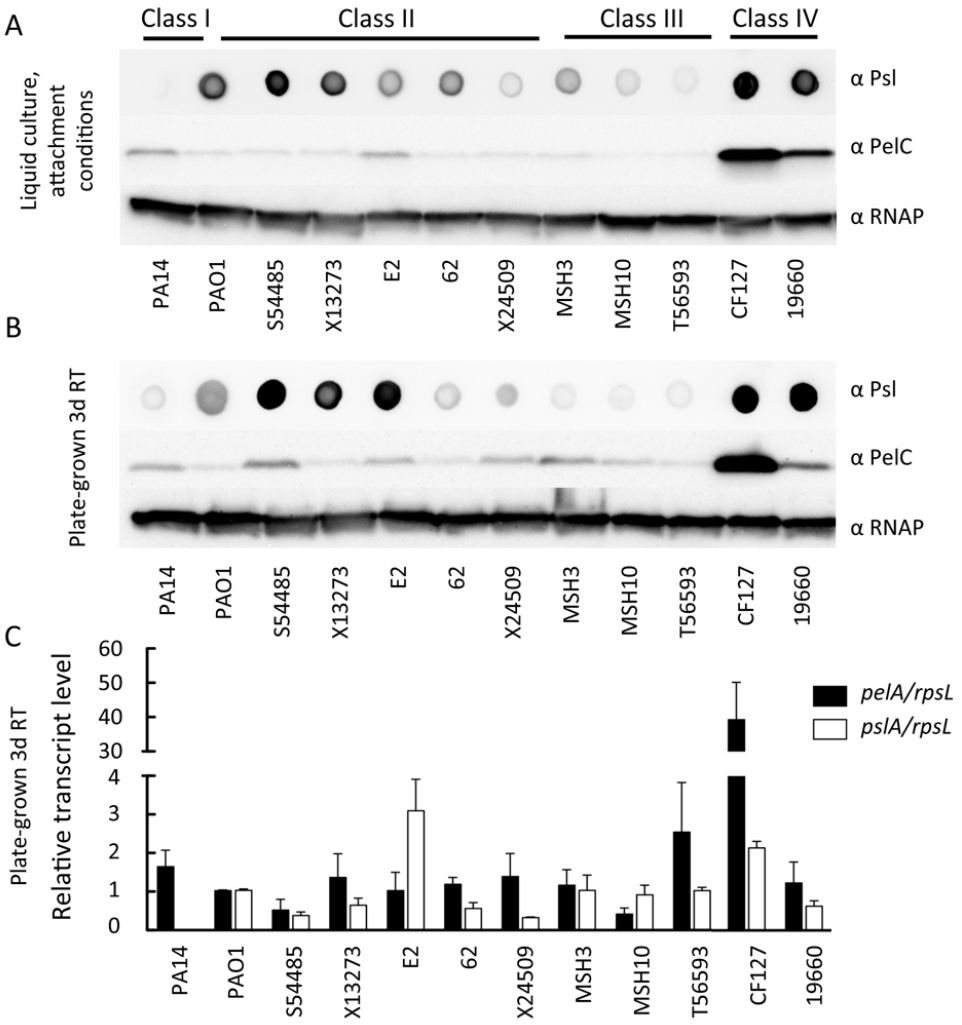

Figure 11. PelC protein, Psl polysaccharide and *pelA* and *pslA* transcript level analysis. Psl polysaccharide dot blot (top panel), PelC protein (middle panel) and RNA polymerase protein loading control (bottom panel) were analyzed for the different isolates. Polysaccharide and protein profiles were assessed for microtiter dish attachment conditions (A) or from plate grown cultures at 25 °C for 3 d (B). qRT-PCR on *pelA*, *pslA* and *rpsL* transcripts were performed from the same culture conditions as analyzed for protein and polysaccharide expression level in part B (C). *pelA* and *pslA* transcripts are normalized to *rpsL* and then to PAO1 for relative transcript level. Error bars indicate standard deviation from three independent experiments.

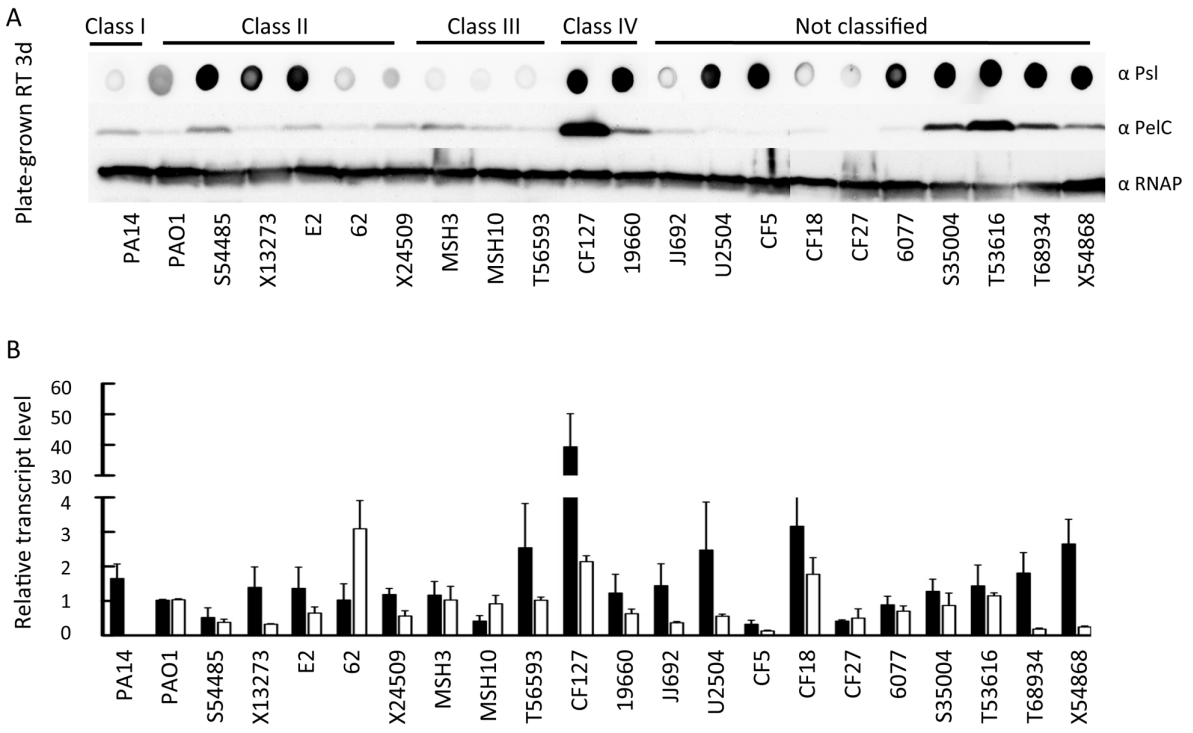

Figure 12. Relative PelC and Psl expression levels of all isolates. Strains were assessed for Psl and PelC expression (A) and *pelA* and *pslA* transcript levels (B) from plate grown cultures at 25 °C for 3 d. (A) Psl polysaccharide dot blot (top panel), PelC protein (middle panel) and RNA polymerase protein loading control (bottom panel) are shown for all isolates. One representative experiment is shown. (B) RNA profiles were assessed by qRT-PCR on *pelA*, *pslA* and *rpsL* transcripts. *pelA* and *pslA* transcripts are normalized to *rpsL* and then to PAO1 for relative transcript level. Error bars indicate standard deviation from three independent experiments.

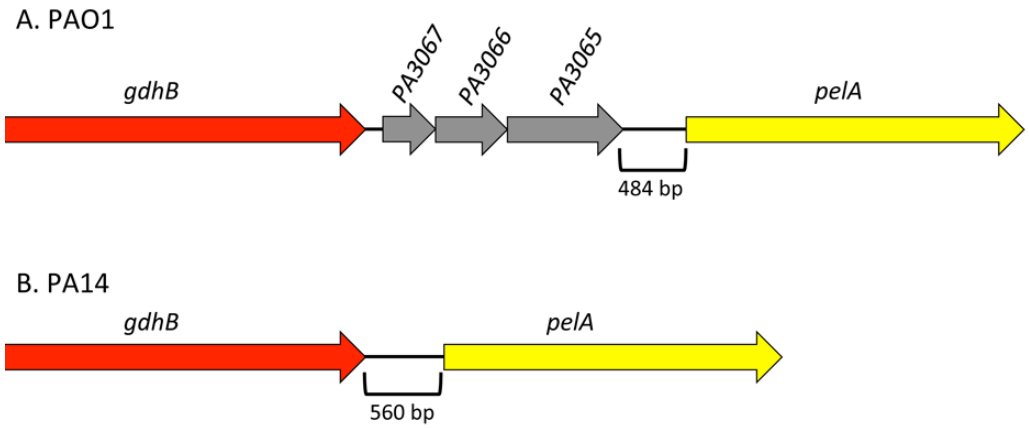

Figure 13. Schematic of the *pelA* 5'UTR. The two different gene organizations found up-stream of *pelA* is represented for PAO1 (A) and PA14 (B). PAO1 has a three-gene insertion between *pelA* and *gdhB*. These genes are colored grey. The length of the intergenic region is specified.

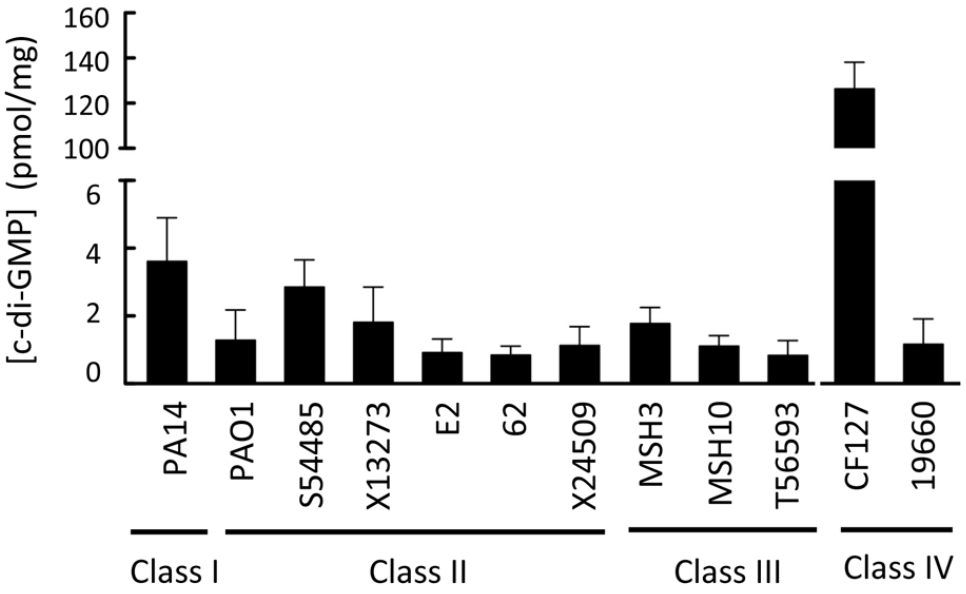

Figure 14. Intracellular c-di-GMP concentrations are quantified for the isolates. Total intracellular c-di-GMP was extracted and measured by LC/MS/MS from plate grown cultures at 25 °C for 3 d. c-di-GMP concentrations were quantified from three individual experiments. C-di-GMP concentrations are normalized to mg of total protein. Error bars represent standard deviation.

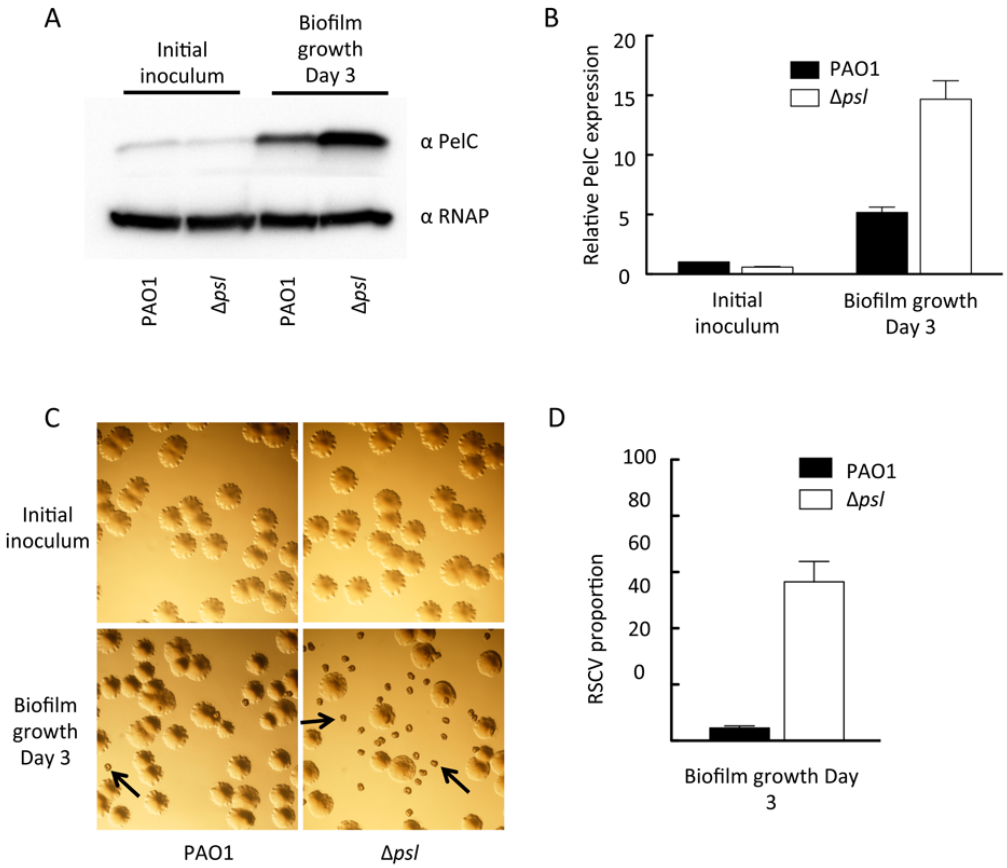

Figure 15. PelC expression is up-regulated in PAO1Δ*psl* during biofilm growth. PAO1 and PAO1Δ*psl* were compared for PelC expression level in planktonic and biofilm grown cells. Protein levels were isolated from the log phase cultures used for the initial inoculum and adhered biomass after 3 d of continuous flow within a tube bioreactor (A). Relative expression levels were quantified using densitometry analysis (B). Representative images of colony morphology of the initial inoculum and post biofilm growth are shown (C). Arrows are pointing toward RSCV morphotypes. The number of RSCVs in each population was quantified from three separate experiments (D). RNAP is a loading control. Error bars represent standard deviation.

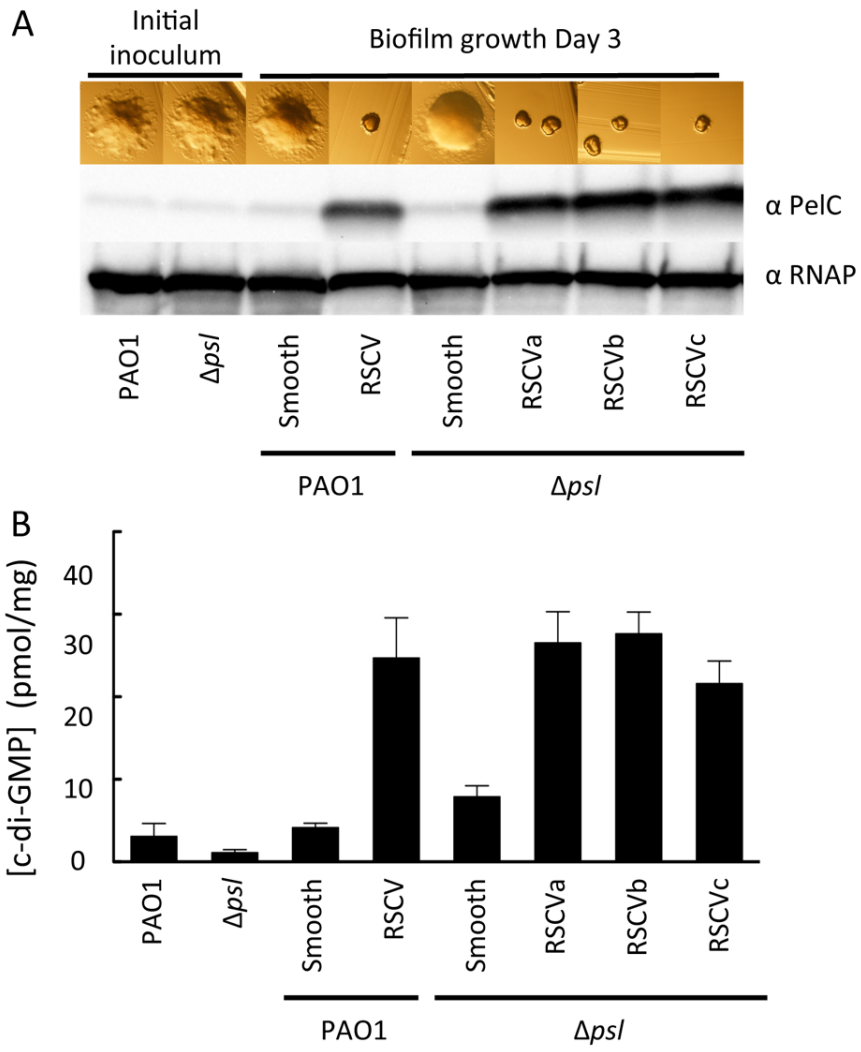

Figure 16. Biofilm-derived RSCVs overexpress PelC and have increased c-di-GMP levels. Representative smooth and RSCV isolates were selected after 3 d of continuous flow within a tube bioreactor for PAO1 and the *psl* mutant. Isolates were streaked onto LB agar and allowed to grow for 1 d at 37°C. Images of colony morphology were acquired and relative PelC expression levels measured (A). Total intracellular c-di-GMP was extracted and measured by LC/MS/MS from plate grown cultures at 37°C for 1 d. c-di-GMP concentrations were quantified from three individual experiments (B). C-di-GMP concentrations are normalized to mg of total protein. RNAP is a loading control. Error bars represent standard deviation. c-di-GMP extraction and analysis performed by Yasuhiko Irie.

A

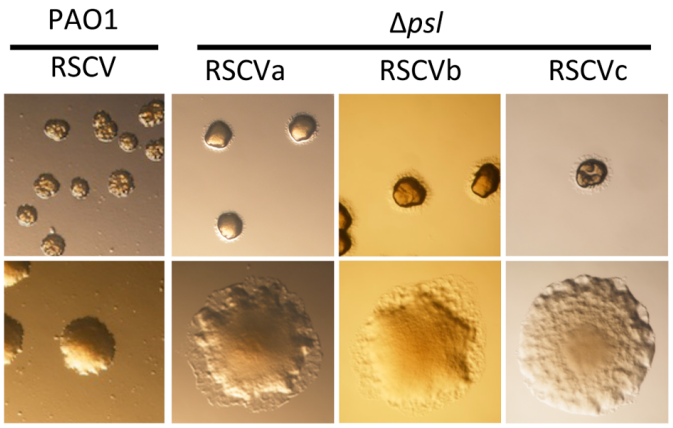

B

Isolate	Identified *wspF*-linked mutation
PAO1 RSCV	-36-164del
Δ*psl* RSCVa	315-316insG
Δ*psl* RSCVb	455-456insG
Δ*psl* RSCVc	440-441insGG

Figure 17. Mutations in the gene *wspF* are responsible for RSCV conversion. RSCVs were complemented by supplying *wspF* in trans (pWspF). Colony morphologies are shown for both the vector control (VC) and pWspF (A). Each isolate was sequenced to determine the nature of the *wspF* mutation and described in the figure (B).

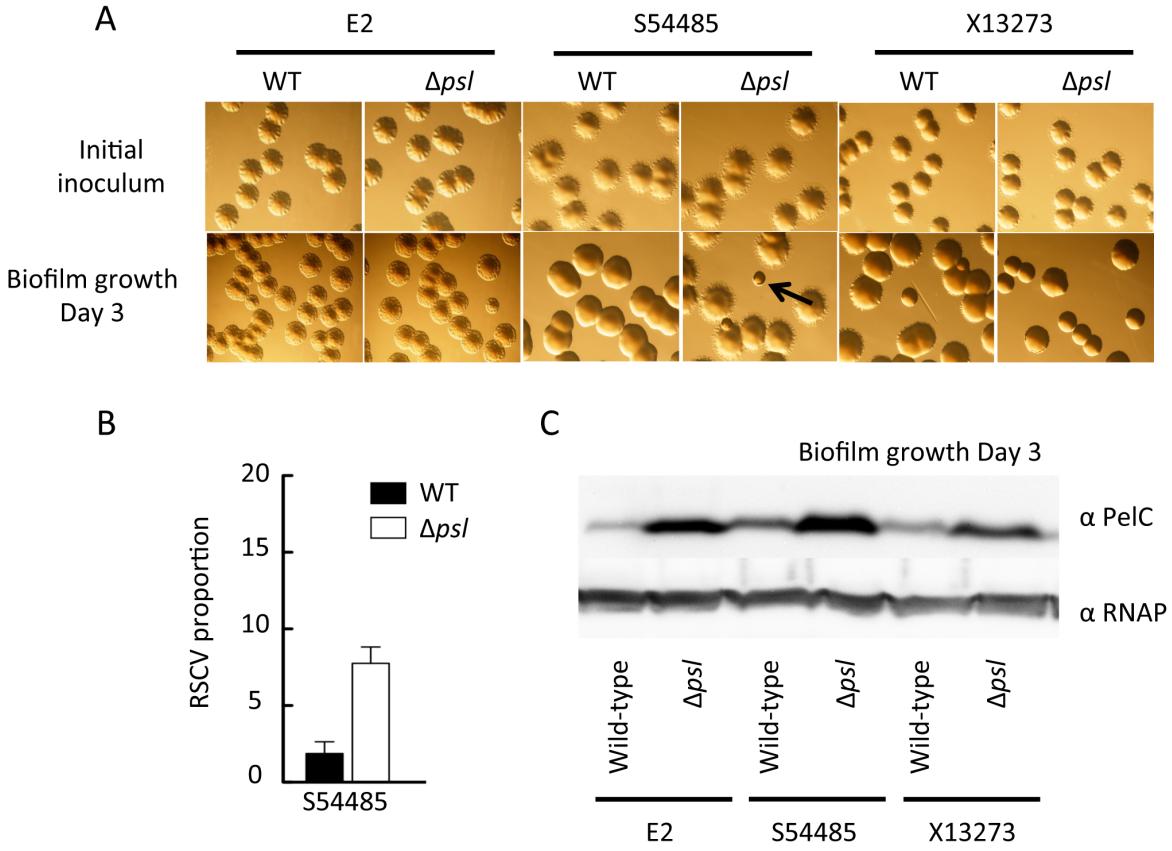

Figure 18. Class II clinical and environmental isolates up-regulate PelC in a *psl* mutant during biofilm growth. Representative images of colony morphology of the initial inoculum and after 3 d of continuous growth in a tube bioreactor (biofilm growth) are shown (A). Arrows point toward RSCV morphotypes. The number of RSCVs in each population was quantified (B). PelC expression was measured from the adhered biomass of wild-type and *psl* mutants for E2, S54485 and X13273. RNAP is a loading control. Error bars indicate standard deviation.

CONCLUSIONS AND FUTURE DIRECTIONS

Biofilms are complex differentiated communities encased in an extracellular matrix and are regarded as the prominent mode of bacterial growth in natural, clinical and industrial settings (41). Biofilms can be composed of a single bacterial species or a community consisting of multiple microbes (48). Cells residing within a biofilm community are afforded many benefits including protection, increased nutrient acquisition through metabolic cooperation and elevated horizontal gene transfer (192, 222, 256). The developmental process begins with a planktonic cell attaching to a surface and proliferating, followed by structural development and finally dispersion. Each of these stages is dependent on either the reinforcement of, or modulation of, the extracellular matrix. A key component of the biofilm matrix is extracellular polysaccharides.

In this thesis work, I have characterized one of the matrix polysaccharides produced by *P. aeruginosa*, the paradigm organism for biofilm research. This work has demonstrated that Pel can serve two key functional roles in a biofilm, one structural and one protective. Pel serves as an initiator of intercellular adhesion and stabilizer of adhesion once formed. This function is essential for bacterial aggregation and mature biofilm development. Pel also provides a measure of protection from aminoglycoside antibiotics. The antibiotic susceptibility experiments suggest that Pel is capable of protecting planktonic cells when artificially overexpressed. However, in both wild-type strains PAO1 and PA14, the *pel* operon is not expressed during planktonic growth. Instead, the *pel* operon is expressed upon surface contact and continues to maintain a high level of expression throughout biofilm development. Therefore, the protection afforded to *P. aeruginosa* by Pel from aminoglycosides appears to be a biofilm-associated mechanism of antimicrobial tolerance. To date, only the cyclic glucans encoded by the *ndvB* locus has been shown to be a biofilm-specific mechanism of antimicrobial tolerance in this species (139).

Additionally, this work has laid the foundation for Pel purification and carbohydrate structural analysis. Our analysis demonstrates that Pel may be rich in glucose, rhamnose and ribose. While the exact structure remains unknown, one gene important

in LPS synthesis was important in Pel-dependent phenotypes. This gene is *orfN* and the gene product is predicted to be the initiating glycosyltransferase in the synthesis of both O-linked antigen (OSA) and common antigen found in LPS (CSA) (194). In addition, this work has begun the biochemical analysis of two proteins involved in Pel synthesis, PelD and PelF. In collaboration with Lynne Howell's group we have purified and crystallized PelD in the presence and absence of c-di-GMP. Predicted amino acids involved in binding c-di-GMP have been mutated and confirmed to lose the ability to synthesize Pel. In addition PelF was purified and mutated in amino acids predicted to be required for nucleotide sugar binding. Finally, a genetic approach was taken to identify common sugar nucleotides involved in Pel synthesis. The *galU* gene product important in UDP-D-Glc synthesis impaired Pel-dependent colony morphology.

Lastly, I demonstrated that Pel and Psl polysaccharides provide unique and redundant functions in the biofilm matrix. By evaluating a range of clinical and environmental *P. aeruginosa* isolates, we can begin to assign functions to each polysaccharide. Psl is an important surface adhesin. However, both Pel and Psl can serve as a structural scaffold for mature biofilm development. The contribution of Pel and Psl to structural maturity was variable between isolates and correlated with the relative expression level of each polysaccharide. Evolution experiments revealed that in the absence of one structural polysaccharide, the evolved population selects for the up-regulation of the secondary structural polysaccharide.

Both the detailed analysis of polysaccharide synthesis and the functional consequence of differential polysaccharide production uncovered in this work provide avenues for future work. Several specific questions remain and suggested experiments towards addressing them are detailed below.

What is/are the mechanisms of Pel-mediated cell-cell adhesion?

Pel is critical for initiating and maintaining cell-cell interactions. This function appears to be a crucial mechanism that biofilm cells employ to retain daughter cells in the

community. In addition, cell-cell interactions are necessary for a biofilm to progress beyond the monolayer stage in PA14. The mechanism mediating cell-cell adhesion remains unknown. There are two potential possibilities. Pel can facilitate cell-cell adhesion by binding to itself or another extracellular matrix component, such as surface appendages, proteins or other polysaccharides. Precedence for both adhesion models exists. Cellulose mediates cell-to-cell adhesion by forming extensive hydrogen bonds between individual strands of glucose polymers (230). The extracellular appendage, Curli, has been demonstrated to be important in anchoring polysaccharides to the cell, in both *S. typhimurium* and *E. coli* (105, 147, 259). In addition, the large extracellular protein adhesin, CdrA was demonstrated to directly bind to the Psl polysaccharide (20). This binding is important in facilitating cell-cell adhesion.

To examine how Pel is enabling cell-cell adhesion, co-cultures experiments should be performed. Two PA14 strains differentially labeled, one synthesizing Pel (PA14P_{BAD}*pel*) while the other does not (PA14P_{BAD}*pel*Δ*pelF*), can be monitored for aggregation in liquid culture. If Pel binds to itself, cells incapable of Pel expression will be excluded from the aggregates. Similar analysis can also be performed with laser tweezers. If Pel participates in cell adhesion by binding to other matrix components, a targeted genetic approach should be taken. One candidate is the extracellular proteinaceous appendages, Cup fimbriae. In PA14, four gene clusters have been identified (241). The second candidates are the paralogs of CdrA. *P. aeruginosa* has five additional predicted gene clusters to be involved in the synthesis of large protein adhesins and, like CdrA, may specifically bind to extracellular polysaccharides (20). The third sets of candidates are two lectins, LecA and LecB. Lectins are proteins that reversibly bind to specific carbohydrate structures with high affinity. LecA and LecB have both been identified as important contributors to biofilm formation(53, 236). Candidate genes should be mutated in a PA14P_{BAD}*pel* background and strains will subsequently be assessed for biofilm development. Laser tweezer experiments can be conducted to corroborate the biofilm analysis. Otherwise, a random mutagenesis screen will be conducted in PA14P_{BAD}*pel* to identify mutants that fail to aggregate in the presence of the inducer.

Genes identified may provide information regarding the gene products important in cell-cell adhesion.

What is the mechanism of Pel-mediated aminoglycoside tolerance?

Aminoglycoside antibiotics are one of the few antibiotics that fail to completely permeate through a biofilm. Just as their name indicates, aminoglycosides are molecules that are composed of amino-modified sugars. One mechanism of resisting these antibiotics is decreased permeability. Extracellular polymers that confer resistance against aminoglycosides bind and possibly sequester the antibiotic. This is true for both alginate and NdvB glucans (139, 163, 201, 253). So one possibility is that Pel is a negatively charged polysaccharide capable of physically interacting with aminoglycosides.

Future experiments can test if Pel directly binds to aminoglycoside antibiotics. Once Pel is purified, an experiment can test whether Pel directly binds aminoglycoside antibiotics using hydrophobic interaction chromatography on Sep-Pak C-18 cartridges as previously described (43). In these experiments, tobramycin and Pel would be mixed, injected onto the hydrophobic column, extensively washed, followed by elution in an appropriate solution (e.g. 25% acetonitrile). The flow through and eluted fractions would be tested for antibiotic activity and Pel. If the antibiotic is retained on the column and only elutes with Pel, these results would suggest that they interact. A second experiment using fluorescently derived aminoglycosides could monitor the spatial distribution of tobramycin in comparison to Pel-derived and Pel-independent biofilms, such as PAO1Δ*wspF*Δ*psl* and PAO1Δ*wspF*Δ*pel*. An ideal experiment would be able to monitor Pel with a fluorescent lectin or antibody, tobramycin and the bacterial cells simultaneously in a biofilm. If Pel and tobramycin co-localize this is a second piece of evidence that they directly bind.

A second possibility is that Pel expression indirectly alters the expression of another matrix component that is important in aminoglycoside tolerance. One candidate is the

NdvB glucans. An *ndvB* mutant may alter aminoglycoside sensitivity in a Pel-dependent manner.

What is the composition and structure of Pel?

In order to completely appreciate the complexity and function Pel provides to a biofilm, the chemical composition needs to be identified. Structural properties including size, complexity, charge, and modifications will affect the physicochemical properties of the polymer. Purifying Pel proved to be challenging but a continued effort may be fruitful. First, Pel needs to be removed from the cell. Depending on how tightly bound Pel is to the cell surface, different methods of various stringency can be used (e.g. mechanical or chemical disruption). Once the polysaccharide is removed from the cell, contaminating proteins, LPS and nucleic acids need to be removed (e.g. digestion, separation). Samples can then be separated by size-exclusion chromatography and individual fractions analyzed for carbohydrate composition.

A parallel approach is to use a lectin microarray. This technique was recently described in a Nature Protocols paper for the rapid profiling of glycans on bacterial cell surfaces (95). Lectins are proteins that bind carbohydrates with a high specificity and therefore can discriminate between distinct carbohydrates with subtle differences. The lectin microarray enables multiple, distinct binding interactions to be observed simultaneously. By using lectins with known targets, this technique may be extremely beneficial towards identifying Pel-specific sugar moieties. The microarray was originally described to include 21 lectins, but the number and carbohydrate specificity can be modified. Regardless of whether this approach is useful in identifying Pel's composition, this novel technique may provide insight into the glycan biology of biofilm cells compared to planktonic cells.

Is Pel modified and if so, how does it affect biofilm development?

One piece of evidence that suggests Pel may be modified is in regulatory backgrounds that lead to *pel* up-regulation (e.g. Δ*wspF* and Δ*fleQ*), a two-gene operon *PA2440-PA2441* is also up-regulated (89, 90, 221). *PA2440* has homology to polysaccharide deacetylases and preliminary experiments show that overexpressing this operon alters the colony morphology and reduces aggregation in liquid culture in PAO1Δ*wspF*. Similarly a mutant in *PA2440* in the PAO1Δ*wspF* background results in increased aggregation. It remains to be determined if Pel or Psl is acetylated and how these alterations would affect biofilm development. Alginate is a highly acetylated polymer and a non-acetylated mucoid strain is significantly impaired in attachment and biofilm development (167). Further studies demonstrated that alginate acetylation was necessary for the aggregation of bacteria into microcolonies (235). Thus, it appears that acetyl groups help mediate interactions between neighbor cells and surface colonization and may be important in Pel- or Psl-mediated adhesion.

Why maintain the genetic capacity to synthesize several unique polysaccharides?

The structure of a polysaccharide is important for its function, and production of several structurally different polysaccharides may allow cells to adapt to certain environments. There are a few hypotheses (not mutually exclusive) as to why a species might retain the capacity to synthesize several unique polysaccharides. One hypothesis is that each polysaccharide is important for niche biology. This is seen in other organisms that also retain to the genetic capacity to synthesize multiple polysaccharides. For example, *Salmonella enterica serovar Typhimurium* produces three known extracellular polysaccharides, colanic acid, cellulose and an O-antigen capsule (44). Interestingly, each polysaccharide has a niche-specific role in biofilm formation. For example, O-antigen capsule is critical to form a biofilm on gallstone surfaces but is not involved in glass or plastic binding (44). Colanic acid is important in biofilm formation on HEp-2 cells and chicken intestinal tissue but does not play a role in plastic surface or gallstone biofilm development (127). Finally, cellulose does not contribute to gallstone biofilm formation but it does to biofilm formation on HEp-2 cells, chicken

intestinal epithelium and plastic surfaces (44, 127). Thus, *P. aeruginosa* might utilize Psl, Pel and alginate in a similar niche-specific manner.

A second hypothesis is that maintaining the genetic capacity to produce multiple polysaccharides protects against deleterious mutations. This redundancy may confer survival advantages in adverse environments. Redundancy of matrix polysaccharides might help reconcile high mutation rates with the maintenance of a key survival mechanism such as biofilm formation.

A third hypothesis is that each polysaccharide contributes unique survival advantages to the organism. In the case of alginate, overexpression inhibits phagocytosis by monocytes and neutrophils both *in vitro* and *in vivo* and protects cells from reactive oxygen species by savaging free radicals released by activated macrophages (9, 74). Psl is extremely important for initial adherence to biotic and abiotic surfaces, including glass, polyvinyl chloride (PVC), mucin and epithelial cells (26, 136). Additionally, Psl protects against the immune system by limiting complement-mediated opsonization and promoting intracellular survival in neutrophils (160). In the case of Pel, overexpression provides protection against certain antibiotics (39). Thus, it appears that each polysaccharide may have a distinct role in *P. aeruginosa* biofilm biology.

Furthermore, each polysaccharide has all been shown to provide cohesive and adhesive properties that allow cells to aggregate, form pellicles, microcolonies and/or biofilms. While, this analysis suggests that structural scaffolding is a redundant property of *P. aeruginosa* polysaccharides, the physical properties afforded by each polysaccharide to the biofilm remains to be determined. The structural differences of each polysaccharide combined with the local environment can greatly affect the physical properties of the polymer (e.g. hydrophobicity, elasticity and tensile strength). Mucoid strains and RSCV strains greatly differ in their physical properties despite both being adept at biofilm formation. Further experiments on the full functional repertoire each polysaccharide provides to the biofilm may contribute insight as to why the genetic capacity to produce multiple polysaccharides is maintained.

Do environmental signals induce production of one polysaccharide compared to another?

Maintaining the capacity to produce structurally distinct extracellular polysaccharides may allow cells to adapt to certain environments. For example, stressful environments may promote the switching of or differential regulation of the polysaccharides. During the course of the chronic CF infection, *P. aeruginosa* undergoes mutational changes that select for phenotypic variants. Two prominent variants are mucoid and RSCV isolates. It is estimated that in 90% of CF patients colonized with *P. aeruginosa*, mucoid conversion occurs. Studies have demonstrated that the extremely inflammatory environment of the CF airway rich in PMNs and their toxic oxygen by-products may select for mucoid conversion (144). The appearance of RSCVs in CF patients was associated with daily inhalation of tobramycin and colistin and correlated with declining lung function (100). In addition, RSCVs are selected for in the laboratory from biofilm reactors (111). These laboratory conditions may simulate the pressures involved in the CF lung and may provide insights as to the survival advantage conferred by RSCVs. Future experiments identifying the signal(s) responsible for altering polysaccharide production may be important in developing prediction models for biofilm growth kinetics and resistance properties.

Biofilm research began as a simple observation that bacterial cells were surrounded by "slime". Uncovering the components involved in the construction of the matrix has led to the discovery of an extremely complex, highly organized and highly regulated network. The biofilm matrix is a web of interactions, most of which remain to be discovered. This work provides a glimpse into the function of one polysaccharide in *P. aeruginosa*.

REFERENCES

1. **Adams, P. D., P. V. Afonine, G. Bunkoczi, V. B. Chen, I. W. Davis, N. Echols, J. J. Headd, L. W. Hung, G. J. Kapral, R. W. Grosse-Kunstleve, A. J. McCoy, N. W. Moriarty, R. Oeffner, R. J. Read, D. C. Richardson, J. S. Richardson, T. C. Terwilliger, and P. H. Zwart.** 2010. PHENIX: a comprehensive Python-based system for macromolecular structure solution. Acta Crystallogr D Biol Crystallogr **66:**213-221.
2. **Aldridge, P., R. Paul, P. Goymer, P. Rainey, and U. Jenal.** 2003. Role of the GGDEF regulator PleD in polar development of *Caulobacter crescentus*. Mol Microbiol **47:**1695-1708.
3. **Alkawash, M. A., J. S. Soothill, and N. L. Schiller.** 2006. Alginate lyase enhances antibiotic killing of mucoid *Pseudomonas aeruginosa* in biofilms. APMIS **114:**131-138.
4. **Allesen-Holm, M., K. B. Barken, L. Yang, M. Klausen, J. S. Webb, S. Kjelleberg, S. Molin, M. Givskov, and T. Tolker-Nielsen.** 2006. A characterization of DNA release in *Pseudomonas aeruginosa* cultures and biofilms. Mol Microbiol **59:**1114-1128.
5. **Anriany, Y. A., R. M. Weiner, J. A. Johnson, C. E. De Rezende, and S. W. Joseph.** 2001. *Salmonella enterica* serovar Typhimurium DT104 displays a rugose phenotype. Appl Environ Microbiol **67:**4048-4056.
6. **Ashkin, A., and J. M. Dziedzic.** 1989. Internal cell manipulation using infrared laser traps. Proc Natl Acad Sci U S A **86:**7914-7918.
7. **Banin, E., M. L. Vasil, and E. P. Greenberg.** 2005. Iron and *Pseudomonas aeruginosa* biofilm formation. Proc Natl Acad Sci U S A **102:**11076-11081.
8. **Barken, K. B., S. J. Pamp, L. Yang, M. Gjermansen, J. J. Bertrand, M. Klausen, M. Givskov, C. B. Whitchurch, J. N. Engel, and T. Tolker-Nielsen.** 2008. Roles of type IV pili, flagellum-mediated motility and extracellular DNA in the formation of mature multicellular structures in *Pseudomonas aeruginosa* biofilms. Environ Microbiol **10:**2331-2343.
9. **Bayer, A. S., D. P. Speert, S. Park, J. Tu, M. Witt, C. C. Nast, and D. C. Norman.** 1991. Functional role of mucoid exopolysaccharide (alginate) in antibiotic-induced and polymorphonuclear leukocyte-mediated killing of *Pseudomonas aeruginosa*. Infect Immun **59:**302-308.
10. **Benach, J., S. S. Swaminathan, R. Tamayo, S. K. Handelman, E. Folta-Stogniew, J. E. Ramos, F. Forouhar, H. Neely, J. Seetharaman, A. Camilli, and J. F. Hunt.** 2007. The structural basis of cyclic diguanylate signal transduction by PilZ domains. EMBO J **26:**5153-5166.
11. **Beveridge, T. J.** 1999. Structures of gram-negative cell walls and their derived membrane vesicles. J Bacteriol **181:**4725-4733.
12. **Beveridge, T. J., S. A. Makin, J. L. Kadurugamuwa, and Z. Li.** 1997. Interactions between biofilms and the environment. FEMS Microbiol Rev **20:**291-303.
13. **Bieber, D., S. W. Ramer, C. Y. Wu, W. J. Murray, T. Tobe, R. Fernandez, and G. K. Schoolnik.** 1998. Type IV pili, transient bacterial aggregates, and virulence of enteropathogenic *Escherichia coli*. Science **280:**2114-2118.
14. **Bodey, G. P., R. Bolivar, V. Fainstein, and L. Jadeja.** 1983. Infections caused by *Pseudomonas aeruginosa*. Rev Infect Dis **5:**279-313.

15. **Boles, B. R., and P. K. Singh.** 2008. Endogenous oxidative stress produces diversity and adaptability in biofilm communities. Proc Natl Acad Sci U S A **105:**12503-12508.
16. **Boles, B. R., M. Thoendel, and P. K. Singh.** 2005. Rhamnolipids mediate detachment of *Pseudomonas aeruginosa* from biofilms. Mol Microbiol **57:**1210-1223.
17. **Boles, B. R., M. Thoendel, and P. K. Singh.** 2004. Self-generated diversity produces "insurance effects" in biofilm communities. Proc Natl Acad Sci U S A **101:**16630-16635.
18. **Bollinger, N., D. J. Hassett, B. H. Iglewski, J. W. Costerton, and T. R. McDermott.** 2001. Gene expression in *Pseudomonas aeruginosa*: evidence of iron override effects on quorum sensing and biofilm-specific gene regulation. J Bacteriol **183:**1990-1996.
19. **Bonafonte, M. A., C. Solano, B. Sesma, M. Alvarez, L. Montuenga, D. Garcia-Ros, and C. Gamazo.** 2000. The relationship between glycogen synthesis, biofilm formation and virulence in salmonella enteritidis. FEMS Microbiol Lett **191:**31-36.
20. **Borlee, B. R., A. D. Goldman, K. Murakami, R. Samudrala, D. J. Wozniak, and M. R. Parsek.** 2010. *Pseudomonas aeruginosa* uses a cyclic-di-GMP-regulated adhesin to reinforce the biofilm extracellular matrix. Mol Microbiol **75:**827-842.
21. **Boyd, A., and A. M. Chakrabarty.** 1994. Role of alginate lyase in cell detachment of *Pseudomonas aeruginosa*. Appl Environ Microbiol **60:**2355-2359.
22. **Brown, M. J., and J. N. Lester.** 1980. Comparison of bacterial extracellular polymer extraction methods. Appl Environ Microbiol **40:**179-185.
23. **Buckstein, M. H., J. He, and H. Rubin.** 2008. Characterization of nucleotide pools as a function of physiological state in *Escherichia coli*. J Bacteriol **190:**718-726.
24. **Bullen, J. J., H. J. Rogers, P. B. Spalding, and C. G. Ward.** 2005. Iron and infection: the heart of the matter. FEMS Immunol Med Microbiol **43:**325-330.
25. **Byrd, M. S., B. Pang, W. Hong, E. A. Waligora, R. A. Juneau, C. E. Armbruster, K. E. Weimer, K. Murrah, E. E. Mann, H. Lu, A. Sprinkle, M. R. Parsek, N. D. Kock, D. J. Wozniak, and W. E. Swords.** 2011. Direct evaluation of *Pseudomonas aeruginosa* biofilm mediators in a chronic infection model. Infect Immun **79:**3087-3095.
26. **Byrd, M. S., B. Pang, M. Mishra, W. E. Swords, and D. J. Wozniak.** 2010. The *Pseudomonas aeruginosa* Exopolysaccharide Psl Facilitates Surface Adherence and NF-kappaB Activation in A549 Cells. MBio **1**.
27. **Byrd, M. S., I. Sadovskaya, E. Vinogradov, H. Lu, A. B. Sprinkle, S. H. Richardson, L. Ma, B. Ralston, M. R. Parsek, E. M. Anderson, J. S. Lam, and D. J. Wozniak.** 2009. Genetic and biochemical analyses of the *Pseudomonas aeruginosa* Psl exopolysaccharide reveal overlapping roles for polysaccharide synthesis enzymes in Psl and LPS production. Mol Microbiol **73:**622-638.
28. **Campa, M., M. Bendinelli, and H. Friedman.** 1993. *Pseudomonas aeruginosa* as an Opportunistic Pathogen. Plenum Press, New York, NY.

29. **Chan, C., R. Paul, D. Samoray, N. C. Amiot, B. Giese, U. Jenal, and T. Schirmer.** 2004. Structural basis of activity and allosteric control of diguanylate cyclase. Proc Natl Acad Sci U S A **101:**17084-17089.
30. **Chandler, J. R., B. A. Duerkop, A. Hinz, T. E. West, J. P. Herman, M. E. Churchill, S. J. Skerrett, and E. P. Greenberg.** 2009. Mutational analysis of *Burkholderia thailandensis* quorum sensing and self-aggregation. J Bacteriol **191:**5901-5909.
31. **Chang, W. S., M. van de Mortel, L. Nielsen, G. Nino de Guzman, X. Li, and L. J. Halverson.** 2007. Alginate production by *Pseudomonas putida* creates a hydrated microenvironment and contributes to biofilm architecture and stress tolerance under water-limiting conditions. J Bacteriol **189:**8290-8299.
32. **Cheng, H. P., and G. C. Walker.** 1998. Succinoglycan is required for initiation and elongation of infection threads during nodulation of alfalfa by Rhizobium meliloti. J Bacteriol **180:**5183-5191.
33. **Choi, K. H., D. DeShazer, and H. P. Schweizer.** 2006. mini-Tn7 insertion in bacteria with multiple glmS-linked attTn7 sites: example *Burkholderia mallei* ATCC 23344. Nat Protoc **1:**162-169.
34. **Choi, S. H., and E. P. Greenberg.** 1991. The C-terminal region of the Vibrio fischeri LuxR protein contains an inducer-independent lux gene activating domain. Proc Natl Acad Sci U S A **88:**11115-11119.
35. **Christen, B., M. Christen, R. Paul, F. Schmid, M. Folcher, P. Jenoe, M. Meuwly, and U. Jenal.** 2006. Allosteric control of cyclic di-GMP signaling. J Biol Chem **281:**32015-32024.
36. **Chua, T. K., J. M. Bujnicki, T. C. Tan, F. Huynh, B. K. Patel, and J. Sivaraman.** 2008. The structure of sucrose phosphate synthase from *Halothermothrix orenii* reveals its mechanism of action and binding mode. Plant Cell **20:**1059-1072.
37. **Chugani, S. A., M. Whiteley, K. M. Lee, D. D'Argenio, C. Manoil, and E. P. Greenberg.** 2001. QscR, a modulator of quorum-sensing signal synthesis and virulence in *Pseudomonas aeruginosa*. Proc Natl Acad Sci U S A **98:**2752-2757.
38. **Ciornei, C. D., A. Novikov, C. Beloin, C. Fitting, M. Caroff, J. M. Ghigo, J. M. Cavaillon, and M. Adib-Conquy.** 2010. Biofilm-forming *Pseudomonas aeruginosa* bacteria undergo lipopolysaccharide structural modifications and induce enhanced inflammatory cytokine response in human monocytes. Innate Immun **16:**288-301.
39. **Colvin, K. M., V. D. Gordon, K. Murakami, B. R. Borlee, D. J. Wozniak, G. C. Wong, and M. R. Parsek.** 2011. The Pel polysaccharide can serve a structural and protective role in the biofilm matrix of *Pseudomonas aeruginosa*. PLoS Pathog **7:**e1001264.
40. **Colvin, K. M., Y. Irie, C. S. Tart, R. Urbano, J. C. Whitney, C. Ryder, P. L. Howell, D. J. Wozniak, and M. R. Parsek.** 2011. The Pel and Psl polysaccharides provide *Pseudomonas aeruginosa* structural redundancy within the biofilm matrix. Environ Microbiol.
41. **Costerton, J. W., Z. Lewandowski, D. E. Caldwell, D. R. Korber, and H. M. Lappin-Scott.** 1995. Microbial biofilms. Annu Rev Microbiol **49:**711-745.
42. **Costerton, J. W., P. S. Stewart, and E. P. Greenberg.** 1999. Bacterial biofilms: a common cause of persistent infections. Science **284:**1318-1322.

43. **Coulon, C., E. Vinogradov, A. Filloux, and I. Sadovskaya.** 2010. Chemical analysis of cellular and extracellular carbohydrates of a biofilm-forming strain *Pseudomonas aeruginosa* PA14. PLoS One **5:**e14220.
44. **Crawford, R. W., D. L. Gibson, W. W. Kay, and J. S. Gunn.** 2008. Identification of a bile-induced exopolysaccharide required for *Salmonella* biofilm formation on gallstone surfaces. Infect Immun **76:**5341-5349.
45. **D'Argenio, D. A., M. W. Calfee, P. B. Rainey, and E. C. Pesci.** 2002. Autolysis and autoaggregation in *Pseudomonas aeruginosa* colony morphology mutants. J Bacteriol **184:**6481-6489.
46. **Danese, P. N., L. A. Pratt, and R. Kolter.** 2000. Exopolysaccharide production is required for development of *Escherichia coli* K-12 biofilm architecture. J Bacteriol **182:**3593-3596.
47. **Davey, M. E., N. C. Caiazza, and G. A. O'Toole.** 2003. Rhamnolipid surfactant production affects biofilm architecture in *Pseudomonas aeruginosa* PAO1. J Bacteriol **185:**1027-1036.
48. **Davey, M. E., and G. A. O'toole.** 2000. Microbial biofilms: from ecology to molecular genetics. Microbiol Mol Biol Rev **64:**847-867.
49. **Davies, D. G., M. R. Parsek, J. P. Pearson, B. H. Iglewski, J. W. Costerton, and E. P. Greenberg.** 1998. The involvement of cell-to-cell signals in the development of a bacterial biofilm. Science **280:**295-298.
50. **Davies, G. J.** 2001. Sweet secrets of synthesis. Nat Struct Biol **8:**98-100.
51. **De, N., M. Pirruccello, P. V. Krasteva, N. Bae, R. V. Raghavan, and H. Sondermann.** 2008. Phosphorylation-independent regulation of the diguanylate cyclase WspR. PLoS Biol **6:**e67.
52. **Delorenzi, M., and T. Speed.** 2002. An HMM model for coiled-coil domains and a comparison with PSSM-based predictions. Bioinformatics **18:**617-625.
53. **Diggle, S. P., R. E. Stacey, C. Dodd, M. Camara, P. Williams, and K. Winzer.** 2006. The galactophilic lectin, LecA, contributes to biofilm development in *Pseudomonas aeruginosa*. Environ Microbiol **8:**1095-1104.
54. **Douthit, S. A., M. Dlakic, D. E. Ohman, and M. J. Franklin.** 2005. Epimerase active domain of *Pseudomonas aeruginosa* AlgG, a protein that contains a right-handed beta-helix. J Bacteriol **187:**4573-4583.
55. **Drenkard, E.** 2003. Antimicrobial resistance of *Pseudomonas aeruginosa* biofilms. Microbes Infect **5:**1213-1219.
56. **Drenkard, E., and F. M. Ausubel.** 2002. *Pseudomonas* biofilm formation and antibiotic resistance are linked to phenotypic variation. Nature **416:**740-743.
57. **DUBOIS, M., K. GILLES, J. K. HAMILTON, P. A. REBERS, and F. SMITH.** 1951. A colorimetric method for the determination of sugars. Nature **168:**167.
58. **E.F. Fritsch, J., and T. Maniatis.** 1989. Molecular Cloning: A Laboratory Manual. Cold Spring Harbor Laboratory Press, Woodbury (New York).
59. **Emsley, P., and K. Cowtan.** 2004. Coot: model-building tools for molecular graphics. Acta Crystallogr D Biol Crystallogr **60:**2126-2132.
60. **Farrow, J. M., Z. M. Sund, M. L. Ellison, D. S. Wade, J. P. Coleman, and E. C. Pesci.** 2008. PqsE functions independently of PqsR-Pseudomonas quinolone signal and enhances the rhl quorum-sensing system. J Bacteriol **190:**7043-7051.

61. **Fine, M. J., M. A. Smith, C. A. Carson, S. S. Mutha, S. S. Sankey, L. A. Weissfeld, and W. N. Kapoor.** 1996. Prognosis and outcomes of patients with community-acquired pneumonia. A meta-analysis. JAMA **275:**134-141.
62. **Flemming, H. C., and J. Wingender.** 2010. The biofilm matrix. Nat Rev Microbiol **8:**623-633.
63. **Franklin, M. J., D. E. Nivens, J. T. Weadge, and P. L. Howell.** 2011. Biosynthesis of the *Pseudomonas aeruginosa* Extracellular Polysaccharides, Alginate, Pel, and Psl. Front Microbiol **2:**167.
64. **Friedman, L., and R. Kolter.** 2004. Genes involved in matrix formation in *Pseudomonas aeruginosa* PA14 biofilms. Mol Microbiol **51:**675-690.
65. **Friedman, L., and R. Kolter.** 2004. Two genetic loci produce distinct carbohydrate-rich structural components of the *Pseudomonas aeruginosa* biofilm matrix. J Bacteriol **186:**4457-4465.
66. **Fuqua, C., and E. P. Greenberg.** 2002. Listening in on bacteria: acyl-homoserine lactone signalling. Nat Rev Mol Cell Biol **3:**685-695.
67. **Gacesa, P.** 1988. Alginates. Carbohydrate Polymers **8:**161-182.
68. **Galperin, M. Y.** 2005. A census of membrane-bound and intracellular signal transduction proteins in bacteria: bacterial IQ, extroverts and introverts. BMC Microbiol **5:**35.
69. **Ghafoor, A., I. D. Hay, and B. H. Rehm.** 2011. The role of exopolysaccharides in *Pseudomonas aeruginosa* biofilm formation and architecture. Appl Environ Microbiol.
70. **Gibiansky, M. L., J. C. Conrad, F. Jin, V. D. Gordon, D. A. Motto, M. A. Mathewson, W. G. Stopka, D. C. Zelasko, J. D. Shrout, and G. C. Wong.** 2010. Bacteria use type IV pili to walk upright and detach from surfaces. Science **330:**197.
71. **Gilbert, M. M., C. K. Beam, B. S. Robinson, and K. H. Moberg.** 2009. Genetic interactions between the Drosophila tumor suppressor gene ept and the stat92E transcription factor. PLoS One **4:**e7083.
72. **Goldberg, J. B., K. Hatano, and G. B. Pier.** 1993. Synthesis of lipopolysaccharide O side chains by *Pseudomonas aeruginosa* PAO1 requires the enzyme phosphomannomutase. J Bacteriol **175:**1605-1611.
73. **Goodman, A. L., B. Kulasekara, A. Rietsch, D. Boyd, R. S. Smith, and S. Lory.** 2004. A signaling network reciprocally regulates genes associated with acute infection and chronic persistence in *Pseudomonas aeruginosa*. Dev Cell **7:**745-754.
74. **Govan, J. R., and V. Deretic.** 1996. Microbial pathogenesis in cystic fibrosis: mucoid *Pseudomonas aeruginosa* and *Burkholderia cepacia*. Microbiol Rev **60:**539-574.
75. **Grimmecke, H. D., M. Voges, Y. A. Knirel, A. S. Shashkov, W. Lauk, and B. Kiesel.** 1994. Structure of the capsular polysaccharide and the O-side-chain of the lipopolysaccharide from *Acetobacter methanolicus* MB 135 (IMET 11402). Carbohydr Res **253:**283-286.
76. **Guerin, M. E., A. Buschiazzo, J. Korduláková, M. Jackson, and P. M. Alzari.** 2005. Crystallization and preliminary crystallographic analysis of PimA, an

essential mannosyltransferase from *Mycobacterium smegmatis*. Acta Crystallogr Sect F Struct Biol Cryst Commun **61:**518-520.
77. **Hall-Stoodley, L., J. W. Costerton, and P. Stoodley.** 2004. Bacterial biofilms: from the natural environment to infectious diseases. Nat Rev Microbiol **2:**95-108.
78. **Hancock, R. E., L. M. Mutharia, L. Chan, R. P. Darveau, D. P. Speert, and G. B. Pier.** 1983. *Pseudomonas aeruginosa* isolates from patients with cystic fibrosis: a class of serum-sensitive, nontypable strains deficient in lipopolysaccharide O side chains. Infect Immun **42:**170-177.
79. **Hao, Y., and J. Lam.** 2011. Pathways for the Biosynthesis of NDP sugars, p. 195-235. *In* Y. Knirel and M. Valvano (ed.), Bacterial Lipopolysaccharides. Springer-Verlag, Wien.
80. **Hardalo, C., and S. C. Edberg.** 1997. *Pseudomonas aeruginosa*: assessment of risk from drinking water. Crit Rev Microbiol **23:**47-75.
81. **Harrison, J. J., H. Ceri, C. A. Stremick, and R. J. Turner.** 2004. Biofilm susceptibility to metal toxicity. Environ Microbiol **6:**1220-1227.
82. **Hatch, R. A., and N. L. Schiller.** 1998. Alginate lyase promotes diffusion of aminoglycosides through the extracellular polysaccharide of mucoid *Pseudomonas aeruginosa*. Antimicrob Agents Chemother **42:**974-977.
83. **Haussler, S., and M. R. Parsek.** 2010. Biofilms 2009: new perspectives at the heart of surface-associated microbial communities. J Bacteriol **192:**2941-2949.
84. **He, X., P. Szewczyk, A. Karyakin, M. Evin, W. X. Hong, Q. Zhang, and G. Chang.** 2010. Structure of a cation-bound multidrug and toxic compound extrusion transporter. Nature **467:**991-994.
85. **Helm, R. F., Z. Huang, D. Edwards, H. Leeson, W. Peery, and M. Potts.** 2000. Structural characterization of the released polysaccharide of desiccation-tolerant Nostoc commune DRH-1. J Bacteriol **182:**974-982.
86. **Hengge, R.** 2009. Principles of c-di-GMP signalling in bacteria. Nat Rev Microbiol **7:**263-273.
87. **Hentzer, M., G. M. Teitzel, G. J. Balzer, A. Heydorn, S. Molin, M. Givskov, and M. R. Parsek.** 2001. Alginate overproduction affects *Pseudomonas aeruginosa* biofilm structure and function. J Bacteriol **183:**5395-5401.
88. **Heydorn, A., B. K. Ersboll, M. Hentzer, M. R. Parsek, M. Givskov, and S. Molin.** 2000. Experimental reproducibility in flow-chamber biofilms. Microbiology **146 (Pt 10):**2409-2415.
89. **Hickman, J. W., and C. S. Harwood.** 2008. Identification of FleQ from *Pseudomonas aeruginosa* as a c-di-GMP-responsive transcription factor. Mol Microbiol **69:**376-389.
90. **Hickman, J. W., D. F. Tifrea, and C. S. Harwood.** 2005. A chemosensory system that regulates biofilm formation through modulation of cyclic diguanylate levels. Proc Natl Acad Sci U S A **102:**14422-14427.
91. **Hitchcock, P. J., and T. M. Brown.** 1983. Morphological heterogeneity among *Salmonella* lipopolysaccharide chemotypes in silver-stained polyacrylamide gels. J Bacteriol **154:**269-277.
92. **Hoang, T. T., R. R. Karkhoff-Schweizer, A. J. Kutchma, and H. P. Schweizer.** 1998. A broad-host-range Flp-FRT recombination system for site-specific

excision of chromosomally-located DNA sequences: application for isolation of unmarked *Pseudomonas aeruginosa* mutants. Gene **212:**77-86.
93. **Hoffman, L. R., E. Déziel, D. A. D'Argenio, F. Lépine, J. Emerson, S. McNamara, R. L. Gibson, B. W. Ramsey, and S. I. Miller.** 2006. Selection for *Staphylococcus aureus* small-colony variants due to growth in the presence of *Pseudomonas aeruginosa*. Proc Natl Acad Sci U S A **103:**19890-19895.
94. **Holloway, B. W.** 1955. Genetic recombination in *Pseudomonas aeruginosa*. J Gen Microbiol **13:**572-581.
95. **Hsu, K. L., and L. K. Mahal.** 2006. A lectin microarray approach for the rapid analysis of bacterial glycans. Nat Protoc **1:**543-549.
96. **Hsu, K. L., K. T. Pilobello, and L. K. Mahal.** 2006. Analyzing the dynamic bacterial glycome with a lectin microarray approach. Nat Chem Biol **2:**153-157.
97. **Hu, S. Q., Y. G. Gao, K. Tajima, N. Sunagawa, Y. Zhou, S. Kawano, T. Fujiwara, T. Yoda, D. Shimura, Y. Satoh, M. Munekata, I. Tanaka, and M. Yao.** 2010. Structure of bacterial cellulose synthase subunit D octamer with four inner passageways. Proc Natl Acad Sci U S A **107:**17957-17961.
98. **Hung, R. J., H. S. Chien, R. Z. Lin, C. T. Lin, J. Vatsyayan, H. L. Peng, and H. Y. Chang.** 2007. Comparative analysis of two UDP-glucose dehydrogenases in *Pseudomonas aeruginosa* PAO1. J Biol Chem **282:**17738-17748.
99. **Huse, H. K., T. Kwon, J. E. Zlosnik, D. P. Speert, E. M. Marcotte, and M. Whiteley.** 2010. Parallel evolution in *Pseudomonas aeruginosa* over 39,000 generations in vivo. MBio **1**.
100. **Häussler, S., B. Tümmler, H. Weissbrodt, M. Rohde, and I. Steinmetz.** 1999. Small-colony variants of *Pseudomonas aeruginosa* in cystic fibrosis. Clin Infect Dis **29:**621-625.
101. **Irie, Y., M. Starkey, A. N. Edwards, D. J. Wozniak, T. Romeo, and M. R. Parsek.** 2010. *Pseudomonas aeruginosa* biofilm matrix polysaccharide Psl is regulated transcriptionally by RpoS and post-transcriptionally by RsmA. Mol Microbiol **78:**158-172.
102. **Jackson, K. D., M. Starkey, S. Kremer, M. R. Parsek, and D. J. Wozniak.** 2004. Identification of psl, a locus encoding a potential exopolysaccharide that is essential for *Pseudomonas aeruginosa* PAO1 biofilm formation. J Bacteriol **186:**4466-4475.
103. **Jenal, U., and J. Malone.** 2006. Mechanisms of cyclic-di-GMP signaling in bacteria. Annu Rev Genet **40:**385-407.
104. **Jin, F., J. C. Conrad, M. L. Gibiansky, and G. C. Wong.** 2011. Bacteria use type-IV pili to slingshot on surfaces. Proc Natl Acad Sci U S A **108:**12617-12622.
105. **Jonas, K., H. Tomenius, A. Kader, S. Normark, U. Romling, L. M. Belova, and O. Melefors.** 2007. Roles of curli, cellulose and BapA in *Salmonella* biofilm morphology studied by atomic force microscopy. BMC Microbiol **7:**70.
106. **Kaku, H., E. J. Van Damme, W. J. Peumans, and I. J. Goldstein.** 1990. Carbohydrate-binding specificity of the daffodil (*Narcissus pseudonarcissus*) and amaryllis (*Hippeastrum hybr.*) bulb lectins. Arch Biochem Biophys **279:**298-304.
107. **Kaneko, Y., M. Thoendel, O. Olakanmi, B. E. Britigan, and P. K. Singh.** 2007. The transition metal gallium disrupts *Pseudomonas aeruginosa* iron metabolism and has antimicrobial and antibiofilm activity. J Clin Invest **117:**877-888.

108. **Karatan, E., and P. Watnick.** 2009. Signals, regulatory networks, and materials that build and break bacterial biofilms. Microbiol Mol Biol Rev **73:**310-347.
109. **Kelley, L. A., and M. J. Sternberg.** 2009. Protein structure prediction on the Web: a case study using the Phyre server. Nat Protoc **4:**363-371.
110. **King, J. D., D. Kocíncová, E. L. Westman, and J. S. Lam.** 2009. Review: Lipopolysaccharide biosynthesis in *Pseudomonas aeruginosa*. Innate Immun **15:**261-312.
111. **Kirisits, M. J., L. Prost, M. Starkey, and M. R. Parsek.** 2005. Characterization of colony morphology variants isolated from *Pseudomonas aeruginosa* biofilms. Appl Environ Microbiol **71:**4809-4821.
112. **Klausen, M., A. Aaes-Jørgensen, S. Molin, and T. Tolker-Nielsen.** 2003. Involvement of bacterial migration in the development of complex multicellular structures in *Pseudomonas aeruginosa* biofilms. Mol Microbiol **50:**61-68.
113. **Klausen, M., A. Heydorn, P. Ragas, L. Lambertsen, A. Aaes-Jørgensen, S. Molin, and T. Tolker-Nielsen.** 2003. Biofilm formation by *Pseudomonas aeruginosa* wild type, flagella and type IV pili mutants. Mol Microbiol **48:**1511-1524.
114. **Koch, B., L. E. Jensen, and O. Nybroe.** 2001. A panel of Tn7-based vectors for insertion of the gfp marker gene or for delivery of cloned DNA into Gram-negative bacteria at a neutral chromosomal site. J Microbiol Methods **45:**187-195.
115. **Kohanski, M. A., D. J. Dwyer, and J. J. Collins.** 2010. How antibiotics kill bacteria: from targets to networks. Nat Rev Microbiol **8:**423-435.
116. **Kohanski, M. A., D. J. Dwyer, B. Hayete, C. A. Lawrence, and J. J. Collins.** 2007. A common mechanism of cellular death induced by bactericidal antibiotics. Cell **130:**797-810.
117. **Kowalska, K., C. Soscia, H. Combe, P. Vasseur, R. Voulhoux, and A. Filloux.** 2010. The C-terminal amphipathic alpha-helix of *Pseudomonas aeruginosa* PelC outer membrane protein is required for its function. Biochimie **92:**33-40.
118. **Krissinel, E., and K. Henrick.** 2007. Inference of macromolecular assemblies from crystalline state. J Mol Biol **372:**774-797.
119. **Kulasakara, H., V. Lee, A. Brencic, N. Liberati, J. Urbach, S. Miyata, D. G. Lee, A. N. Neely, M. Hyodo, Y. Hayakawa, F. M. Ausubel, and S. Lory.** 2006. Analysis of *Pseudomonas aeruginosa* diguanylate cyclases and phosphodiesterases reveals a role for bis-(3'-5')-cyclic-GMP in virulence. Proc Natl Acad Sci U S A **103:**2839-2844.
120. **Kulasekara, H. D., I. Ventre, B. R. Kulasekara, A. Lazdunski, A. Filloux, and S. Lory.** 2005. A novel two-component system controls the expression of *Pseudomonas aeruginosa* fimbrial cup genes. Mol Microbiol **55:**368-380.
121. **Köhler, T., L. K. Curty, F. Barja, C. van Delden, and J. C. Pechère.** 2000. Swarming of *Pseudomonas aeruginosa* is dependent on cell-to-cell signaling and requires flagella and pili. J Bacteriol **182:**5990-5996.
122. **Köhler, T., V. Donner, and C. van Delden.** 2010. Lipopolysaccharide as shield and receptor for R-pyocin-mediated killing in *Pseudomonas aeruginosa*. J Bacteriol **192:**1921-1928.

123. **Lairson, L. L., B. Henrissat, G. J. Davies, and S. G. Withers.** 2008. Glycosyltransferases: structures, functions, and mechanisms. Annu Rev Biochem **77:**521-555.
124. **Lam, J. S., V. L. Taylor, S. T. Islam, Y. Hao, and D. Kocíncová.** 2011. Genetic and Functional Diversity of *Pseudomonas aeruginosa* Lipopolysaccharide. Front Microbiol **2:**118.
125. **Lam, M. Y., E. J. McGroarty, A. M. Kropinski, L. A. MacDonald, S. S. Pedersen, N. Høiby, and J. S. Lam.** 1989. Occurrence of a common lipopolysaccharide antigen in standard and clinical strains of *Pseudomonas aeruginosa*. J Clin Microbiol **27:**962-967.
126. **Lambertsen, L., C. Sternberg, and S. Molin.** 2004. Mini-Tn7 transposons for site-specific tagging of bacteria with fluorescent proteins. Environ Microbiol **6:**726-732.
127. **Ledeboer, N. A., and B. D. Jones.** 2005. Exopolysaccharide sugars contribute to biofilm formation by *Salmonella enterica* serovar typhimurium on HEp-2 cells and chicken intestinal epithelium. J Bacteriol **187:**3214-3226.
128. **Lee, D. G., J. M. Urbach, G. Wu, N. T. Liberati, R. L. Feinbaum, S. Miyata, L. T. Diggins, J. He, M. Saucier, E. Deziel, L. Friedman, L. Li, G. Grills, K. Montgomery, R. Kucherlapati, L. G. Rahme, and F. M. Ausubel.** 2006. Genomic analysis reveals that *Pseudomonas aeruginosa* virulence is combinatorial. Genome Biol **7:**R90.
129. **Lee, V. T., J. M. Matewish, J. L. Kessler, M. Hyodo, Y. Hayakawa, and S. Lory.** 2007. A cyclic-di-GMP receptor required for bacterial exopolysaccharide production. Mol Microbiol **65:**1474-1484.
130. **Lewis, K.** 2008. Multidrug tolerance of biofilms and persister cells. Curr Top Microbiol Immunol **322:**107-131.
131. **Lewis, K.** 2005. Persister cells and the riddle of biofilm survival. Biochemistry (Mosc) **70:**267-274.
132. **Lewis, K.** 2010. Persister cells. Annu Rev Microbiol **64:**357-372.
133. **Liu, H., and H. H. Fang.** 2002. Extraction of extracellular polymeric substances (EPS) of sludges. J Biotechnol **95:**249-256.
134. **Lyczak, J. B., C. L. Cannon, and G. B. Pier.** 2002. Lung infections associated with cystic fibrosis. Clin Microbiol Rev **15:**194-222.
135. **Ma, L., M. Conover, H. Lu, M. R. Parsek, K. Bayles, and D. J. Wozniak.** 2009. Assembly and development of the *Pseudomonas aeruginosa* biofilm matrix. PLoS Pathog **5:**e1000354.
136. **Ma, L., K. D. Jackson, R. M. Landry, M. R. Parsek, and D. J. Wozniak.** 2006. Analysis of *Pseudomonas aeruginosa* conditional psl variants reveals roles for the Psl polysaccharide in adhesion and maintaining biofilm structure postattachment. J Bacteriol **188:**8213-8221.
137. **Ma, L., H. Lu, A. Sprinkle, M. R. Parsek, and D. J. Wozniak.** 2007. *Pseudomonas aeruginosa* Psl is a galactose- and mannose-rich exopolysaccharide. J Bacteriol **189:**8353-8356.
138. **Mah, T. F., and G. A. O'Toole.** 2001. Mechanisms of biofilm resistance to antimicrobial agents. Trends Microbiol **9:**34-39.

139. **Mah, T. F., B. Pitts, B. Pellock, G. C. Walker, P. S. Stewart, and G. A. O'Toole.** 2003. A genetic basis for *Pseudomonas aeruginosa* biofilm antibiotic resistance. Nature **426:**306-310.
140. **Mahenthiralingam, E., M. E. Campbell, and D. P. Speert.** 1994. Nonmotility and phagocytic resistance of *Pseudomonas aeruginosa* isolates from chronically colonized patients with cystic fibrosis. Infect Immun **62:**596-605.
141. **Makin, S. A., and T. J. Beveridge.** 1996. The influence of A-band and B-band lipopolysaccharide on the surface characteristics and adhesion of *Pseudomonas aeruginosa* to surfaces. Microbiology **142 (Pt 2):**299-307.
142. **Marmont, L. S., J. C. Whitney, H. Robinson, K. M. Colvin, M. R. Parsek, and P. L. Howell.** 2012. Expression, purification, crystallization and preliminary X-ray analysis of *Pseudomonas aeruginosa* PelD. Acta Crystallogr Sect F Struct Biol Cryst Commun **68:**181-184.
143. **Marshall, B., and L. Hazle.** 2010. Cystic Fibrosis Foundation Patient Registry: Annual Data Report 2010.
144. **Mathee, K., O. Ciofu, C. Sternberg, P. W. Lindum, J. I. Campbell, P. Jensen, A. H. Johnsen, M. Givskov, D. E. Ohman, S. Molin, N. Høiby, and A. Kharazmi.** 1999. Mucoid conversion of *Pseudomonas aeruginosa* by hydrogen peroxide: a mechanism for virulence activation in the cystic fibrosis lung. Microbiology **145 (Pt 6):**1349-1357.
145. **Matilla, M. A., M. L. Travieso, J. L. Ramos, and M. I. Ramos-Gonzalez.** 2011. Cyclic diguanylate turnover mediated by the sole GGDEF/EAL response regulator in Pseudomonas putida: its role in the rhizosphere and an analysis of its target processes. Environ Microbiol **13:**1745-1766.
146. **Matsukawa, M., and E. P. Greenberg.** 2004. Putative exopolysaccharide synthesis genes influence *Pseudomonas aeruginosa* biofilm development. J Bacteriol **186:**4449-4456.
147. **May, T., and S. Okabe.** 2008. *Escherichia coli* harboring a natural IncF conjugative F plasmid develops complex mature biofilms by stimulating synthesis of colanic acid and Curli. J Bacteriol **190:**7479-7490.
148. **Mayrand, D., and D. Grenier.** 1989. Biological activities of outer membrane vesicles. Can J Microbiol **35:**607-613.
149. **McAvoy, M. J., V. Newton, A. Paull, J. Morgan, P. Gacesa, and N. J. Russell.** 1989. Isolation of mucoid strains of *Pseudomonas aeruginosa* from non-cystic-fibrosis patients and characterisation of the structure of their secreted alginate. J Med Microbiol **28:**183-189.
150. **McGrath, S., D. S. Wade, and E. C. Pesci.** 2004. Dueling quorum sensing systems in *Pseudomonas aeruginosa* control the production of the Pseudomonas quinolone signal (PQS). FEMS Microbiol Lett **230:**27-34.
151. **Merighi, M., V. T. Lee, M. Hyodo, Y. Hayakawa, and S. Lory.** 2007. The second messenger bis-(3'-5')-cyclic-GMP and its PilZ domain-containing receptor Alg44 are required for alginate biosynthesis in *Pseudomonas aeruginosa*. Mol Microbiol **65:**876-895.
152. **Merkle, R. K., and I. Poppe.** 1994. Carbohydrate composition analysis of glycoconjugates by gas-liquid chromatography/mass spectrometry. Methods Enzymol **230:**1-15.

153. **Merritt, J. H., K. M. Brothers, S. L. Kuchma, and G. A. O'Toole.** 2007. SadC reciprocally influences biofilm formation and swarming motility via modulation of exopolysaccharide production and flagellar function. J Bacteriol **189:**8154-8164.
154. **Merritt, J. H., D. G. Ha, K. N. Cowles, W. Lu, D. K. Morales, J. Rabinowitz, Z. Gitai, and G. A. O'Toole.** 2010. Specific control of *Pseudomonas aeruginosa* surface-associated behaviors by two c-di-GMP diguanylate cyclases. MBio **1**.
155. **Merritt, J. H., D. E. Kadouri, and G. A. O'Toole.** 2005. Growing and analyzing static biofilms. Curr Protoc Microbiol **Chapter 1:**Unit 1B.1.
156. **Mikkelsen, H., G. Ball, C. Giraud, and A. Filloux.** 2009. Expression of *Pseudomonas aeruginosa* CupD fimbrial genes is antagonistically controlled by RcsB and the EAL-containing PvrR response regulators. PLoS One **4:**e6018.
157. **Mikkelsen, H., M. Sivaneson, and A. Filloux.** 2011. Key two-component regulatory systems that control biofilm formation in *Pseudomonas aeruginosa*. Environ Microbiol.
158. **Miller, M. B., and B. L. Bassler.** 2001. Quorum sensing in bacteria. Annu Rev Microbiol **55:**165-199.
159. **Mireles, J. R., A. Toguchi, and R. M. Harshey.** 2001. *Salmonella enterica* serovar typhimurium swarming mutants with altered biofilm-forming abilities: surfactin inhibits biofilm formation. J Bacteriol **183:**5848-5854.
160. **Mishra, M., M. S. Byrd, S. Sergeant, A. K. Azad, M. R. Parsek, L. McPhail, L. S. Schlesinger, and D. J. Wozniak.** 2012. *Pseudomonas aeruginosa* Psl polysaccharide reduces neutrophil phagocytosis and the oxidative response by limiting complement-mediated opsonization. Cell Microbiol **14:**95-106.
161. **Morici, L. A., A. J. Carterson, V. E. Wagner, A. Frisk, J. R. Schurr, K. Höner zu Bentrup, D. J. Hassett, B. H. Iglewski, K. Sauer, and M. J. Schurr.** 2007. *Pseudomonas aeruginosa* AlgR represses the Rhl quorum-sensing system in a biofilm-specific manner. J Bacteriol **189:**7752-7764.
162. **Nguyen, D., A. Joshi-Datar, F. Lepine, E. Bauerle, O. Olakanmi, K. Beer, G. McKay, R. Siehnel, J. Schafhauser, Y. Wang, B. E. Britigan, and P. K. Singh.** 2011. Active starvation responses mediate antibiotic tolerance in biofilms and nutrient-limited bacteria. Science **334:**982-986.
163. **Nichols, W. W., S. M. Dorrington, M. P. Slack, and H. L. Walmsley.** 1988. Inhibition of tobramycin diffusion by binding to alginate. Antimicrob Agents Chemother **32:**518-523.
164. **Nickel, J. C., J. B. Wright, I. Ruseska, T. J. Marrie, C. Whitfield, and J. W. Costerton.** 1985. Antibiotic resistance of *Pseudomonas aeruginosa* colonizing a urinary catheter in vitro. Eur J Clin Microbiol **4:**213-218.
165. **Nielsen, L., X. Li, and L. J. Halverson.** 2011. Cell-cell and cell-surface interactions mediated by cellulose and a novel exopolysaccharide contribute to *Pseudomonas putida* biofilm formation and fitness under water-limiting conditions. Environ Microbiol **13:**1342-1356.
166. **Nilsson, M., W. C. Chiang, M. Fazli, M. Gjermansen, M. Givskov, and T. Tolker-Nielsen.** 2011. Influence of putative exopolysaccharide genes on *Pseudomonas putida* KT2440 biofilm stability. Environ Microbiol **13:**1357-1369.

167. **Nivens, D. E., D. E. Ohman, J. Williams, and M. J. Franklin.** 2001. Role of alginate and its O acetylation in formation of *Pseudomonas aeruginosa* microcolonies and biofilms. J Bacteriol **183:**1047-1057.
168. **O'Toole, G. A.** 2003. To build a biofilm. J Bacteriol **185:**2687-2689.
169. **O'Toole, G. A., and R. Kolter.** 1998. Flagellar and twitching motility are necessary for *Pseudomonas aeruginosa* biofilm development. Mol Microbiol **30:**295-304.
170. **O'Toole, G. A., L. A. Pratt, P. I. Watnick, D. K. Newman, V. B. Weaver, and R. Kolter.** 1999. Genetic approaches to study of biofilms. Methods Enzymol **310:**91-109.
171. **Oglesby, L. L., S. Jain, and D. E. Ohman.** 2008. Membrane topology and roles of *Pseudomonas aeruginosa* Alg8 and Alg44 in alginate polymerization. Microbiology (Reading, Engl) **154:**1605-1615.
172. **Oliver, A., R. Cantón, P. Campo, F. Baquero, and J. Blázquez.** 2000. High frequency of hypermutable *Pseudomonas aeruginosa* in cystic fibrosis lung infection. Science **288:**1251-1254.
173. **Olvera, C., J. B. Goldberg, R. Sánchez, and G. Soberón-Chávez.** 1999. The *Pseudomonas aeruginosa* algC gene product participates in rhamnolipid biosynthesis. FEMS Microbiol Lett **179:**85-90.
174. **Ophir, T., and D. L. Gutnick.** 1994. A role for exopolysaccharides in the protection of microorganisms from desiccation. Appl Environ Microbiol **60:**740-745.
175. **Otwinowski, Z., and W. Minor.** 1997. Processing of X-ray diffraction data collection in oscillation mode. Methods in Enzymology **276:**307-326.
176. **Pamp, S. J., M. Gjermansen, H. K. Johansen, and T. Tolker-Nielsen.** 2008. Tolerance to the antimicrobial peptide colistin in *Pseudomonas aeruginosa* biofilms is linked to metabolically active cells, and depends on the pmr and mexAB-oprM genes. Mol Microbiol **68:**223-240.
177. **Pandit, J., M. D. Forman, K. F. Fennell, K. S. Dillman, and F. S. Menniti.** 2009. Mechanism for the allosteric regulation of phosphodiesterase 2A deduced from the X-ray structure of a near full-length construct. Proc Natl Acad Sci U S A **106:**18225-18230.
178. **Pape, T. a. S. T. R.** 2004. HKL2MAP: a graphical user interface for phasing with SHELX programs. Journal of applied crystallography **37:**843-844.
179. **Parkins, M. D., H. Ceri, and D. G. Storey.** 2001. *Pseudomonas aeruginosa* GacA, a factor in multihost virulence, is also essential for biofilm formation. Mol Microbiol **40:**1215-1226.
180. **Parsek, M. R., and P. K. Singh.** 2003. Bacterial biofilms: an emerging link to disease pathogenesis. Annu Rev Microbiol **57:**677-701.
181. **Parsonage, D., G. L. Newton, R. C. Holder, B. D. Wallace, C. Paige, C. J. Hamilton, P. C. Dos Santos, M. R. Redinbo, S. D. Reid, and A. Claiborne.** 2010. Characterization of the N-acetyl-α-D-glucosaminyl l-malate synthase and deacetylase functions for bacillithiol biosynthesis in *Bacillus anthracis*. Biochemistry **49:**8398-8414.

182. **Patriquin, G. M., E. Banin, C. Gilmour, R. Tuchman, E. P. Greenberg, and K. Poole.** 2008. Influence of quorum sensing and iron on twitching motility and biofilm formation in *Pseudomonas aeruginosa*. J Bacteriol **190:**662-671.
183. **Pesci, E. C., J. B. Milbank, J. P. Pearson, S. McKnight, A. S. Kende, E. P. Greenberg, and B. H. Iglewski.** 1999. Quinolone signaling in the cell-to-cell communication system of *Pseudomonas aeruginosa*. Proc Natl Acad Sci U S A **96:**11229-11234.
184. **Poornam, G. P., A. Matsumoto, H. Ishida, and S. Hayward.** 2009. A method for the analysis of domain movements in large biomolecular complexes. Proteins **76:**201-212.
185. **Pratt, L. A., and R. Kolter.** 1998. Genetic analysis of *Escherichia coli* biofilm formation: roles of flagella, motility, chemotaxis and type I pili. Mol Microbiol **30:**285-293.
186. **Proctor, R. A., C. von Eiff, B. C. Kahl, K. Becker, P. McNamara, M. Herrmann, and G. Peters.** 2006. Small colony variants: a pathogenic form of bacteria that facilitates persistent and recurrent infections. Nat Rev Microbiol **4:**295-305.
187. **Qin, Z., L. Yang, D. Qu, S. Molin, and T. Tolker-Nielsen.** 2009. *Pseudomonas aeruginosa* extracellular products inhibit staphylococcal growth, and disrupt established biofilms produced by *Staphylococcus epidermidis*. Microbiology **155:**2148-2156.
188. **Rahme, L. G., E. J. Stevens, S. F. Wolfort, J. Shao, R. G. Tompkins, and F. M. Ausubel.** 1995. Common virulence factors for bacterial pathogenicity in plants and animals. Science **268:**1899-1902.
189. **Razatos, A., Y. L. Ong, M. M. Sharma, and G. Georgiou.** 1998. Molecular determinants of bacterial adhesion monitored by atomic force microscopy. Proc Natl Acad Sci U S A **95:**11059-11064.
190. **Remminghorst, U., and B. H. Rehm.** 2006. Bacterial alginates: from biosynthesis to applications. Biotechnol Lett **28:**1701-1712.
191. **Remminghorst, U., and B. H. Rehm.** 2006. In vitro alginate polymerization and the functional role of Alg8 in alginate production by *Pseudomonas aeruginosa*. Appl Environ Microbiol **72:**298-305.
192. **Rickard, A. H., P. Gilbert, N. J. High, P. E. Kolenbrander, and P. S. Handley.** 2003. Bacterial coaggregation: an integral process in the development of multi-species biofilms. Trends Microbiol **11:**94-100.
193. **Rocchetta, H. L., L. L. Burrows, and J. S. Lam.** 1999. Genetics of O-antigen biosynthesis in *Pseudomonas aeruginosa*. Microbiol Mol Biol Rev **63:**523-553.
194. **Rocchetta, H. L., L. L. Burrows, J. C. Pacan, and J. S. Lam.** 1998. Three rhamnosyltransferases responsible for assembly of the A-band D-rhamnan polysaccharide in *Pseudomonas aeruginosa*: a fourth transferase, WbpL, is required for the initiation of both A-band and B-band lipopolysaccharide synthesis. Mol Microbiol **28:**1103-1119.
195. **Rodrigue, A., Y. Quentin, A. Lazdunski, V. Méjean, and M. Foglino.** 2000. Two-component systems in *Pseudomonas aeruginosa*: why so many? Trends Microbiol **8:**498-504.
196. **Rose, H. D., M. G. Heckman, and J. D. Unger.** 1973. *Pseudomonas aeruginosa* pneumonia in adults. Am Rev Respir Dis **107:**416-422.

197. **Ross, P., R. Mayer, and M. Benziman.** 1991. Cellulose biosynthesis and function in bacteria. Microbiol Rev **55:**35-58.
198. **Ryder, C., M. Byrd, and D. J. Wozniak.** 2007. Role of polysaccharides in *Pseudomonas aeruginosa* biofilm development. Curr Opin Microbiol **10:**644-648.
199. **Ryjenkov, D. A., R. Simm, U. Romling, and M. Gomelsky.** 2006. The PilZ domain is a receptor for the second messenger c-di-GMP: the PilZ domain protein YcgR controls motility in enterobacteria. J Biol Chem **281:**30310-30314.
200. **Römling, U., M. Gomelsky, and M. Y. Galperin.** 2005. C-di-GMP: the dawning of a novel bacterial signalling system. Mol Microbiol **57:**629-639.
201. **Sadovskaya, I., E. Vinogradov, J. Li, A. Hachani, K. Kowalska, and A. Filloux.** 2010. High-level antibiotic resistance in *Pseudomonas aeruginosa* biofilm: the ndvB gene is involved in the production of highly glycerol-phosphorylated beta-(1->3)-glucans, which bind aminoglycosides. Glycobiology **20:**895-904.
202. **Sakuragi, Y., and R. Kolter.** 2007. Quorum-sensing regulation of the biofilm matrix genes (pel) of *Pseudomonas aeruginosa*. J Bacteriol **189:**5383-5386.
203. **Samuel, G., and P. Reeves.** 2003. Biosynthesis of O-antigens: genes and pathways involved in nucleotide sugar precursor synthesis and O-antigen assembly. Carbohydr Res **338:**2503-2519.
204. **Schaefer, A. L., E. P. Greenberg, and M. R. Parsek.** 2001. Acylated homoserine lactone detection in *Pseudomonas aeruginosa* biofilms by radiolabel assay. Methods Enzymol **336:**41-47.
205. **Schooling, S. R., and T. J. Beveridge.** 2006. Membrane vesicles: an overlooked component of the matrices of biofilms. J Bacteriol **188:**5945-5957.
206. **Schooling, S. R., A. Hubley, and T. J. Beveridge.** 2009. Interactions of DNA with biofilm-derived membrane vesicles. J Bacteriol **191:**4097-4102.
207. **Schuster, M., and E. P. Greenberg.** 2006. A network of networks: quorum-sensing gene regulation in *Pseudomonas aeruginosa*. Int J Med Microbiol **296:**73-81.
208. **Shrout, J. D., D. L. Chopp, C. L. Just, M. Hentzer, M. Givskov, and M. R. Parsek.** 2006. The impact of quorum sensing and swarming motility on *Pseudomonas aeruginosa* biofilm formation is nutritionally conditional. Mol Microbiol **62:**1264-1277.
209. **Singh, P. K.** 2004. Iron sequestration by human lactoferrin stimulates *P. aeruginosa* surface motility and blocks biofilm formation. Biometals **17:**267-270.
210. **Singh, P. K., M. R. Parsek, E. P. Greenberg, and M. J. Welsh.** 2002. A component of innate immunity prevents bacterial biofilm development. Nature **417:**552-555.
211. **Singh, P. K., A. L. Schaefer, M. R. Parsek, T. O. Moninger, M. J. Welsh, and E. P. Greenberg.** 2000. Quorum-sensing signals indicate that cystic fibrosis lungs are infected with bacterial biofilms. Nature **407:**762-764.
212. **Skjak-Brak, G., F. Zanetti, and S. Paoletti.** 1989. Effect of Acetylation on some Solution and Gelling Properties of Alginates. Carbohydrate Research **185:**131-138.
213. **Skjåk-Braek, G., H. Grasdalen, and B. Larsen.** 1986. Monomer sequence and acetylation pattern in some bacterial alginates. Carbohydr Res **154:**239-250.

214. **Slifkin, M., and R. Cumbie.** 1988. Congo red as a fluorochrome for the rapid detection of fungi. J Clin Microbiol **26:**827-830.
215. **Smith, E. E., D. G. Buckley, Z. Wu, C. Saenphimmachak, L. R. Hoffman, D. A. D'Argenio, S. I. Miller, B. W. Ramsey, D. P. Speert, S. M. Moskowitz, J. L. Burns, R. Kaul, and M. V. Olson.** 2006. Genetic adaptation by *Pseudomonas aeruginosa* to the airways of cystic fibrosis patients. Proc Natl Acad Sci U S A **103:**8487-8492.
216. **Smith, R. L., and E. Gilkerson.** 1979. Quantitation of glycosaminoglycan hexosamine using 3-methyl-2-benzothiazolone hydrazone hydrochloride. Anal Biochem **98:**478-480.
217. **Smith, R. S., and B. H. Iglewski.** 2003. *P. aeruginosa* quorum-sensing systems and virulence. Curr Opin Microbiol **6:**56-60.
218. **Snyder, D. S., D. Gibson, C. Heiss, W. Kay, and P. Azadi.** 2006. Structure of a capsular polysaccharide isolated from *Salmonella enteritidis*. Carbohydr Res **341:**2388-2397.
219. **Spiers, A. J., J. Bohannon, S. M. Gehrig, and P. B. Rainey.** 2003. Biofilm formation at the air-liquid interface by the *Pseudomonas fluorescens* SBW25 wrinkly spreader requires an acetylated form of cellulose. Mol Microbiol **50:**15-27.
220. **Spoering, A. L., M. Vulic, and K. Lewis.** 2006. GlpD and PlsB participate in persister cell formation in *Escherichia coli*. J Bacteriol **188:**5136-5144.
221. **Starkey, M., J. H. Hickman, L. Ma, N. Zhang, S. De Long, A. Hinz, S. Palacios, C. Manoil, M. J. Kirisits, T. D. Starner, D. J. Wozniak, C. S. Harwood, and M. R. Parsek.** 2009. *Pseudomonas aeruginosa* rugose small-colony variants have adaptations that likely promote persistence in the cystic fibrosis lung. J Bacteriol **191:**3492-3503.
222. **Stewart, P. S.** 2001. Multicellular resistance: biofilms. Trends Microbiol **9:**204.
223. **Stewart, P. S., and J. W. Costerton.** 2001. Antibiotic resistance of bacteria in biofilms. Lancet **358:**135-138.
224. **Stewart, P. S., and M. J. Franklin.** 2008. Physiological heterogeneity in biofilms. Nat Rev Microbiol **6:**199-210.
225. **Stoodley, P., R. Cargo, C. J. Rupp, S. Wilson, and I. Klapper.** 2002. Biofilm material properties as related to shear-induced deformation and detachment phenomena. J Ind Microbiol Biotechnol **29:**361-367.
226. **Stoodley, P., K. Sauer, D. G. Davies, and J. W. Costerton.** 2002. Biofilms as complex differentiated communities. Annu Rev Microbiol **56:**187-209.
227. **Stover, C. K., X. Q. Pham, A. L. Erwin, S. D. Mizoguchi, P. Warrener, M. J. Hickey, F. S. Brinkman, W. O. Hufnagle, D. J. Kowalik, M. Lagrou, R. L. Garber, L. Goltry, E. Tolentino, S. Westbrock-Wadman, Y. Yuan, L. L. Brody, S. N. Coulter, K. R. Folger, A. Kas, K. Larbig, R. Lim, K. Smith, D. Spencer, G. K. Wong, Z. Wu, I. T. Paulsen, J. Reizer, M. H. Saier, R. E. Hancock, S. Lory, and M. V. Olson.** 2000. Complete genome sequence of *Pseudomonas aeruginosa* PAO1, an opportunistic pathogen. Nature **406:**959-964.
228. **Sutherland, I. W.** 1969. The structure of colanic acid. J Gen Microbiol **57:**18.
229. **Tarchevsky, I., and G. Marchenko.** 1991. Cellulose: biosynthesis and structure. Springer-Verlag.

230. **Tarchevsky, I. A., and G. N. Marchenko.** 1991. Cellulose: Biosynthesis and Structure. Springer-verlag, berlin.
231. **Teitzel, G. M., and M. R. Parsek.** 2003. Heavy metal resistance of biofilm and planktonic *Pseudomonas aeruginosa*. Appl Environ Microbiol **69:**2313-2320.
232. **Terwilliger, T. C., and J. Berendzen.** 1999. Automated MAD and MIR structure solution. Acta Crystallogr D Biol Crystallogr **55:**849-861.
233. **Thormann, K. M., S. Duttler, R. M. Saville, M. Hyodo, S. Shukla, Y. Hayakawa, and A. M. Spormann.** 2006. Control of formation and cellular detachment from *Shewanella oneidensis* MR-1 biofilms by cyclic di-GMP. J Bacteriol **188:**2681-2691.
234. **Tielen, P., F. Rosenau, S. Wilhelm, K. E. Jaeger, H. C. Flemming, and J. Wingender.** 2010. Extracellular enzymes affect biofilm formation of mucoid *Pseudomonas aeruginosa*. Microbiology **156:**2239-2252.
235. **Tielen, P., M. Strathmann, K. E. Jaeger, H. C. Flemming, and J. Wingender.** 2005. Alginate acetylation influences initial surface colonization by mucoid *Pseudomonas aeruginosa*. Microbiol Res **160:**165-176.
236. **Tielker, D., S. Hacker, R. Loris, M. Strathmann, J. Wingender, S. Wilhelm, F. Rosenau, and K. E. Jaeger.** 2005. *Pseudomonas aeruginosa* lectin LecB is located in the outer membrane and is involved in biofilm formation. Microbiology **151:**1313-1323.
237. **Tischler, A. D., and A. Camilli.** 2004. Cyclic diguanylate (c-di-GMP) regulates *Vibrio cholerae* biofilm formation. Mol Microbiol **53:**857-869.
238. **Tusnady, G. E., and I. Simon.** 2001. The HMMTOP transmembrane topology prediction server. Bioinformatics **17:**849-850.
239. **Ueda, A., and T. K. Wood.** 2009. Connecting quorum sensing, c-di-GMP, pel polysaccharide, and biofilm formation in *Pseudomonas aeruginosa* through tyrosine phosphatase TpbA (PA3885). PLoS Pathog **5:**e1000483.
240. **Vallet, I., S. P. Diggle, R. E. Stacey, M. Camara, I. Ventre, S. Lory, A. Lazdunski, P. Williams, and A. Filloux.** 2004. Biofilm formation in *Pseudomonas aeruginosa*: fimbrial cup gene clusters are controlled by the transcriptional regulator MvaT. J Bacteriol **186:**2880-2890.
241. **Vallet, I., J. W. Olson, S. Lory, A. Lazdunski, and A. Filloux.** 2001. The chaperone/usher pathways of *Pseudomonas aeruginosa*: identification of fimbrial gene clusters (cup) and their involvement in biofilm formation. Proc Natl Acad Sci U S A **98:**6911-6916.
242. **van Schaik, E. J., C. L. Giltner, G. F. Audette, D. W. Keizer, D. L. Bautista, C. M. Slupsky, B. D. Sykes, and R. T. Irvin.** 2005. DNA binding: a novel function of *Pseudomonas aeruginosa* type IV pili. J Bacteriol **187:**1455-1464.
243. **Varki, A., R. Cummings, J. Esko, H. Freeze, G. Hart, and J. Marth.** 1999. Essentials of Glycobiology. Cold Spring Harbor Laboratory Press, Cold Spring Harboy (NY).
244. **Vasseur, P., C. Soscia, R. Voulhoux, and A. Filloux.** 2007. PelC is a *Pseudomonas aeruginosa* outer membrane lipoprotein of the OMA family of proteins involved in exopolysaccharide transport. Biochimie **89:**903-915.

245. **Vasseur, P., I. Vallet-Gely, C. Soscia, S. Genin, and A. Filloux.** 2005. The pel genes of the *Pseudomonas aeruginosa* PAK strain are involved at early and late stages of biofilm formation. Microbiology **151:**985-997.
246. **Velraeds, M. M., B. van de Belt-Gritter, H. C. van der Mei, G. Reid, and H. J. Busscher.** 1998. Interference in initial adhesion of uropathogenic bacteria and yeasts to silicone rubber by a *Lactobacillus acidophilus* biosurfactant. J Med Microbiol **47:**1081-1085.
247. **Ventre, I., A. L. Goodman, I. Vallet-Gely, P. Vasseur, C. Soscia, S. Molin, S. Bleves, A. Lazdunski, S. Lory, and A. Filloux.** 2006. Multiple sensors control reciprocal expression of *Pseudomonas aeruginosa* regulatory RNA and virulence genes. Proc Natl Acad Sci U S A **103:**171-176.
248. **Vetting, M. W., P. A. Frantom, and J. S. Blanchard.** 2008. Structural and enzymatic analysis of MshA from *Corynebacterium glutamicum*: substrate-assisted catalysis. J Biol Chem **283:**15834-15844.
249. **Wagner, V. E., and B. H. Iglewski.** 2008. *P. aeruginosa* Biofilms in CF Infection. Clin Rev Allergy Immunol **35:**124-134.
250. **WAHBA, A. H., and J. H. DARRELL.** 1965. THE IDENTIFICATION OF ATYPICAL STRAINS OF *PSEUDOMONAS AERUGINOSA*. J Gen Microbiol **38:**329-342.
251. **Waldor, M. K., R. Colwell, and J. J. Mekalanos.** 1994. The *Vibrio cholerae* O139 serogroup antigen includes an O-antigen capsule and lipopolysaccharide virulence determinants. Proc Natl Acad Sci U S A **91:**11388-11392.
252. **Walker, T. S., H. P. Bais, E. Déziel, H. P. Schweizer, L. G. Rahme, R. Fall, and J. M. Vivanco.** 2004. *Pseudomonas aeruginosa*-plant root interactions. Pathogenicity, biofilm formation, and root exudation. Plant Physiol **134:**320-331.
253. **Walters, M. C., F. Roe, A. Bugnicourt, M. J. Franklin, and P. S. Stewart.** 2003. Contributions of antibiotic penetration, oxygen limitation, and low metabolic activity to tolerance of *Pseudomonas aeruginosa* biofilms to ciprofloxacin and tobramycin. Antimicrob Agents Chemother **47:**317-323.
254. **Wang, X., J. F. Preston, 3rd, and T. Romeo.** 2004. The pgaABCD locus of *Escherichia coli* promotes the synthesis of a polysaccharide adhesin required for biofilm formation. J Bacteriol **186:**2724-2734.
255. **Wang, Z., S. Larocque, E. Vinogradov, J. R. Brisson, A. Dacanay, M. Greenwell, L. L. Brown, J. Li, and E. Altman.** 2004. Structural studies of the capsular polysaccharide and lipopolysaccharide O-antigen of *Aeromonas salmonicida* strain 80204-1 produced under in vitro and in vivo growth conditions. Eur J Biochem **271:**4507-4516.
256. **Watnick, P., and R. Kolter.** 2000. Biofilm, city of microbes. J Bacteriol **182:**2675-2679.
257. **Weinhouse, H., S. Sapir, D. Amikam, Y. Shilo, G. Volman, P. Ohana, and M. Benziman.** 1997. c-di-GMP-binding protein, a new factor regulating cellulose synthesis in *Acetobacter xylinum*. FEBS Lett **416:**207-211.
258. **Whitchurch, C. B., T. Tolker-Nielsen, P. C. Ragas, and J. S. Mattick.** 2002. Extracellular DNA required for bacterial biofilm formation. Science **295:**1487.

259. **White, A. P., D. L. Gibson, W. Kim, W. W. Kay, and M. G. Surette.** 2006. Thin aggregative fimbriae and cellulose enhance long-term survival and persistence of *Salmonella*. J Bacteriol **188:**3219-3227.
260. **Whitfield, C.** 2006. Biosynthesis and assembly of capsular polysaccharides in *Escherichia coli*. Annu Rev Biochem **75:**39-68.
261. **Whitfield, C., and I. S. Roberts.** 1999. Structure, assembly and regulation of expression of capsules in *Escherichia coli*. Mol Microbiol **31:**1307-1319.
262. **WILKINSON, J. F.** 1958. The extracellualr polysaccharides of bacteria. Bacteriol Rev **22:**46-73.
263. **Williams, P., and M. Cámara.** 2009. Quorum sensing and environmental adaptation in *Pseudomonas aeruginosa*: a tale of regulatory networks and multifunctional signal molecules. Curr Opin Microbiol **12:**182-191.
264. **Wolfgang, M. C., B. R. Kulasekara, X. Liang, D. Boyd, K. Wu, Q. Yang, C. G. Miyada, and S. Lory.** 2003. Conservation of genome content and virulence determinants among clinical and environmental isolates of *Pseudomonas aeruginosa*. Proc Natl Acad Sci U S A **100:**8484-8489.
265. **Wozniak, D. J., T. J. Wyckoff, M. Starkey, R. Keyser, P. Azadi, G. A. O'Toole, and M. R. Parsek.** 2003. Alginate is not a significant component of the extracellular polysaccharide matrix of PA14 and PAO1 *Pseudomonas aeruginosa* biofilms. Proc Natl Acad Sci U S A **100:**7907-7912.
266. **Yang, L., W. Hengzhuang, H. Wu, S. D. Pedersen, N. Jochumsen, Z. Song, M. Givskov, N. Høiby, and S. Molin.** 2012. Polysaccharides serve as scaffold of biofilms formed by mucoid *Pseudomonas aeruginosa*. FEMS Immunol Med Microbiol.
267. **Yang, L., Y. Hu, Y. Liu, J. Zhang, J. Ulstrup, and S. Molin.** 2011. Distinct roles of extracellular polymeric substances in *Pseudomonas aeruginosa* biofilm development. Environ Microbiol.
268. **Yildiz, F. H., and G. K. Schoolnik.** 1999. *Vibrio cholerae* O1 El Tor: identification of a gene cluster required for the rugose colony type, exopolysaccharide production, chlorine resistance, and biofilm formation. Proc Natl Acad Sci U S A **96:**4028-4033.
269. **Zielinski, N. A., A. M. Chakrabarty, and A. Berry.** 1991. Characterization and regulation of the *Pseudomonas aeruginosa* algC gene encoding phosphomannomutase. J Biol Chem **266:**9754-9763.
270. **Zogaj, X., M. Nimtz, M. Rohde, W. Bokranz, and U. Römling.** 2001. The multicellular morphotypes of *Salmonella typhimurium* and *Escherichia coli* produce cellulose as the second component of the extracellular matrix. Mol Microbiol **39:**1452-1463.

APPENDICES

Appendix 1. Abbreviations

Abbreviation	Description
CF	Cystic fibrosis
CFTR	Cystic fibrosis transmembrane regulator
LPS	Lipopolysaccharide
PMN	Polymorphonuclear leukocytes
Cup fimbriae	Chaperone-usher pathway
eDNA	Extracellular DNA
CPA	Common polysaccharide antigen (formerly A-band)
OSA	O-specific antigen (formerly B-band)
QS	Quorum sensing
PQS	Pseudomonas quinolone signal
C-di-GMP	Bis-(3',5')-cyclic-di-guanidine monophosphate
DGC	Diguanylate cyclase
PDE	phosphodiesterase
TCS	Two-component systems
MATE	Multidrug and toxic compound extrusion
TM	Transmembrane
TPR	Tetratricopeptide
ITC	Isothermal titration calorimetry
TPR	Differential scanning fluorimetry
CLSM	Confocal laser scanning microscopy
RSCV	Rugose small colony variant

VITA

Kelly Marie Colvin was born in Cupertino, CA on September 19, 1983, the daughter of Linda Lechner and Jim Colvin. After completing high school at Homestead High in Sunnyvale, CA, she attended University of California, San Diego from 2001 to 2005. She graduated with a bachelor of science in both Biochemistry/Cell Biology and Psychology. In 2012 she earned a Doctor of Philosophy at University of Washington in Microbiology.